



## City Research Online

### City, University of London Institutional Repository

---

**Citation:** Eon Kang, Shin (2014). Hot ductility of TWIP steels. (Unpublished Doctoral thesis, City University London)

This is the accepted version of the paper.

This version of the publication may differ from the final published version.

---

**Permanent repository link:** <https://openaccess.city.ac.uk/id/eprint/13703/>

**Link to published version:**

**Copyright:** City Research Online aims to make research outputs of City, University of London available to a wider audience. Copyright and Moral Rights remain with the author(s) and/or copyright holders. URLs from City Research Online may be freely distributed and linked to.

**Reuse:** Copies of full items can be used for personal research or study, educational, or not-for-profit purposes without prior permission or charge. Provided that the authors, title and full bibliographic details are credited, a hyperlink and/or URL is given for the original metadata page and the content is not changed in any way.

# **HOT DUCTILITY OF TWIP STEELS**

**by**

**Shin Eon Kang**

**A Thesis Submitted for the Degree of  
Doctor of Philosophy  
at the City University London**

**School of Mathematics, Computer Science and Engineering  
City University London**

**December 2014**

## TABLE OF CONTENTS

<b>TABLE OF CONTENTS</b> .....	i
<b>LIST OF TABLES</b> .....	v
<b>LIST OF FIGURES</b> .....	vi
<b>ACKNOWLEDGEMENTS</b> .....	xviii
<b>DECLARATION</b> .....	xix
<b>ABSTRACT</b> .....	xx
<b>LIST OF SYMBOLS</b> .....	xxii
<b>CHAPTER 1: INTRODUCTION</b> .....	1
1.1 Background of research .....	1
1.2 Aim of the thesis .....	3
1.3 Scope of the work .....	4
<b>CHAPTER 2: LITERATURE REVIEW</b> .....	5
2.1 Surface defect of continuously cast products .....	5
2.2 Transverse cracking .....	7
2.2.1 Mechanism for formation of transverse cracks .....	8
2.2.2 Factors influencing formation of transverse cracking .....	11
2.2.3 Prevention of transverse cracking .....	14
2.3 Hot ductility of steels .....	16
2.3.1 Hot ductility test .....	18
2.3.2 Hot ductility region .....	21
Low ductility regions (embrittlement region) .....	22
High ductility regions .....	25
2.3.3 Factors that influence hot ductility .....	29
Strain rate .....	30
Grain size .....	32

Precipitation .....	36
Inclusions .....	39
Cooling rate .....	41
Thermal cycle .....	45
2.3.4 Influence of compositions on hot ductility .....	46
Carbon .....	47
Silicon .....	50
Manganese .....	52
Phosphorus .....	63
Sulphur .....	66
Aluminum .....	72
Niobium .....	77
Vanadium .....	81
Boron .....	84
Titanium .....	94
Copper .....	99
<b>CHAPTER 3: EXPERIMENTAL METHODS .....</b>	<b>108</b>
3.1 Preparation of specimens .....	108
3.2 Equipment for tensile testing .....	110
3.2.1 Hot tensile testing machine .....	110
3.2.2 Gleeble 3500 .....	112
3.3 Evaluation of hot ductility .....	113
3.4 Metallography .....	114
3.4.1 Optical Microscopy (OM) .....	114
3.4.2 Scanning Electron Microscopy (SEM) .....	115
3.4.3 Transmission Electron Microscopy (TEM) .....	115
3.4.4 Secondary Ion Mass Spectrometry (SIMS) .....	116
<b>CHAPTER 4: THE INFLUENCE OF Al AND N ON THE HOT DUCTILITY OF TWIP STEELS .....</b>	<b>117</b>
4.1 Introduction .....	117
4.2 Experimental .....	117
4.3 Results .....	120
4.4 Discussion .....	127
4.5 Conclusions .....	129

<b>CHAPTER 5: HOT DUCTILITY OF Nb/V CONTAINING HIGH Al, TWIP STEELS</b>	131
5.1 Introduction	131
5.2 Experimental	131
5.3 Results	134
5.4 Discussion	142
5.5 Conclusions	145
<b>CHAPTER 6: INFLUENCE OF S ON HOT DUCTILITY OF HIGH Al, TWIP STEELS</b>	147
6.1 Introduction	147
6.2 Experimental	147
6.3 Results	148
6.4 Discussion	163
6.5 Conclusions	167
<b>CHAPTER 7: INFLUENCE OF B AND Ti ON HOT DUCTILITY OF HIGH Al, TWIP STEELS</b>	168
7.1 Introduction	168
7.2 Experimental	169
7.3 Results	170
7.4 Discussion	174
7.5 Conclusions	177
<b>CHAPTER 8: INFLUENCE OF B AND Ti ON HOT DUCTILITY OF ‘AS-CAST HIGH Al, Nb CONTAINING TWIP STEELS</b>	178
8.1 Introduction	178
8.2 Experimental	178
8.3 Results	179
8.4 Discussion	185
8.5 Conclusions	187
<b>CHAPTER 9: INFLUENCE OF B ON HOT DUCTILITY OF HIGH Al TWIP</b>	

<b>STEELS</b> .....	189
9.1 Introduction .....	189
9.2 Experimental .....	189
9.3 Results .....	191
9.4 Discussion .....	199
9.5 Conclusions .....	205
<b>CHAPTER 10: SUMMARY AND CONCLUSIONS</b> .....	206
<b>REFERENCE</b> .....	209
<b>APPENDIX A</b> .....	226

## LIST OF TABLES

Table 4.1 Compositions of TWIP steels.....	120
Table 4.2 AlN precipitation and its influence on the minimum depth of the trough.....	128
Table 5.1 Composition of Nb/V containing TWIP steels.....	132
Table 6.1 Compositions of TWIP steels.....	147
Table 6.2 Inclusion and precipitate sizes and shapes in low S and higher S steels.....	152
Table 6.3 Volume fraction of MnS and AlN assuming equilibrium conditions.....	165
Table 7.1 Composition of steels examined.....	169
Table 8.1 Composition of steels examined.....	178
Table 9.1 Compositions of the high Al containing TWIP steels.....	190
Table A1 Composition of steels, wt.%, used for comparing the tensile results from Gleeble with those obtained from Induction heating machine.....	226

## LIST OF FIGURES

Fig.1.1 Relationship of tensile strength and elongation for automotive steel sheets.....	1
Fig.1.2 Comparison of strength-strain curves between TWIP and other automotive steels and how twin density increases with strain.....	3
Fig.2.1 Schematic drawing of strand cast section showing different types of cracks.....	6
Fig.2.2 Typical transverse corner crack (a) and cross-section of transverse corner crack (b) .....	8
Fig.2.3 Intergranular microvoid coalescence of low alloy steels by deformation in (a) ~ (c) low temperature $\gamma$ region and (d)~(f) $\alpha/\gamma$ duplex phase region [19].....	10
Fig.2.4 Low ductility (brittle) temperature ranges [24].....	11
Fig.2.5 Effect of oscillation mark depth on ductility [25].....	13
Fig.2.6 A typical temperature profile measured at various positions in the slab for 1880mm $\times$ 250mm strand.....	18
Fig.2.7 Heating method of tensile testing machine.....	19
Fig.2.8 A typical commercial cooling cycle at various positions in the slab.....	21
Fig.2.9 Schematic diagram of ductility curve defining the three characteristic regions of hot ductility [20].....	22
Fig.2.10 Precipitation free zone around grain boundary in Nb-bearing steel fracture at 950 $^{\circ}$ C; grain boundary contains fine precipitates of Nb(C, N) and coarse MnS inclusions [46].....	23
Fig.2.11 Schematic models showing formation of wedge and rounded cracks by grain boundary sliding [48, 49].....	25

Fig.2.12 Schematic diagram illustrating the ductility levels that can be achieved with and without dynamic recrystallisation at the high temperature end of the trough [38].....	29
Fig.2.13 Dependence of ductility on strain rate and test temperature for Nb-bearing steel [22].....	30
Fig.2.14 Influence of strain rate on hot ductility of 0.4%C, 1.5%Mn steel had a relatively fine grain size 110 $\mu$ m [53].....	32
Fig.2.15 Hot ductility curves for 0.19% C steel of various grain sizes [63].....	34
Fig.2.16 Influence of $D_0$ (initial un-deformed grain size after heat treatment) on minimum RA value [20].....	35
Fig.2.17 Influence of (a) particle size and (b) interparticle spacing on hot ductility of Nb-containing steels [20].....	37
Fig.2.18 Effect of increasing Mn level on decreasing depth of trough: all steels give wide ductility troughs due to coarse grain size (450 $\mu$ m) and the trough was deeper and extended to higher temperature in high Al containing steel due to precipitation of AlN [71].....	39
Fig.2.19 Influence of S in solution on depth of steels with similar coarse grain size (~400 $\mu$ m), strain rate ( $10^{-3} \text{ s}^{-1}$ ) and cooling rates [71, 74, 75]: trough changes from narrow to wide trough behaviour as S content increases[73].....	40
Fig.2.20 Influence of cooling rate on hot ductility of given steels at two strain rates [75]...42	
Fig.2.21 Hot ductility curves for as-cast C-Mn-Nb-Al steel, given different cooling rates to the test temperature [76].....	43
Fig.2.22 Effect of reducing cooling rate during casting to 25 $^{\circ}$ C/min on as-cast C-Mn-Nb-Al steel with and without Ti addition (curve for the same Nb-Ti steel cooled at 100 $^{\circ}$ C/min, broken line shown for a comparison) [79] .....	44

Fig.2.23 Thermal schedule used to generate the thermal condition of billet surface in the continuous casting process. $T_m$ is the melting point, $T_{min}$ is the lowest temperature reached during the primary cooling stage and $T_{max}$ is the highest temperature at the start of secondary cooling. $T_u$ is the temperature at the straightener [82] .....	46
Fig.2.24 Dependence on C content of (a) surface cracking frequency and of (b) ductility (RA) and $\gamma$ grain size $D_\gamma$ of as cast steel and (c) their relation to $\gamma$ composition temperature $T_\gamma$ schematic) [19].....	48
Fig.2.25 Effect of C content on grain growth of $\gamma$ phase during continuous cooling of 0.8%Mn steels [66].....	49
Fig.2.26 Hot ductility curves for series of plain C-Mn steels (C contents in wt.%) [51]...50	
Fig.2.27 Influence of silicon on hot ductility of C-Mn-Al steels reduction of area [92]. Steels 1 and 2 have 0.3 and 1.22%Si, respectively and steel 7 is a Nb containing HSLA steel .....	51
Fig.2.28 Influence of manganese content on RA at temperature of 1300 °C for holding time of 300s at a high strain rate ( $22s^{-1}$ ). (a) 0.005 mass% sulfur steels (b) 0.008~0.009 mass% sulfur steels [98].....	53
Fig.2.29 Influence of C and Mn on width of trough [38].....	56
Fig.2.30 Hot ductility curves for steel A-F: occurrence of dynamic recrystallisation indicated by shaded regions [101].....	57
Fig.2.31 Strength and R of A of TWIP steels with various Mn and C contents from 9-23%Mn to 0.6 to 0.9%C [104].....	59
Fig.2.32 Fracture surface and EDX analyses of Fe-16%Mn-0.8%C tested at 1200 °C, RA 21%: (a) At the centre position; (b) High magnification of (a); (c) Position 1 of EDX analysis; (d) Analysis of the droplet (position 1) [104].....	60
Fig.2.33 Hot ductility curve of 3C16MnAl. Curve of 6C22Mn is included for comparison [105]. (Strain rate is $1s^{-1}$ ).....	61

Fig.2.34 Examples of true stress–true strain curves of 6C22Mn and 3C16MnAl at high temperatures [105].....	61
Fig.2.35 Tensile strained microstructures of 3C16MnAl: (a) fracture tip at 800°C (longitudinal cross-section), (b) transverse cross-section of a fracture surface at 900°C, (c) large grain structure after reheating at 1250°C for 120s (SEM-EBSD), (d) dynamic recrystallized structure after straining at 1200°C(SEM-EBSD) [105].....	62
Fig.2.36 Effect of phosphorus on hot ductility in 0.4%C steels. Chemical compositions of each heat are also shown above this figure [108].....	64
Fig.2.37 Effect of C and P content on the embrittlement. Good ductility region is defined as the region where minimum RA value is higher than 60% in the temperature range 1200 to 900°C, melted samples were strained at a strain rate of 5/s [108].....	64
Fig.2.38 Hot ductility curves for as cast high C, Nb containing and Nb free steels, with and without P [113].....	65
Fig.2.39 Variation of reduction of area to failure with temperature of deformation in tensile test for various steels solution treated at 1350°C: $\dot{\epsilon}=2.3s^{-1}$ [60].....	67.
Fig.2.40 Extraction replica image showing sulphide precipitation in steel (0.05C-0.19Mn-0.012S): specimen deformed at 1000°C at $\dot{\epsilon}=2.3s^{-1}$ after solution treatment at 1350°C [60].....	68
Fig.2.41 Effect of cooling rate on hot ductility of steels [95].....	69
Fig.2.42 Effect of Sulfur and Phosphorus on hot ductility, strain rate $2 \times 10^{-3}s^{-1}$ [118].....	71
Fig.2.43 Effect of holding time on hot ductility of an 0.16%C steel [118].....	71
Fig.2.44 Influence of Al on the hot ductility of C-Mn-Al steels [92]. (N and S levels were ~0.005 and 0.006%, respectively).....	74
Fig.2.45 Hot ductility curves for high Al containing steels showing that increasing the Al level from 0.03 to 0.87% widens the trough. However, at the higher Al levels, the depth of the trough becomes shallower. The steels contained 0.2%C, and 1.4%Mn with varying P levels [124].....	75

Fig.2.46 Hot ductility for three steels under examination [122].....	76
Fig.2.47 The effect of Nb contents and deformation temperature on hot ductility [23].....	77
Fig.2.48 Influence of N on hot ductility of C-MnNb-Al steels (Sol.Al, 0.032~0.042%, Nb, 0.034%) [127].....	79
Fig.2.49 Hot ductility curves for C-Mn-Nb-Al steels (solid lines) and calculated curves of the volume fraction of Nb(CN) precipitated as a function of the test temperature assuming equilibrium is achieved (dotted lines) [100].....	79
Fig.2.50 Influence of a 0.04%Ti addition to hot ductility of Nb steel containing 0.004%N for similar grain sizes [21].....	81
Fig.2.51 Hot ductility curves for a series of steels having different levels of V and N. (also included is a curve for a Nb containing steel for comparison). Steel were solution treated at 1330 °C [112].....	82
Fig.2.52 (a) Effect of product of total V and N contents on the width of the trough, (b) Influence of product of total V and N contents on RA values; steels were tested at 850 °C in the trough [112].....	83
Fig.2.53 Hot ductility curves for boron microalloyed steels (RA, reduction of area) [133].	86
Fig.2.54 Hot ductility curves for the specimens doped with different quantities of boron [136].....	88
Fig.2.55 Optical microstructures for the specimens with 7.5 wt.ppm B, (a) and (b) and 35 wt.ppm B, (c) and (d) tensile-tested at 800°C, (a) and (c) and 750°C, (b) and (d) [136].....	88
Fig.2.56 Hot ductility curves at various cooling rates for (a) B-free steel and (b) B containing steel [146].....	89

Fig.2.57 Influence of B precipitate distribution and location on hot ductility of B containing steel at different deformation temperatures and cooling rates. PTA image at non-deformed temperatures of (a) 850°C with a cooling rate of 1°C/s, (b) 900°C with a cooling rate of 1°C/s, (c) 950°C with a cooling rate of 1°C/s, (d) 850°C with a cooling rate of 20°C/s, (e) 900°C with a cooling rate of 20°C/s, and (f) 950°C with a cooling rate of 20°C/s [146].....	90
Fig.2.58 The effect of an addition of B on the hot ductility of C steels in thermal cycles (A) [147].....	91
Fig.2.59 Comparison of hot ductility of C-B steel in thermal cycles (A) direct cooled to straining temperatures and (B) under-cooled and reheated to straining temperatures [147].....	92
Fig.2.60 Effect of N content on BN distributions in the single $\gamma$ temperature range from 900 to 1000°C [147].....	92
Fig.2.61 Hot ductility curves of the B steel, B-Nb steel and B-Nb-Ti steel [148].....	93
Fig.2.62 Distributions of BN precipitates in B-Nb steel and B-Nb-Ti steel for the temperature range of 850~950°C before deformation [148].....	94
Fig.2.63 Influence of small Ti additions on the hot ductility of reheated Nb containing steels. Grain size of the steels after solution treating is indicated on curves [21]. (a) Ref. 107, (b) Ref. 126 .....	93
Fig.2.64 Average particle size against T:N ratio for steels tested at 1000 °C after cooling at 25°Cmin <sup>-1</sup> and 100~200°Cmin <sup>-1</sup> . Ti and N levels were 0.02% and 0.009%, respectively [78].....	96
Fig.2.65 Hot ductility curves for the Nb, Ti and Nb-Ti steels in-situ melted and (a) directly cooled at 4°C/s or 0.4°C/s, (b) cooled at 4°C/s with or without pre-chilling [150].....	97
Fig.2.66 Hot ductility curves for boron as-cast C-Mn-Al-Nb steels tested in "air" (argon flow discontinued) steel1, low residual, steel 2, 0.25%Cu, 0.25%Ni, steel 3, 0.5%Cu, steel 4, 0.5%Ni [157].....	101

Fig.2.67 Micrographs obtained using transmission electron microcopy (TEM) showing copper sulphide particles at $\gamma$ grain boundaries (X18500) and b, c enlarged views of copper (oxy)sulphide showing their various shapes (X51600, X30300) [157].....	103
Fig.2.68 Hot ductility for the high purity ultra-low carbon steels containing copper and/or tin deformed at $1s^{-1}$ [134].....	105
Fig.2.69 Effect of copper on the hot ductility of ultra-low carbon steels containing 0.004% sulphur deformed at $10^{-2}s^{-1}$ and $200s^{-1}$ [134].....	105
Fig.2.70 Hot ductility for the 0.2% carbon steel containing 0.2% tin deformed at $10^{-2}s^{-1}$ and $200s^{-1}$ [134].....	106
Fig.2.71 Effects of deformation temperature and Cu and/or Sn addition on the hot ductility of steels with various C content [135].....	107
Fig.3.1 Position and dimensions of tensile specimens taken from as cast ingot.....	108
Fig.3.2 Details of the tensile test sample used when testing was carried out in the induction heated unit at the City University London.....	109
Fig.3.3 Geometry of Gleeble specimen.....	109
Fig.3.4 Layout of test equipment.....	111
Fig.3.5 Testing arrangement for the hot ductility tests in the as cast condition.....	111
Fig.3.6 Schematic diagram of testing rig at the City University.....	112
Fig.3.7 Layout of Gleeble 3500 .....	113
Fig.3.8 Testing arrangement for carried out the hot ductility tests when re-heating to $1250\sim 1350^{\circ}C$ using the Gleeble.....	113
Fig.3.9 Geometry of sample after fracture.....	114
Fig.4.1 Temperature profile used (a) without and (b) with under cooling step.....	119

Fig.4.2 Hot ductility curve for low Al steels, steels 1 and 2.....	121
Fig.4.3 Hot ductility curves for high Al steels, steels 3(0.0095%N), 4(0.017%N) and 5(0.023%N).....	121
Fig.4.4 Hot ductility curves for 1.42%Al, 0.0043%N TWIP steel (steel 6), after cooling at 60°C/min and 180°C/min and after introducing the under- cooling step.....	122
Fig.4.5 Hot ductility curves for high Al and high N steel (steel 5), at two cooling rates, 60°C (solid line) and 180°C/min (dashed line).....	123
Fig.4.6 Micrograph of TWIP steel, steel 6 (1.42%Al, 0.0043%N) melted and tested at 800 °C showing precipitation at austenite grain boundaries.....	124
Fig.4.7 Micrograph of steel 6 (1.42%Al, 0.0043%N) melted and tested at 900 °C showing precipitation at austenite grain boundaries.....	124
Fig.4.8 Micrograph of TWIP steel 5 (1.53%Al, 0.023%N) melted and tested at 800°C showing longer precipitates at the boundaries compared to the lower N steel 6 (Fig.4.7).125	
Fig.4.9 Micrograph of TWIP steel 5 (1.53%Al, 0.023%N) melted and tested at 900°C showing extensive precipitation at austenite grain boundaries.....	125
Fig.4.10 Copious precipitation of AlN at the austenite grain boundaries in (a) low N TWIP steel 6 (1.43%Al, 0.0043%N) showing very thin films of AlN at the grain boundaries on the fracture surface and (b) coarse AlN particle at the boundary in a high N, TWIP steel 3 (1.53%Al, 0.01%N). Both steels were tested at 800°C after melting and the fracture surfaces examined. ....	126
Fig.4.11 Summary of hot ductility curves for the Al containing in the melted “cast in situ” condition and typical hot ductility curve for a 0.1C-0.42Si-1.39Mn-0.007P-0.01S-0.036Al-0.0075N, HSLA steel. Cooling rate in all cases was 60°C/min.....	129
Fig.5.1 Schematic diagram for the testing conditions for (a) “cast in situ” and (b) “machined as cast or hot rolled” tensile specimens.....	133
Fig.5.2 Hot Ductility curves for Nb/V TWIP steels, in the “cast in situ” condition.....	134

Fig. 5.3 Hot ductility curves for “as cast” and “cast in situ” steels of similar composition .....	135
Fig.5.4 Hot ductility curves for "machined hot rolled" (dashed curves) and "machined as cast” steel (solid curve).....	135
Fig.5.5 Influence of cooling rate on the hot ductility of low and higher N, Nb/V containing TWIP steels.....	136
Fig.5.6 Micrographs of as cast steel, A1, (0.0068%N) tested at (a) 700°C, RA 13%, (b) 800°C, RA 12%, (c) 900°C, RA 38%, (d) 1000°C, RA 36%, (e) 1100°C, RA 24%.....	137
Fig.5.7 Dynamic recrystallisation (DRX) at the fracture surface for steel F (“cast in situ”) tested at 1150°C. (RA was 50%).....	138
Fig.5.8 (a) typical precipitation found in the Nb/V steels with associated analysis for particles (Steel A-1 was “machined as-cast” and tested at 700°C) and (b) position 2 in (a) showing strong Nb peaks with much smaller V peaks.....	139
Fig.5.9 Very coarse AlN precipitation not associated with the grain boundaries in steel AB, "machined hot rolled".....	140
Fig.5.10 Fine Nb(C, N) precipitation (12~40nm) within the austenite grains in steel AB, "machined hot rolled".....	140
Fig.5.11 Films of AlN found on the fracture surface of (a) “machined as rolled” and (b) “machined as cast” steels tested at 700°C.....	142
Fig.5.12 Summary of hot ductility curves for the Al containing Nb/V free high N TWIP steels and the Nb/V containing high Al TWIP steels in the melted “cast in situ” condition also included is a typical hot ductility curve for a 0.1C-0.42Si-1.39Mn-0.007P-0.01S- 0.036Al-0.0075N steel. Cooling rate in all cases was 60°C/min.....	145
Fig.6.1 Schematic diagram of the processing route for the tensile specimens.....	148
Fig. 6.2 Hot ductility curves for the three TWIP steels with varying sulphur contents ....	149

Fig.6.3 Microstructures for the 3 steels examined (a) 0.003%S, (b) 0.010%S, (c) 0.023%S at two magnifications (Optical Microscopy).....	150
Fig.6.4 Types of analysis spectrum (a) MnS inclusions containing Ca, (steel 1) (b) Pure MnS inclusions, (steels 1, 2 and 3) (c) AlN (steels 1, 2 and 3).....	151
Fig.6.5 Sulphides and AlN particles present in (a) low S, 0.003%steel, grey colour is CaMnS and black is AlN, (b) and (c) higher S steel, 0.01%, grey is MnS, black AlN and dark grey is a mixture of MnS and AlN.....	152
Fig.6.6 Large hexagonal AlN particle in low S steel. (SEM).....	155
Fig.6.7 Further examples of these dendritic AlN rods associated with MnS inclusions...	156
Fig.6.8 Flat intergranular fractures formed by grain boundary sliding are encouraged by the long interdendritic AlN rods in high S steels. (SEM) .....	159
Fig.6.9 Very coarse AlN dendritic rods found in higher S steels (TEM) with sulphides at their ends.....	159
Fig.6.10 A typical area for the low S steel is shown in which coarse hexagonal AlN particles are present and very fine MnS sulphide inclusions containing Ca.....	160
Fig.6.11 Typical fracture surface of low S steel showing the presence of plate AlN particles. (SEM).....	161
Fig. 6.12 Fracture surface in 0.023%S steel at 900°C. (SEM).....	162
Fig.6.13 Electron microscope grids showing the absence of these long AlN rods in the low S steel (a) but there presence in the higher S steel (b) and (c). (TEM).....	163
Fig.7.1 Schematic diagram of the processing routes for the tensile specimens for samples machined from the ingots and heated to 1250°C.....	170
Fig.7.2 Hot ductility curves for Ti-B free steel 1 and Ti-B containing steel 2 after “re-heating” to 1250°C and cooling at 60°C/min to the tensile test temperature.....	171

Fig.7.3 Change of TiN particle distribution and size with increasing test temperature from 800 to 1100°C for “re-heated” steel 2 (0.038%Ti, 0.0021%B).....	173
Fig.7.4 Copious precipitation of very coarse AlN particles at the austenite grain boundaries in the Ti-B free TWIP steel, steel 1 “reheated” to 1250°C and cooled at 60°C/min.....	174
Fig.8.1 Hot ductility curves for samples machined from the ingots and re-melted at 1410°C; “as-cast”.....	179
Fig.8.2 Hot ductility curves for cooling rates of 12 and 60°C/min for the Nb, Ti-B steel 2 after melting, the “as-cast” condition. Also included is the hot ductility curve for steel 1, “re-heated” to 1250°C and cooled at 60°C/min.....	180
Fig.8.3 Coarse TiN particles in the “as-cast” steel 2, cooled at 60°C/min, (a) fracture surface showing the presence of precipitation particles A, B and C with typical analysis (b) mainly TiN particles with occasionally a trace of Al (c) mainly MnS particles with Alumina (d)TiN particles with more substantial amounts of Nb. Sample was fractured at 800°C.....	183
Fig.8.4 AlN and Nb(C, N) precipitation in the Ti-B free TWIP steel, steel 1 “reheated” to 1250°C and cooled at 60°C/min. (a) Copious precipitation of very coarse AlN particles at the austenite grain boundaries (b) Fine (Nb(C, N)) precipitation at the boundaries (c) dendritic precipitation of AlN.....	184
Fig.8.5 Hot ductility curves for “as-cast” steel 2 at the two cooling rates, 60 and 12°C/min compared to Zarandi and Yues’ curves for HSLA, Nb containing steels with and without B using a secondary cooling rate of 15°C/min.....	186
Fig.9.1 Schematic diagram of the heating and cooling programme used in the investigation.....	191
Fig.9.2 Hot ductility curves for B-Ti high Al, TWIP steels, Steels 1~3 compared to the hot ductility curve for a B free, Ti containing high Al, TWIP steel, Steel 4.....	192
Fig.9.3 SIMS photographs for steel 1 (1.51%Al, 0.042%Ti, 0.0026%B, 0.0093%N) for the test temperature range 700~1200°C.....	193
Fig.9.4 SIMS photographs for steel 2 (1.48%Al, 0.041%Ti, 0.0026%B, 0.0094%N) for the test temperature range 700~1200°C.....	194

Fig.9.5 SIMS photographs for steel 3 (1.12%Al, 0.038%Ti, 0.0021%B, 0.007%N) for the test temperature range 800~1150°C.....	195
Fig.9.6 SIMS photographs for steel 5 (1.44%Al, 0.098%Ti, 0.0017%B, 0.009%N) for the test temperature range 700~1200°C.....	196
Fig.9.7 Hot ductility curve for high Ti-B containing steel, steel 5, after heating to 1250°C.....	197
Fig.9.8 Particle distribution for (a) 0.04%Ti steel 3, heated to 1250°C and cooled to the test temperature of 1050°C and (b) 0.1% Ti, steel 5, tested at 1000°C and (c) typical analysis for the fine particles.....	199
Fig.9.9 AlN films on the grain surface of as-cast high Al TWIP steels having no Ti or B present [167]. (a) intergranular failure (b) AlN precipitation at the austenite grain boundaries (c) AlN film on fracture surface (d) analysis of particles.....	201
Fig.9.10 PTT diagrams for BN and Fe <sub>23</sub> (CB) <sub>6</sub> [175].....	203
Fig.A1 Comparison of hot ductility behavior between tensile specimens tested using Gleeble with tensile specimens tested using induction heating. Tensile specimens were machined from as cast ingots.....	227

## ACKNOWLEDGEMENTS

I would like to express my sincere gratitude to my supervisors Professor Barrie Mintz and Professor Ranjan Banerjee for their constant encouragement and invaluable discussions throughout the course of this research.

The technical staff, Jim Hooker, assistance staff, Dr. Hujiang Su and Dr. W.D.Gunawardana in particular Jim Hooker for his advice on handling the hot ductility facility in the City University London is deeply appreciated.

I also wish to thank the experimental support from my company POSCO is also acknowledged with gratitude.

I am greatly indebted many people in the Technical Research Labs., POSCO. In particular I would like to thank all my colleagues in the Steelmaking Research Group, Dr. Joongkil Park, Dr. Kyunchul Cho, Dr. Minseok Park and Dr. Hojung Shin(formerly researcher at POSCO), for their cooperation and assistance.

The appreciation is extended to Dr. Sanghoon Joo(Director of Gwangyang Technical Research Labs.), Dr. Sungho Park(President of POSCO Technical Research Labs.), Dr. Joo Choi(formerly Gr. Leader), Dr. Changhee Yim(formerly Director of Gwangyang Technical Research Labs.), Dr. Kwanggeun Chin, Dr. Sungkyu Kim and Dr. Jongmin Park(formerly Gr. leader at POSCO), for their warm word of encouragement.

I sincerely thank my mother and the deceased father for their devoted love, encouragement and support until now. Finally, I am grateful to my wife Sunhee, my daughters Seongah and Seongeun for their love, encouragement and understanding throughout my long endeavor

## **DECLARATION**

I grant powers of discretion to the University Librarian to allow this thesis to be copied in whole or in part without further reference to me. This permission covers only single copies made for study purposes, subject to normal conditions of acknowledgment.

## ABSTRACT

TWIP (Twining Induced Plasticity) steel is very promising AHSS (Advanced High Strength Steel) grade owing to its superior toughness and ductility. Recently it has attracted the interest of the automotive and steelmaking industries, as the need for reducing weight to provide better fuel efficiency is of paramount importance with the gradual depletion of fuel resources. A high Al, TWIP steel is being commercially developed as Al has been found very well in delaying fraction in deep drawn products. However these steels are difficult to continuous cast and cracking can occur at the slab surface. Therefore it becomes very important to gain an understanding of the cause of this cracking, in order to prevent their occurrence.

To assess the likelihood of the cracking in these high Al TWIP steel slabs (1~1.5%Al, 0.6%C, 18%Mn), conventional hot tensile tests were performed to simulate the continuous casting process. A variety of TWIP steels were tested in order to determine the influence of such factors as chemical composition, cooling rate and thermal cycle on hot ductility.

Using a cooling rate of 60°C/min after heating to 1250°C, ductility was generally <40% RA (Reduction of Area) indicating that these high Al TWIP steels it will be difficult to cast without transverse cracking occurring. The 1.5%Al containing steels had worse ductility than the low Al containing steels (0.02%Al) because of the presence of large amounts of AlN precipitated at the austenite grain boundaries. Reducing the Al and N level improved ductility.

Higher strength Nb/V high Al containing TWIP steels were also examined although ductility was likely to be worse than the simpler microalloying free TWIP steels as was confirmed. Increasing the cooling rate from 60 to 180°C/min after melting caused the ductility to further deteriorate and high N levels produced only a small reduction in the ductility, probably because ductility is so poor.

Increasing the S level from 0.003 to 0.01% caused the ductility to deteriorate in TWIP steels free of microalloying. Increasing the S level to 0.023% caused no further deterioration in ductility even though the MnS volume fraction increased

The worse ductility in the higher S steels was not caused by a simple increase in the sulphide volume fraction but more a consequence of the change from coarse hexagonal plate AlN, which are mainly within the matrix and so have little influence on the hot ductility, to very long dendritic rod precipitates, which are situated at the dendritic or close to the austenite grain boundaries. This dendritic precipitation was rarely observed in the low S steel. The MnS inclusions appeared to act as nucleation sites for the precipitation of AlN and when there was few inclusions precipitation of AlN was mainly confined to the matrix.

The ductility of Nb containing high Al, TWIP steels was very poor in the as-cast condition. Adding B and Ti still gave rise to extremely poor ductility when a cooling rate of 60 °C/min was used but reducing it to 12°C/min caused the ductility to improve so that RA values were now close to the 35~40% RA value required to avoid transverse cracking.

To improve ductility B and Ti additions were examined. 0.04%Ti and 0.002%B are

required to ensure good hot ductility in high Al, TWIP steels. Sufficient Ti is needed to remove all the N as TiN so preventing AlN precipitating as films over the austenite grain surfaces. B is also needed as it can segregate to the boundaries and strengthen them. A SIMS technique confirmed that B had indeed segregated to the boundaries. The slower cooling rate 10~15°C/min compared to 60°C/min will result in the optimum segregation of B as well as coarsening the TiN precipitates so they are no longer effective in reducing the ductility.

Following all these recommendations, i.e. a low S level, slow secondary cooling rate, a Ti level above the stoichiometric for TiN and a boron addition of 0.002%, transverse cracking was avoided commercially in these very difficult to cast high strength TWIP steels

## LIST OF SYMBOLS

TWIP	Twining Induced Plasticity
Al	Aluminum
RA	Reduction of Area
AlN	Aluminum Nitride
N	Nitrogen
S	Sulphur
Nb	Niobium
V	Vanadium
MnS	Manganese Sulphide
B	Boron
Ti	Titanium
AHSS	Advanced High Strength Steel
DP	Dual Phase
TRIP	Transformation Induced Plasticity
MART	MARTensitic
HPF	Hot Press Forming
X-AHSS	Extra Advanced High Strength Steel
Mn	Manganese
C	Carbon
HCR	Hot Charge Rolling
HDR	Hot Direct Rolling
Nb(C, N)	Niobium Carbo Nitride
NbC	Niobium Carbide
$\alpha$	Ferrite( alpha iron)
$\gamma$	Austenite (gamma iron)
$\delta$	Ferrite (delta iron)
VN	Vanadium Nitride
V <sub>3</sub> C <sub>3</sub>	Vanadium Carbide
BN	Boron Nitride
HDL	High ductility, Low temperature region
HDH	High ductility, High temperature region
Ar <sub>3</sub>	Temperature which the ferrite formation starts on cooling out of equilibrium
Ae <sub>3</sub>	Temperature which the ferrite starts on cooling on equilibrium
DIF	Deformation Induced Ferrite
PFZ	Precipitate free zones

w	Wedge crack
r	Rounded crack
$D_o$	Grain size
Ti(C, N)	Titanium Carbo Nitride
TiN	Titanium Nitride
$T_m$	Melting point temperature ( $^{\circ}\text{C}$ )
$T_{\min}$	Lowest temperature reached during the primary cooling stage ( $^{\circ}\text{C}$ )
$T_{\max}$	Highest temperature at the start of secondary cooling ( $^{\circ}\text{C}$ )
$\Delta T$	Difference between $T_{\max}$ and $T_{\min}$ ( $^{\circ}\text{C}$ )
$T_u$	Temperature at the straightener ( $^{\circ}\text{C}$ )
wt. %	Weight percent (%)
fcc	Face Centered Cubic
bcc	Body centered Cubic
Fe-C	Iron Carbon
$D_{\gamma}$	Grain size
$T_{\gamma}$	Austenite composition temperature ( $^{\circ}\text{C}$ )
HSLA	High Strength Low Alloy
Si	Silicon
SFE	Stacking Fault Energy
MPa	Mega Pascal
EDX	Energy Dispersive X ray
$\mu\text{m}$	Micrometer
nm	Nanometer
EBSA	Electron Backscatter Diffraction
P	Phosphorus
$\dot{\epsilon}$	Strain rate
min	Minute
s	Second
$V_t$	Total Vanadium
$N_t$	Total Nitrogen
PTA	Particle Tracking Autoradiography
TEM	Transmission Electron Microscope
T	Temperature ( $^{\circ}\text{C}$ )
Ref.	Reference
Cu	Copper
Ni	Nickel
Ar	Argon
$D_i$	Initial diameter (mm)

$D_f$	Final diameter (mm)
$A_0$	Cross-sectional area before test
$A_f$	Cross-sectional area after test
OM	Optical Microscopy
SEM	Scanning Electron Microscope
FE-SEM	Field Emission Scanning Electron Microscope
FEG	Field Emission Gun analyzer
FE-TEM	Field Emission Transmission Electron Microscope
SIMS	Secondary Ion Mass Spectrometry
EPMA	Electron probe micro analyser
AES	Auger electron spectroscopy
HSLA	High Strength Low Alloy
Nb/V	Niobium and Vanadium

## CHAPTER 1: INTRODUCTION

### 1.1 Background of research

Recent trends in automotive industry towards improved passenger safety and reduced weight have led to a great interest in AHSS (Advanced High Strength Steel).

Several new kinds of AHSS which exhibit high strength and superior formability are being developed for automotive industry to achieve improved passenger safety and reduced weight.

So far the lightweight steel materials for cars to attain high strength are DP (Dual Phase), TRIP (Transformation Induced Plasticity), MART (MARTensitic) and HPF (Hot Press Forming) type steels these being the so-called first generation AHSS.

However, as the strength of steel material increases, the elongation decreases as shown in Fig.1.1 [5]. Therefore application of AHSS has been limited, because as shown in Fig.1.1, the martensitic steels and HPF really have very poor elongations.

TWIP (Twinning Induced Plasticity) steel developed since the early 1990s constitute the next generation (X-AHSS) material for the car industry because both elongation and strength exhibit excellent values, Fig.1.1.

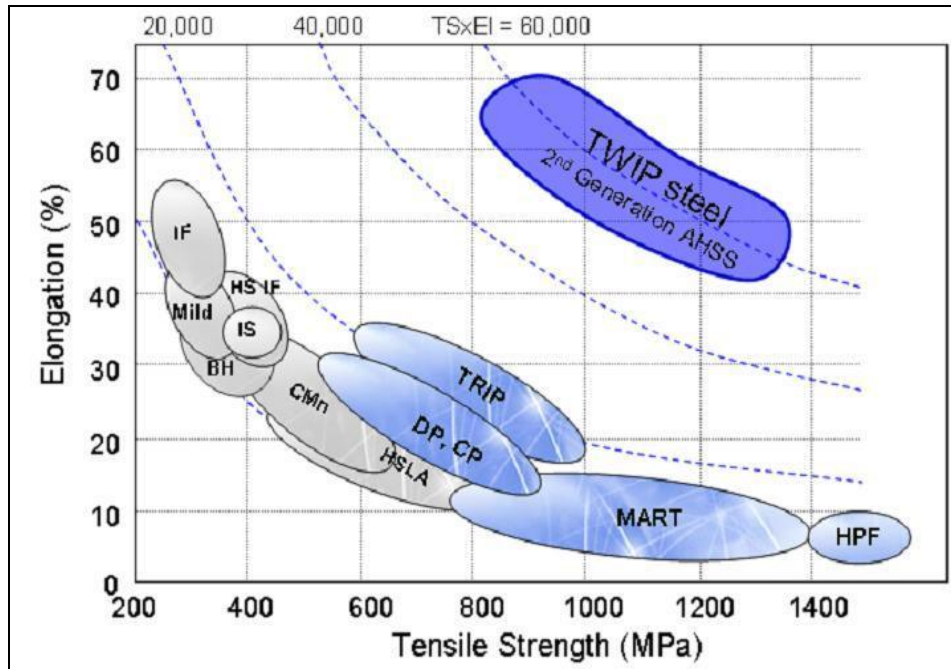


Fig.1.1 Relationship of tensile strength and elongation for automotive steel sheets [5].

High Mn TWIP steel is a very promising AHSS grade owing to its superior toughness and ductility. Extensive studies into the mechanical properties of High Mn TWIP steel of various compositions have been carried out by various research groups and are given in references [1-5].

TWIP steel is a new material for automotive use, which is hardened mainly by twinning in addition to dislocation hardening, and its fully austenitic microstructure is stable at room temperature. As well as the high Mn (15~21%) and high C level required to keep the steel fully austenitic varying amounts of aluminum or silicon are added resulting in an excellent combination of strength and elongation. Recently it has attracted the interest of the automotive and steelmaking industries, as the need for reducing weight to provide better fuel efficiency is of paramount importance with the gradual depletion of fuel resources. Higher energy absorption for improved crash worthiness is also becoming more important as safety requirements become more stringent.

TWIP steel is fully austenitic and has a high-carbon and high-manganese content. Its strength and elongation is excellent due to a high work-hardening rate which occurs under deformation due to the high rate of twin formation, the twin boundaries behaving much in the same way as grain boundaries making it difficult for yielding to be transferred throughout the microstructure.

Fig.1.2 left hand side of figure is the tensile curve of TWIP steel with a tensile strength of 980MPa. Its elongation is about 65% and this level is extraordinary high compared with other automotive steels such as DP and TRIP.

The picture on the right shows how the deformation twins multiply with increase in strain, see Fig.1.2.

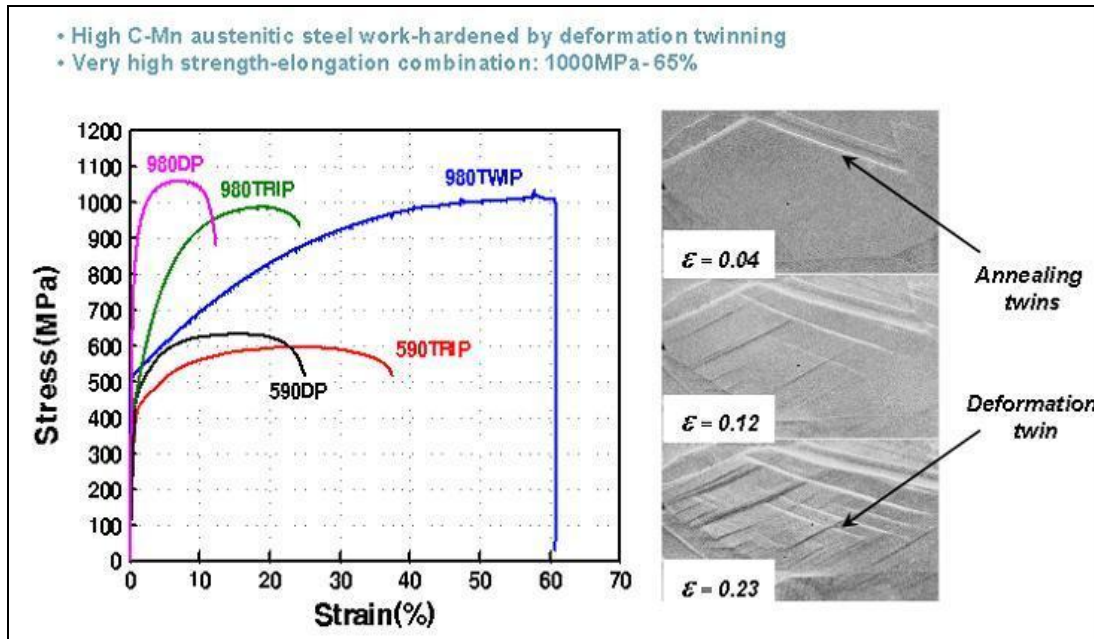


Fig.1.2 Comparison of strength-strain curves between TWIP and other automotive steels and how twin density increases with strain.

## 1.2 Aim of the thesis

In 1994 POSCO first developed an Al-containing high Mn cold rolled steel sheet for automotive parts [1, 2]. The steel was trial stamped successfully to a few auto parts including floor front extension, rear package tray, rear window opening inner and lower cowl. However, because processing conditions such as continuous casting, hot rolling, strip welding before cold rolling, etc. had not been optimized; commercial production was not attempted at that time. Recently POSCO succeeded in the mill production of TWIP steel with reduced Mn content. An innovative continuous casting process using molten mould flux was applied to solve the problem of poor slab surface quality of this highly alloyed material.

The aim of the present thesis is to develop further advanced TWIP steels via the continuous casting process. Because of the importance of slab quality to the continuous casting process and to the properties of the final product, the study of slab quality on the TWIP steels becomes an essential part for the success of their commercial production and application.

These steels are difficult to continuous cast and cracking can occur at the slab surface.

Therefore it becomes very important to gain an understanding of the cause of this cracking, in order to prevent their occurrence. To gain a better understanding of the cracking propensity in TWIP steel slabs, hot tensile tests were performed using the thermal cycle and strain designed to simulate the continuous casting process. These studies have related low ductility failures in the tensile tests to the occurrence of cracking in continuous cast slabs. Hot tensile tests were performed on a variety of TWIP steels, in order to determine the influence of such factors as phase transformation, grain size and precipitation on hot ductility. The influence of chemical composition on hot ductility of plain and micro-alloyed steels has been extensively studied, but there appear to be a few reports in the literature on TWIP steels, relating composition to hot ductility and to slab cracking. Therefore it has been decided to investigate the influence of chemical composition, Al, N, Nb, V, S, B and Ti, on the hot ductility of TWIP steels.

### **1.3 Scope of the work**

In chapter 2, there is a literature review on the areas relevant to the continuous casting of steel, for example, defects present in continuously cast products, mechanisms and formation of cracks, factors influencing the hot ductility and prevention of transverse cracking. The influence of composition on the hot ductility of steels is also reviewed.

The experimental procedure used in the work is described in chapter 3, and results follow in chapter 4~9. Chapter 4 describes the influence of Al and N on the hot ductility of TWIP steels. Chapter 5 details the effect on hot ductility of Nb/V containing high Al, TWIP steels and Chapter 6 explores the influence of S on the hot ductility of high Al, TWIP steels. Chapter 7~9 gives the fulfillment of the objectives of the work in producing a TWIP steel free of cracks using composition which have B and Ti present in these high Al, TWIP steels

Finally, conclusions and future work are given in chapter 10.

## CHAPTER 2: LITERATURE REVIEW

### 2.1 Surface defects of continuously cast products

Many of the surface defects arising in continuous casting result from insufficient control of the casting operation and inadequate machine maintenance. This is particularly the case for casting operations during transient periods as at the start and end of casting, ladle and submerged entry nozzle changes. In these periods, fluctuations in the meniscus level of the melt, turbulence in the melt flow from the submerged entry nozzle, and a decrease in the temperature of the melt and flux take place in the mould. All of these events result in the formation of an irregular solidification shell that allows many types of surface defects to form. Measures to prevent these events have been in place for some time but are still incomplete.

Regarding machine maintenance, wear of the mould plating and mould itself, misalignment of the pass line, an uneven gap and defects on supporting roles and clogged spray nozzle tips for secondary cooling can all produce various surface cracks. Thus, transient operation and machine maintenance must be under good control prior to optimizing steady-state casting conditions to produce strands free from surface defects.

During the steady state casting, the occurrence of surface defects is largely influenced by steel grade, machine design, and casting operation. In the early development of continuous casting, these three factors were entangled due to the underdeveloped state of engineering and technology. Accordingly, it was difficult to clarify the real cause and work out effective countermeasures. After more than 40 years of experience, however, our understanding as well as the hardware and software for continuous casting has advanced to near maturity, enabling us to identify the possible cause and elaborate upon countermeasures.

On the other hand, end-user requirements regarding surface quality of steel products have become more stringent, making tolerable casting defects smaller as years pass. This trend is further enhanced by the increasing implementation in conventional continuous casters of HCR (Hot Charge Rolling) and HDR (Hot Direct Rolling), where scaling-off of minor and shallow surface defects does not occur. In an extreme case, surface cracks of 1mm depth and 10mm length on the strands have caused problems in downstream processing. The tolerance becomes even less for thin-slab casters, as the reduction ratio from the strand to the final product is smaller, the surface/volume ratio of the strands is greater, and off-line conditioning is virtually impossible. An extreme case is that of direct strip casting, for

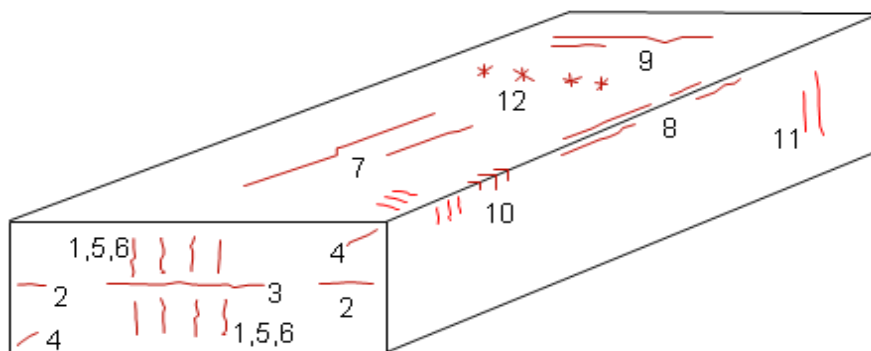
which no amount of surface conditioning is acceptable.

In addition, competition in international steel markets has increased considerably, driving steel mills to increase the productivity of continuous casting machines in order to match the output of the basic oxygen furnace and hot rolling mill with a reduced number of strands. Thus, the casting speed of conventional continuous casting machines will keep increasing. This principle also applies to thin-slab casters, as the productivity of electric arc furnaces will further increase. With an increase in casting speed, surface defects usually increase because the meniscus of steel melt in the mould tends to become more turbulent.

In the light of quality and productivity constraints, therefore, trying to minimize the size and number of surface defects has been and will continue to be like trying to hit a moving target. In fact, the causes and countermeasures for surface defects have changed to some extent due to the changes in machine structure and operation.

There have been many reviews on the type and position of surface cracks on continuous cast slabs, Brimacombe and Sorimachi [6], the Iron and Steel Institute of Japan (ISIJ) [7], McPherson and McLean [8] and Wolf [9].

In Fig.2.1, the defects found in continuously cast products are schematically illustrated, based on a classification system devised by Brimacombe and Sorimachi [6].



#### Internal Cracks

1. Midway
2. Triple-point
3. Centerline
4. Diagonal
5. Straightening/ Bending
6. Pinch Roll

#### Surface Cracks

7. Longitudinal, mid-face
8. Longitudinal, corner
9. Transverse, mid-face
10. Transverse, corner
11. Transverse, narrow face
12. Star

Fig.2.1 Schematic drawing of strand cast section showing different types of cracks [6].

## 2.2 Transverse cracking

A common problem of continuous casting is that the cast strands are produced with cracks along the surfaces and are more extreme at the edges. Studies have shown that a typical crack can have a width of 0.2mm and depths of 1~15mm whilst at the edge can be as much as 50mm in depth [6]. Cracks have been proven to originate from the surface ripples produced by the oscillating mould [10]. As the strand exits out of the mould and feeds along the rollers where it is water cooled and bent, the fracture strength threshold of the strand can be exceeded by frictional stresses, thermal stresses, bending stresses and ferrostatic pressures.

The general features of transverse surface cracks are illustrated in Fig.2.1. Examples of transverse cracks in slabs are shown in Fig.2.2. Transverse cracks may be formed on the broad face, narrow face, or corner of continuously cast slab, but are not always apparent to visual inspection unless the slab surface is dressed. They are usually associated with the depression of oscillation marks, and are predominantly found on the top slab surface. The cracks themselves can be several centimeters in length in extreme cases, and generally follow austenite grain boundaries. The cracks are partially oxidized, but there is little decarburization, and little oxidation of the inner end of the crack [11].

The cracks originate at the bottom of deep oscillation marks, as reported by Harada et al. [12]. In the thickness direction, they develop to a shallow depth, form a kink and further propagate along austenite grain boundaries to a depth of 2~5mm. They run transverse to the withdrawal direction either on the faces or on the corners of strands to a length of 10~100mm along the oscillation marks as shown in Fig.2.2. Subscale is usually formed along the cracks from the surface to the kink.

As many of these cracks result in edge cracks on hot rolling, conditioning after rolling is mandatory. In an extreme case, various forms of metal leakage and bleeding can take place, mostly from the bottom of the oscillation marks with cracks growing more at the corner than at the face of the strands. Excessive bleeding results in breakouts.

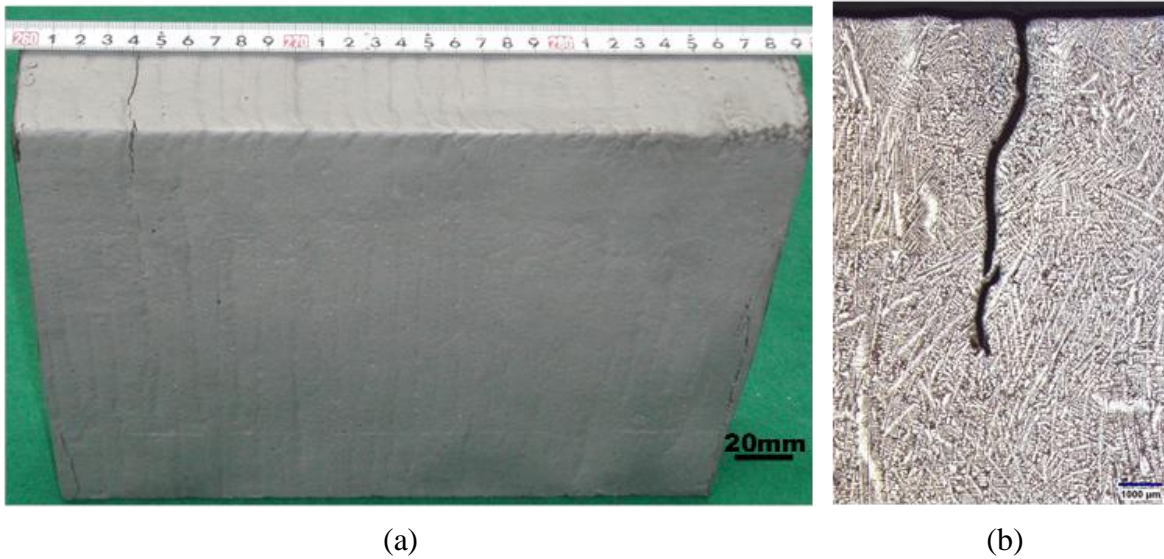


Fig.2.2 Typical transverse corner crack (a) and cross-section of transverse corner crack (b)

Among many types of defect encountered in continuously cast products, only transverse surface cracks are strongly influenced by the presence of microalloying elements. The presence of Nb greatly promotes the formation of transverse cracks [12~14], but V at low N levels has no effect, although combinations of 0.15% V and 0.02% N have been reported to lead to transverse cracking [15, 16].

### 2.2.1 Mechanism for formation of transverse cracks

Transverse cracking occurs when the strand surface is subjected to thermal, mechanical or transformation stress and strains, which are greater than the inherent material strength at the temperature of the strand surface.

Stresses can arise from a large number of different causes during continuous casting, and the subject has been reviewed by Lankford [17]. Stresses may arise due to transformation effects, thermal effects (variable heat transfer within the mould, temperature gradients within slabs, effects of cooling water sprays, contact with rollers, etc.), friction between strand and mould, bulging of the strand caused by ferrostatic pressure, mechanical effects due to misalignment of the casting machine, and straightening strains.

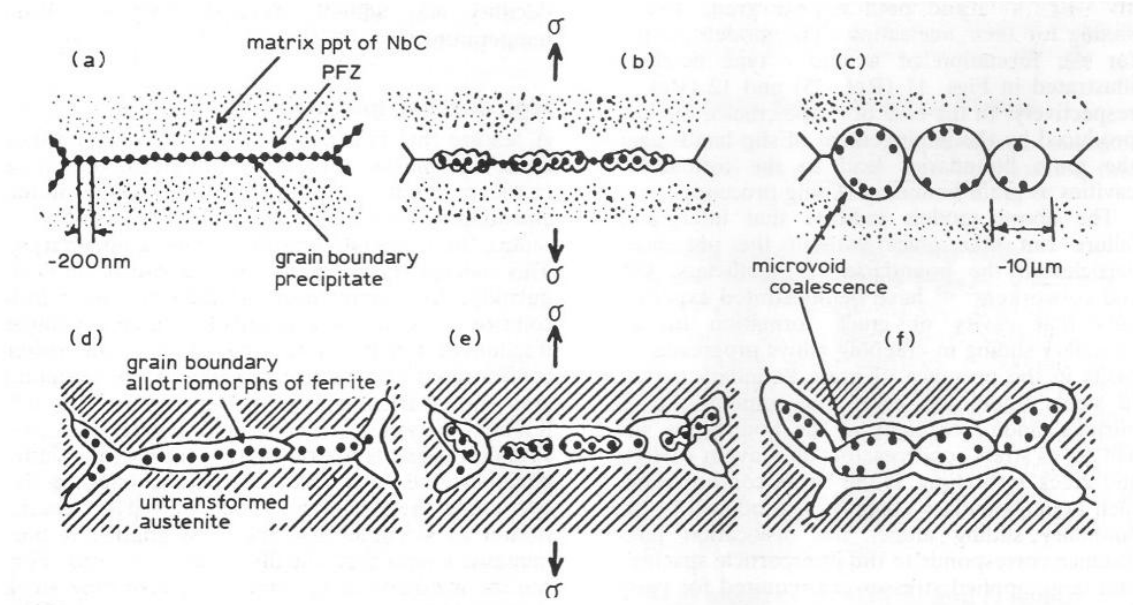
It has been suggested that the earliest stages of transverse crack formation occur in the mould, and are associated with segregation in the vicinity of oscillation marks. The low

melting point of these regions, coupled with higher temperatures due to reduced heat transfer to the mould, lead to hot tearing. Further evidence of the importance of events in the mould to transverse cracking is suggested by the strong effect of carbon on transverse cracking. When the C content is such that some peritectic solidification can occur, transverse cracking increases, and it has been suggested that this is due to transformation strains during solidification. There have been reports suggesting that Nb additions refine the as-cast grain size, which should help to reduce transverse cracking, but these beneficial effects must be overshadowed by the detrimental effect of Nb on hot ductility by the dynamic precipitation of Nb(C, N) on bending [18].

Although the early stages of transverse crack formation may be in the mould, there is evidence to suggest that these defects become larger and more numerous under the application of stresses from various sources below the mould, particularly those encountered during slab straightening [13]. When these stresses occur in the temperature range over which ductility is poor, transverse cracking is severe, and as hot ductility is strongly influenced by microalloys, this is the proposed mechanism by which microalloying elements affect transverse cracking. As well as having a role in the nucleation of transverse cracks, oscillation marks would also tend to favour the propagation of cracks, in that grain size may often be coarse beneath the oscillation mark, and the notch like geometry will also tend to concentrate stresses.

The presence of microalloy precipitates can also reduce the strain to fracture by a number of possible mechanisms: precipitate free zones are often observed adjacent to austenite grain boundaries, and this may lead to strain concentration at the grain boundary; the particles (or groups of particles) at the grain boundaries may act as crack initiation sites; or general matrix precipitation can lead to an increase in strength, and an overall reduction in ductility [19-21]. The proposed mechanism for low ductility failures in the presence of Nb and V carbonitrides is illustrated in Fig.2.3(a)~(c) in this case it being precipitate free zones which allow strain concentration [19].

In the case of plain C-Mn steels, similarly, small voids from around grain boundary particles in plain C-Mn steels, these being MnS and AlN particles coalesce during the progress of deformation and grow into cracks. In Nb containing steels, grain decohesion is further enhanced by very fine NbC particles precipitated within the grains which increase matrix strength and lead to deformation concentration at the grain boundaries, with crack formation occurring above  $Ae_3$  temperature.



a, d dynamic precipitation and strain concentration within soft layers along  $\gamma$  grain boundaries in initial stage of deformation; b, e microvoid formation by decohesion of precipitation/matrix interfaces; c, f coalescence of microvoids, resulting in ductile intergranular fracture austenite.

Fig.2.3 Intergranular microvoid coalescence of low alloy steels by deformation in (a)~(c) low temperature  $\gamma$  region and (d)~(f)  $\alpha/\gamma$  duplex phase region [19].

Fracture surfaces are characterised by intergranular failures, and the facets of the individual grains are often associated with void formation around second phase particles. It is believed that this region of low ductility in the two phase  $\gamma/\alpha$  region in both plain C-Mn steels and microalloyed steels are associated with the austenite to ferrite transformation. On cooling below the transformation temperature, ferrite formation commences at austenite grain boundaries, leading to the formation of films of ferrite around the austenite grains. At temperatures within the transformation range, ferrite is softer than austenite and so when deformation commences, strain is concentrated within the ferrite at grain boundaries, and the processes of ductile failure, i.e. void nucleation at second phase particles, and the growth of these voids, continues within the ferrite film [14, 22, 23]. Thus on a microscopic scale, fracture can be described as ductile, but overall the failure is brittle, ductility as measured by RA (Reduction of Area) being as low as 5%. The mechanism for this type of fracture is illustrated in Fig. 2.3(d) ~ (f).

## 2.2.2 Factors influencing formation of transverse cracking

The occurrence of the cracks is influenced by the strength/ductility of the shell surface and the stress/strain imposed on the shell. The former depends on steel chemistry and the temperature of the shell, whereas the latter depends on thermal and mechanical origins.

The peritectic steels give rise to strain due to the contraction upon peritectic transformation and become brittle due to coarse austenite grain formation. In steels containing [C], [N], [Al], [Nb] and [V] fine precipitates formed in the secondary cooling zone at the grain boundaries of the shell surface. These precipitates make the strand surface brittle at 700~900°C, where unbending is usually practiced. The brittleness in this temperature range has been confirmed to be due to hardening by the precipitation of fine Nb(C, N), VN and/or V<sub>4</sub>C<sub>3</sub> and/or precipitation of a ferrite film along the austenite grain boundaries during the austenite to ferrite transformation, as shown in detail by Thomas et al. [24] in Fig.2.4. AlN although not hardening the steel concentrates preferentially at the boundaries, weakening them and is particularly deleterious.

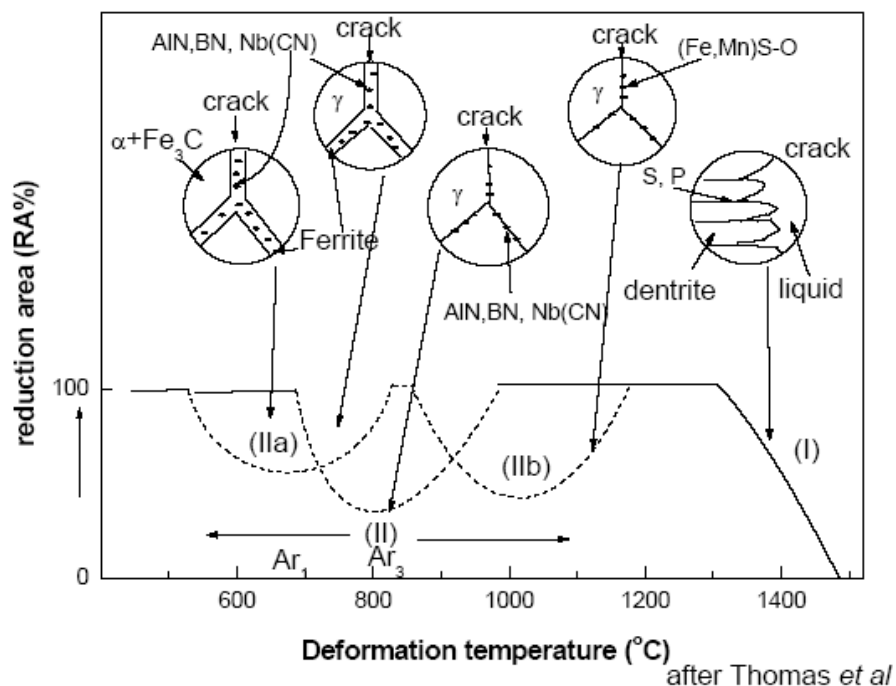


Fig.2.4 Low ductility (brittle) temperature ranges [24].

Thermal stresses and surface structure can be influenced by heat transfer in the mould. It is important to consider the type of mould powder used, particularly viscosity, and ensure good and uniform fluxing.

The crack formation is enhanced by non-uniform formation of the initial shell that is caused by an uneven inflow of mould flux melt into the mould/shell gap when the sub-meniscus flow is turbulent, the meniscus level fluctuates, the meniscus temperature is low and/or the viscosity of the flux melt is too high. When the flow of flux melt into the mould/shell boundary decreases particularly at high casting speeds, the friction at the boundary increases locally with viscous flux melts and the frictional force causes the transverse cracks to form at the bottom of the oscillation marks while still in the mould.

Deep oscillation marks effectively increase the occurrence of the transverse cracks by decreasing the critical strain above which the cracks can form on the strand surface. Suzuki et al. [25] have shown that the oscillation marks act as a notch to considerably decrease the high-temperature ductility of the cast strand. The solid curve in Fig.2.5 indicates thus determined critical strain as a function of the depth of oscillation marks. The critical strain decreased to about 8%.

The importance of oscillation marks to transverse crack formation has already been mentioned, and the depth of these oscillation marks can be reduced by increasing the mould oscillation frequency and/or decreasing the stroke to reduce the heel time. Increasing the oscillation frequency has been shown to reduce the incidence of transverse cracking. Deep, irregular oscillation marks may also be formed due to poor mould level control and other factors.

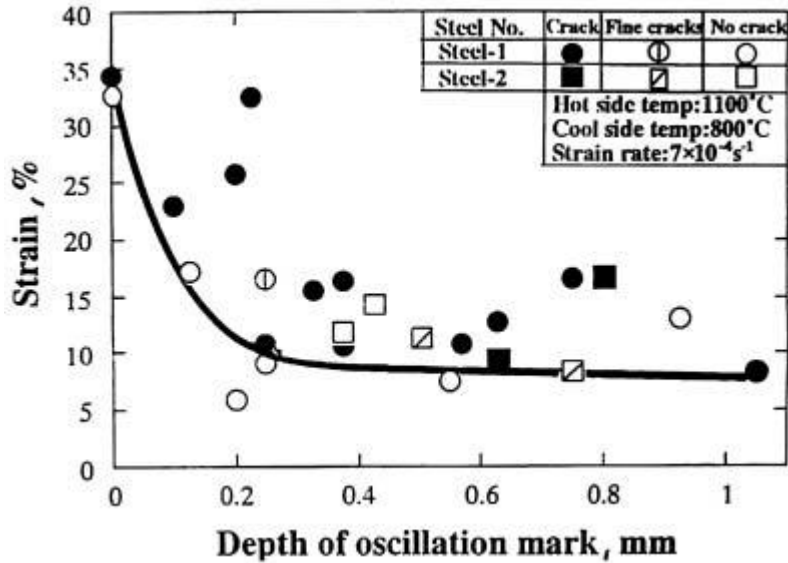


Fig.2.5 Effect of oscillation mark depth on ductility [25].

The secondary cooling strategy is very important in minimizing transverse cracking. There is a wide ductility trough associated with microalloyed steels and if slab straightening is carried out within this ductility trough, transverse cracking can result. If slab straightening is carried out at temperatures either above or below this temperature range, cracking should be minimised. Both these different cooling strategies ("soft" cooling and "hard" cooling) have been used on various machines around the world [15].

It should be noted that the use of these cooling strategies requires knowledge of the temperature range over which low ductility exists, and this temperature range may not necessarily correspond to those obtained in a hot tensile test. Non-uniform secondary cooling can promote thermal stresses, and hence lead to cracking. This requires good nozzle design and maintenance, and preferably the use of air-mist cooling [26].

Intensive water-spray cooling, results in nonuniform and excessive cooling of the strand surface. The surface undergoes over cooling below the  $A_{r3}$  in the water pool above the support roll/strand contacts in the top zone of the strand, and subsequent reheating above  $A_{r3}$  after passing the support rolls. The fine precipitates of  $AlN$  do not form until 800°C (770~850°C) on cooling, but they do precipitate at 700~1000°C on heating. Accordingly, the above thermal cycles, repeated cooling and reheating across the critical temperature between the rolls in the secondary cooling zone can promote fine precipitation, making the grain boundaries even more brittle.

Mechanical stresses can be introduced by poor alignment of the components of the machine, and from many other sources, but of most relevance to transverse cracking is the straightening operation. Straightening may be carried out over a single point, or by multi-point straightening. The effect of these two types of straightening operation on transverse cracking are not clear, but there are reasons to suppose that multi-point bending will not improve hot ductility as the strain rate will be reduced, which will reduce hot ductility and more time will be allowed for dynamic precipitation. Furthermore, at least for Nb containing steels, stress relaxation between each bending point seems to be minimal [27].

Tensile strain arising from unbending above the brittle temperature zone enhances the propagation of the cracks. Thus, the upper surface of the strand shows more cracks in curved continuous casting machines. Thicker slabs also form more cracks. Additional strains caused by insufficient lubrication in the mould; misalignment; seized, bent and/or worn support rolls; and bulging of the strand all contribute, to a different degree, to the occurrence and propagation of cracks in more than just the upper surface.

### **2.2.3 Prevention of transverse cracking.**

From the previous sections, it is apparent that if stresses and strains are introduced during the continuous casting process over certain critical temperature ranges for which ductility is low, transverse surface cracks can occur in continuously cast products. There are many steps which can be taken to minimize the likelihood that these cracks will form, but it may not be possible to completely eliminate them, in which case some form of slab repair operation is required. The following sections discuss methods to minimize cracking, and the implications of slab repair prior to final rolling.

In continuous casting transverse cracking is the most commonly experienced serious form of cracking found on slabs, blooms and billets. The mechanism of their formation together with measures to prevent them, have been the subject of much research and much progress has been made into understanding the problem and preventing it from occurring. However, the increased popularity of high rate production of microalloyed steels and hot direct rolling has made implementation of the measures not always satisfactory. Complete prevention of transverse cracks remains a moving target.

It is evident from the above discussion that composition, and particularly the use of microalloying elements, can strongly influence transverse cracking by their influence on

hot ductility. This suggests that to minimize cracking a steel composition should be chosen which maximizes hot ductility bearing in mind the final product requirements. The following guidelines should help to maximize hot ductility and minimize transverse cracking: 1) Choose C and alloy additions to avoid peritectic solidification, and particularly avoid 0.1~0.14%C range. 2) Reduce the [Nb], [Al] and [N] so as not to exceed the solubility product while keeping within the specification. 3) Consider the use of Ti additions.

In order to reduce transverse cracks it is necessary to optimize mould flux viscosity and mould oscillations to result in an oscillation mark depth  $<0.2\text{mm}$ .

In case of poor lubrication or/and other irregularities in meniscus shell formation (e.g. abrupt mould level change or overcritical level turbulence), the initial shell may tear and stick to the mould wall. Shell tearing is aggravated by high relative velocity between strand and mould (“drag”) due to a high oscillation frequency. Accordingly, a frequency reduction at short negative strip time (“healing time”) is found effective in reducing sticking (and “bleeding”) of high carbon steel billets [28].

In the case of mould powder application, sticking tendency is to be respected by the selection of adequate slag properties, i.e. a low basicity slag with glassy solidification which assures high lubricity. Sticking can also occur for steel types without intrinsic sticking tendency in cases where the meniscus shell is infected by local carbon pickup from the powder as shown in the investigation of breakout shells of low carbon steel [29]. This clearly points to the detrimental effect of irregular mould operation i.e. inadequate liquid slag layer thickness which permits a direct contact between liquid steel and the carbon rich slag rim [30]. Since the rate of carbon burning during powder melting is limited, mould powders should not contain more than a free carbon content of 1.5~5.0 %.

The effect of carbon content is primarily connected with deep oscillation marks formed around 0.1%C content. The depth of oscillation marks can be reduced by decreasing the negative strip time, which is achieved by increased oscillation frequency and/or reduced oscillation stroke [31, 32]. The incidence of surface defects strongly increases at low casting speed attributable to the common direct synchronization of speed with oscillation frequency i.e. low frequency (and high negative strip time) at low speed. Such deficiency can only be overcome by the innovative “inverse synchronization” which increases oscillation frequency with speed reduction.

There are two ideas for overcoming transverse cracking and they involve varying the cooling rates of the strand during straightening, to take the temperature above or below the low ductility trough. These are obtained by adjusting the cooling pattern and casting speed

to match.

Under a 'soft' cooling pattern, the amount of cooling water is reduced and in consequence the temperature during straightening is raised. Small increases of temperature would lead to the coarsening of precipitates and the prevention of grain boundary pinning and sliding [33]. However, this cooling pattern can present difficulties [34]. Firstly, at higher temperatures, preventing transverse cracking by avoiding the trough is much more composition dependent than at lower temperatures. Secondly, correct casting speeds are crucial at these higher temperatures, as too fast could produce incomplete solidification of the strand as it is straightened, and too slow would mean the strand temperature falls back into the trough.

Under a 'hard' cooling pattern, the amount of cooling water is increased and the temperature during the straightening falls below that of the trough. The elimination of coarse austenite grains is identified as the reason for transverse cracking prevention and hence fast cooling should refine the grain size [35]. However, this regime also has its associated problems. Firstly cooling the outer shell to the desired temperature could mean the core is still molten. Not only could this risk breakout, but more fundamentally, the core temperature could still be high enough to fall into the low ductility trough and cause subsurface cracking. Secondly, careful control of the cooling sprayers is required. Uneven distribution of cooling would lead to discrepancies of surface temperatures across the strand. This induces extra thermal stresses that aid transverse cracking. Reducing the amount of thermal cyclic oscillations by ensuring uniform cooling has also been found to reduce precipitation such as Nb(C, N) and AlN at the austenite grain boundaries and improve ductility [36].

If slab cracking cannot be avoided by any of the above methods, the only options to avoid losses in the final product are to repair the continuously cast product prior to rolling. In the most extreme case, slab repair could involve machine scarfing of top and bottom broad faces, removing several mm from each face, together with scarfing of the narrow faces or rolling wide and trimming off the edges containing the cracks. After machine scarfing, it may be necessary to inspect the slabs, and remove any remaining defects by hand scarfing.

### **2.3 Hot ductility of steels**

Over the past forty years, the difficulty in casting some steels has led to great efforts in understanding the science behind the cracking processes. Although there are still many instances of transverse cracking occurring in continuously cast steel, the problem for the continuous casting operation has to a large degree been reduced through the extensive research programmes which have been devoted to the subject in the last 40 years [17,

19~24, 37]. The continuous casting process can to some degree be simulated using a simple laboratory hot tensile test. Investigating the hot ductility of the steel under these laboratory conditions does give great insight into the viability of producing continuous cast steel free from transverse cracking. It has been quantified that under standardized testing conditions after straining a steel sample to failure, a ductility displayed as a RA (Reduction of Area) value of greater than 40 % will allow for successful casting in industry [38].

In the simple hot ductility test, conditions are kept as close as possible to those pertaining to the commercial continuous casting operation. The tensile specimen is heated to a high temperature to dissolve all the microalloying elements or for an even better simulation melted. It is then cooled at the average cooling rate that the strand undergoes to test temperatures in the range 1000 to 700°C; this being the temperature range in which poor ductility occurs in a tensile test and is the same temperature range in which cracking occurs when the strand is unbent at the straightener. This is followed by straining the tensile specimen to failure at the same strain rate used in the bending operation and the RA is taken as a measure of the hot ductility.

Although the simple hot ductility test is a good simulator of the continuous casting operation there are nevertheless important differences; one of the most important being that in continuous casting, cooling conditions are quite complex and very different from those used in the simple test. The temperature on cooling from the melting point is observed to fall rapidly, reach a minimum and then increase again and this is followed by the temperature cycling; the temperature first rising as the strand goes into the guide rolls and then falling as it exits and the water sprays impinge on the surface. A typical temperature profile is shown in Fig.2.6.

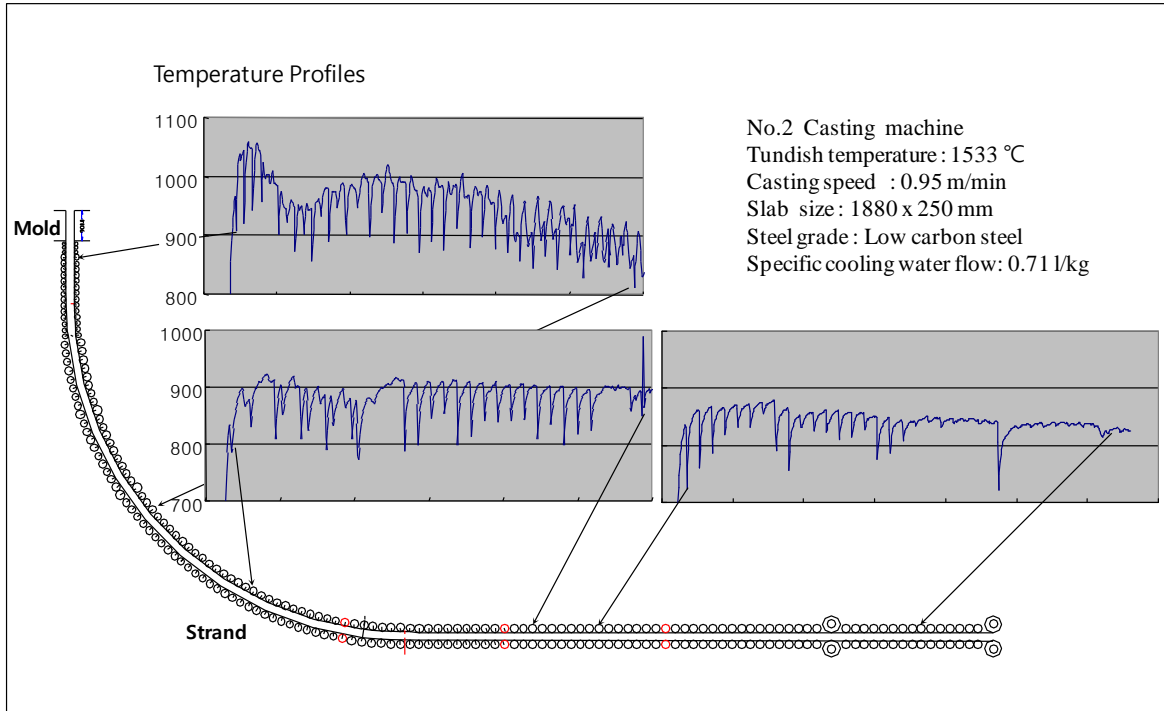


Fig.2.6 A typical temperature profile measured at various positions in the slab for 1880mm × 250mm strand.

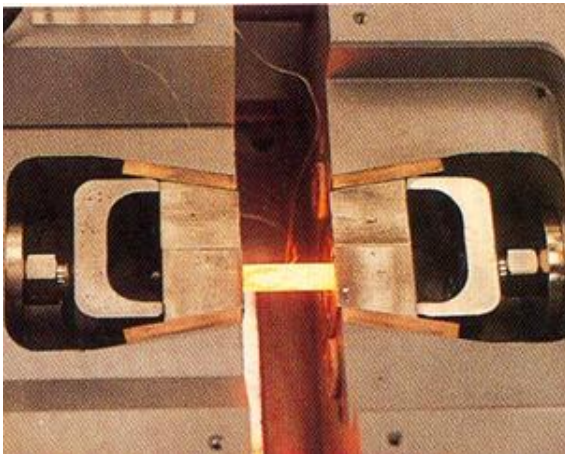
### 2.3.1 Hot ductility test

In the hot ductility laboratory test, the tensile sample is heated to a sufficiently high temperature to take all the microalloying additions back into solution and produce a coarse austenite grain size reminiscent of that found after casting. Generally, it is sufficient to heat the tensile specimen to 1350°C but when Ti is present or high Al and N levels, the specimen has to be taken to the melting point to ensure all the microalloying additions are in solution. After cooling to test temperatures in the range 700-1000°C, the tensile sample is strained at a similar strain rate to that used in the unbending operation ( $10^{-2}$  to  $10^{-3}$  s $^{-1}$ ) and the cooling rate to the test temperature is chosen as the average cooling rate close to the surface of the strand during cooling

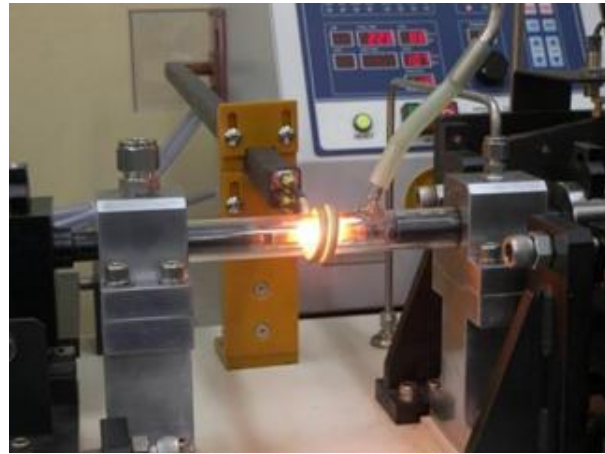
The laboratory test which best simulates the unbending operation during continuous casting has been found to be the hot bend test. However, it is difficult to quantify the severity of surface cracking from such tests, and for this reason it has only been used rarely [17]. An alternative testing method has been developed in which a hot compression test is carried out on a flanged sample, the hoop strain corresponding to the first appearance of a

crack being taken as a measure of hot ductility [39]. Torsion testing has also been used [40], but the large strains associated with this method and difficulties in interpreting the fracture appearance after failure make it unsuitable.

Of all the laboratory tests, the one that has proved the most popular for the study of transverse cracking is the simple hot tensile test. Generally, tests are carried out using a servo hydraulic load frame equipped with either a furnace or an induction heater, in a protective atmosphere. The Gleeble machine has also proved to be popular for the investigation of hot ductility because of its ability to melt samples and versatility in simulating thermal cycles. In this case, heating is by electrical resistance, which has the advantage that there is no practical limit to the possible rate of heating, and temperature gradients can be kept to minimum. Heating methods used on the tensile machine are shown in Fig.2.7 (a) for when the Gleeble machine is used and (b) for induction heating.



(a) heating by electrical resistance



(b) heating by induction heater

Fig.2.7 Heating method of tensile testing machine.

Samples are usually heated to a temperature above the solution temperature of the microalloying precipitates, both to dissolve all these particles and to produce a coarse grain size reminiscent of the continuously cast microstructure before the unbending operation. The sample is cooled at the rate experienced by the surface of the strand during the continuous casting operation, these being based on the average cooling rate close to the surface of the strand from the melting point to the test temperatures (this being often taken as  $60^{\circ}\text{C}/\text{min}$  for 220mm thick slab [17, 21]. More sophisticated simulations of the continuous casting operation involve actually melting the samples, either by induction or

electrical resistance, in a quartz tube placed over the mid span region to retain the liquid. This can be combined with the complex cooling patterns that are experienced in the secondary cooling zone before straightening, although unfortunately this has rarely been used. Some of the more recent work [41] has included both primary and secondary cooling to better simulate the commercial process rather than have one average cooling rate.

Some investigators [42, 43] have used total elongation to fracture as a measure of the ductility rather than RA and it can certainly provide useful information regarding the role played by dynamic recrystallisation in influencing the ductility but not transverse cracking where the strains are too low for dynamic recrystallisation to occur [42]. The majority of researchers have used the RA at fracture to provide quantitative information on the fracture strain. This measurement has the advantage that it is independent of fracture geometry of sample.

As well as the hot ductility curve being very useful for predicting the likelihood of transverse cracking occurring with new steel compositions, the information from the curve can also be used to operate the continuous casting plant so that by adjustment of the cooling conditions and/or composition as well as the temperature range, the poor ductility that occurs on straightening can be avoided.

Generally, commercially useful results have been obtained by considerably simplifying this cooling pattern. After solution treatment, the specimen is cooled at the average cooling rate undergone by the strand as it cools from the mould to the straightening temperature, this being taken as 60~100 °C/min [14] for conventional casting (220 to 250mm thick slab) and 200~300 °C/min for thin slab casting (60~80mm thick slab), the cooling rate being calculated for the mid-width position at a 1/10 thickness below the surface of the slab.

Cooling rates at the corners are always going to be faster and cooling rates for billet casting will be higher than for slab casting. Furthermore, the cooling rate below the mould, primary cooling is an order of magnitude faster than the secondary cooling as shown in Fig.2.8.

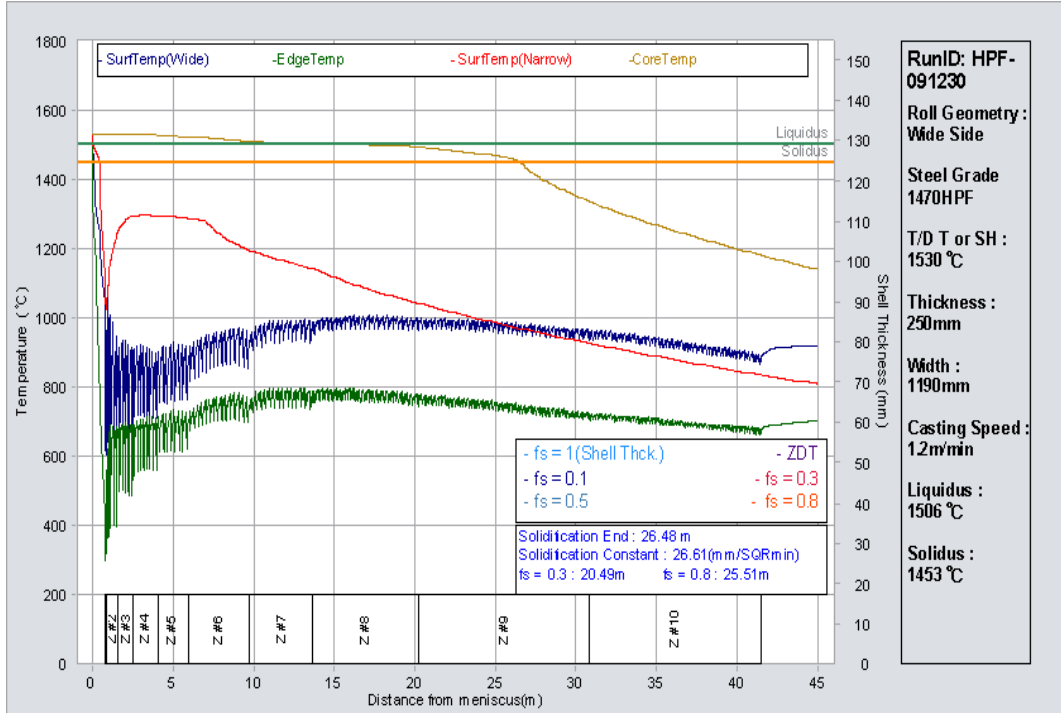


Fig.2.8 A typical commercial cooling cycle calculated at various positions in the slab.

After cooling, the tensile specimens are held at a temperature in the temperature range at which the unbending operation is carried out in the continuous casting process, 1000 to 700°C and then strained to failure at  $3 \times 10^{-3} \text{s}^{-1}$  or  $1.5 \times 10^{-2} \text{s}^{-1}$ , this being the strain rate during bending for thick and thin slab casting, respectively, i.e. the strain rate for thin slab casting is  $\sim 5$  times greater. The RA value is taken as the measure of the hot ductility and is then plotted against the test temperature.

### 2.3.2 Hot ductility region

The key to the prevention of transverse cracking of micro-alloying steels is the understanding of the hot ductility curve in which the RA values are plotted against the test temperature; the test temperature range being chosen to correspond to when the cracking occurs during the straightening operation. A typical hot ductility curve that is generally obtained for plain C-Mn steels is shown in Fig.2.9 [20]. It consists of three distinct regions: 1) the trough or region of embrittlement, 2) a high ductility, low temperature (HDL) region, 3) a high ductility, high temperature (HDH) region.

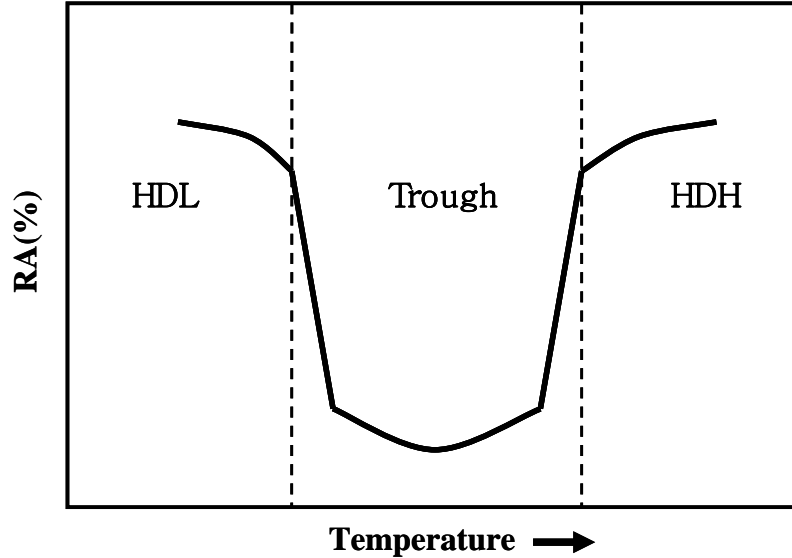


Fig.2.9 Schematic diagram of ductility curve defining the three characteristic regions of hot ductility [20].

### Low ductility regions (embrittlement region)

The poor ductility in the trough is always related to intergranular failure at the  $\gamma$  grain boundaries [20]. The fracture facets are either covered with fine dimples or microvoids, or they are smooth. Cracks are formed along these boundaries and can be caused by two mechanisms, grain boundary sliding in the austenite and/or transformation controlled intergranular failure. Grain boundary sliding, occurs with single phase austenite grains and is illustrated by smooth fracture facets on the fracture surface. Transformation controlled intergranular failure is due to the formation of thin films of ferrite surrounding the  $\gamma$  grain boundaries. The austenitic grains begin to change phase and appear as ferrite films at grain boundaries. At this stage since ferrite is softer than  $\gamma$  and the temperature and strain rate are such as to allow ready recovery, all the strain concentrates in these thin films, encouraging voiding around the MnS inclusions situated at the boundaries and these voids gradually link up to give failure. Without deformation on cooling below the  $A_{r3}$  the films rapidly change during transformation to large islands of ferrite and soon there is sufficient ferrite to prevent strain concentration. With deformation, however, as in the straightening operation ferrite is able to form readily at temperatures above the  $A_{r3}$  but only in the form of thin films.

The thin film of ferrite at the boundaries is indeed generally deformation induced and forms readily at temperatures from just below the  $A_{r3}$  up to the  $A_{e3}$  [20]. This temperature region is of low ductility since with only a small amount of soft deformation induced ferrite (DIF)

around the prior  $\gamma$  grain boundaries in an essentially austenitic microstructure, strain concentration is excessive. The DIF can often form over a very wide temperature range ( $100^{\circ}\text{C}$ ) from the  $A_{r3}$  to the  $A_{e3}$  and ductility remains poor throughout this region.

Recovery in ductility at the low temperature end of the trough (HDL) depends only on significant amounts of ferrite being present ( $\sim 45\%$  to give RA values of 60%) independent of whether it is produced by normal transformation or strain induced [38, 44, 45].

Steels that contain Nb and are solution treated before cooling to test temperatures are often observed with fine matrix and boundary precipitation along with precipitate free zones (PFZ) on either side of the boundaries (500nm wide), Fig.2.10 [46]. Fine matrix precipitation can also take place, leading to significant matrix strengthening. With the presence of soft PFZ's the situation is then similar to the soft films of deformation induced ferrite and microvoid coalescence fractures are frequently observed. This fracture process is shown schematically in Fig.2.3 [19]. In this case, the void formation is at the micro alloying precipitates which are believed to have formed during deformation as well as sulphides present at the austenite grain boundaries. At the higher temperatures within the low ductility trough, fracture surfaces have been observed with both smooth facets and dimples illustrating a combination of grain boundary sliding and microvoid coalescence. This is evidence that intergranular fracture in this steel type can occur both from grain boundary sliding and micro void coalescence [46].

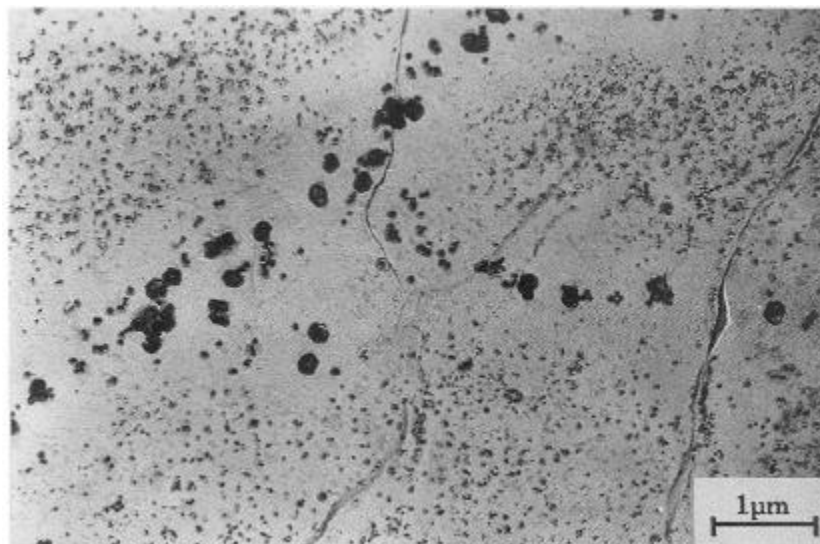


Fig.2.10 Precipitation free zone around grain boundary in Nb-bearing steel fracture at  $950^{\circ}\text{C}$ ; grain boundary contains fine precipitates of Nb(C, N) and coarse MnS inclusions [46].

When deformation is taking place in the single phase austenitic region, grain boundary sliding is likely to be one of the most important embrittlement processes, most probably contributing to crack enlargement.

Grain boundary sliding followed by cracking is seen in austenite rather than ferrite, because the former shows only limited dynamic recovery. This gives rise to high flow stresses and work hardening rates, preventing the accommodation, by lattice deformation, of the stresses built up triple points or grain boundary particles, leading in this way to intergranular failure by the nucleation of grain boundary cracks. This rupture mechanism is usually associated with creep, the latter occurring at strain rates typically below  $10^{-4}\text{s}^{-1}$ . However, fracture characteristic of failure initiated by grain boundary sliding are frequently found at the strain rate generally used in hot tensile testing  $10^{-3}\text{s}^{-1}$ . Ouchi and Matsumoto have observed grain boundary sliding at strain rates as high as  $10^{-1}\text{s}^{-1}$  in a 0.0054%Nb containing steel strained at  $900^{\circ}\text{C}$  [23]. Much can be learned therefore about the factors that influence intergranular crack nucleation and growth at high temperatures from a study of creep literature [47].

Cracks formed by intergranular creep have been classified as either ‘grain edge’ or ‘r’ type (r for rounded) or as ‘grain corner’ or ‘w’ (w for wedge) cavities. Both types of cracks are observed in samples tensile tested at strain rates in the range  $10^{-3}\text{s}^{-1} \sim 10^{-4}\text{s}^{-1}$ , and both require grain boundary sliding for their nucleation. The models proposed for the formation of w and r type cracks are illustrated in Fig.2.11 (a) and (b), respectively [48, 49].

Cracking occurs when the stresses that are built up at grain boundary triple points exceed the stress required for grain boundary failure, as shown in Fig.2.11 (a). Although, in this model, no precipitates are necessary, the presence of precipitates at the boundary makes grain boundary sliding much easier. Grain boundary sliding is generally considered the main deformation and fracture mechanism where conditions of creep prevail, i.e. at strain rates below  $10^{-4}\text{s}^{-1}$  but there is no doubt that grain boundary sliding has been observed at higher strain rates up to  $10^{-1}\text{s}^{-1}$  [23].

Grant [48] have demonstrated experimentally that cavity or crack formation by grain boundary sliding in creep resistant alloys progresses most easily in the presence of grain boundary particles. In steels, there are invariably sulphides, oxides, nitrides, and/or carbides at the boundaries which will act as stress concentrators and favour cavitation and crack formation. If the stress concentration at such grain boundary particles is produced by grain boundary sliding alone, the dislocation pile-up distance corresponds to the interparticle spacing, so that the large applied stresses are required for particle fracture or particle-matrix decohesion. However, for the ease of intra granular slip band impingement against a grain

boundary particle, much smaller applied stresses are required for particle fracture, as the slip distances are much greater. It should be noted that the critical stresses required for the nucleation of r type cavities are much lower than those required for w cavity nucleation, and so the former is favoured in low stress, high temperature creep tests, or low strain rate, hot workability tests.

There are many proposed mechanisms for nucleating r-type cavities which either involve the deformation or vacancy diffusion mechanisms [47]. A possible mechanism pictures cavities appearing as ledges. Impinging slip bands on grain boundaries allow for these 'ledge' cavities to form as the grain boundary slides away.

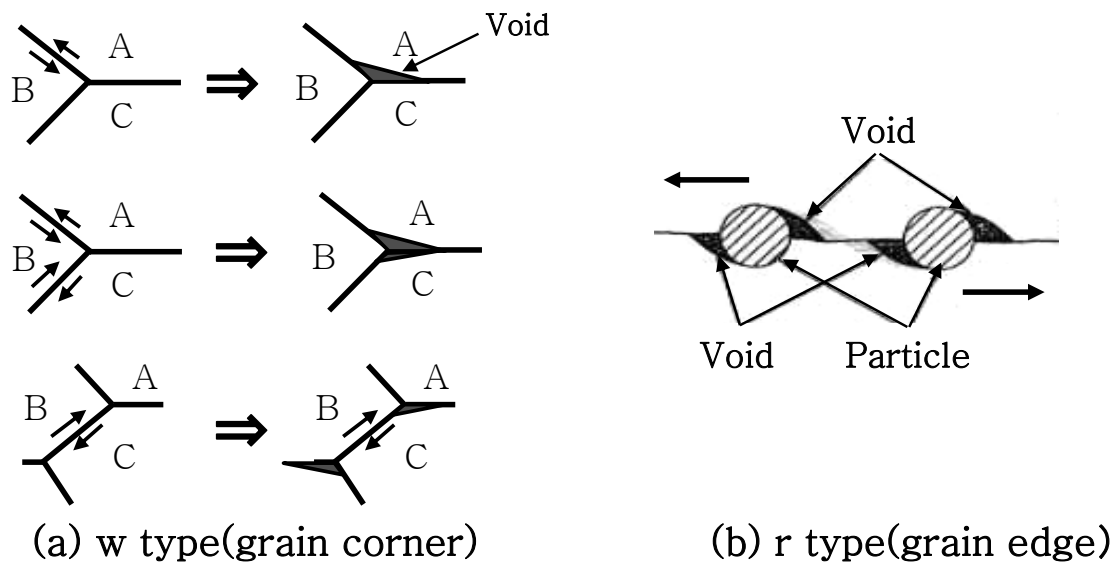


Fig.2.11 Schematic models showing formation of wedge and rounded cracks by grain boundary sliding [48, 49].

### High ductility regions

One of the essentials in avoiding embrittlement is to reduce the strain concentration at grain boundaries. This concept readily applies to the case of the high ductility, low temperature (HDL) region, which coincides with a relatively high volume fraction of ferrite.

As sufficient ferrite will always eventually be present at the low temperature end, ductility will always improve as ferrite has excellent ductility [38]. This ferrite is formed either via

normal transformation prior to deformation, or by the deformation itself. Here the strain is no longer concentrated in a thin ferrite film at austenite grain boundaries. Furthermore, the strength differential between austenite and ferrite decreases with decrease in temperature, thus increasing plastic strain in the austenite and more importantly, decreasing the strain in the ferrite [50]. The concentration of strain at the grain boundaries is thus minimized, and high ductilities are observed.

Generally, the ductility is very good when high percentages of ferrite are present in the microstructure, which often corresponds to a test temperature of  $\sim 700^{\circ}\text{C}$  [23, 51]. At this temperature, recovery in the ferrite take place with ease, the subgrain size is large, and the flow stress is low. Thus, ferrite flows readily at triple points to relieve stress concentrations, therefore discouraging the initiation of w type cracks.

In addition, metals and phases that are susceptible to dynamic recovery like ferrite may form ‘scalped’ grain boundaries, which reduce grain boundary sliding and hence impede the nucleation of intergranular cracks [52].

Studies [53-55] have therefore been carried out in recent years to examine the conditions required to produce deformation induced ferrite and how it can be encouraged to form in large enough amounts to improve ductility. It is found that increasing the strain rate and refining the  $\gamma$  grain size encourage its formation [53, 54]. Composition also plays an important part as this controls the temperature at which the transformation takes place and elements which raise the  $A_{e3}$  temperature are favoured for aiding ferrite formation at higher temperatures [44].

Ductility generally starts to recover at higher temperatures (HDH) when the ferrite film no can longer form and the microstructure is fully austenitic. However, this recovery in ductility is small normally about a 10% increase in the RA value, since un-recrystallised  $\gamma$  has in itself relatively poor ductility.

Full restoration of ductility, the final region, only occurs when dynamic recrystallisation (DRX) can occur and this requires not only the removal of the ferrite film but re-solution of all the  $\gamma$  grain boundary pinning precipitates such as Nb(C, N) and in the case of steels with high concentrations of Al and N, AlN precipitation.

The high ductility, high temperature (HDH) region is encountered when the temperature is in excess of the  $A_{e3}$ , i.e. fully austenitic. Continuing with the concept of reduction in the strain concentration at grain boundaries, one obvious reason for this improvement in ductility is the eventual absence of the thin ferrite film. This, of course, is only effective in

the austenite plus ferrite two phase region, and does not affect the embrittlement in the single phase austenite region, which occurs either by grain boundary sliding or through strain concentration in the PFZ. However higher temperatures also lead to less precipitation in the matrix and at grain boundaries, which offsets the latter embrittling mechanisms. Increased temperature also leads to low flow stresses via increased dynamic recovery, which reduces the stress concentrations at the crack nucleation sites.

However, a very important further mechanism affecting ductility which applies to the HDH region requires the occurrence of grain boundary migration. In this case, cracks which have already been initiated are isolated from the prior grain boundaries, and high ductilities result because the growth and coalescence of these cracks is not readily achieved away from grain boundaries. This is evident from the large voids, characteristic of the fracture surface generated by testing in the HDH region, which apparently are not associated with second phase particles [56]. These grow from the intergranular cracks which form at early stages of the deformation, and which become isolated within the grains as a result of grain boundary migration. The original cracks are then distorted into elongated voids, until final failure occurs by necking between these voids.

Although grain boundary migration can isolate cracks from grain boundaries, the cracks can also exert a grain boundary drag force and 'capture' moving grain boundaries. Crack growth will then resume along the captured boundary by combined effects of vacancy diffusion and the applied tensile stress, until the boundary breaks away once more. If the capture frequency and/or the crack drag force are high, intergranular failure may ultimately occur, even if the prior grain boundaries had moved away from the initiated cracks at an earlier stage in the deformation. Thus, in order to offset embrittlement adequately, the driving force for grain boundary migration must be substantially higher than the drag force exerted by cracks that are present.

One way to achieve a high driving force for grain boundary migration is by dynamic recrystallisation and this in steels is the main cause of the recovery in ductility at the high temperature end of the trough. The nucleation of dynamic recrystallisation takes place at existing boundaries at low strain rates [57]. Poorly developed sub-boundaries pin sections of the original boundaries, which bulge out and migrate relatively rapidly because of the strain energy difference across a given boundary. This is clearly a potent mechanism for bringing about grain boundary movement. It is not surprising therefore that the HDH region has been observed to coincide with the onset of dynamic recrystallisation in many studies [42, 58].

As noted, at the high temperature end of the trough, ductility dramatically improves when dynamic recrystallisation occurs, Fig.2.12 [38]. Any cracks that are formed at the grain boundaries become isolated as the grain boundary moves away from the cracks and new grains are formed and in consequence crack growth is halted. However, dynamic recrystallisation is not possible during conventional continuous casting since the strain involved in straightening (2%) is too small and the grain size is too coarse [20]. (Although strains can be greater in thin slab casting when pre-deformation is used and the grain size will be finer, it is still too coarse and dynamic recrystallisation does not take place). Nevertheless commercially some improvement in ductility occurs at higher temperature since there are no ferrite films at the austenite boundaries to cause embrittlement and the high temperature discourages precipitation in the matrix and at grain boundaries which can aid grain boundary sliding. The improvement in ductility from these sources when DRX doesn't occur is in the region of 10 to 20% increase in the RA value and importantly is often sufficient to avoid transverse cracking.

The use of the high temperature end of the trough in predicting what happens on straightening during continuous casting must therefore be treated with great caution. Nevertheless, raising the temperature at the straightener into the HDH region can improve ductility by coarsening precipitates or reducing the amount of precipitates formed in the boundary regions and removal of the ferrite film but the improvement in ductility is often small and may not be sufficient to entirely eliminate the problem of transverse cracking [38]. The form of the hot ductility curve in this case, when dynamic recrystallisation is absent, is shown schematically in Fig.2.12, (dashed curve), and this is the curve that is relevant to the problem of transverse cracking [38].

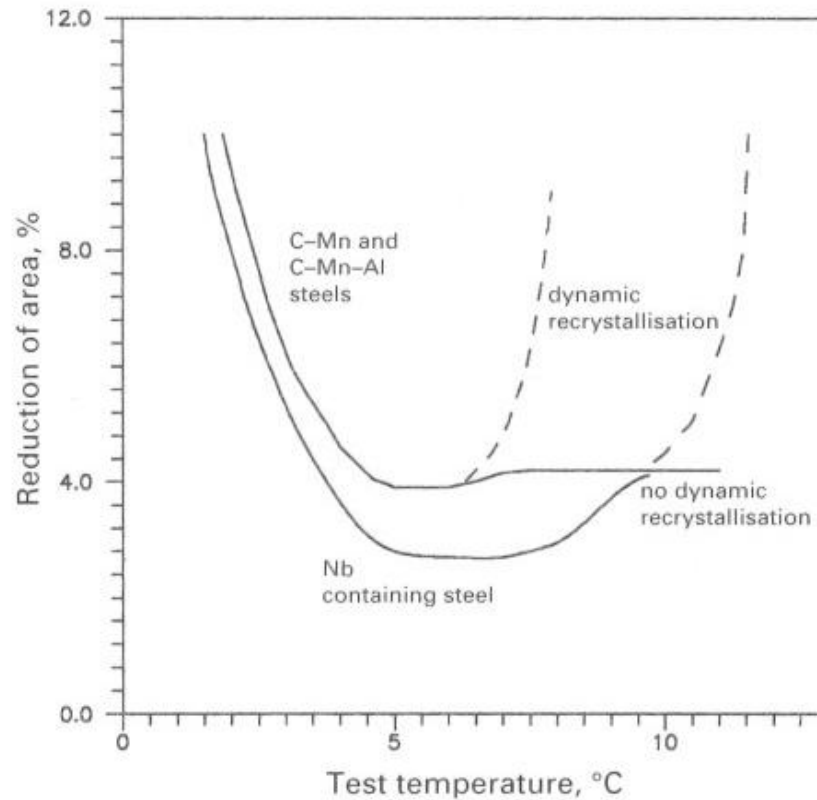


Fig.2.12 Schematic diagram illustrating the ductility levels that can be achieved with and without dynamic recrystallisation at the high temperature end of the trough [38].

### 2.3.3 Factors that influence hot ductility

It is necessary to mention the four most important variables that control ductility; strain rate, grain size, precipitation and inclusion content, (their size, volume fraction and distribution being important). Increasing the strain rate and refining the grain size (and this has to be generally below 200 $\mu$ m to have any significant effect [20]) both give rise to improved ductility; the former by reducing the amount of grain boundary sliding and the latter by making it more difficult for cracks to propagate along the boundaries. Unfortunately, it is not generally possible to alter either of these sufficiently in conventional continuous casting to make any significant difference to ductility.

The other two variables which have a major influence on the hot ductility are precipitation and the presence of inclusions; the finer the precipitation, the worse is the ductility. Grain boundary precipitation is particularly deleterious [20]. This arises because for a given

volume fraction of precipitate and/or inclusions, the finer the particles at the boundaries, the closer they are to each other and the easier it is for cracks to interlink. Again, strain induced precipitation is always finer and more detrimental to ductility than precipitation that is present before strain [59]. In the case of Nb and V containing steels, a large part of the precipitation comes out dynamically during the straightening operation and so can be very detrimental to ductility [20].

### Strain rate

When recreating the conditions of continuous casting in a laboratory, a strain rate of  $3 \times 10^{-3} \text{ s}^{-1}$  is normally used as it is comparable to that experienced by the cast strand during the straightening process. It is found that an increase in strain rate will give better ductility, such that an increase of a factor of ten would give increases in RA values of 20% and often changes the failure from intergranular to ductile. This can be seen in Fig.2.13 for the 700 ~1000 °C temperature range, relevant to the straightening process [22].

Increasing the strain rate from  $10^{-3} \text{ s}^{-1}$  to  $10^{-1} \text{ s}^{-1}$  usually improves the hot ductility [22, 23, 58, 61], often eradicating the trough entirely [22]. Furthermore, the high temperature boundary of the trough is moved to lower temperatures, narrowing the trough as shown in Fig.2.13.

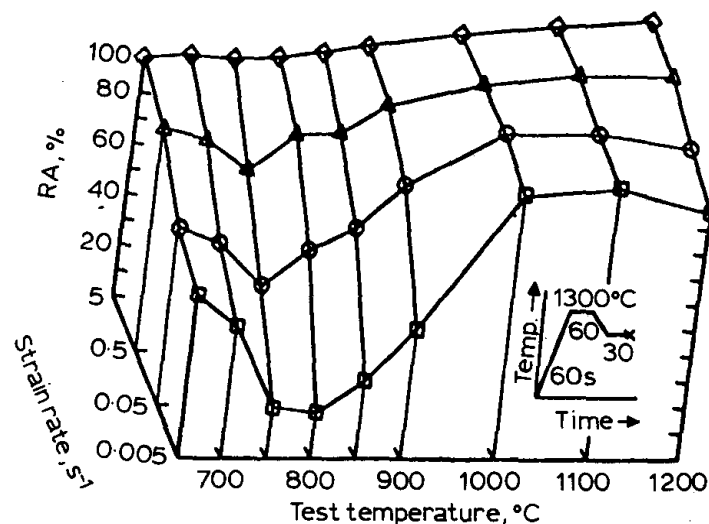


Fig.2.13 Dependence of ductility on strain rate and test temperature for Nb-bearing steel [22].

This observation indicates that strain rate changes have an effect via the kinetics of critical events. Thus, higher strain rates decrease the time available for dynamic precipitation, and diffusion assisted void nucleation and growth.

In other words, by the time these phenomena have progressed to a significant level, the specimen has already been subjected to a relatively high strain.

Other effects of increasing the strain rate include the observed decrease in the extent of grain boundary sliding [23] and precipitate coarsening [60]. The latter is presumably due to the higher dislocation densities, which can increase the pipe diffusion rates. However, very low strain rates can increase the time available for precipitate coarsening, and can also lead to increases in hot ductility.

In Fig.2.14 [53] it can be seen that a high C (0.4%C) and high Mn (1.5%Mn) steel with a relatively fine  $\gamma$  grain size of 110  $\mu\text{m}$  when tested at  $3 \times 10^{-4} \text{ s}^{-1}$  gives a wide trough, the strain rate being low enough to allow recovery in the ferrite band so that is not able to strengthen up. The strain then becomes localised so that there is no spread of ferrite into the interior and ductility remains poor. For ductility to improve, the temperature has to fall below the  $A_{r3}$  giving rise to a large amount of ferrite, leading to a wide trough. Increasing the strain rate to  $3 \times 10^{-3} \text{ s}^{-1}$  allows the thin band of ferrite to work harden so that the DIF can now spread into the interior and improve ductility at temperatures above the  $A_{r3}$ , giving rise to narrow trough behaviour. The width of this trough can always vary, but what now differentiates this narrow trough from the wide is that full recovery in ductility at the low temperature end is due to the rapid formation of DIF in large quantities below the  $A_{e3}$  not to the normal transformation induced ferrite.

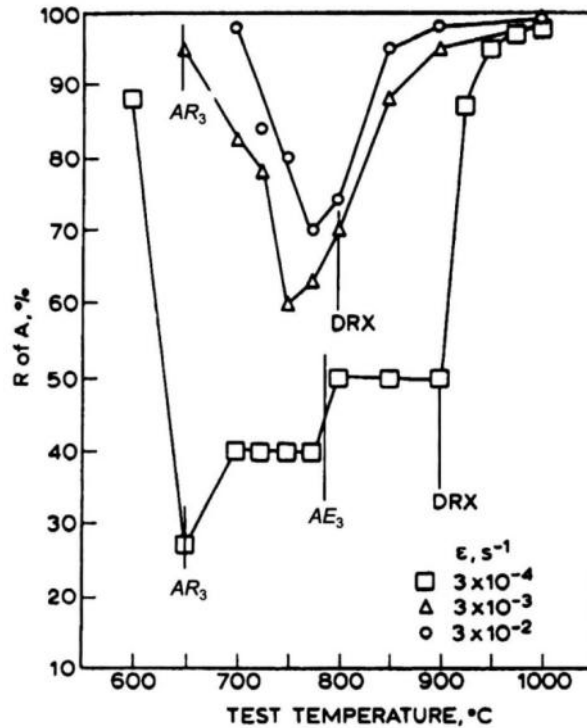


Fig.2.14 Influence of strain rate on hot ductility of 0.4%C, 1.5%Mn steel had a relatively fine grain size 110 $\mu\text{m}$  [53].

There are two instances when an increase in strain rate has been found to yield worse ductility [60, 62]. However, in both these cases this occurred at high strain rates such as  $10^1 \sim 10^2 \text{ s}^{-1}$  and is therefore not applicable to typical tensile test strain rates. In one case, the steel contained unstable precipitates such as FeMn sulphides, so that lower strain rates allowed for rapid coarsening of inclusions so they were not able to pin austenite grain boundaries [60]. In the other instance, the high strain rate resulted in there being insufficient time for recovery or dynamic recrystallisation processes to occur and so ductility can be impaired [62].

### Grain size

In general, finer grain sizes should lead to higher ductilities. The possible reasons for this depend on the fracture mode, or the ductility recovery mechanism in operation.

There have been many investigations into the relationship between grain size and hot

ductility of many materials including austenitic steel. The majorities conclude that the high temperature ductility in a creep study increases as the grain size is decreased [47, 64]. When the failure is intergranular, refining the grain size makes crack growth more difficult because the crack aspect ratio is decreased, thus decreasing the stress concentration at the crack tip. Furthermore, crack propagation through triple points is more difficult than along grain boundaries [64]. The increase in grain boundary area per unit volume will also decrease the number of precipitates per unit area of grain boundary [23]. This reduces the critical strain for dynamic recrystallisation by increasing the number of grain boundary nucleation sites [65], and thereby increases the possibility of ductility improving via grain boundary migration. All these effects outweigh any detrimental influence on the hot ductility due to the small increase in flow stress brought about by grain refinement.

The influence of grain size on hot ductility has been examined under conditions which involve the absence of precipitation [56, 63]. These studies have shown that refining the grain size leads to reduction both in the depth and width of the trough in Fig.2.15 [63].

Finer grain sizes can also affect the transformation rate, because grain boundaries are preferential ferrite nucleation sites. This has the effect of narrowing the trough because of relatively rapid thickening of the ferrite film at the austenite grain boundaries; thus increasing the ductility. It has also been observed that finer austenite grain sizes promote the formation of ferrite that is equi-axed, as opposed to being present in the form of a ferrite thin film [63].

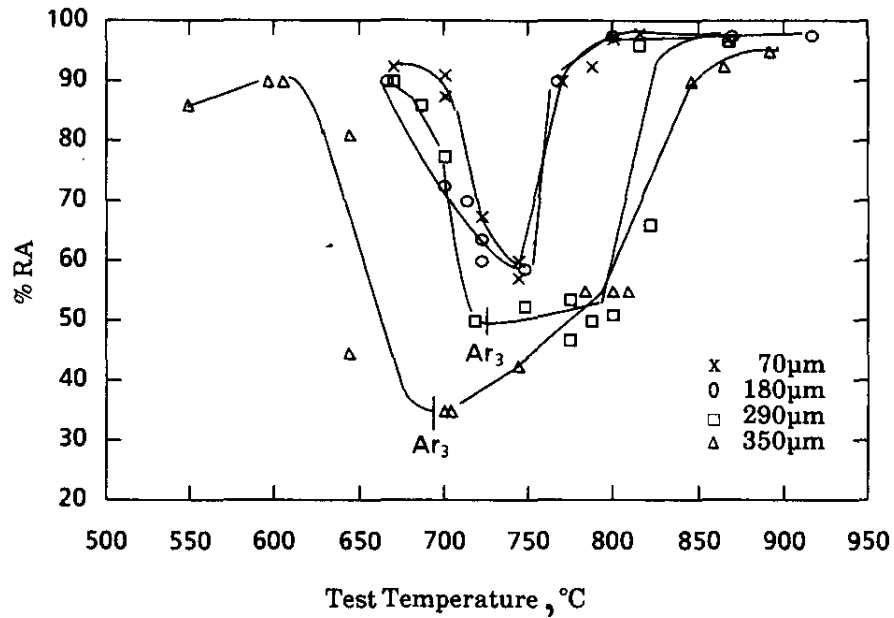
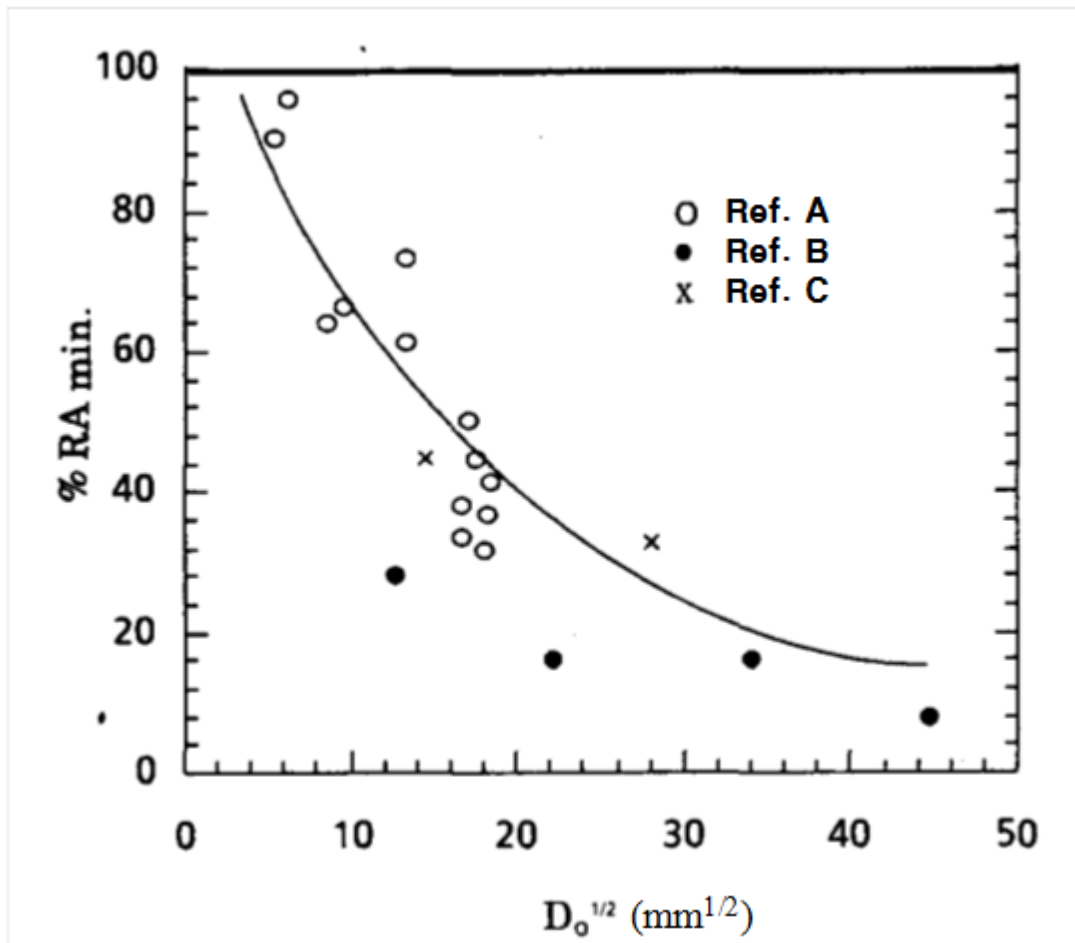


Fig.2.15 Hot ductility curves for 0.19% C steel of various grain sizes [63].

Microalloyed steels generally show little indication, from the hot tensile test, that grain size has a significant influence on their hot ductility, because of the overriding effect of precipitation of AlN or Nb(C, N) at the austenite grain boundaries. Where an attempt has been made to keep the precipitate distribution constant [66], the changes in hot ductility with grain size were similar to those observed in plain C-Mn steels in Fig.2.16. When the degree of precipitation is such that the ductility trough extends into the austenite, the beneficial effects from grain refinement are readily apparent [20].



○ Ref. A: D. N. Crowther et al.; Material Science and Technology, 1986, 2, p1099

● Ref. B: Y. Maehara et al.; Trans. Iron Steel Inst. Japan, 1985, 25, p1045

x Ref. C: D. P. Rizio et al.; 'Physical metallurgy of thermomechanical processing and other metals, Thermec 88', 178, Tokyo, The Iron and steel Institute of Japan.

Fig.2.16 Influence of  $D_0$  (initial un-deformed grain size after heat treatment) on minimum RA value [20].

However, there have been other studies on the relationship between grain size and ductility whereby grain refinement has led to worse ductility suggesting that grain size in this case may have a negligible bearing on ductility [67]. The reason for these differences in opinions is attributed to difficulties in isolating the affect of grain size from that of precipitation.

Ouchi et al. found that for C-Mn-Nb-Al steels, with austenite grain sizes in the range 100~300 $\mu\text{m}$ , that there was no relationship between the grain size and ductility when tested at 900°C [23]. This was most likely due to the overriding influence of Nb(C, N) precipitation on the ductility in these steels.

## **Precipitation**

It has been shown that the likelihood of transverse cracking is reduced when the temperature at the straightener is raised. This effect can be linked directly to the reduction in the extent of nitride and carbonitride precipitation, the higher temperature decreasing the degree of precipitation. Higher temperatures at the straightener can be achieved by reducing the amount of secondary cooling, or increasing the casting speed.

It is well known that Nb steels are more susceptible to transverse cracking than plain C-Mn or C-Mn-Al steels. Precipitates have been associated with such cracks, and, as can be seen in Fig.2.17 fine precipitates and close interparticle spacing lead to low ductilities, and high incidence of product rejections. Such a correlation can be explained on the basis of enhanced grain boundary pinning, due to the presence of fine precipitates, and short void coalescence distances, i.e. interparticle spacing. Fig.2.17 also suggests, perhaps more practically, that a hot ductility of >40% RA is desirable if transverse cracking problems are to be avoided [20].

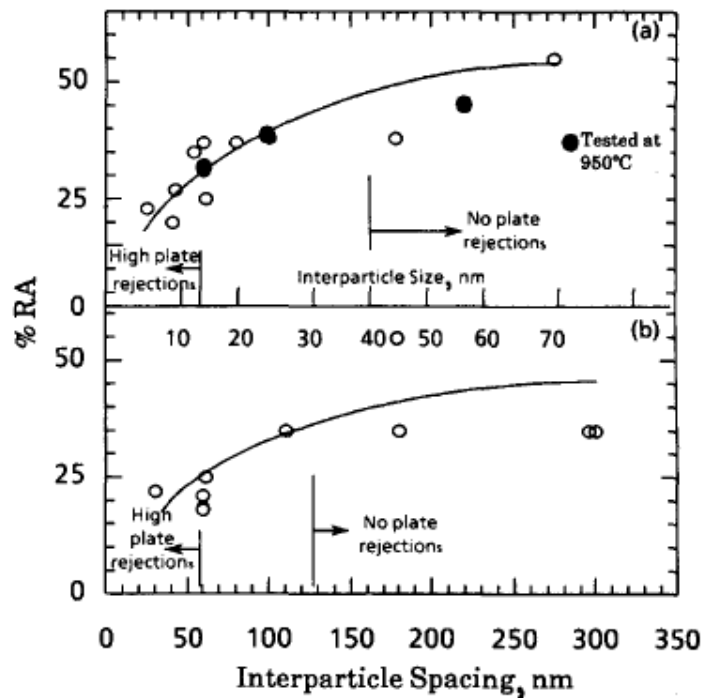


Fig.2.17 Influence of (a) particle size and (b) interparticle spacing on hot ductility of Nb-containing steels [20].

The role of precipitates in promoting embrittlement has been clearly defined [19, 24, 68]. In the case of grain boundary sliding in the austenite, fine precipitation pins the boundaries, allowing the cracks to join up [14]. In addition, both precipitates and inclusions cause void formation, extending the crack length in this way [69]. Microvoid coalescence failures are also encouraged by an increase in the precipitate or inclusion density at the boundaries, these being preferential sites for void initiation.

It is clear that the precipitation of microalloy carbides and nitrides has a crucial role to play in determining the depth, position and width of the ductility trough, through their influence on dynamic recrystallisation, strain to fracture and transformation. The influence of precipitates on dynamic recrystallisation is dependent on their size and volume fraction, large volume fractions of fine particles having the greatest effect in delaying recrystallisation. Similarly, large volume fractions of fine precipitates are likely to increase strength, and hence reduce ductility.

Precipitation and the presence of microalloying elements in solution, as well as increasing the depth of the trough can also widen the trough at both the low and high temperature ends of the trough. At the high temperature end, this is because precipitation slows down the process of dynamic recrystallisation and pins the austenite grain boundaries encouraging grain boundary sliding [44]. In the case of Nb containing steels, the trough is also widened at the low temperature end, as the presence of Nb in solution markedly reduces the  $A_{r3}$  temperature [70] and dynamically induced precipitation of Nb(C, N) can occur over a wide range of temperature with the result that Nb containing steels can have exceptionally wide troughs making it difficult to successfully cast.

Precipitation from VN, Nb(C, N) and Ti(C, N) has been shown to deepen the trough [21]. Precipitates are generally very much finer than inclusions and so will not in themselves be as effective as inclusions in encouraging void formation at the boundaries. It is likely that the increased depth of the trough in this case is due to precipitation in the austenite increasing the stress on the ferrite band encouraging cavitation processes around the inclusions within the ferrite film. Surprisingly, even AlN which does not cause precipitation hardening in the austenite has been found to deepen the trough Fig.2.18 and this probably arises because it precipitates mainly at the austenite grain boundaries and is coarser than the other precipitates [71]. Again, increasing the cooling rate by producing a finer precipitate distribution decreases the spacing between the particles making it easier for cracks to interlink and separate the grain surfaces.

The precipitate size and distribution are influenced by whether the precipitates are formed statically before the material is tested, or dynamically during deformation. Deformation accelerates the rate of precipitation as the process produces dislocations and sub-boundaries within the matrix that act as their nucleation sites [23]. To argue which type of precipitation, statically produced or dynamically produced, is most detrimental to a material's ductility is unclear. One study has shown that in steel containing V and Al static precipitates were more detrimental to hot ductility than deformation produced ones [43, 59]. However, this has not generally been found to be the case, particularly for Nb containing steels. For Nb containing steels, precipitates produced dynamically have been found to be more detrimental than those produced statically [59]. It has been suggested the hot ductility of Nb containing steels can be improved by reducing the cooling rate allowing, the formation of coarse statically precipitated Nb(C, N), thus reducing the amount of dynamically precipitated Nb(C, N) [56].

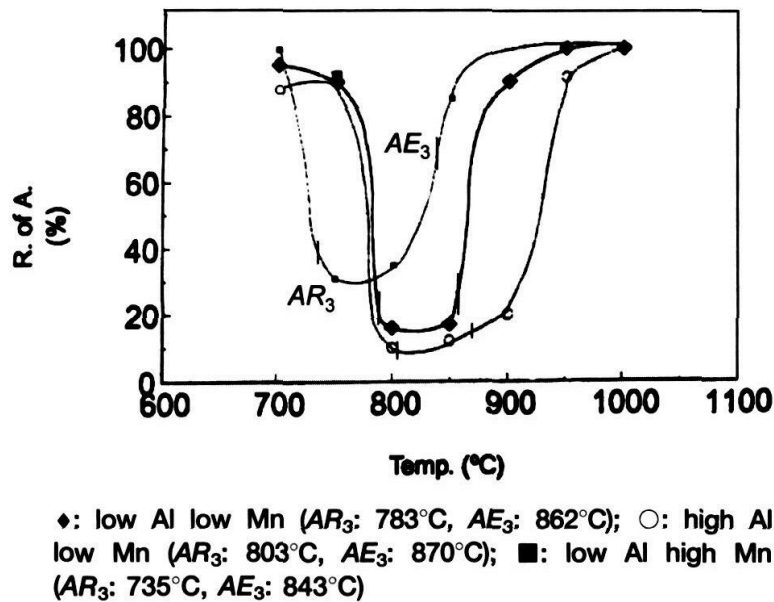


Fig.2.18 Effect of increasing Mn level on decreasing depth of trough: all steels give wide ductility troughs due to coarse grain size (450 $\mu$ m) and the trough were deeper and extended to higher temperature in high Al containing steel due to precipitation of AlN [71].

## Inclusions

Non-metallic inclusions have proved to be detrimental to the hot ductility of steels. Hot tensile tests have found that iron of varying purities showed a decrease in hot ductility as the inclusion volume fraction increases [182]. The reasoning for this is that inclusions act as nucleation sites for cracks on deformation.

Fracture in the lower temperature range of the trough is always intergranular ductile and it occurs by voids being produced on deformation around the second phase particles that are situated in the softer ferrite band surrounding the  $\gamma$  grains, these voids gradually linking up to give failure. Thus, the greater the volume fraction of second phase particles, normally MnS inclusions, the worse is the ductility. However, for plain C-Mn steels which are heated to about 1300~1400°C and then cooled to the test temperature, it is the amount of S that redissolves at the solution temperature and subsequently reprecipitates as fine spherical sulphides, which controls the ductility not the total S content [45].

The amount that re-dissolves on reheating depends on the Mn level and for steels with 1.4%Mn, only a very small amount re-dissolves (0.001~0.002%) whereas for a 0.5%Mn steel, the amounts are much higher 0.006~0.007% [72]. Thus, one would expect the depth to be generally, shallower for high Mn steels as shown in Fig.2.18, taken from the work of Cardoso et al. [71]. The influence of S in solution in deepening the trough for steels with a coarse  $\gamma$  grain ( $\sim 400\mu\text{m}$ ) is clearly shown in Fig.2.19 where the curves have been taken from a variety of sources [73].

However, the depth of the trough is also influenced by the grain size, cooling rate, precipitation and strain rate.

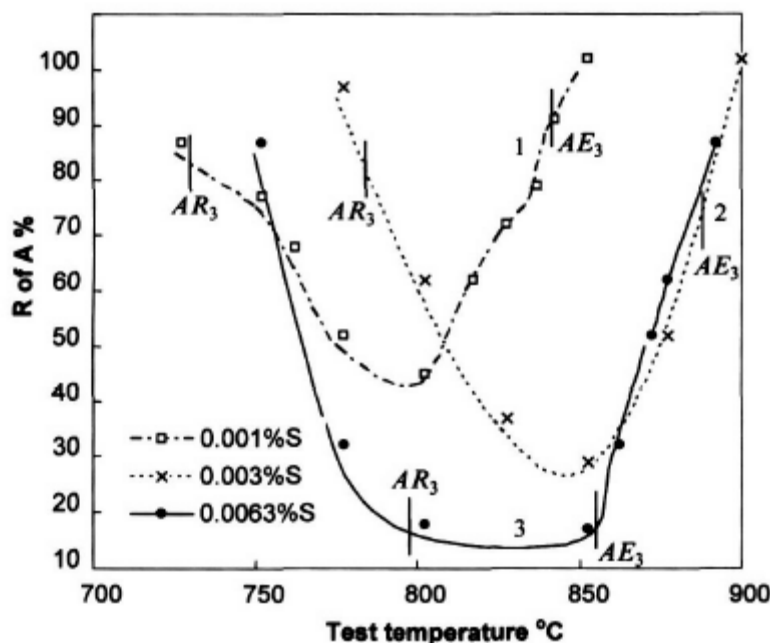


Fig.2.19 Influence of S in solution on depth of steels with similar coarse grain size ( $\sim 400\mu\text{m}$ ), strain rate ( $10^{-3}\text{ s}^{-1}$ ) and cooling rates [71, 74, 75]: trough changes from narrow to wide trough behaviour as S content increases [73].

The influence of S in solution, which dictates the amount of fine spherical MnS inclusions reprecipitated out in the ferrite band, is clearly shown in Fig.2.19, which also highlights the importance of S in solution in not only controlling the depth of the trough but also at times the width. It can be seen for the two low Mn coarse grained steels, steels 2 and 3 that at the higher S level, steel 3 (based on the S in solution at  $1300^\circ\text{C}$ ), not only is the trough very deep but now the trough is wide and ductility only improves when the temperature has

fallen below the  $Ar_3$ . It can be inferred that if the sulphur in solution at the solution temperature is sufficiently high, large amounts of fine sulphides are precipitated at the  $\gamma$  grain boundaries, causing so much cavitation at the boundaries that failure occurs before the ferrite has had time to work harden sufficiently to allow more austenite to deform and so produce enough DIF (Deformation Induce Ferrite) to avoid localised failure.

Hence not only is the fracture strain in the trough related to the volume fraction of the inclusions at the austenite grain boundaries, it can also influence the width of the trough at the lower temperature end.

### **Cooling rate**

An area which has received little attention is the influence of cooling rate to the test temperature on the hot ductility. This has become particularly important with the advent of thin slab casting, where cooling rates are much higher than in conventional continuously cast steel. Generally, the average cooling rate from the mould to the straightening temperature are 60~100°C/min for conventional casting (220 to 250mm thick slab) and 200~300°C/min for thin slab casting (60~80mm thick slab).

It is found that increasing the cooling rate to the test temperature after solution treatment results in deeper troughs Fig.2.20 [75]. This has been shown to be related to a finer sulphide re-precipitation at the  $\gamma$  grain boundaries produced by the higher cooling rate so that again the spacing between the particles is reduced making it easier for ductile cracks to link up and give failure [75]. It should be appreciated that for a given inclusion volume fraction, although finer inclusions will generally increase the energy required for ductile fracture at room temperature because they are less deformable, this does not apply to the present situation where the failures are intergranular and the linking up of the cavities is more important than their ease of formation [75].

Decreasing the cooling rate from the 'solution treatment' temperature can be seen from Fig. 2.20 to result in narrower troughs. Part of the explanation is that slow cooling coarsens the sulphide inclusions which for a given volume fraction results in more space between them making ductile intergranular failure more difficult and therefore results in a shallower trough, this also has the effect of reducing the width.

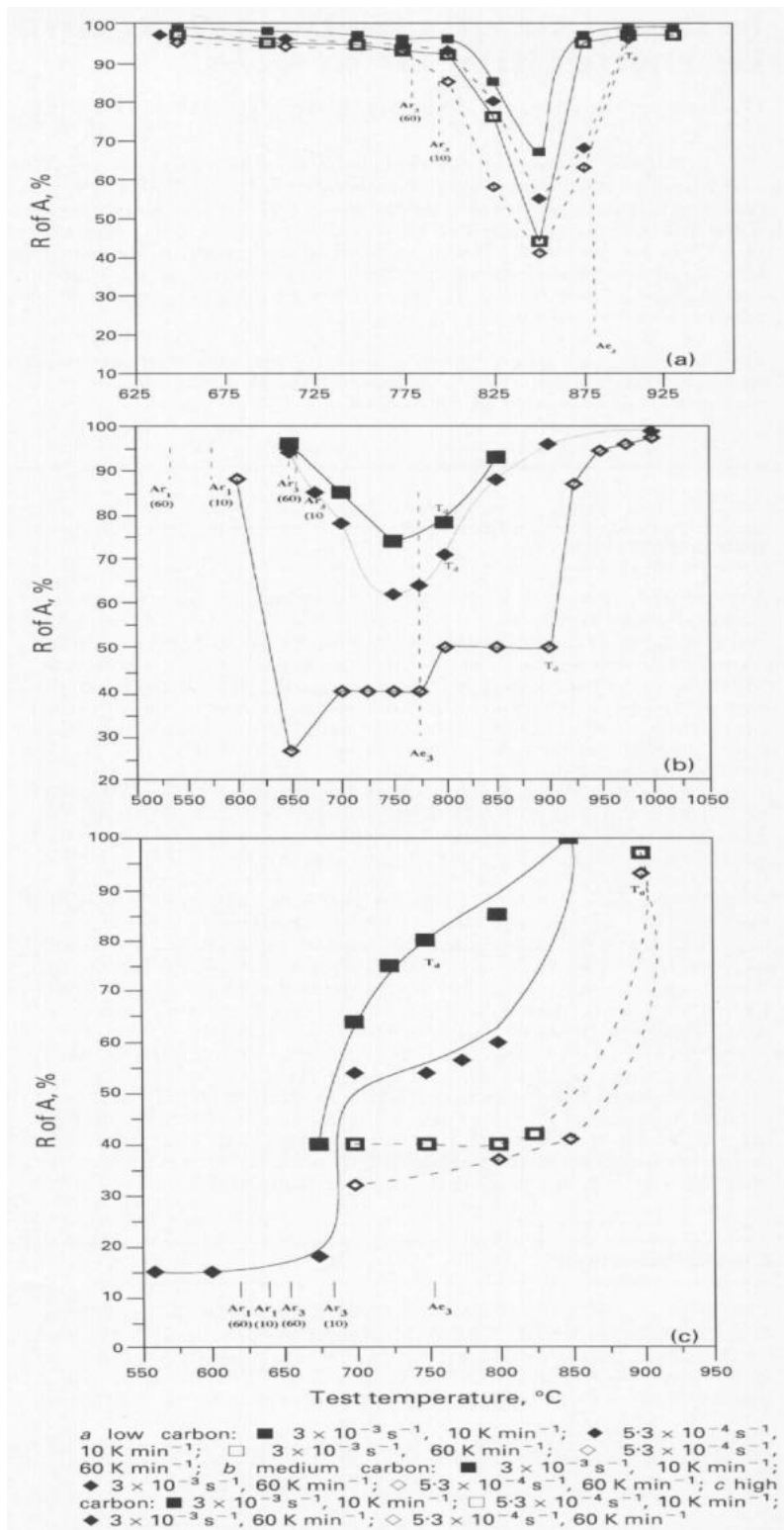


Fig.2.20 Influence of cooling rate on hot ductility of given steels at two strain rates [75].

The faster cooling rate close to the surface of the thin slab strand ( $\sim 200^{\circ}\text{C}/\text{min}$ ), causes precipitation to be refined leading to reduced ductility, Fig.2.21 [76, 77] and this to a large extent, offsets the improvement in ductility from the increased strain rate. Because of this, the hot ductility data and information already obtained from conventional thick slab casting is still likely to be relevant to the thin slab casting operation.

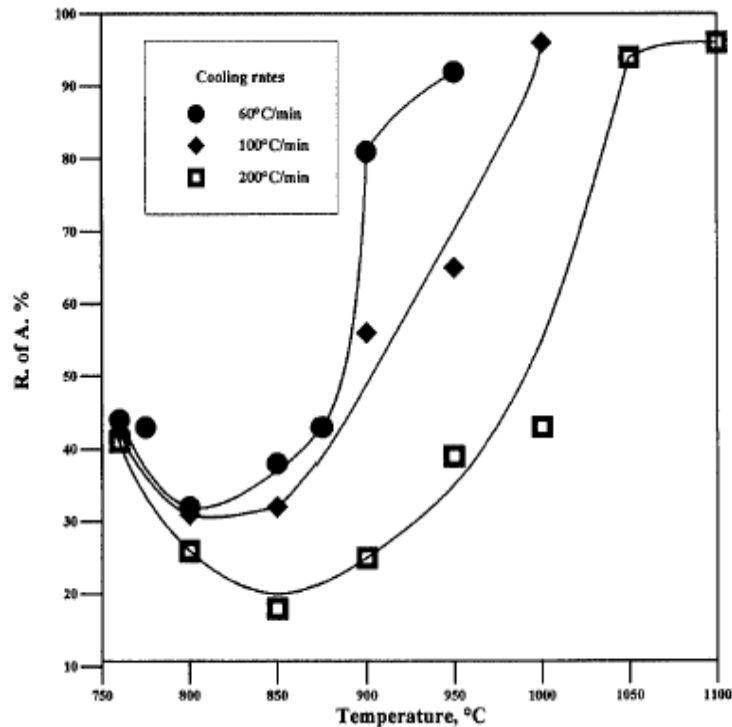


Fig.2.21 Hot ductility curves for as-cast C-Mn-Nb-Al steel, given different cooling rates to the test temperature [76].

Considerable work [75, 77, 78] has been carried out into the influence of cooling rate in the range 25 to  $200^{\circ}\text{C}/\text{min}$  on hot ductility for a wide variety of steels including Ti containing steels. Invariably increasing the cooling rate results in worse ductility, Fig.2.21, and this is even so for plain C-Mn steels. In all cases, the better ductility could be ascribed to either a finer particle size or finer inclusion distribution.

The greatest improvement in ductility that has been found so far on adding Ti to as-cast steel, is when slow cooling to the test temperature has been used [79]. Whereas cooling an Nb containing steel at  $100^{\circ}\text{C}/\text{min}$  to the test temperature only gave a small improvement in

ductility when Ti was present, reducing the cooling rate to 25°C/min resulted in a significant benefit, Fig.2.22. This slower cooling rate allowed the NbC to precipitate out at high temperatures on the coarse TiN precipitates. Precipitation was then generally coarser and there was less Nb available to precipitate out dynamically on deformation.

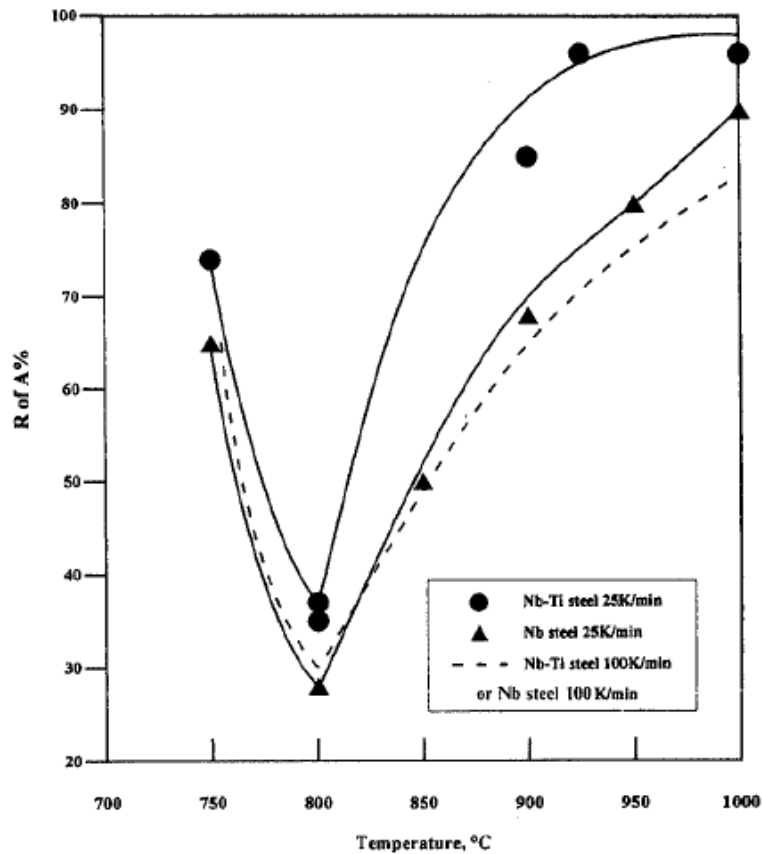


Fig.2.22 Effect of reducing cooling rate during casting to 25°C/min on as-cast C-Mn-Nb-Al steel with and without Ti addition (curve for the same Nb-Ti steel cooled at 100°C/min, broken line shown for a comparison) [79].

## **Thermal cycle**

During continuous casting, the surface of steel is in contact with a variety of different media, including water sprays, air, guides and rolls, Fig.2.6. This leads to complex cycle fluctuations of temperature, during which the surface can momentarily drop to temperatures as low as 600°C, followed by rapid reheating from the specimen interior [15].

Simulations of these cycle heat treatments have been carried out in association with tensile tests. These have shown that, if the temperature drops below the final test temperature during cycling, an increased amount of fine precipitation occurs, giving rise to a greater volume fraction of precipitate present at the test temperature, and therefore to reduced ductility. This has been demonstrated both for C-Mn-Al and C-Mn-Nb-Al steels [15, 71, 80, 81].

Furthermore, if the temperature falls below the transformation so that ferrite is present, precipitation is still further enhanced, because nitride and carbo-nitrides have lower solubilities in ferrite than in austenite. This is again expected to be detrimental to the hot ductility.

There has been a move to make the hot tensile test more representative of the commercial process. Melting of the tensile samples and testing in situ is more common and cooling conditions after melting are often closer to the actual cooling conditions found close to the surface of the strand as shown in Fig.2.23, where both the primary and secondary cooling are dealt with separately. This closer simulation of the commercial process normally results in worse ductility [82]. In addition, pilot continuous casting machines are now available which can represent the casting conditions and bending at the straightener more realistically but on a smaller scale.

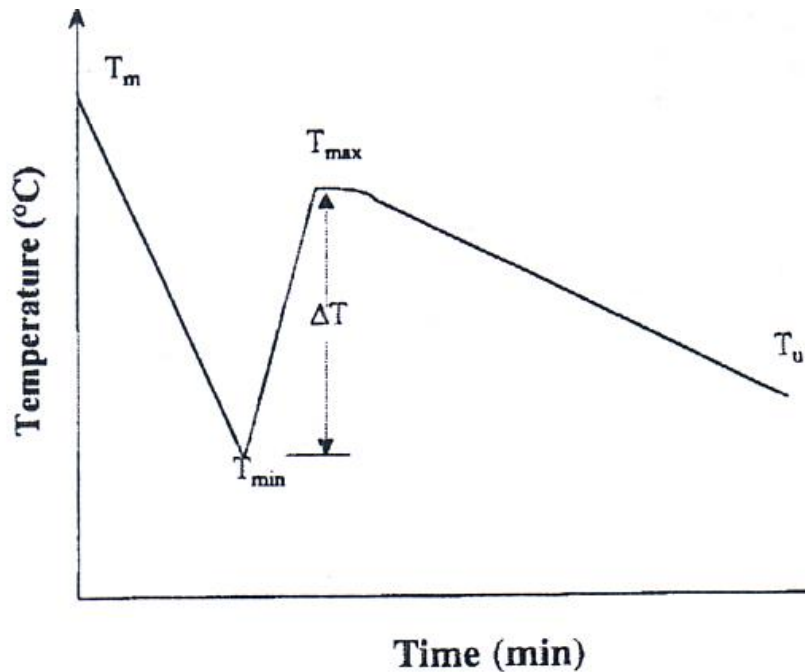


Fig.2.23 Thermal schedule used to generate the thermal condition of billet surface in the continuous casting process.  $T_m$  is the melting point,  $T_{min}$  is the lowest temperature reached during the primary cooling stage and  $T_{max}$  is the highest temperature at the start of secondary cooling.  $T_u$  is the temperature at the straightener [82].

### 2.3.4 Influence of compositions on hot ductility

From the discussions in section 2.3.2 on the occurrence of ductility troughs, and the previous section on the influential factors on the hot ductility, it is clear that the precipitation of microalloy carbides and nitrides has a crucial role to play in determining the depth, position and width of the ductility trough, through their influence on dynamic recrystallisation, strain to fracture and transformation. The influence of precipitates on dynamic recrystallisation is dependent on their size and interparticle spacing, particularly at grain boundaries.

It is evident from the above discussion that composition, and particularly the use of microalloying elements, can strongly influence transverse cracking by their influence on hot ductility.

In this section, the effect of the different microalloying elements on hot ductility will be compared, and the mechanisms by which they influence hot ductility will be discussed in more detail.

## Carbon

The surface cracking susceptibility of low alloy steel slabs during continuous casting depends on the C content [83, 84], attaining a maximum in the range 0.1~0.15%C. Such a dependence on C content cannot be reproduced by hot tensile testing of reheated specimens [66]. This suggests that the C content dependence originates from the microstructural change during solidification. This phenomenon has been studied in relation to the peritectic reaction during solidification. It has confirmed that the solidified shell of the steels in this C region becomes uneven in the mould by the shrinkage owing to transformation from bcc  $\delta$  ferrite to the close packed fcc structure of austenite within a liquid phase [85-87], resulting in the marked reduction of heat extraction in the mould [88]. Since the thinner parts of the unevenly solidified shell break easily, cracking just below the solidus temperature could be explained by such a mechanism. However, it is difficult to explain surface cracking that occurs in the temperature region from low temperature  $\gamma$  to  $\alpha/\gamma$  duplex phase, where solidification has been completed already.

Since the surface cracking occurs mostly by intergranular fracture, the ductility should depend largely on the  $\gamma$  grain size [56, 63, 66]. Thus the grain growth behaviour of austenite during both solidification and cooling has been examined [66]. It was found that the  $\gamma$  grain size of as cast materials attains a maximum in the medium C range. Such a C dependence of austenite grain size corresponds to that of ductility loss and is in good agreement with the variation of austenite formation temperature in the Fe-C binary phase diagram as shown in Fig.2.24 [19]. In fact the growth of austenite grains occurred rapidly after the completion of either transformation to or solidification into the  $\gamma$  phase [66] as shown in Fig.2.25. Such grain growth behaviour after solidification into or transformation to  $\gamma$  single phase can also be explained theoretically [66]. It can be seen from Fig.2.25 that the austenite grain structure of continuous casting slab surface is determined in the mould, since the surface temperature is approximately 1300°C at the outlet of the conventional mould. Although the C content giving the maximum  $\gamma$  grain size shows good agreement with that of the maximum surface cracking susceptibility, it is considerably less than the 0.18%C of peritectic point in the Fe-C binary system. This can be explained in terms of both the effects of other alloying elements such as Mn and segregation of impurity atoms such as P and S, as pointed out by Yasumoto et al. [89]. It is, nevertheless, not clear that the movement of the constitutional diagram by alloying elements accounts for the gap.

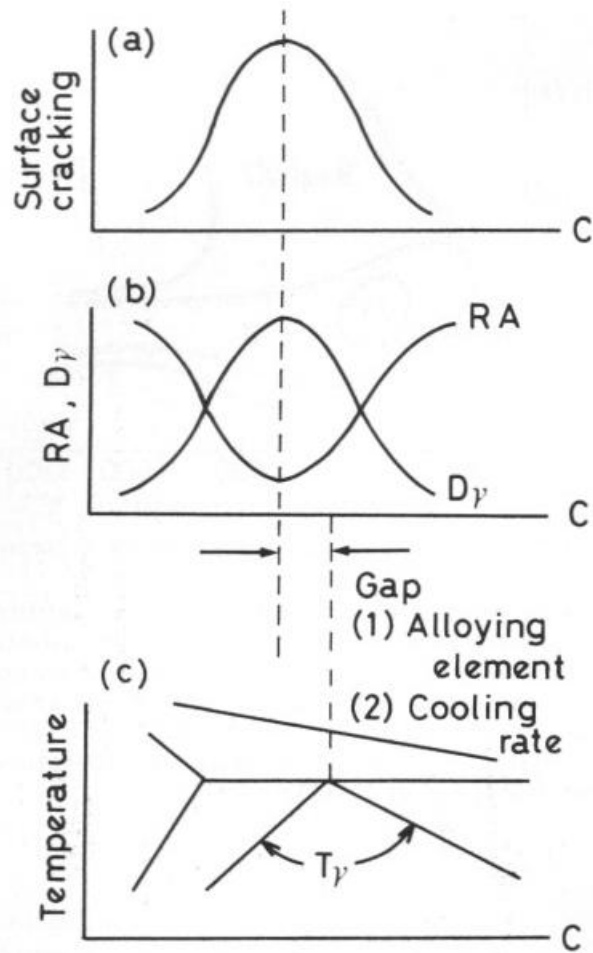


Fig.2.24 Dependence on C content of (a) surface cracking frequency and of (b) ductility (RA) and  $\gamma$  grain size ( $D_\gamma$ ) of as cast steel and (c) their relation to  $\gamma$  composition temperature  $T_\gamma$  (schematic) [19].

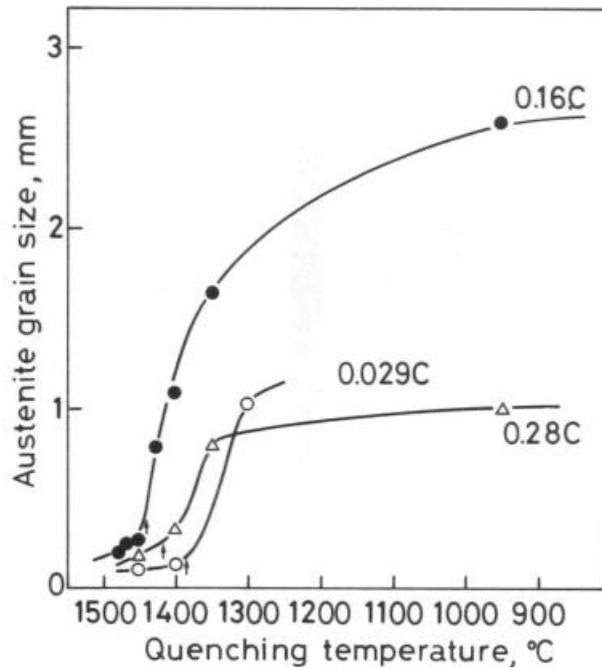


Fig.2.25 Effect of C content on grain growth of  $\gamma$  phase during continuous cooling of 0.8%Mn steels [66].

In the case of the ductility trough obtained on cooling from high temperature, say 1350°C, the mechanism proposed for intergranular failure has been linked to the onset of austenite to ferrite transformation. As raising the C level lowers the transformation temperature, it moves the trough to lower temperatures. Such behaviour has indeed been observed by many investigators in both plain C-Mn-Al and C-Mn steels as shown Fig.2.26 [22, 51, 90]. Generally, the curves move bodily down to lower temperatures as the C level is increased in the range 0.05 to 0.3%C, but Suzuki et al. [22] have noted that the trough is deepened as well.

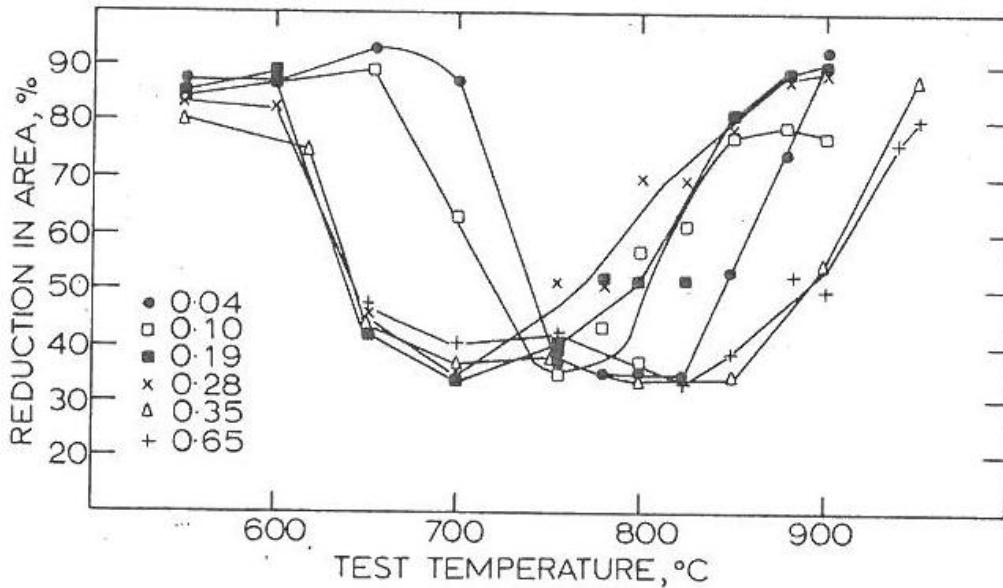


Fig.2.26 Hot ductility curves for series of plain C-Mn steels (C contents in wt. %) [51].

### Silicon

There is little information in the literature on the influence of silicon on the hot ductility of high strength low alloy (HSLA) steels, because generally the silicon level for most steels in the range 0.02~0.5%Si, and there is no evidence of any problem with transverse cracking for this narrow range. However, electrical steels, which contain 3%Si, have presented major casting problems, although this has been shown to be a result of the Mn/S ratio being low rather than the silicon content being high [91].

Hot ductility results obtained by Mintz et al. [92] show in Fig.2.27 that raising the silicon from 0.3% to that normally found in high silicon TRIP (Transformation Induced Plasticity) steels, 1.22% (steels 1 and 2, respectively), causes the ductility to deteriorate but mainly by a shift of the trough to higher temperatures as Si increases the transformation temperatures. Nevertheless, the ductility is still much better than that for a HSLA niobium containing steel (steel 7).

It has been found that the ferrite films are deformation induced, and start to form at temperatures just below  $Ae_3$ . The poor ductility then spans the region from  $Ae_3$  to  $\sim 20^\circ\text{C}$  below  $Ar_3$ , when normal transformation induced ferrite forms in sufficient quantities to prevent strain concentration occurring, and ductility then recovers. The hot ductility of plain C-Mn steels is controlled by the austenite-ferrite transformation. When ferrite starts to

form from coarse grained austenite, it does so by nucleating at the austenite grain boundaries, resulting in a thin band surrounding the austenite grain. When the two phases austenite and ferrite are present together, the ferrite is generally the softer phase, and it has been shown that most of the strain becomes concentrated in this thin band. Voiding occurs around MnS inclusions at the boundary, leading to intergranular cracks which link up to give low ductility, ductile, intergranular failure [21].

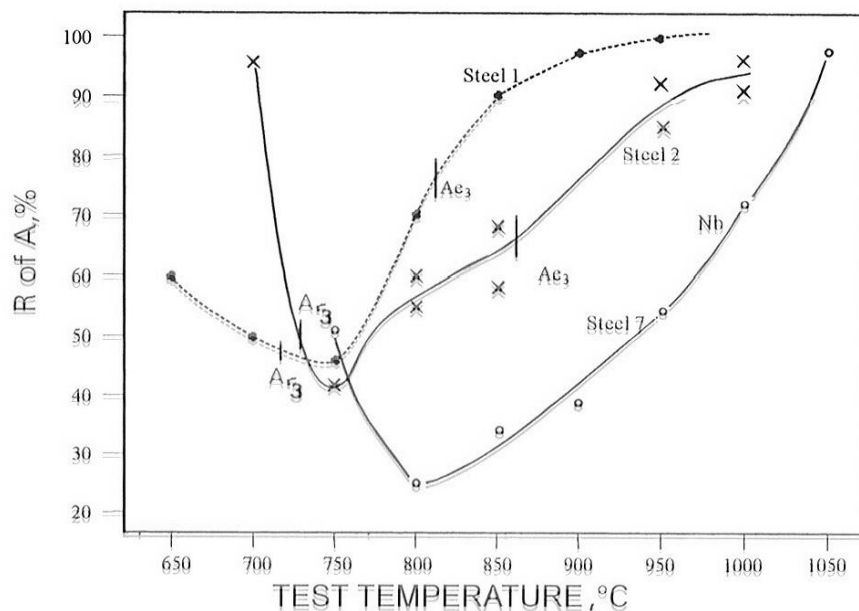


Fig.2.27 Influence of silicon on hot ductility of C-Mn-Al steels reduction of area [92]. Steels 1 and 2 have 0.3 and 1.22%Si, respectively and steel 7 is a Nb containing HSLA steel.

Silicon, being a ferrite former, raises the  $A_{e3}$  temperature, and from the work of Andrews [93], a 1% increase in silicon would be expected to raise the  $A_{e3}$  by  $\sim 60^\circ\text{C}$ . Calculations from Calphad program give a somewhat smaller increase of  $30^\circ\text{C}$ . This increase in  $A_{e3}$  with increasing silicon level is therefore in accord with the ductility trough extending to higher temperatures (Fig.2.27).

For the low silicon steel (steel 1) in Fig.2.27, the calculated  $A_{e3}$  temperature from Calphad program [94] is  $820^\circ\text{C}$ , and for the high silicon steel (steel 2) it is  $857^\circ\text{C}$ . These temperatures correspond approximately to when the ductility starts to deteriorate (Fig.2.27).

The presence of the ferrite band was noted at temperatures as high as 800°C in steels 1 and 2, which is a temperature well above their Ar<sub>3</sub> temperatures of 720 and 732°C respectively, indicating that the ferrite was deformation induced. Although these steels have 0.02% Al in solution, it has been shown that, without temperature cycling, AlN precipitation is very sluggish at these low levels, and has only small influence on ductility [21]. As the reduction of area values are in excess of 40% and this is sufficiently high to avoid transverse cracking [21], high silicon steel should be readily cast. Certainly, the presence of higher silicon steel level by extending the width of trough will make the steel more difficult to cast, but provided that aluminium levels are kept low there should be no problem.

## **Manganese**

Previous reports described hot ductility with respect to manganese and sulphur contents, and concluded hot ductility improves with increased manganese content and decreased sulphur content [17, 60, 71, 95~97]. Furthermore, a decrease in the reheating temperature and an increase in the holding time before deformation also reduce the loss in hot ductility [60, 97]. Manganese sulfides have been quoted [97] as being associated with intergranular fracture in the low temperature austenite range for C-Mn steels, where the sulphur content exceeds 30ppm or when the Mn/S ratio is less than 20. The critical ratio of manganese to sulphur to prevent embrittlement is about 30 when the manganese content is above 0.1 mass%. Lower ratios encourage, (Fe, Mn)S precipitates or segregated sulphur at the austenite grain boundaries may deteriorate the strength of the austenite grain boundary.

Kizu et al. [98] investigated the hot ductility of sulphur containing low manganese steels at a high strain rate (22s<sup>-1</sup>) more relevant to hot rolling rather than the straightening operation during continuous casting. The manganese contents varied from 0.06 to 0.26 mass%, and two sulphur contents were examined 0.0008 and 0.0209 mass%.

Fig.2.28 shows the influence of manganese content on RA for 0.005 and 0.008~0.009 mass% sulphur steels. With 0.005 mass% sulphur steels, Fig.2.28 (a), RA values are very high at temperatures above 1100°C at the manganese content of 0.06 mass%. However, with these low manganese steels, the drop in RA with decreasing temperature is large and the RA decreases as the manganese content decreases at below 1050°C. On the other hand, the improvement of RA which occurs on substantial ferrite transformation is retarded in high manganese steels. With 0.008~0.009mass% sulphur steels, RA increases with increasing manganese content in the austenite region, and the reversal of RA is not seen at high temperature. That is, in the hot tensile test at high strain rate, RA shows its minimum

value in the low temperature austenite region, and an increase in manganese content and a decrease in sulphur content improve hot ductility.

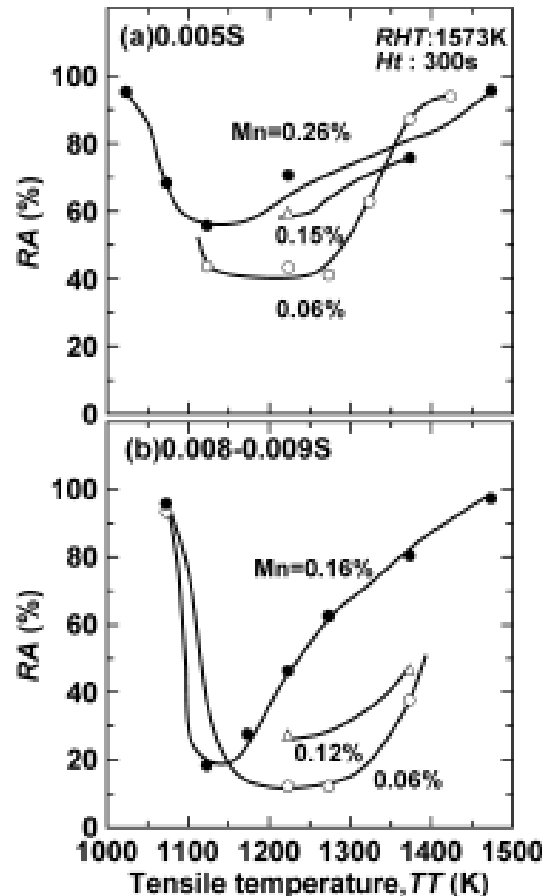


Fig.2.28 Influence of manganese content on RA at temperature of 1300°C for holding time of 300s at a high strain rate ( $22s^{-1}$ ). (a) 0.005 mass% sulphur steels (b) 0.008~0.009 mass% sulphur steels [98].

Cardoso et al. [71] state that manganese sulfides can have a strong effect on hot ductility. They have found in C-Mn steels where no precipitates are present that intergranular failure occurs due to the presence of a thin film of ferrite surrounding the austenite grains. This allows a strain concentration to be built up round the manganese sulfide inclusions. It is obvious that the more manganese sulfides that are present in the boundary regions then the easier it will be for microvoid coalescence and growth to occur. The finer the inclusion size

for a given volume fraction of MnS, then the poorer the ductility, as more of the boundary will be covered. This is the same conclusion that was reached in the case of niobium carbonitride precipitates.

In the early survey by Lankford [17], the importance of the Mn/S ratio on the hot ductility of the as-cast state was clearly shown. High Mn/S ratios were considered important to prevent the formation of the low melting point compound, FeS, which forms liquid films at the austenite grain boundaries. Theoretically, a Mn/S ratio of 1.7 is required for this purpose, but because of the marked tendency of S to segregate, much higher values are needed in practice. With the very high Mn/S ratios pertaining to HSLA steels, FeS is not a problem in these materials.

Nevertheless, there is a considerable body of work which indicates that, even when the Mn/S ratio is increased to 60/1, the hot ductility continues to improve with further increase in ratio [17]. It should be remembered that hot ductility troughs are observed in plain C-Mn steels in the absence of the microalloying additions. In this case, intergranular failure has been shown to be due to void formation at sulphide inclusions situated in the deformation induced ferrite films. Thus, the beneficial effect of raising the Mn/S ratio above 2 or 3, by reducing the S levels, can be simply interpreted in terms of the reduction in the volume fraction of MnS inclusions. Similarly, the effect of lowering the S content in reducing the depth and narrowing the hot ductility trough in as cast low Mn steels [61] is readily understood. Lankford [17] has also suggested that, in addition to reducing the volume fraction of MnS that precipitates at the austenite boundaries, the driving force for precipitation increases with Mn concentration, encouraging precipitation within the matrix rather than, more detrimentally, at the austenite boundaries.

The detrimental effect of sulphides at the boundaries increases with the fineness of their distribution, presumably because the shorter the interparticle distance, the easier it is for cracks to link up. In addition, Yasumoto et al. [60], working with low Mn steels, reported that very fine (100nm) (Fe, Mn)S precipitates form at the boundaries, leading in this way to the formation of PFZ (Precipitate Free Zones), encouraging intergranular failure. Where such fine sulphides are present, prior heat treatment and strain rate have been found to be important, as the growth of these sulphides can take place, leading to improvements in the hot ductility [60,61]. It is perhaps worth noting that the formation of (Fe, Mn)S is favoured in both low (0.6%) and high (1.4%) Mn steels when the cooling rate is slow enough to allow the intense segregation of S to the interdendritic boundaries [46].

Although increasing the volume fraction of sulphides will enable intergranular ductile failure to occur more readily when deformation induced ferrite is present, the sulphides also influence intergranular failure when failure is by grain boundary sliding in the austenite [99]. Generally, very fine particles (<50nm) are required to prevent the austenite grain boundaries from migrating, so allowing time for the cracks that may have formed to join up by grain boundary sliding [56]. In the HSLA steels, the MnS inclusions are often an order of magnitude larger than the AlN or Nb(C, N) precipitates, and are not expected to influence the hot ductility by this mechanism. However, such behaviour could arise if both coarse MnS particles are at boundaries and the fine microalloy carbide and nitride precipitates pin the boundaries. This allows strain concentrations to develop at the boundaries aiding the process of intergranular failure in this way.

Because the Mn content influences the amount of S that redissolves and is able to reprecipitate out, high Mn levels will give shallower troughs Fig.2.18 [71]. However, it should be noted that this is not likely to be so for the as cast situation, where the total sulphur content, independent of the Mn level, is available for precipitating out at the interdendritic boundaries [100].

It has been found experimentally that low (0.4%) Mn and low (0.1%) C levels favour narrower troughs although why this should be so is not always too clear (Fig.2.29) [38].

However, even at a strain rate of  $\sim 10^{-3} \text{ s}^{-1}$  and a coarse grain size of  $370\mu\text{m}$  a high Mn (1.4% Mn) steel can give narrow type trough behaviour when the S level is low, 0.001%S in solution in Fig.2.19. The increased Mn level, although slowing down the  $\gamma$  to DIF reaction, still allows full recovery in ductility to occur above the  $A_{r3}$ , although a slightly wider trough is noted [74].

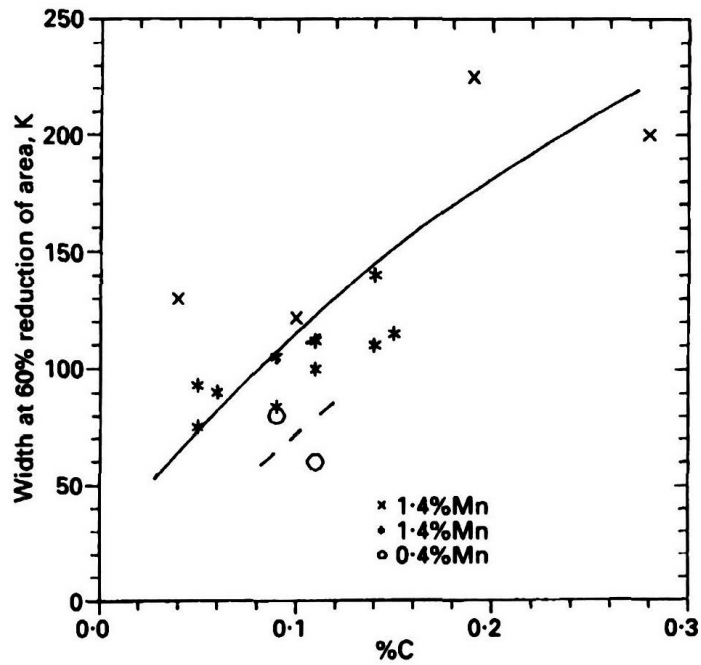
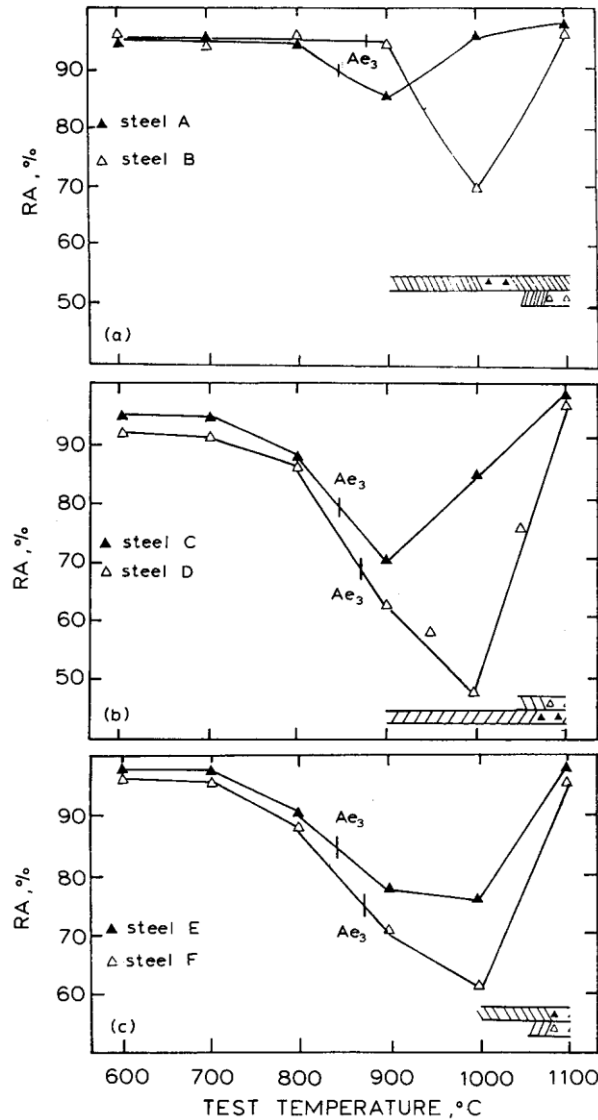


Fig.2.29 Influence of C and Mn on width of trough [38].

For microalloyed steels heated directly to test temperatures in the range 700~1100°C after normalizing, increasing the Mn content at a constant S level improves hot ductility as shown, Fig.2.30 [101]. This arises because increasing the Mn content leads to a refinement of the  $\gamma$  grain size which reduces the critical deformation required for dynamic recrystallisation.



(a) Steel A: 1.42% Mn, 0.002% S, Steel B: 0.32% Mn, 0.003% S

(b) Steel C: 1.42% Mn, 0.030% S, Steel D: 0.31% Mn, 0.032% S

(c) Steel E: 1.41% Mn, 0.007% S, Steel F: 0.29% Mn, 0.007% S

Fig.2.30 Hot ductility curves for steel A-F: occurrence of dynamic recrystallisation indicated by shaded regions [101].

Mn is the main alloying element in TWIP steel. Its principal role is to expand the  $\gamma$  phase region and stabilise the austenite microstructure of the steel. When the carbon content of steel is constant increasing the Mn level, results in the microstructure formed at room temperature being martensitic rather than pearlitic; further increase leads to a fully austenitic

microstructure of the steel. Another role of Mn is to control the SFE (Stacking Fault Energy) of steel so as to suppress the martensitic transformation. With the appropriate Mn content, the twinning mechanism is favoured.

The hot ductility behaviour of the high Mn TWIP steels has received little attention. However, these steels are becoming important and such knowledge is required to ensure slab surface cracking is not a problem in the continuous casting process and subsequent hot rolling stages. Recently, Wang et al. [102] pointed out large edge cracks occur in strips of TWIP steel (Fe-23Mn-3Si-3Al) fabricated by conventional hot rolling. They believe that lack of hot workability is the major cause for edge cracking in hot rolled TWIP steel. Liao et al. [103] also studied the surface cracking in hot rolled plates of Fe-23Mn-2Al-V austenitic steel. Fine cracks are found to be distributed on the surface of hot rolled plate. To assess the hot ductility of steels, hot tensile tests have been proven to be a very useful technique in designing optimum hot working schedules to avoid cracking during hot working.

Bleck et al. [104] have studied the processing conditions to produce the new high Mn-high C austenitic steels ( $R_m > 700\text{MPa}$ ) to determine a suitable window of process parameters. In-situ melting hot tensile tests were carried out to investigate the hot ductility, fracture characteristics and flow behaviour during continuous casting and hot deformation of 3 steels with Mn and C contents between 9~23% and 0.6~0.9%, respectively. The results showed that these steels are susceptible to interdendritic fracture at high temperatures.

Decreasing Mn content to 9%Mn improved the hot ductility of the steels. For instance, the RA values of Fe-9%Mn-0.9%C are higher than those of Fe-23%Mn-0.6%C and Fe-16%Mn-0.9%C as shown in Fig.2.31 [104]. The RA of the Fe-9%Mn-0.9%C steel is higher than 60% in the temperature range of 1050~1200°C. The hot ductility of the investigated steels is however, significantly lower compared to the conventional austenitic stainless steel 1.4301 (Fig.2.31(c)). The wide solidification ranges of high Mn steels promote segregation and shrinkage.

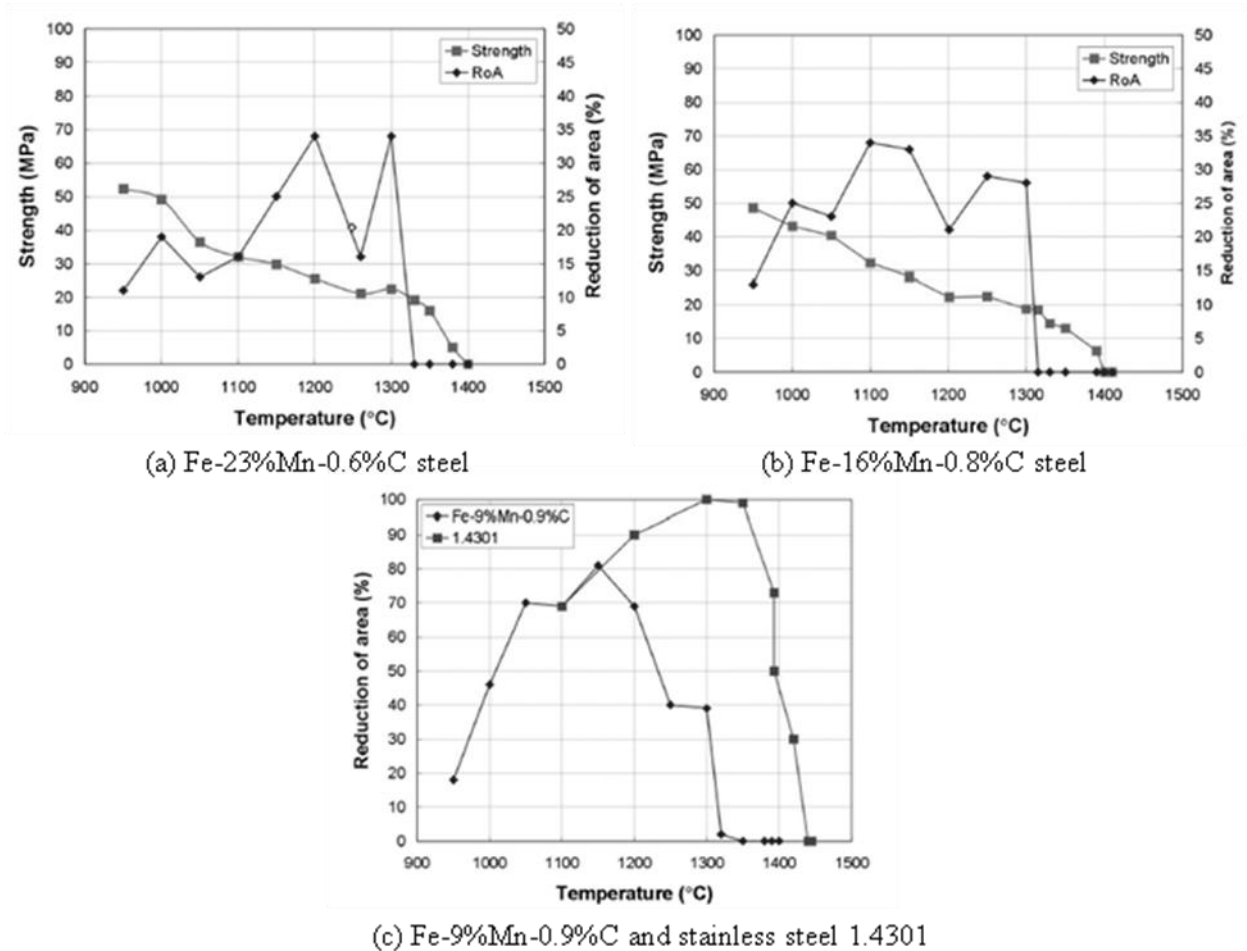


Fig.2.31 Strength and RA of TWIP steels with various Mn and C contents from 9-23%Mn to 0.6 to 0.9%C [104].

The fracture surface and EDX analyses of the Fe-16%Mn-0.8%C steel tested at 1200°C are shown in Fig.2.32 [104]. Microporosity was observed in the interdendritic areas (Fig.2.32 (b)). Precipitate droplets were found on the dendrite surface (Fig.2.32 (c)). The analysis of the droplets found high contents of S, Mn and Se (Fig.2.32 (d)). At some dendrites, rod-like precipitates of  $MnS_xSe_{1-x}$  were observed. Therefore, countermeasures to reduce microshrinkage and segregation in the primary structure are interesting aspects for developing and improving yield and quality of high Mn steels [104].

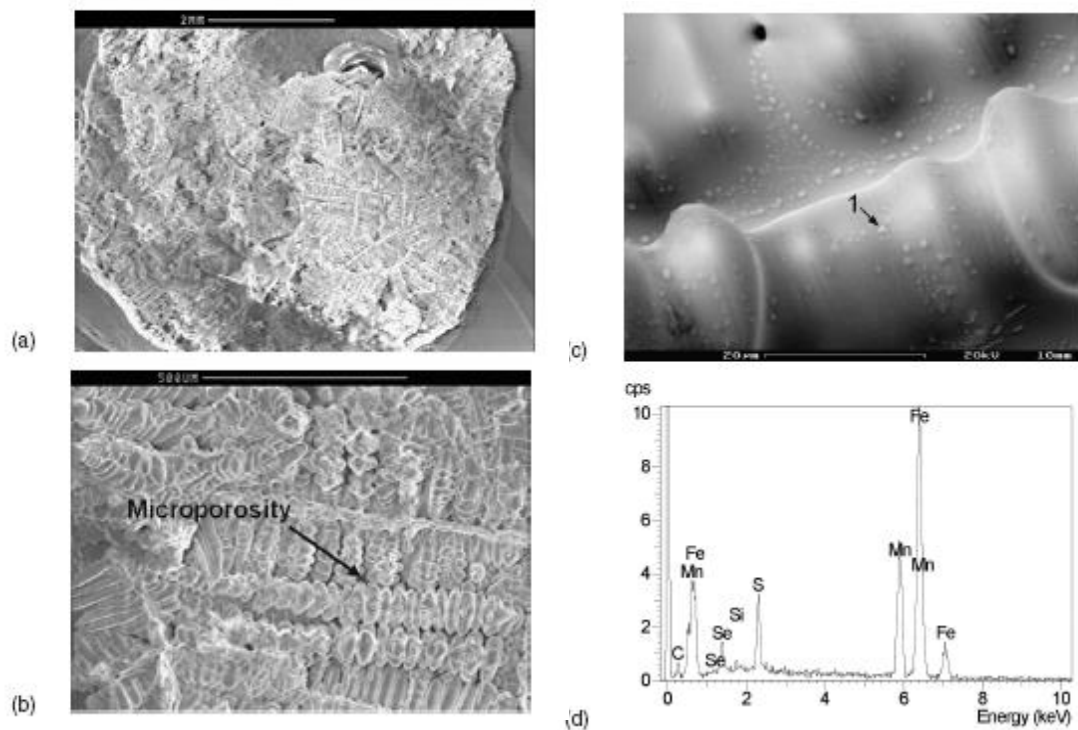


Fig.2.32 Fracture surface and EDX analyses of Fe-16%Mn-0.8%C tested at 1200°C, RA 21%: (a) At the centre position; (b) High magnification of (a); (c) Position 1 of EDX analysis; (d) Analysis of the droplet (position 1) [104].

There is limited data in the literature on the hot ductility of high Mn steels similar to those in the present work so the data that is available will be dealt with now in detail.

Hamada et al. [105] have carried out a hot ductility study of four high Mn TWIP steel using hot tensile tests in the temperature range 700~1300 °C. Their strain rate was high,  $1s^{-1}$  more appropriate to that used in hot rolling than in the straightening operation.

All four investigated steels qualitatively displayed similar behaviour over the temperature range 700~900°C. The hot ductility improved significantly in the temperature range 1000~1200 °C for the austenitic steels due to the onset of dynamic recrystallization.

The hot ductility curve for 3C16MnAl is shown in Fig.2.33. For comparison, the hot ductility curve of 6C22Mn is also included in Fig.2.33. It is seen that both steels have almost same RA values up to 1000°C. Above 1000°C, ductility continues to improve to 1200°C, the ductility being better for the lower Mn steel. The true stress–true strain curves

of both steels at different high temperatures are given in Fig.2.34. It can be observed that 3C16MnAl possesses higher strength but also higher ductility than that of 6C22Mn. It is known that Al additions strengthen steel at high deformation temperatures [106].

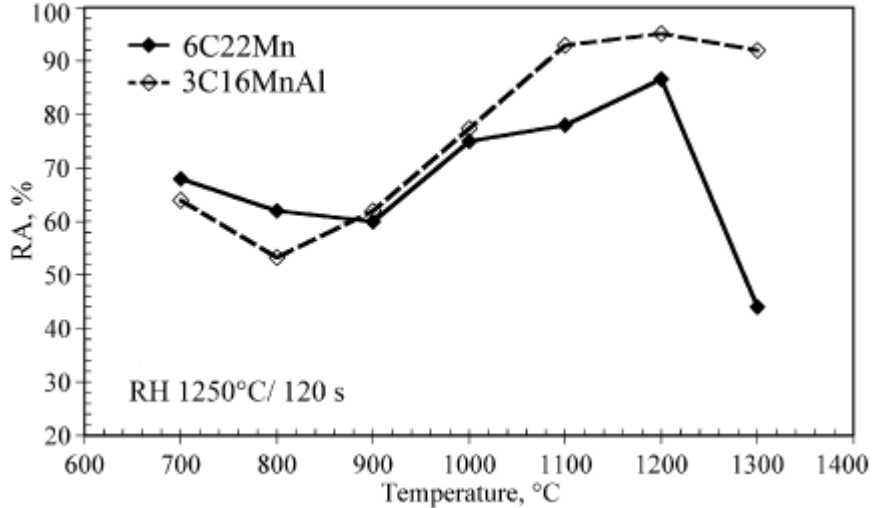


Fig.2.33 Hot ductility curve of 3C16MnAl. Curve of 6C22Mn is included for comparison [105]. (Strain rate is  $1s^{-1}$ )

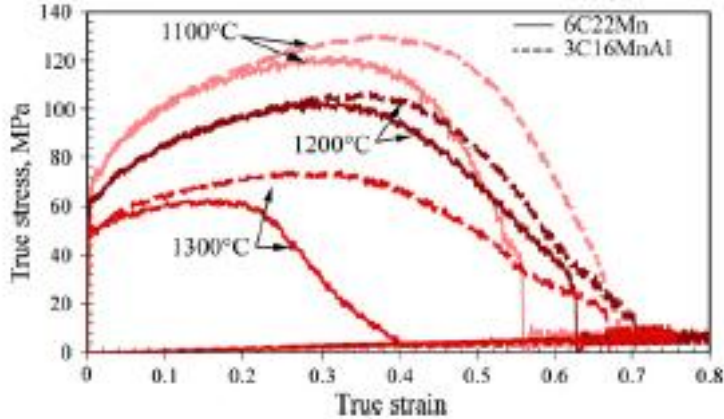


Fig.2.34 Examples of true stress–true strain curves of 6C22Mn and 3C16MnAl at high temperatures [105].

The microstructures of 3C16MnAl after the hot ductility tests at different temperatures are given in Fig.2.35. It can be seen from Fig.2.35 (a) that in the un-recrystallised state cracks form along the boundaries. At 900°C, transverse ductile intergranular cracks having a length ~200µm could be observed from Fig.2.35 (b). In principle, these cracks might cause problems during the rolling of such steels which may lead to them being scrapped. In Fig.2.35(c) it can be seen that the initial grain size is coarse with an average grain size of 136µm after reheating at 1250°C for 120s. However, after reheating at 1250°C for 120s followed by straining at 1200°C, it refines due to dynamically recrystallisation with average grain size 32µm and 13µm when the twin boundaries are included, Fig.2.35(d). Mintz and Abushosha [107] reported that dynamic recrystallisation and the movement of grain boundaries prevents the voids from linking up and thereby leads to high RA values. Such refinement of grain size by itself would lead to good ductility. Intergranular cracking as a result of grain boundary sliding was recognized as the main fracture mechanism during hot tensile tests for all the studied steels.

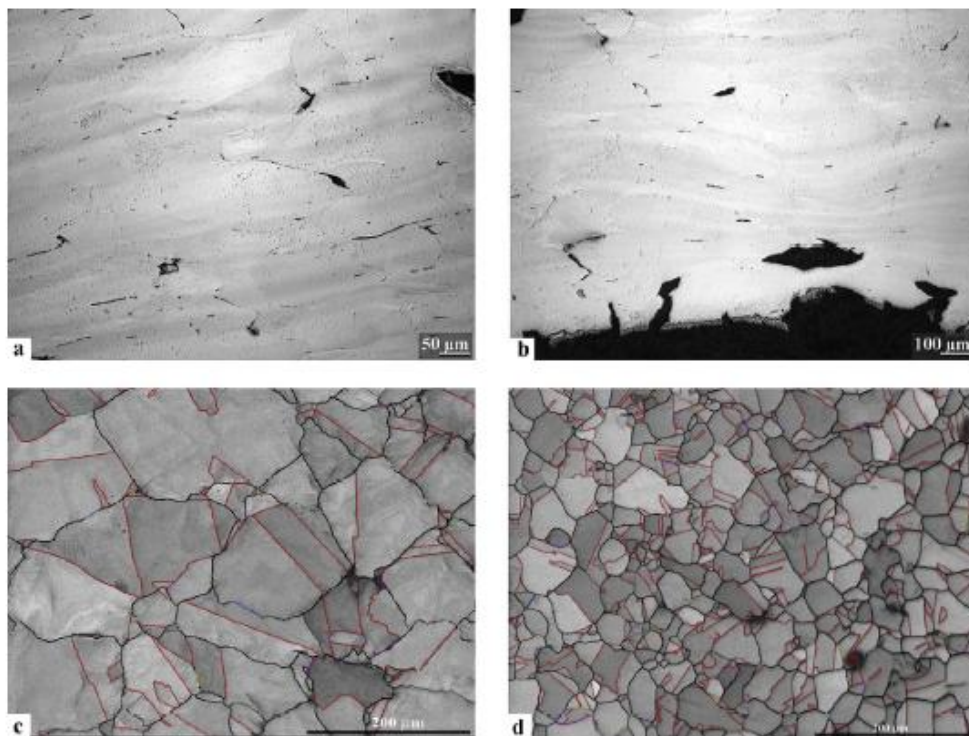


Fig.2.35 Tensile strained microstructures of 3C16MnAl: (a) fracture tip at 800°C (longitudinal cross-section), (b) transverse cross-section of a fracture surface at 900°C, (c) large grain structure after reheating at 1250°C for 120s (SEM-EBSD), (d) dynamic recrystallised structure after straining at 1200°C (SEM-EBSD) [105].

## Phosphorus

Phosphorus is an element which segregates readily to grain boundaries in both ferrite and austenite and might therefore be expected to weaken the cohesion at the boundaries and so reduce hot ductility, favouring intergranular failure [108-111].

Suzuki et al. [108] have mapped out the temperature range over which P additions will give rise to poor hot ductility and have shown its dependence on the C content for plain C-Mn steels as shown Fig.2.36. For low C steel ( $<0.2\%C$ ), they indicated that P segregation should not be a problem as shown Fig.2.37. In the case of low C steels, solidification produces a bcc structure whereas above  $\sim 0.02\%C$  solidification results in a fcc structure and the more close packed structure results in more P being rejected into the dendritic liquid. In contrast to these findings, Harada et al. [12] have suggested that both longitudinal and transverse cracking of continuous cast slabs have the same origin and this can be related to the intense microsegregation of P to regions below the roots of oscillation markings, a phenomenon that embrittles the austenite grain boundaries. They show that this can occur even at a relatively low C levels ( $0.1\sim 0.2\%C$ ) in the peritectic C composition range, a range which has been shown to be particularly susceptible to the problem of transverse cracking [14]. The micro-segregation of P takes place during solidification and cracking can be related to the formation of oscillation marks, i.e. to the manner in which the partially solidified shell is deformed and then entraps liquid high in segregation between the dendrites.

	C	Si	Mn	P	S	Al	N	O
○	.45	.21	.90	.002	.001	.026	—	—
△	.42	.24	1.2	.01	"	.023	.0035	—
□	"	"	"	.02	.004	"	"	—
◇	.41	"	1.18	.03	.003	.021	.0046	.001
●	"	"	"	.057	.004	.024	.0045	"

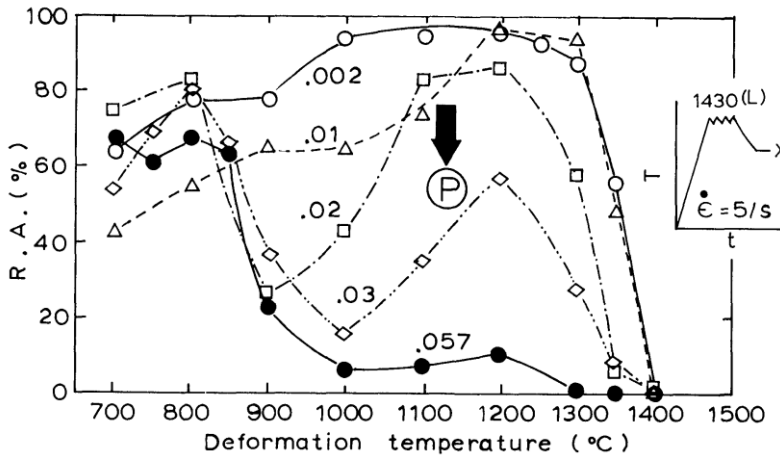


Fig.2.36 Effect of phosphorus on hot ductility in 0.4%C steels. Chemical compositions of each heat are also shown above this figure [108].

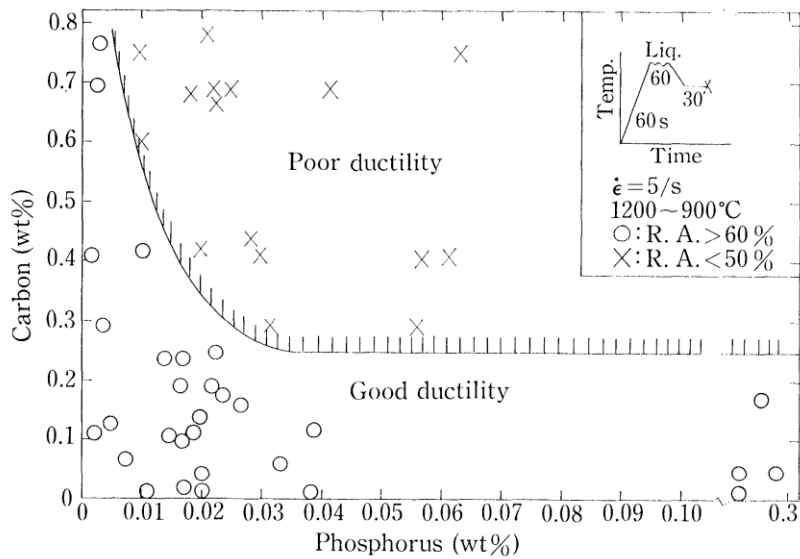
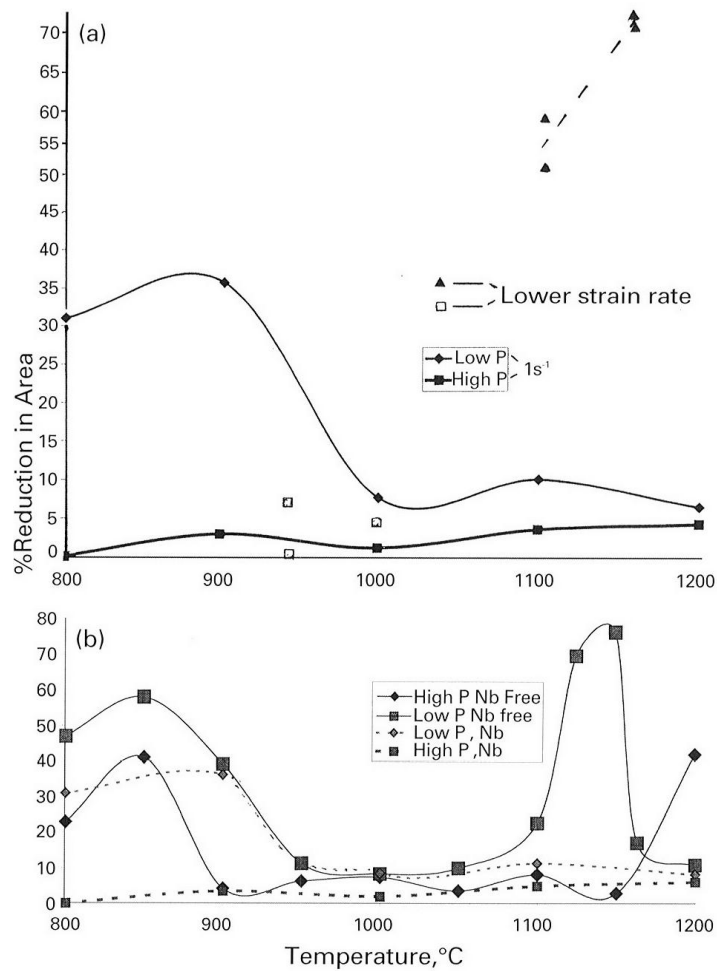


Fig.2.37 Effect of C and P content on the embrittlement. Good ductility region is defined as the region where minimum RA value is higher than 60% in the temperature range 1200 to 900°C melted samples were strained at a strain rate of 5/s [108].

Recent work by Mintz et al. [113] have also shown that in high C steels(0.6%C), high P contents(0.04~0.05%), are detrimental to hot ductility for both C-Mn-Al and Nb containing steels as shown Fig.2.38 but there is considerable evidence that for low C, Nb containing steels(<0.2%C) where the P segregation to the inter-dendritic boundaries is not intense enough to form the low melting point phosphide phase, a small addition of P(0.02%), can be actually beneficial [21]. It is believed that P occupies vacant sites which would otherwise be used to allow the detrimental precipitation of fine Nb(C, N) particles to occur.



*a* for as cast Nb containing steels C and D tested at a strain rate of 0.1 s<sup>-1</sup> (also included are a few results for tests at the lower strain rate of 7 × 10<sup>-3</sup> s<sup>-1</sup>; *b* for as cast Nb free and Nb containing steels tested at a strain rate of 0.1 s<sup>-1</sup>

Fig.2.38 Hot ductility curves for as cast high C, Nb containing and Nb free steels, with and without P [113].

There is considerable evidence in the literature that phosphorus at levels up to 0.02%P improves the ductility of the continuously cast strand at temperatures between 700~1200°C, provided the carbon content is less than 0.25% [14, 22, 90].

Phosphorus up to 0.02% has also been found by Mintz [14] to be beneficial for C-Mn-Nb-Al steels, possibly because although P is normally regarded as detrimental, it segregates to boundaries and vacant sites, preventing the precipitation of the more detrimental fine Nb(C, N) precipitation from taking place [14]. Works data and laboratory work both confirm the benefits of this P level for the Nb containing steels [14]. A similar trend has been found by Hannerz [90] using regression analysis on works data indicating that phosphorus reduces the incidence of surface defects for microalloyed and C-Mn steels. Similar benefits were noted on tensile testing. Suzuki et al. [22] have tested a plain C-Mn steel (0.05%C, 1.4%Mn) with a P range of 0.003 to 0.32%. Again hot ductility improved as the phosphorus content increased.

Mintz et al. [113] summarized that P is likely to improve the hot ductility of the continuously cast strand provided its segregation to the boundaries can be reduced so that the low melting point 'iron phosphide' phase is prevented from forming and when this occurs transverse cracking during straightening may be avoided. However, if too much segregation of P has occurred and this is most likely in the higher C steels (>0.25%), then iron phosphide interdendritic liquid will be present at a temperature well below the bulk solidus temperature. The presence of these liquid films at the austenite grain boundaries will severely reduce the ductility of as cast steel, making the cast steel susceptible to cracking both early on after casting (in the mould) and at the solidification front. In the higher C, P and Nb containing steels, the presence of both the NbC eutectic and extensive films of Fe<sub>3</sub>P lead to very poor ductility throughout the whole temperature range 800~1200°C.

## **Sulphur**

The effect of S on hot ductility in low C steels has been studied extensively [17, 60, 61]. The embrittlement is observed usually in low Mn Al-killed steels, and is well known as overheating, because the hot embrittlement accompanying  $\gamma$  intergranular fracture occurs by straining after heating above critical temperatures. The embrittlement is due to the solute S atoms, formed by coarse MnS particles dissolving owing to overheating, precipitating dynamically as fine sulphide particles during subsequent high strain rate deformation. Suzuki et al. [61] demonstrated that S is essentially detrimental in high strain rate tensile

deformation after remelting. The ductility trough found for high temperature solution treatment, 1350°C [60] ranges from 750 to 1150°C, as shown in Fig.2.39. The trough is deepened and widened significantly by either raising the solution treatment temperature or increasing the S content. It should be noted that marked hardening is observed typically in the low ductility region. This can be explained in terms of fine precipitation of sulphide particles within the matrix, as shown in Fig.2.40. In the low ductility specimens, sulphide particles are observed to form densely at the prior  $\gamma$  grain boundaries, and extremely fine sulphide particles are formed in the matrix outside the PFZs, in the vicinity of the boundaries. Such sulphide particles exhibit cubic FeS structure and consist of Fe, Mn and S as Fe rich (Fe, Mn)S. From these results, it can be seen that almost the same mechanism as that for surface cracking by carbide and/or nitride precipitation can be adopted in this case, although there are some differences in fracture mode between them.

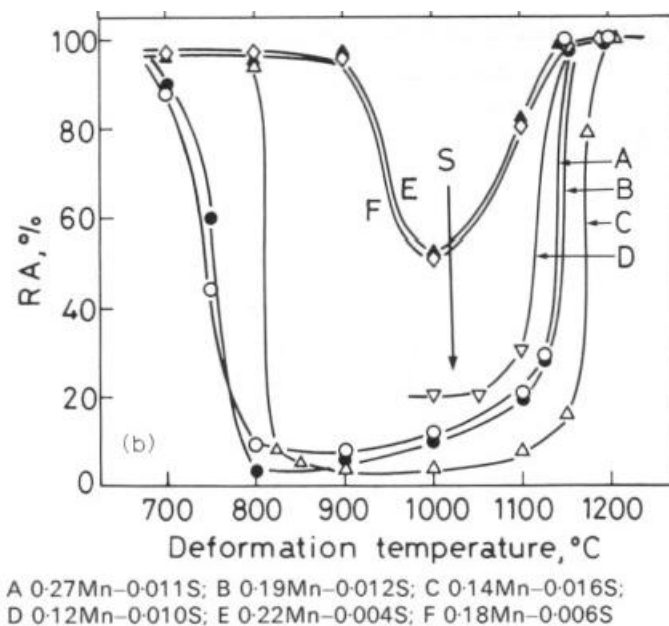


Fig.2.39 Variation of reduction of area to failure with temperature of deformation in tensile test for various steels solution treated at 1350°C:  $\dot{\epsilon}=2.3s^{-1}$  [60].

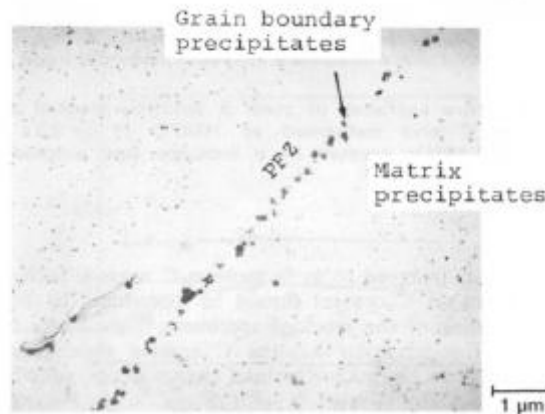


Fig.2.40 Extraction replica image showing sulphide precipitation in steel (0.05C-0.19Mn-0.012S): specimen deformed at 1000°C at  $\dot{\epsilon}=2.3\text{s}^{-1}$  after solution treatment at 1350°C [60].

At the outset it is important to note that it is the boundary regions which are embrittled by S and, in contrast to their effects at room temperature, any sulphides situated within the matrix have little influence on the hot ductility. Sulphur can impair hot ductility by weakening the grain boundary regions for a variety of reasons (a) S segregation to the boundary [114], (b) the formation of low melting point Fe-S compounds [115] and (c) the effect of Mn sulphides on the formation of cavities [15], which then link up to produce low ductility intergranular failure. Although the segregation of atomic S may play a part in influencing the hot ductility of HSLA steels, there is much evidence to indicate that it is the sulphides that have the dominating influence on fracture [46, 75, 100, 101].

Analysis of works data by Hannerz [90] invariably shows that raising the S level in steels leads to an increased incidence of cracking. Reducing the S level in as-cast steel gives improved ductility and Ca treatment has been found to be particularly beneficial [71,99]. This is not surprising as intergranular failure is favoured by having sulphides present at the boundaries and wide, deep hot ductility troughs are common even when no microalloying precipitates are present.

However, a considerable amount of work has been carried out by Koblyanski and co-workers on ultra pure Fe alloys [114], which would indicate that S segregation to the boundaries weakening the boundaries was an important cause of transverse cracking.

In contrast, other work [46, 75, 100] has suggested that in HSLA and plain C-Mn steels, it is the precipitation of fine sulphides at the  $\gamma$  grain boundaries which reduces ductility, rather than segregation. Generally, in as-cast steel, the segregation of S is so rapid and concentrations so high, that sulphide are able to form on cooling. These are not always pure MnS but often FeMnS [46, 60].

Cooling rate from the melting point to the test temperature has been shown to have a very important influence on the size of these sulphides, increasing the rate producing finer particles. The influence of cooling rate on ductility when segregation alone is important can be seen from the work of Kobayashi [95]. It is clear from Fig.2.41 that faster cooling rates prevent segregation and ductility improves. However, the cooling rates used in Kobayashi's examination are very high as was the strain rate, the exercise being designed to examine hot cracking during rolling. When more conventional cooling rates are used, 0.5~1°C/sec, and slower strain rates, then increasing the cooling rate makes the ductility worse, Fig.2.41. This is because segregation has already taken place so that precipitation of sulphides can occur. Faster cooling then produces a finer distribution of sulphides at the  $\gamma$  boundaries, which are more detrimental [78].

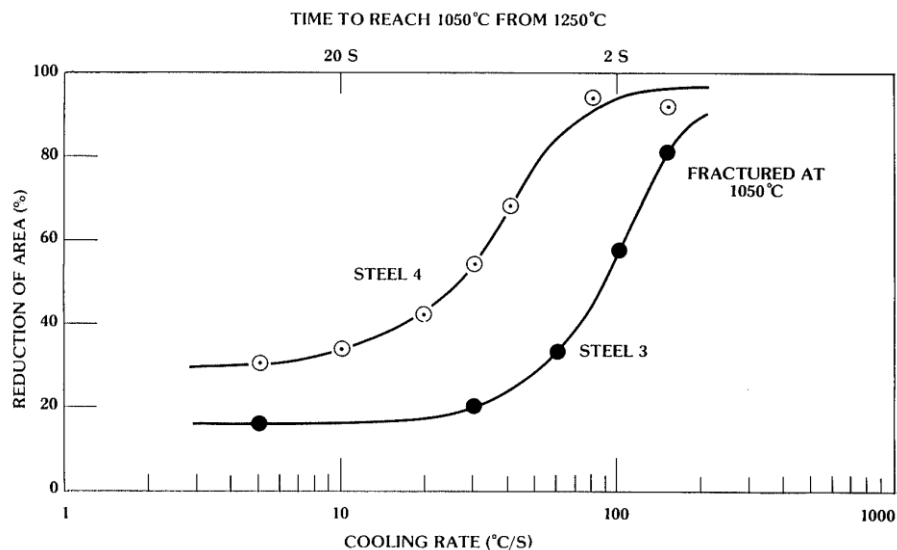


Fig.2.41 Effect of cooling rate on hot ductility of steels [95].

Vopodivec et al. [116], has also examined the role played by S in influencing the ductility, and although not coming to any conclusion with regards to the origins of the intergranular sulphides could find no S gradient in the grain boundary areas. Whereas fine precipitation of sulphides seems to be the major cause of intergranular failure during the straightening operation when there are no microalloying additions, hot cracking during rolling or forging has been found to be very susceptible to the amount of S segregated to the boundaries. This is much influenced by the composition (Mn and S levels), and processing conditions (temperature and cooling conditions), often but not always in the same way as transverse cracking.

However, Maehara and Nagamichi [117] have shown even under normal continuous casting conditions, cooling at 120°C/min and straining at  $4 \times 10^{-4} \text{ s}^{-1}$ , Nb containing steels are very sensitive to the amount of S in solution which is able to segregate to the boundaries; the greater this is the worse the ductility. They suggest that this is due to S encouraging voiding to occur at the interface between the Nb(C, N) precipitates situated at the boundaries and the  $\gamma$ . To avoid this problem they recommend that S levels should be below 0.001%. They suggest that there is little difference between the poor ductility often noted at high strain rates and that observed at low strain rates both being due to S segregation. However, in the Mintz et al's experience [75, 101], it is the amount of S in solution either at solidification or when solution treated that subsequently segregates to the  $\gamma$  boundaries and then re-precipitates on cooling in the form of fine sulphides which are responsible for the ductility trough in plain C-Mn steels. Such an explanation would be entirely in keeping with Maehara and Nagamichi's results. For their high Mn steel only 0.001% S would go back into solution and therefore, only when the S level was less than this would there be any improvement in ductility in accordance with their observations. For lower Mn levels more will go into solution and ductility will start to improve as the S level is reduced below this higher value.

Inoe et al. [118] have looked at the influence of both S and P on the hot ductility of a steel with 0.16%C and 0.6%Mn. The S level varied from 0.003 to 0.009%, (Mn/S ratio of 200:1 and 66:1) and P was examined at two levels, a trace and 0.017%. At these high Mn/S ratios little influence could be found of the S level on the hot ductility as shown Fig.2.42. Also, these steels were solution treated not as-cast. However, the steel with both ultra low S (0.0006%) and P (<0.001%) gave the best ductility, open square in Fig.2.42. Increasing the holding time, at temperatures above the  $A_{r3}$  to over 20min prior to testing, resulted in a marked improvement in ductility for the P containing steels as shown in Fig.2.43 due to re-precipitation and coarsening of the MnS inclusions [118]. Abushosha et al have, however, also shown that for plain C-1.4%Mn steels even in the as-cast condition, increasing the S from 0.002 to 0.016% only causes a small deterioration in the hot ductility. Furthermore, the same change in S levels for a Nb containing steel only resulted in a slight deterioration of the ductility [100].

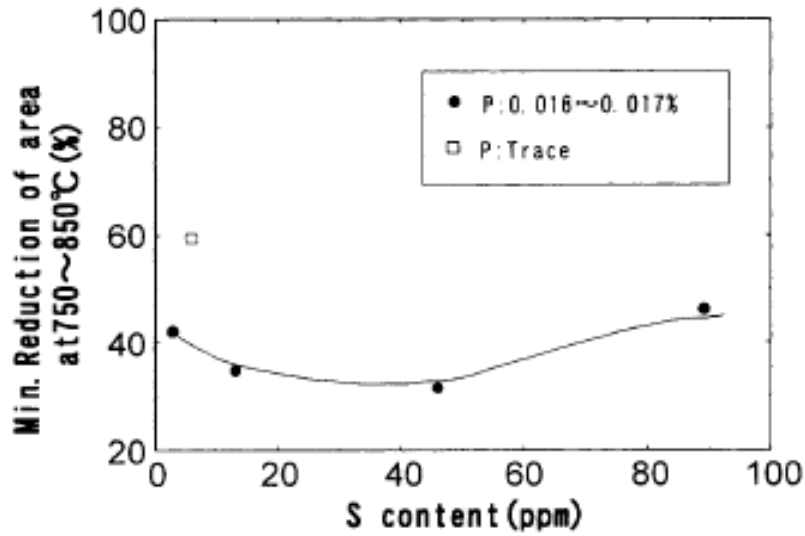


Fig.2.42 Effect of sulphur and phosphorus on hot ductility, strain rate  $2 \times 10^{-3} \text{ s}^{-1}$  [118].

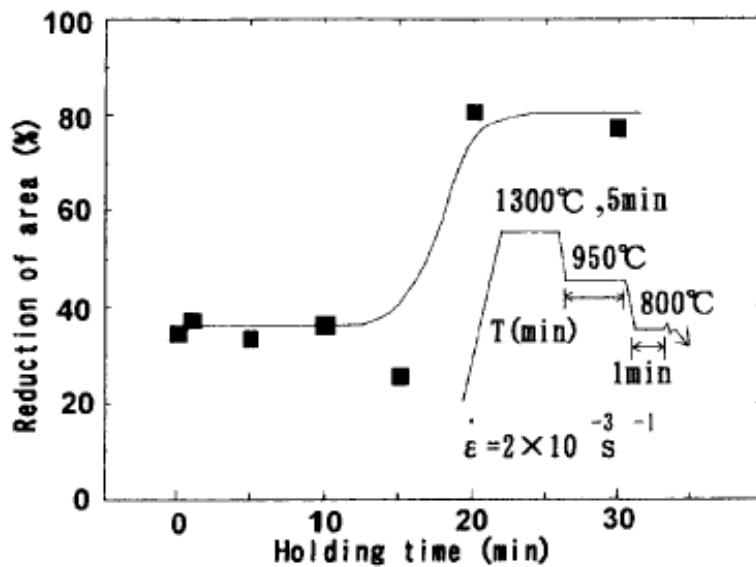


Fig.2.43 Effect of holding time on hot ductility of a 0.16% C steel [118].

As with Ti, the effect of S on the hot ductility of Nb steels also depends upon the thermal cycle used in the test. For steels reheated to a solution temperature prior to testing, S has little effect on hot ductility [46]. However, for in-situ melted test pieces increasing S levels have a detrimental effect on hot ductility, as the more S that is present in solution, the more is available to precipitate out on grain boundaries [107].

## Aluminium

Al additions to steels have always created problems when it comes to continuous casting and if not controlled can lead to transverse and edge cracking of the continuously cast slab [20, 21]. The problem results from the formation of AlN which forms preferentially at the austenite grain boundaries often in a wafer thin plate morphology which for low Al contents, <0.08%Al can be very difficult to extract for examination under the electron microscope [20, 21]. These precipitates can pin the austenite grain boundaries encouraging grain boundary sliding and the development of inter-granular cracks. Previous work [119] has shown that for C-Mn-Al steels, it is important not to exceed 0.04% as an addition, if ductility is not to significantly deteriorate. In the case of Nb-Al containing steels, it is believed that it is not so much the AlN precipitation, that is responsible for the poor hot ductility but the observation that Al additions refine the intra-granular niobium rich precipitation; the finer the precipitation the worse being the ductility [14]. The low ductility values were therefore attributed to the precipitation of niobium carbonitride.

However, there is marked evidence [120] to show that increasing the aluminum level of C-Mn-Al steels causes a drop in the hot ductility. This would suggest that under certain circumstances, aluminum nitride precipitation will occur. Work by Crowther et al. [59] has shown that aluminum nitride does not precipitate dynamically. Aluminum nitride will not precipitate unless the  $[Al] \times [N]$  exceeds  $3 \times 10^{-4}$ . Mintz and Arrowsmith [14] established that increasing the soluble aluminum content of steel from 0.02% to 0.07% caused a reduction in the interparticle spacing, and a reduction in the mean particle size.

Subsequent work by Cardoso et al. [71] on C-Mn-Al steels has shown that the ductility trough in these steels is due to the production of thin films of deformation induced ferrite which form within the  $Ar_3$  and  $Ae_3$  temperature range. As the strain concentrates in the ferrite film, microvoid coalescence occurs around the manganese sulphide inclusions situated within the boundaries. The recovery of ductility at high temperatures is due to dynamic recrystallisation of austenite, as long as the temperature is above  $Ae_3$ . The recovery of ductility at lower temperature is due to the presence of significant amounts of ferrite which distribute the strain more uniformly. Cardoso et al. [71] have also shown that an increase in the aluminum level in C-Mn-Al steel extends the ductility trough to higher temperatures and this is related to the aluminum nitride which has precipitated out, delaying the onset of dynamic recrystallisation. In this work the  $[Al] \times [N]$  value is  $4.25 \times 10^{-4}$  which is above the level quoted earlier [79]. AlN when it precipitates out of solution is particularly damaging to ductility and there is increasing evidence [122, 123] that it can precipitate out from the melt as a very thin film, which covers the austenite grain surfaces. This may

account for the great difficulty in finding microscopic evidence for AlN precipitation.

Previous hot ductility work [21] has been mainly concerned with steels with  $<0.08\%$  Al but the recent interest in the development of TRIP (transformation induced plasticity) assisted steels has widened this interest in Al to much higher levels 1~2% Al. Aluminium in the same way as silicon, can slow down the precipitation of carbides in bainite allowing retained austenite of high carbon content, (1~2% C) to be formed at room temperature in a mainly ferritic structure. This can subsequently transform to martensite on deformation and so strengthen up regions which would otherwise neck down to failure during press forming. Whereas, the conventional high Si levels of TRIP steels can give surface problems on galvanising, this is not believed to be the case for Al or P [121].

Recent work [92] has examined the hot ductility of two very high Al containing, P free TRIP steels, one containing 0.98% Al and the other 1.93% Al as shown in Fig.2.44. Ductility for the 0.98% Al steel was found to be poor, particularly in the temperature range 750~850°C presumably due to a combination of AlN precipitation and the presence of thin bands of ferrite surrounding the austenite grain boundaries. In contrast, the steel with 1.93% Al, gave very good ductility. Although AlN was precipitated in large amounts, the precipitation was always coarse and more importantly a large volume fraction of ferrite was always present, since it was not possible to form  $<45\%$  ferrite with this composition, and therefore strain concentration was prevented.

It has been found with lower additions of Al ( $<0.08\%$  Al) that precipitation of AlN extends the trough to higher temperatures [71]. Although, the control that is required to prevent transverse cracking with normal aluminium additions to C-Mn-Al and C-Mn-Nb-Al steels is well established ( $<0.04\%$  Al), with the development of this new breed of TRIP and TWIP steels which can have very high Al contents, 1~2% Al, considerable research work is being carried out to establish their optimum casting conditions.

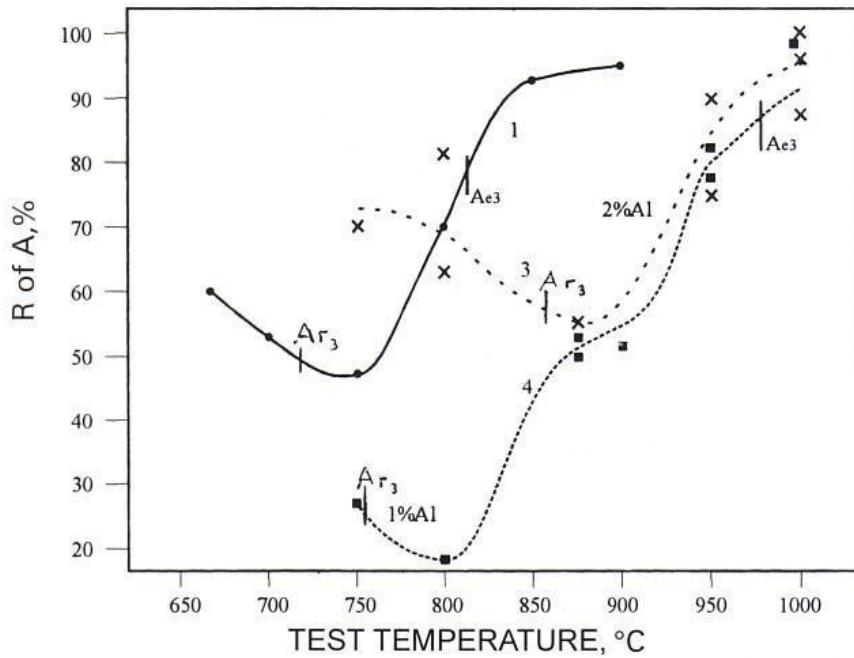


Fig.2.44 Influence of Al on the hot ductility of C-Mn-Al steels [92]. (N and S levels were ~0.005 and 0.006%, respectively)

Increasing the Al level from 0.03 to 0.41% in steels with a very low N level ~0.002% has been shown to lead to a progressive widening of the trough due probably to the increase in the  $A_{e3}$  by the Al in solution and the presence of the ferrite band to much higher temperatures, solid lines in Fig.2.45 [124].

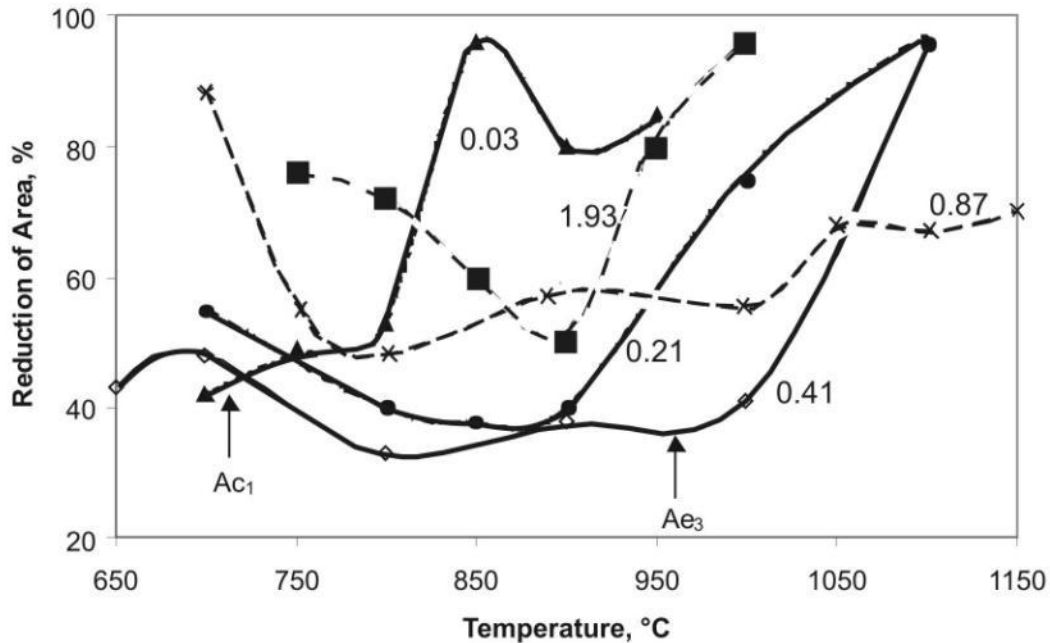


Fig.2.45 Hot ductility curves for high Al containing steels showing that increasing the Al level from 0.03 to 0.87% widens the trough. However, at the higher Al levels, the depth of the trough becomes shallower. The steels contained 0.2% C, and 1.4% Mn with varying P levels [124].

A very wide trough was present when testing steel with 0.87% Al, Fig.2.45. For this steel, the  $A_{e3}$  temperature was  $980^{\circ}\text{C}$  and the temperature when all the AlN precipitation goes back into solution is  $\sim 1200^{\circ}\text{C}$ . The ductility can be seen to exceed 40% RA at the 0.87% Al level but such good ductility is probably a result of the very low N and S level in this steels.

Recently, Tuling et al. [122], have examined the influence of Al in the range of 0.05%~1.5% on Nb containing TRIP steels. The curves for these steels are shown in Fig.2.46, and it can be seen that the best ductility is given by the 1.5% Al steel. The low Al steel has poor ductility at  $750^{\circ}\text{C}$ , but it starts to recover at temperature  $> 800^{\circ}\text{C}$ . The 1% Al containing steel not only has deep trough, it is also very wide, stretching up to  $1000^{\circ}\text{C}$  before ductility materially starts to improve.

Generally, at low Al levels, AlN is not detected. When the test temperature is above  $1000^{\circ}\text{C}$  in Nb containing steel, ductility is good, as dynamic recrystallisation can take place and the precipitates are coarse and few [14, 23]. A similar behaviour is noted here for higher Mn, low Al steel. The absence of AlN precipitation means that the ductility behaviour noted in

Fig.2.46 can be ascribed to a combination of having a thin film of ferrite present concentrating the strain, which encourages intergranular failure and at high temperature above the  $Ae_3$  (795 °C), the presence of Nb(C, N) delaying dynamic recrystallisation.

Increasing the Al to 1% considerably widens trough (Fig.2.46) and, from the TEM work, results in the copious precipitation of AlN at prior  $\gamma$  grain boundaries, causing ‘rock candy’ type failures. Although Nb(C, N) is precipitated in the lower temperature range, it is the AlN precipitation that is controlling ductility in this steel. However, a further increase in Al level to 1.5% leads to much better ductility and a return to the narrower trough given by the 0.05%Al steel since at this high Al level the steel is outside the peritectic and most of the AlN precipitates in a coarse form in the delta phase and so is ineffective in influencing ductility. A major difference between 0.05 and 1.53%Al was that increasing the Al level changed the steel from hypo-peritectic to hyper-peritectic, but both steels avoided the peritectic C range, which has been shown to particularly susceptible to cracking during continuous casting. In contrast the 1%Al containing steel sat squarely in the peritectic range leading to a coarse grain size and copious precipitation of AlN in a dendritic form at the austenite grain boundaries.

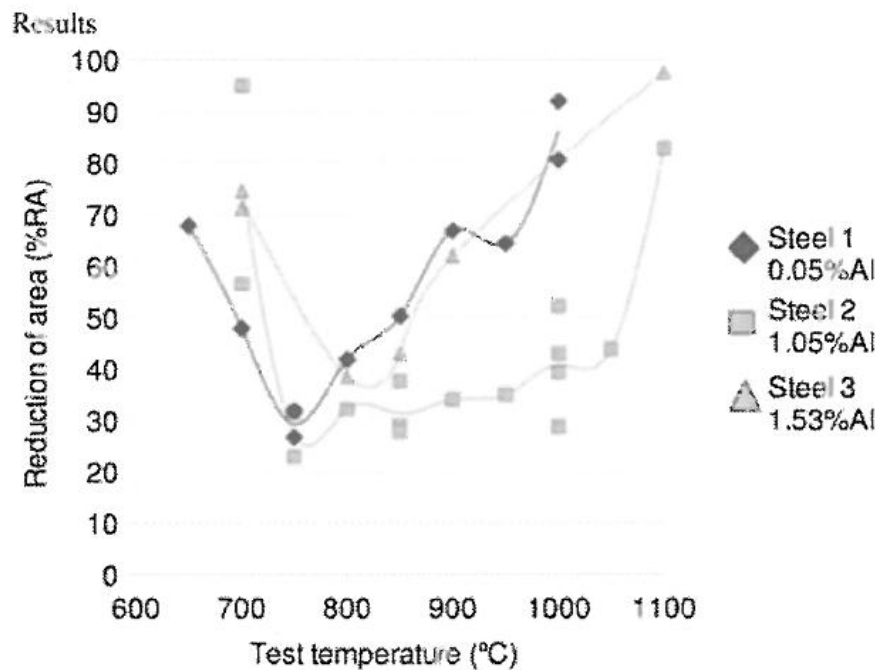


Fig.2.46 Hot ductility for three steels under examination [122].

## Niobium

Niobium is a popular micro-alloy in HSLA (High Strength Low Alloy) steels as it is both a grain refiner and precipitation hardener. Niobium has been frequently found to cause transverse cracking. Hot tensile testing has found that there is a widening and deepening of low ductility troughs as the Nb content increases. This has been explained as Nb(C, N) precipitation pinning austenite grain boundaries and aiding grain boundary sliding and intergranular fractures [14].

There have been a very large number of studies of the effect of Nb on hot ductility, and the activity in this field is probably related to the perceived detrimental effect of Nb on slab surface quality [14, 23, 39, 42, 61, 90, 125, 126]. These results can be summarised by saying that Nb additions deepen and broaden the ductility trough extending the trough to higher temperatures. Nb additions of as little as 0.017% has a detrimental effect, and ductility continues to deteriorate up to at least 0.074%. Typical results are shown in Fig.2.47 [23].

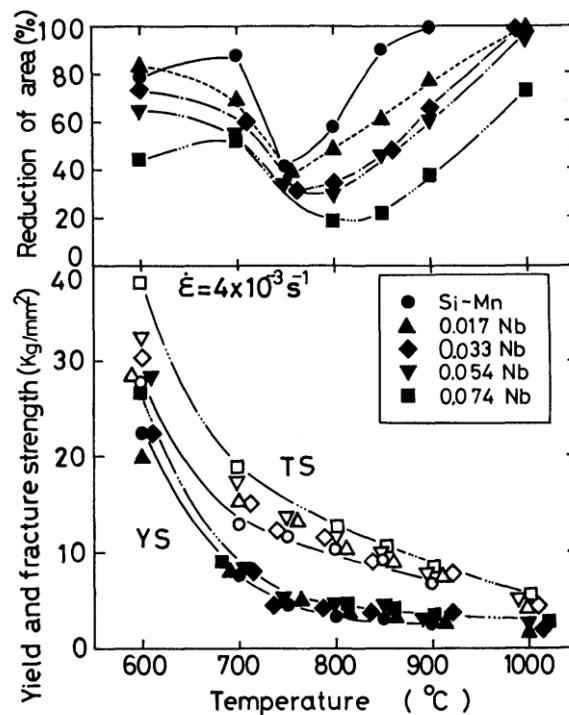


Fig.2.47 The effect of Nb contents and deformation temperature on hot ductility [23].

Mintz and Crowther [37] have explained that Nb containing steels are found to be one of the steel groups most prone to transverse cracking during continuous casting for the following reasons:

- (i) Nb has a powerful influence in decreasing the  $A_{r3}$  so widening the trough at the low temperature end [44].
- (ii) Nb precipitates out very rapidly as Nb(C, N) in a fine form in the  $\gamma$  on deformation in the temperature range of the straightening operation. The increased matrix strength encourages grain boundary sliding in the  $\gamma$  and void formation in the ferrite film so increasing the depth of the trough. The precipitates at the boundaries make it easy for cracks to interlink giving intergranular failure [21]. The presence of precipitates also widens the trough at the higher temperature end.
- (iii) Often there are coarser Nb(C, N) precipitates at the  $\gamma$  grain boundaries which are surrounded by a soft precipitate free zone. These soft precipitate free zones behave in a similar manner to the ferrite film so that poor ductility continues for temperatures in excess of the  $A_{e3}$ , so widening the trough at the high temperature end [21].

Nb is of course added for its ability to refine the  $\gamma$  grain size and provide precipitation hardening so that high strength and toughness can be achieved in the final product but the same precipitation of Nb(C, N) which causes these desirable qualities also make it more difficult to cast these steels.

Work by Mintz and Arrowsmith [127] has however, shown that the deterioration in hot ductility is progressive throughout the range 0.004 to 0.011%N and changes in ductility are relatively small, Fig.2.48. This is probably because an increase in the nitrogen level will have only a small influence on the volume fraction of Nb(C, N) that is precipitated out. Compared to the other microalloying additions, Nb(C, N) precipitates out very rapidly during deformation and often all or a very large part of the Nb is precipitated out in the time of the test at these low strain rates, (i.e., equilibrium conditions are achieved), Fig.2.49 [100]. Again, because the N level would not be expected to have much influence on the volume fraction of Nb(C, N) that is precipitated, the detrimental influence of N on transverse cracking is most likely related to the enhancement of AlN precipitation, which occurs during the temperature oscillations to which the strand is subject.

Clearly, whatever the exact mechanism of embrittlement it is nevertheless, important to keep the N as well as the Al levels as low as possible. Raising the Nb level at constant N level, as would be expected, also causes the hot ductility to deteriorate [23, 42, 127] as well as encouraging transverse cracking [23, 24].

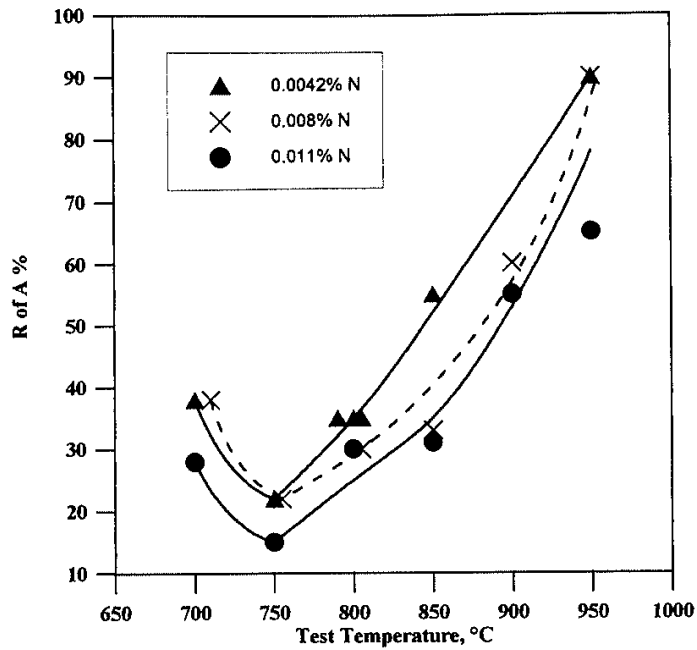


Fig.2.48 Influence of N on hot ductility of C-MnNb-Al steels (Sol. Al, 0.032~0.042%, Nb, 0.034%) [127].

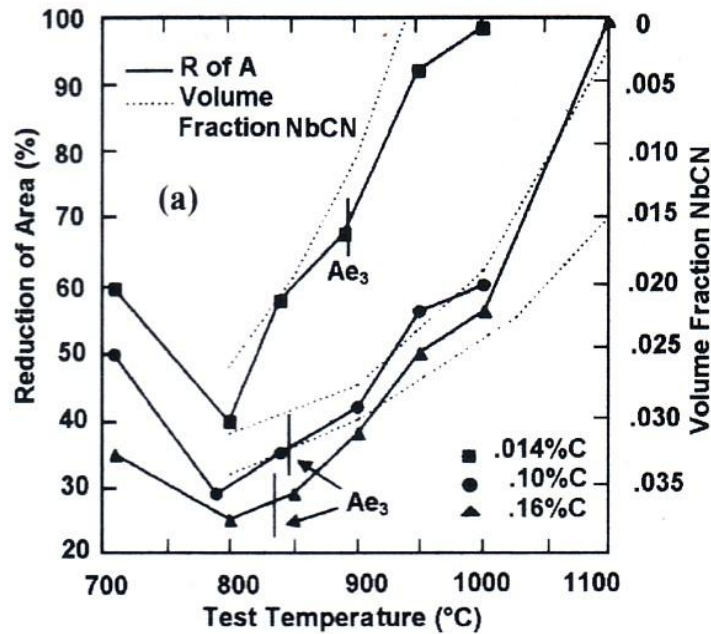


Fig.2.49 Hot ductility curves for C-Mn-Nb-Al steels (solid lines) and calculated curves of the volume fraction of Nb(C, N) precipitated as a function of the test temperature assuming equilibrium is achieved (dotted lines) [100].

Al additions to Nb containing steels deepened and broadened the ductility trough [14, 15, 125], as did increasing N contents [23]. When expressed in terms of Al×N, the combination of increased Al and/or N was also detrimental to the hot ductility of Nb containing steels.

C-Mn-Nb-Al steels are notoriously hard to cast as the presence of both Nb and Al produce a fine Nb(C, N) precipitate within the grain matrix which concentrates strain at the austenite boundaries [14]. Further to this, Nb has been attributed to hinder dynamic recrystallisation so reducing the hot ductility. This can be explained by the critical strain for fracture propagation being lower than that needed to activate dynamic recrystallisation. Metallographic work has shown that there is no recrystallisation of coarse austenite grains during the hot ductility test [42].

In C-Mn-Nb steels, it was found that the Nb(C, N) precipitation was main culprit in reducing hot ductility and not the prevention of dynamic recrystallisation [42]. In general terms, Nb(C, N) is seen as having a large affect on grain boundary mobility and that refinement of this precipitation by techniques such as increasing the cooling rate, further reduces hot ductility [14].

When examining the influence of Ti additions on the hot ductility of Nb steels, care must be taken to ensure that the thermal cycle is appropriate to continuous casting conditions. It is common practice when performing hot ductility tests to carry out a solution treatment at a high temperature, prior to cooling down to and testing at a lower temperature. Whilst this is acceptable for many steels, for steels containing Ti, it can lead to the formation of a fine austenite grain size, due to the grain boundary pinning effects of TiN precipitates which are stable to high temperatures. Thus there are several reports of the apparent benefits of Ti additions to hot ductility, but when the finer grain sizes of these steels are taken into account, the benefits are not as apparent [126, 127], Fig.2.50. Thus for simulating the continuous cast condition for Ti containing steels, it is particularly important that the test pieces are melted in-situ. When only tests from samples melted in-situ are considered, Ti additions to Nb steels have only a very small beneficial effect on hot ductility, or even a detrimental effect, and it is believed that this is due to the influence of Ti:N ratio in controlling precipitate size [21]. If compositions and cooling conditions are carefully chosen so that a coarse precipitate size is obtained, then good ductility can be achieved in Nb-Ti steels. The picture is complicated further still by cooling rate effects; at relatively slow cooling rate of 25°C/min, Ti can give a large improvement to the hot ductility of Nb steels, again due to the formation of coarse precipitates [79].

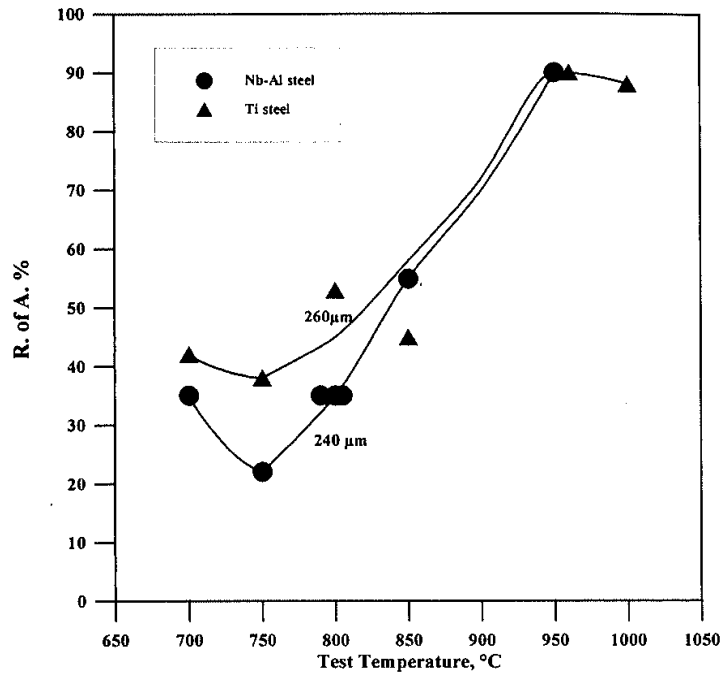


Fig.2.50 Influence of a 0.04%Ti addition to hot ductility of Nb steel containing 0.004%N for similar grain sizes [21].

## Vanadium

Vanadium is added to a number of structural steels. The hot ductility behaviour of the vanadium bearing steels has been found to be similar to those of C-Mn steels.

There have been several studies of the influence of V on hot ductility using hot tensile tests [15, 90, 112, 128~130]. It is known that high V, high N steels are susceptible to transverse cracking [15]. Hannerz's[90] statistical analysis of work's data gave only a small detrimental effect of V on transverse cracking but only a few V containing steels were included in the analysis. Hannerz's hot ductility work [90] suggested that with a high N steel (0.016%N), the V content had to be in excess of 0.07% to produce a significant deterioration in ductility.

Mintz and Abushosha [112] have carried out a more detailed study of the effect of vanadium on hot ductility and typical results are illustrated in Fig.2.51. The results from all the various studies are consistent in that V additions of up to 0.1% at low N contents (<0.005%) have only a small detrimental effect on hot ductility. At higher N levels, the effect of V additions becomes more marked, and the ductility trough becomes deeper and

broader. In fact, a good relationship can be constructed between the product  $V \times N$ , and the depth and breadth of the ductility trough, Fig.2.52 [112]. It should also be noted that in this example it is only at the highest  $V \times N$  product,  $0.1\%V \times 0.01\%N$ , that hot ductility approaches that of a  $0.028\%Nb$  steel of otherwise similar composition.

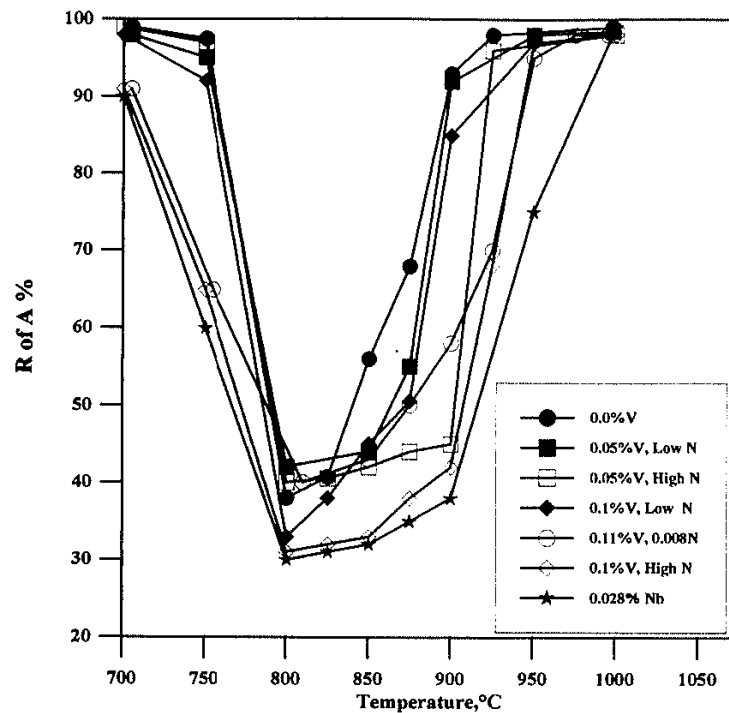


Fig.2.51 Hot ductility curves for a series of steels having different levels of V and N. (also included is a curve for a Nb containing steel for comparison). Steel were solution treated at  $1330\text{ }^{\circ}\text{C}$  [112].

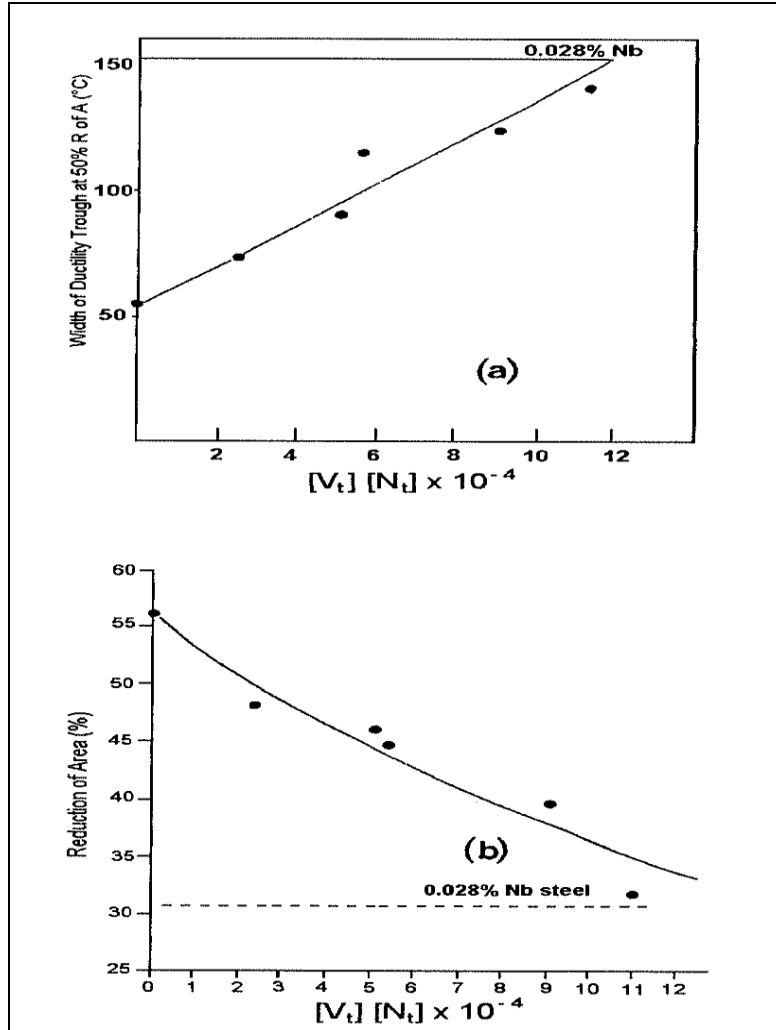


Fig.2.52 (a) Effect of product of total V and N contents on the width of the trough, (b) Influence of product of total V and N contents on RA values; steels were tested at 850°C in the trough [112].

It is apparent from these curves that the ductility decreases with increase in V and N levels but provided the product  $[V_t] \times [N_t]$  is  $1.2 \times 10^{-3}$ , e.g. 0.1%V and 0.012%N, V-N steels will show a reduced propensity to cracking compared with a conventional Nb containing steel. It should be noted, that again, no AlN precipitation was observed in any of these steels, all the nitrogen being combined with the vanadium. Wilson and Gladman [130] have also noted that VN can form in preference to AlN, despite the greater thermodynamic stability of the latter. Precipitates were coarser in the V containing steels than in the Nb steel probably as a result of the higher solubility of V in the austenite compared to Nb. Thus V is less detrimental to

ductility than Nb because it precipitates in a coarser form and a greater volume fraction of precipitate is required to cause the ductility to deteriorate.

Banks et al. [128] have noted that using cooling rates applicable to thin slab casting; a small addition of Nb (0.015%) can actually be of benefit to the hot ductility of high V (0.085%) low C (0.05%) steels with N contents in the range 0.0065 to 0.012%. Improved ductility in the temperature range 800~900°C occurred and stress relaxation tests showed that this was due to Nb delaying dynamic and post dynamic precipitation of NbV(C, N). The combination of Nb with V looks very attractive as a means of tackling the problem of transverse cracking in these HSLA steels and there is a need for more research on this, particularly on the hot ductility of higher N steels.

## **Boron**

Microalloyed steels with strong carbide forming elements such as Nb have been the subject of numerous investigations because they are particularly susceptible to transverse cracking [80, 100, 131].

A considerable amount of research has been conducted to improve the hot ductility of Nb-containing steel, mostly by addition of alloying elements such as Ti [78, 79, 131], Ca [99], Zr and Y [81]. B has been considered as another possible element likely to enhance the hot ductility in similar grades. At low temperatures where austenite and ferrite phases coexist, such beneficial effect of B was suggested to be due to the precipitation of  $Fe_{23}(B, C)_6$  in the matrix [132]. This precipitate acts as the preferential sites for the intragranular nucleation of ferrite. In this way, less ferrite is available to form at grain boundaries. This not only decreases the number of voids and cavities formed at grain boundaries, but also makes the austenite grain interior more deformable because of the soft intragranular ferrite. The final result is an improvement in the hot ductility.

It has been suggested that B improves the hot ductility by reacting strongly with nitrogen in a similar way to titanium [90]. Hence, less nitrogen will be available for precipitation of the detrimental Nb(C, N), which is known to be responsible for the loss of hot ductility in the Nb-containing steel. On the other hand, it can be argued that BN precipitation resembles that of Nb(C, N), resulting in grain boundary embrittlement.

Some production statistics have clearly pointed out the beneficial influence of boron on hot ductility [82, 90]. This improvement can be ascribed to several factors such as preferential BN precipitation, retardation of the austenite/ferrite transformation, which presumably

avoids ferrite film formation at austenite grain boundaries, and increasing resistance to grain boundary sliding during straightening operation, which results in better creep ductility [90].

Boron additions can improve the hot ductility as shown by the work of Loprez-Chipres et al. [133]. They examined a low C, 0.04%C, 0.025%Al steel with 0.008%N and found that the hot ductility markedly improved as the B/N ratio increased from 0.33 to 1.25, (the stoichiometric ratio for BN is 0.8); the minimum depth at 800°C increasing from an RA value of 45 to 70%, as shown in Fig.2.53. The cooling rate in their work was 100°C/min. The improved ductility of the boron microalloyed steels is associated to the enhanced grain boundary cohesion and an easier flow in the austenite lattice, where grain boundary segregation and precipitation of boron have an important role.

It has been reported that in contrast to impurities such as P and S which segregate to grain boundaries causing the hot ductility to deteriorate, B can improve the ductility. Thin proeutectoid ferrite layer formation and the precipitation of carbides or nitrides of V, Ti, Nb, Al or B at austenite boundaries cause ductility to deteriorate [19, 20, 100, 134~137]. Soluble boron in steel can strongly segregate towards boundaries at high temperature and occupy the thickness of about several atom layers near boundaries [138]. Accordingly, Lagerquist and Langenborg [139] showed that the addition of boron to an alloy can reduce grain boundary sliding and improve creep ductility. At low temperatures (700°C) where recrystallization is absent, recovery of hot ductility is related to a high volume fraction of ferrite so that strain concentration does not occur [107].

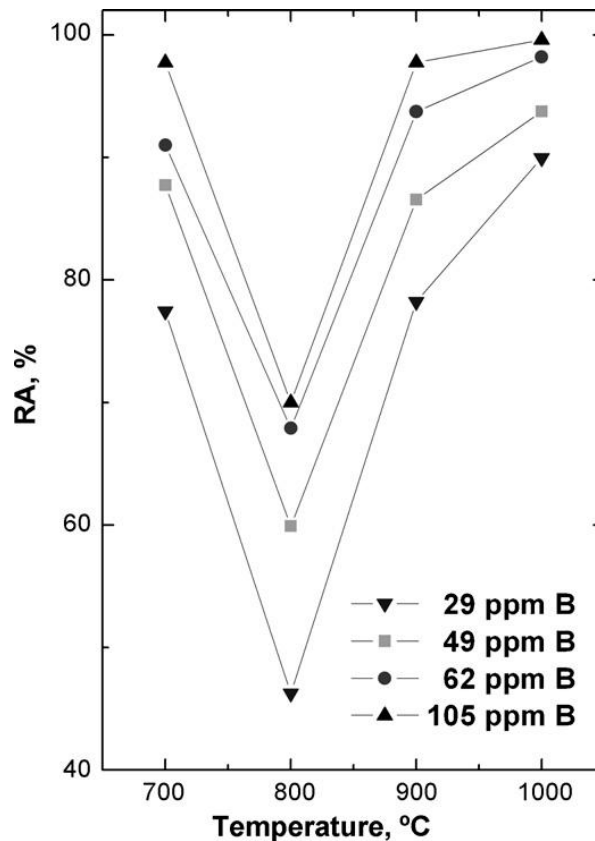


Fig.2.53 Hot ductility curves for boron microalloyed steels (RA, reduction of area) [133].

In the Nb-containing steel, it is known that the hot ductility trough at high temperatures is associated with fine precipitation of Nb(C, N) particles at both grain boundaries and grain interiors. At room temperature, on the other hand, poor ductility is usually associated with coarse precipitates and inclusions [132]. As well, it has been shown that the coarsening of precipitates is quite effective in improving the hot ductility of various steels at high temperatures [20, 78, 81]. Hence, at first sight, the reason for better hot ductility in the Nb-B steels than the Nb-steel can be ascribed to the  $Fe_{23}(B,C)_6$  particles which, although at grain boundaries, are relatively coarse[132], and then not as much detrimental to the hot ductility.

Furthermore,  $Fe_{23}(B, C)_6$  particles contain N, as shown by Kim et al. [132]. Thus, precipitation of  $Fe_{23}(B, C)_6$  reduces the amounts of both N and C, available for precipitation of fine Nb(C, N) not only at the grain boundary but also in the grain interior. Therefore, the density of mobile dislocations is increased, as the density of dislocation pinning precipitates decreases, and more flow in the grain interior can alleviate strain concentration at austenite grain boundaries.

Zarandi and Yue [138] have shown with a Ti stabilised steel that when B (0.002~0.004%) is added to a low C (0.05~0.15%) and Nb (0.035~0.05%) containing steel, boron not only improves the ductility in the  $\gamma+\alpha$  phase field but also in the  $\gamma$  temperature range, RA values  $\geq 40\%$  being achieved throughout the temperature range, 700~1200°C. Their steels contained sufficient Ti to combine with the entire N. They suggest that the beneficial effect of adding B to the Nb containing steel could be due to either: (i) enhancement of nucleation and growth of precipitates, in the temperature range of precipitation, that leads to the depletion of carbonitride precipitants in the lattice, and (ii) depletion of strengthening elements, above the dissolution temperature of precipitants, especially Nb, in the grain interior owing to the non-equilibrium co-segregation of B and Nb to the grain boundary. The effect of B atoms in solute at grain boundaries can be viable in both of these scenarios.

There are just a few studies on the boron effect on the steel hot ductility [107, 132, 140]. It has been shown that boron can segregate to austenite grain boundaries and occupy vacancy sites induced by deformation so as to prevent the formation and propagation of microcracks at boundaries and in turn improve the steel hot ductility.

Song et al. [136] have investigated the effect of boron on the hot ductility of 2.25Cr1Mo steel. A trough in the hot ductility temperature curve is located between 1000 and 700 °C in Fig.2.54. The ductility trough shifts to lower temperatures with increasing boron content and the hot brittle range becomes shallow and narrow.

The shift of the ductility trough to lower temperatures by the addition of boron is due to the decrease in the formation temperature of pro-eutectoid ferrite at austenite grain boundaries in Fig.2.55. The large improvement in the hot ductility of the examined steel by the addition of boron should be due mainly to the increase in grain boundary cohesion, causing the trough to narrow and become less deep. This can arise from grain boundary segregation of boron [141~143], which could occupy nucleation sites and lower austenite grain boundary energy, suppressing the decomposition transformation of austenite and increasing grain boundary cohesion [144]. Also, the segregation of boron may restrain the segregation of impurities like phosphorus because the competition capability of boron for grain boundary sites is much higher than that of phosphorus [145]. Furthermore, boron atoms at the boundary can occupy vacancy sites induced by deformation so as to prevent the formation and propagation of microcracks at the boundary and in turn improve the steels hot ductility.

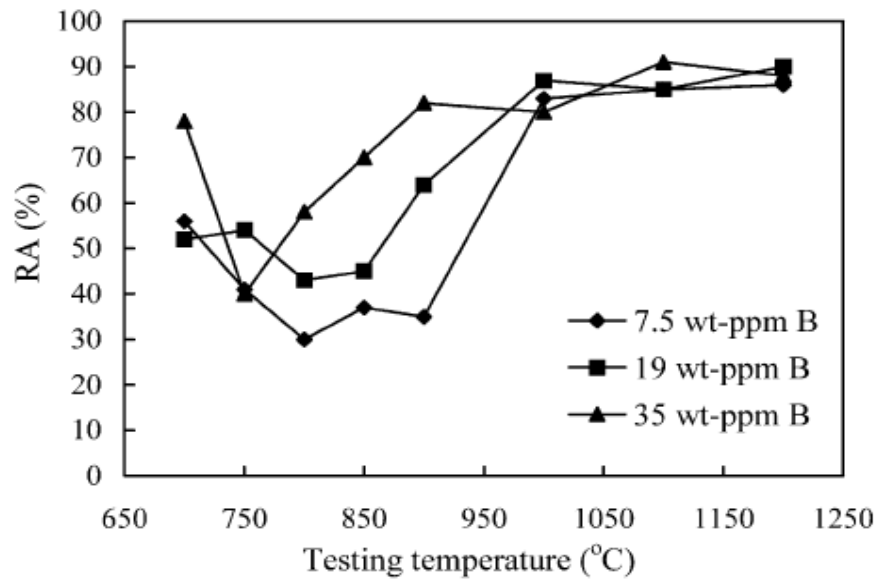


Fig.2.54 Hot ductility curves for the specimens doped with different quantities of boron [136].

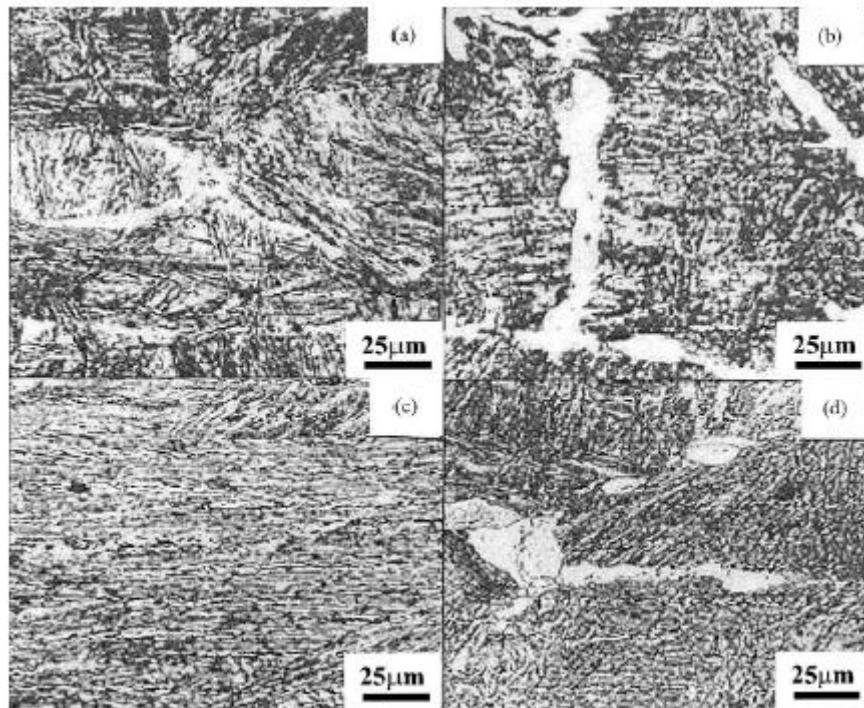


Fig.2.55 Optical microstructures for the specimens with 7.5 wt.ppm B, (a) and (b) and 35 wt.ppm B, (c) and (d) tensile-tested at 800°C, (a) and (c) and 750°C, (b) and (d) [136].

Recently, the effect of boron precipitation behavior on the hot ductility of B containing steel was investigated by Cho et al. [146, 147]. The hot ductility of the B containing steel was found to be sensitive to the cooling rate in the range of 1 to 20°C/s, whereas that of B-free steel showed little change with cooling rate. Increased cooling rate causes deepening and widening of the ductility trough in B containing steel as shown Fig.2.56 [146]. Particle tracking autoradiography (PTA) analysis and transmission electron microscope (TEM) images of the samples showed that BN particles formed along prior austenite grain boundaries, and that as cooling rate increases, these particles become smaller and more numerous as shown Fig.2.57 [146]. This increase in the number of small BN precipitates may promote intergranular fracture, leading to a decrease in hot ductility in the lower austenite temperature region (900 to 1000°C). Furthermore, the formation of film like ferrite at ~850°C causes a decrease in the hot ductility of this steel regardless of B addition and cooling rate.

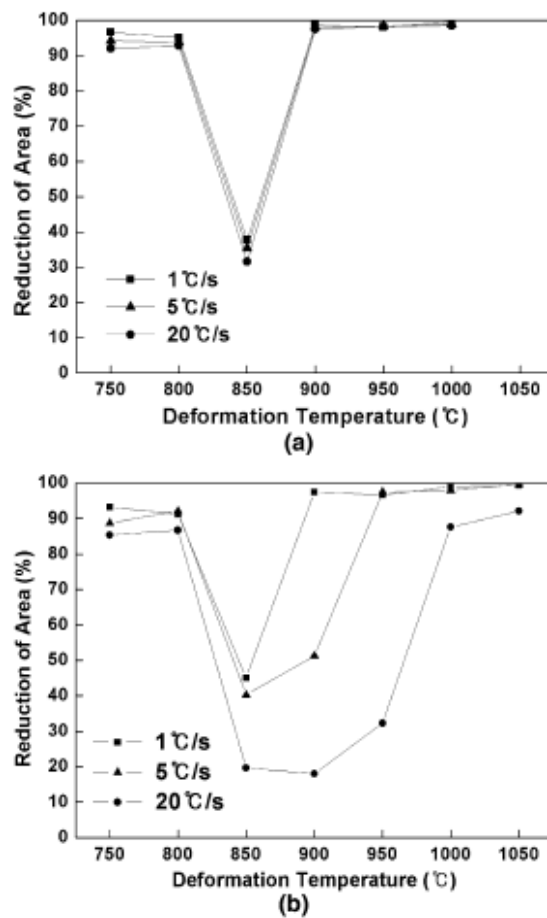


Fig.2.56 Hot ductility curves at various cooling rates for (a) B-free steel and (b) B containing steel [146].

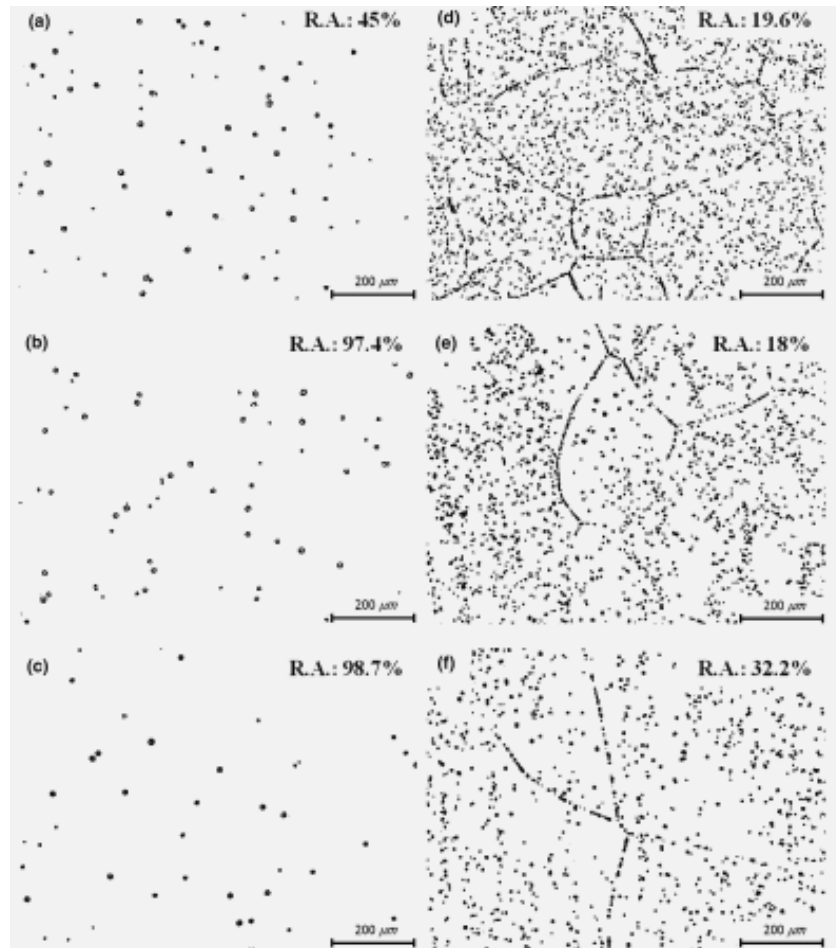


Fig.2.57 Influence of B precipitates distribution and location on hot ductility of B containing steel at different deformation temperatures and cooling rates.

PTA image at non-deformed temperatures of (a) 850°C with a cooling rate of 1°C/s, (b) 900 °C with a cooling rate of 1°C/s, (c) 950°C with a cooling rate of 1°C/s, (d) 850°C with a cooling rate of 20°C/s, (e) 900°C with a cooling rate of 20°C/s, and (f) 950°C with a cooling rate of 20°C/s [146].

The hot ductility of a B-bearing steel was investigated by hot tensile tests under two types of thermal cycles; (a) direct cooled to straining temperatures and (b) under-cooled and reheated to the straining temperatures. The effect of N content on the hot ductility of B-bearing steel was also investigated [147]. Addition of B to plain carbon steel deteriorated hot ductility under the thermal cycle which introduced direct fast cooling to straining

temperature (Fig.2.58) because of the precipitation of BN in the lower temperature region of the  $\gamma$  single phase.

The rapid temperature drop and reheating to the straining temperature caused a marked deterioration in the hot ductility of the B-bearing steels (Fig.2.59) because the precipitation of BN was encouraged. The thermal cycle before straining leads to formation of a large number of BN precipitates in the B-bearing steel.

PTA (particle tracking autoradiography) results showed that the hot ductility of B-bearing steel depended strongly on the distribution of BN precipitates, which were in turn determined by the thermal cycle and N content of the steels. With high N content; BN precipitates were randomly distributed in the interior of the prior austenite and preferentially at austenite grain boundaries, whereas, the precipitates were rather sparsely distributed and larger in the B-bearing steel of low N content as shown Fig.2.60 [147].

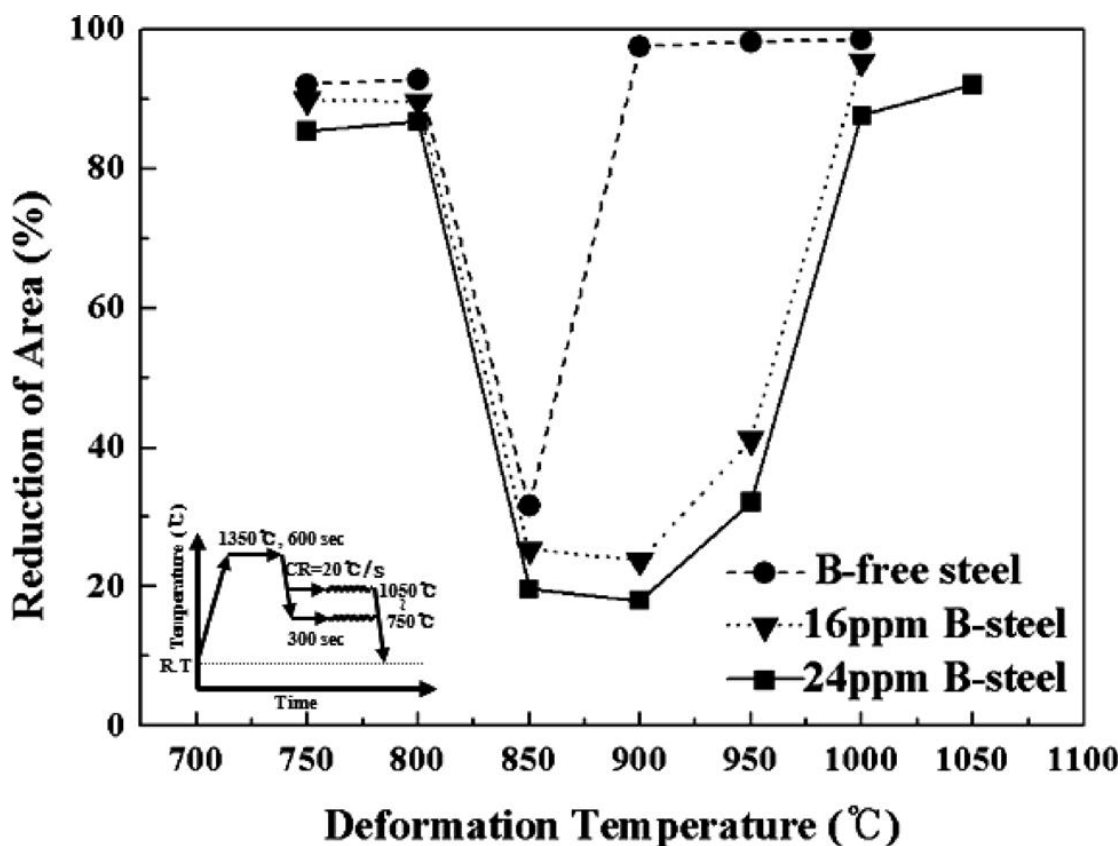


Fig.2.58 The effect of an addition of B on the hot ductility of C steels in thermal cycles (A) [147].

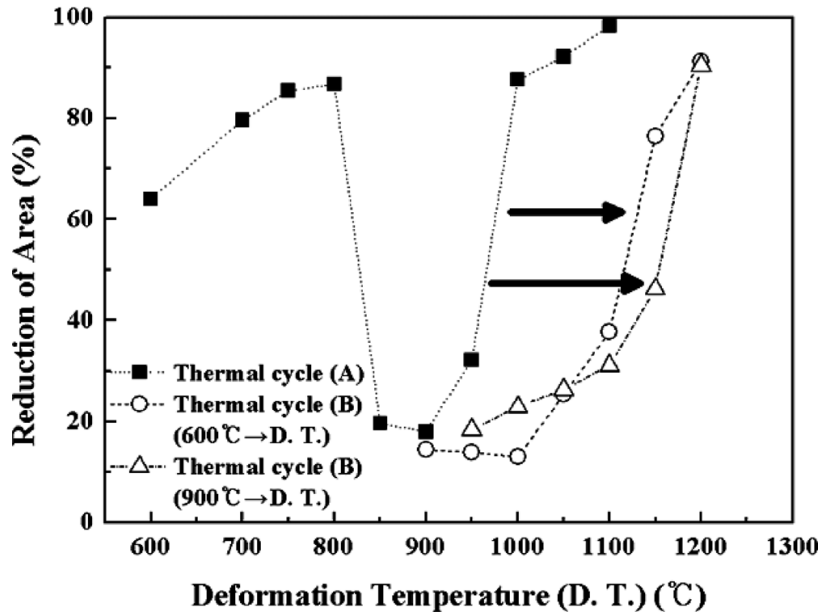


Fig.2.59 Comparison of hot ductility of C-B steel in thermal cycles (A) direct cooled to straining temperatures and (B) under-cooled and reheated to straining temperatures [147].

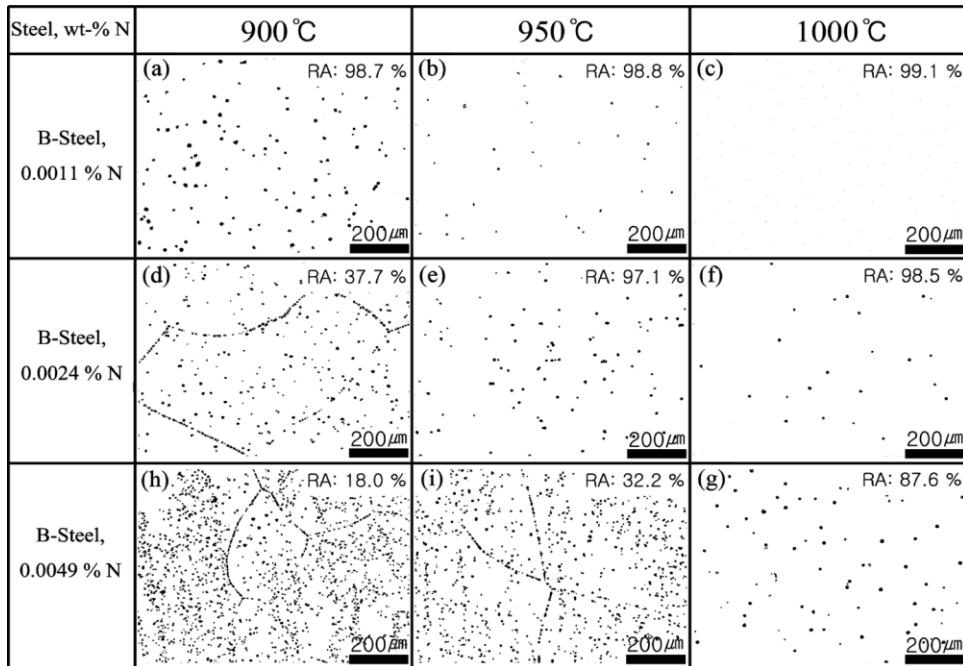


Fig.2.60 Effect of N content on BN distributions in the single  $\gamma$  temperature range from 900 to 1000°C [147].

Cho et al. [148] have also investigated the hot ductility of boron containing steel (B steel) with an addition of Nb (0.03 wt.%) (B-Nb steel) and B-Nb steel with an addition of Ti (0.0079 wt.%) (B-Nb-Ti steel) using hot tensile tests. The specimens were solution-treated at 1350°C and cooled at 20°C/s to tensile test temperatures in the range of 750~1050°C. After that, they were strained to failure at a strain rate of  $2.5 \times 10^{-3} \text{ s}^{-1}$ . For the B-Nb steel, severe hot ductility loss was observed at 850~950°C as shown in Fig.2.61, which covered the low temperature range in which austenite single phase exists, and the high temperature range in which  $\gamma$  and ferrite coexist. Ductility loss in the B-Nb steel was caused by the presence of a network of BN precipitates, rather than by Nb(C, N) precipitates at the  $\gamma$  grain boundaries as shown in Fig.2.62. In contrast, the hot ductility of the B-Nb-Ti steel was substantially improved at  $850 \leq T \leq 950^\circ\text{C}$  as shown in Fig.2.61. In the B-Nb-Ti steel, BN precipitates preferentially on TiN particles, resulting in increased BN precipitation in the  $\gamma$  grain interior and a decrease in the network of BN precipitates at the  $\gamma$  grain boundaries shown in Fig.2.62. These changes reduce strain localization at the  $\gamma$  grain boundaries and therefore increase the hot ductility of the steel.

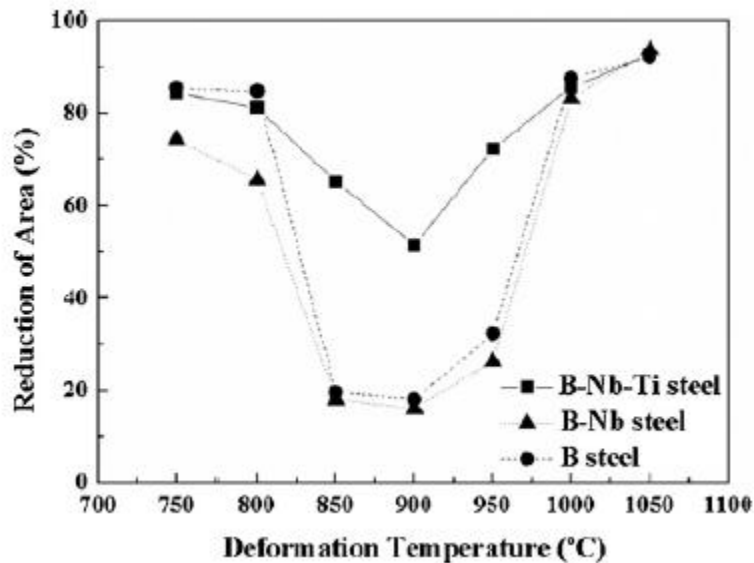


Fig.2.61 Hot ductility curves of the B steel, B-Nb steel and B-Nb-Ti steel [148].

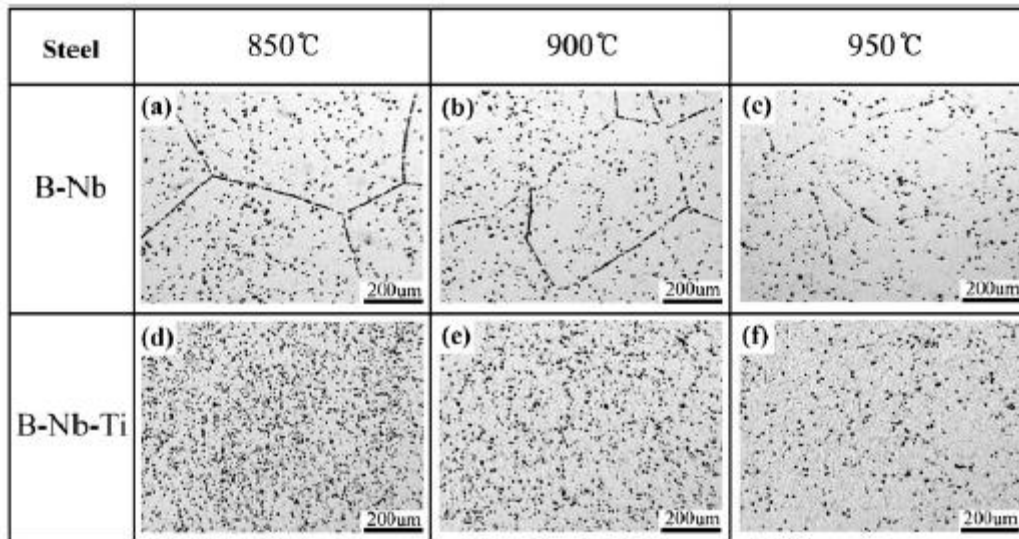


Fig.2.62 Distributions of BN precipitates in B-Nb steel and B-Nb-Ti steel for the temperature range of 850~950°C before deformation [148].

## Titanium

The use of titanium as a microalloying addition to steels has increased considerably over the past 40 years as a means of refining the grain size. TiN precipitation has a low solubility and resists particle coarsening and hence can be used as grain refiners up to very high temperatures. Their presence has therefore been found useful as means of refining the grain size of as cast structures as well as in welding applications where the heat affect zone can be markedly refined.

Ti has been reported [11, 15, 16, 68] to reduce the incidence of transverse cracking during continuous casting, particularly for the more difficult to cast grades of niobium containing steels. It has been suggested that when titanium is present, coarse titanium rich particles are produced on solidification and these act as nucleation sites for the precipitation of NbC at high temperatures so that there is little niobium available for precipitating out in a fine detrimental form at low temperatures where bending of the cast from vertical to straight horizontal occurs [68].

Most of the papers on hot ductility in which Ti has been added to steels suggests that it is the prescription for avoiding transverse cracking, ductility always improving dramatically, [23, 90, 126] Curves from such examinations are shown in Fig.2.63 [21].

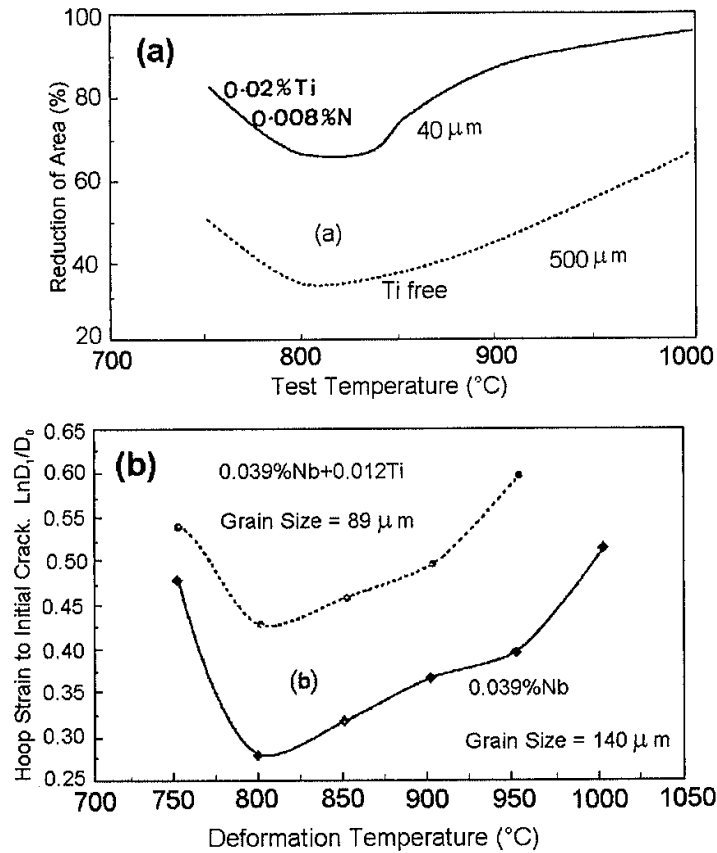


Fig.2.63 Influence of small Ti additions on the hot ductility of reheated Nb containing steels. Grain size of the steels after solution treating is indicated on curves [21].

(a) Ref. 107, (b) Ref. 126

Ti being a powerful nitride former will virtually remove the entire N from solution and for a given N content, increasing the Ti addition will increase the precipitate volume fraction. When the stoichiometric composition for TiN is reached, i.e. Ti: N ratio 3.4:1 the maximum volume fraction of precipitate can form. Furthermore, the Ti containing particles then precipitate at the lowest temperature so that they are fine 10nm as shown Fig.2.64.

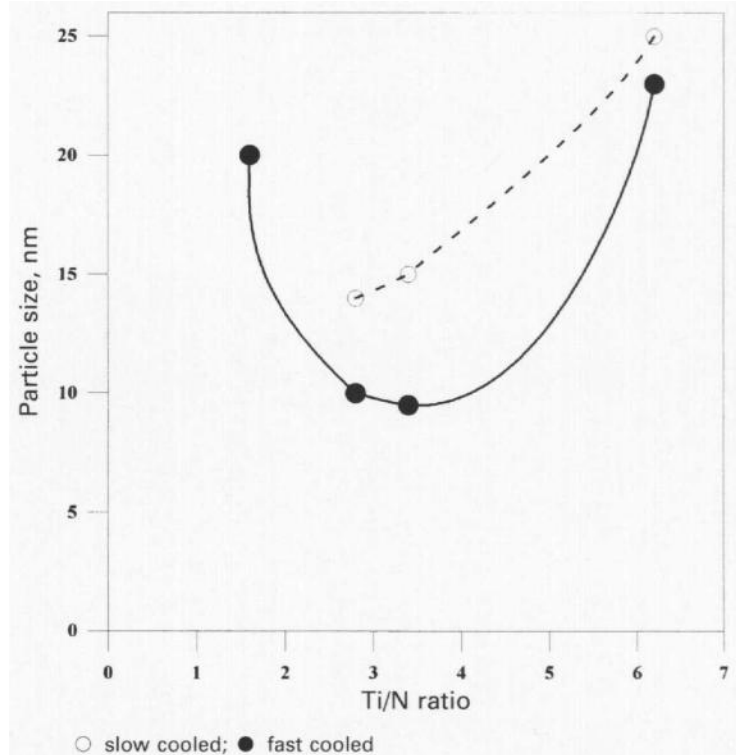


Fig.2.64 Average particle size against T: N ratio for steels tested at 1000°C after cooling at 25°C/min and 100~200°C/min. Ti and N levels were 0.02% and 0.009%, respectively [78].

It is believed of the two precipitates AlN and TiN, AlN has often the most detrimental influence on ductility [78, 149] as although it is slow to precipitate out, when it does so, it precipitates preferentially at the grain boundaries.

From previous work [78] to obtain the optimum ductility for C-Mn-Al steels having a low N (0.005%) level, the Ti addition should be greater than the stoichiometric level for TiN so as to remove the entire N as TiN and produce a coarse precipitation. The stoichiometric ratio for TiN is not recommended unless very low N levels are present ( $\leq 0.004\%$ ) as it gives rise to the maximum precipitation volume fraction and the finest particle size, Fig.2.64 [78]. However, from the large amount of laboratory work [78, 79, 149] carried out on as-cast C-Mn-Al-Ti steels there have been only two cases in which Ti containing steels have given superior hot ductility to Ti free steels of otherwise similar composition. This occurred when a relatively slow cooling rate to the test temperature of 60°C/min was used and when the steels in question (0.05%C and 0.15%C) had a high N content. This combination of 0.02%Ti, 0.009%N (a high [Ti][N] product) ensured that the TiN precipitation took place at a high temperature and was coarse. However, even then, the

improvements were very small amounting to an increase in RA of only 5% over the Ti free steel of similar composition [79].

Luo et al. [150] have examined the influence of Ti/N ratio on the hot ductility of a higher C, 0.1C, 1.4%Mn, 0.03%Nb, low N (0.005%) steel having Ti/N ratios of 0 to 6.4. Hot tensile testing of in situ melted samples, led to a large volume fraction of fine strain induced precipitates at temperatures as high as 1000°C seriously impairing ductility as shown Fig.2.65 [150]. An increase in the Ti level led to even worse ductility. Two cooling rates, 24°C/min and 240°C/min were examined. The slower cooling rate improved ductility due to the coarser precipitation but nevertheless had no influence on the detrimental influence of Ti.

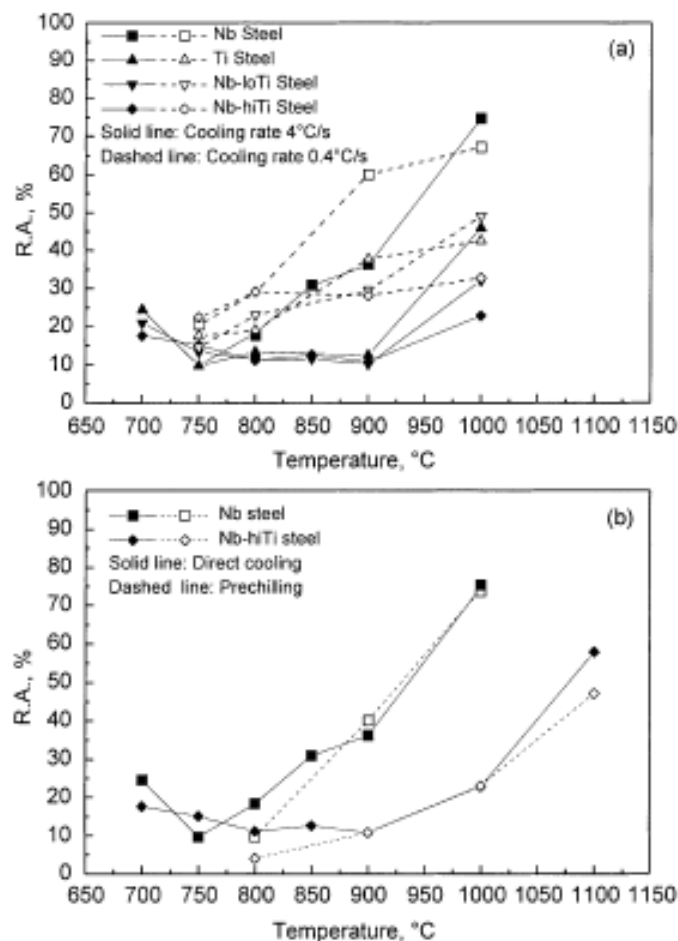


Fig.2.65 Hot ductility curves for the Nb, Ti and Nb-Ti steels in-situ melted and (a) directly cooled at 4°C/s or 0.4°C/s, (b) cooled at 4°C/s with or without pre-chilling [150].

Whereas Al was found to be detrimental in Ti containing C-Mn-Al steels with Ti/N ratio < 3.4 this was not found to be so for Nb containing steels [131]. It was found that on adding Ti to a 0.03%Nb containing 0.1%C steel, precipitation occurred at higher temperatures [131] and hence was coarser. Thus the expected deterioration in ductility from an increased volume fraction of precipitates from having both Nb and Ti present was balanced by the precipitation taking place at higher temperatures.

Again in selecting the Ti and N levels to avoid cracking the same philosophy as for the C-Mn-Al-Ti steels would apply. However, if there is less worry from AlN precipitation giving rise to poor ductility in steels with less than the stoichiometric composition, lower Ti levels might be used for both low and high N steels, particularly if slow cooling can be used. Nevertheless, for the faster cooling conditions applying to thin slab casting, a high Ti/N ratio of 8 would seem to be needed [78].

It is inevitable that the thermal history of the surface of a slab that is subjected to straightening be simulated as accurately as possible in the hot tensile tests. It is therefore more appropriate to use tensile specimens that have been melted in situ (direct cast structures) than specimens that have been reheated to the test temperature [19, 21, 107]. It is especially important to use in situ melting of tensile specimens to evaluate hot ductility of steels containing Ti and S [21, 79, 107]. In these steels, in situ melting ensures complete resolution of Ti and sulfide particles and provides a segregated, coarse grained microstructure similar to that observed in continuous casting practice.

Some practical experiences indicate that the addition of Ti reduces the incidence of transverse cracking and improves the surface quality [21]. Turkdogan [68] suggested that in the Nb microalloyed steels most of Nb can precipitate on the coarse TiN particles before the straightening stage of the slab, leaving less Nb in solution to precipitate out in a more detrimental form during straining. Abushosha et al. [79] found that a 0.02% Ti addition was beneficial regarding the hot ductility of Nb-containing steels (0.023% Nb, 0.009 % N), particularly after a slow cooling. Suzuki et al. [81] similarly found that nitride-forming microalloying elements could improve hot ductility by causing niobium carbonitride precipitation at higher temperatures. In these tests, the thermal cycle of steel slab surface as it passes through the spray cooling and bending zones was simply simulated. Contrary to these observations, Comineli et al. [131] recently reported a significant deterioration in ductility caused by a small addition of Ti to Nb-bearing steels. Mintz [21] put forward the opinion that the beneficial effect of addition of Ti can be noted only when temperature fluctuations equivalent to those in real continuous casting are introduced into the hot ductility tests and the optimum levels of titanium and nitrogen are used.

Small titanium additions to steel have generally been found to be beneficial to surface quality and in reducing transverse cracking susceptibility [11, 15, 16, 20, 68]. Commercially, for low nitrogen steels (0.005%N), titanium levels are recommended to be 2~4 times the nitrogen level, although Turkdogan [68] has stated that the favoured ratio is 4. In contrast, when laboratory hot tensile tests are carried out, it is found that small additions of titanium lead to poor ductility [78, 131, 150], unless the cooling rate after casting is slow [79]. When simulated cooling rates are fast, as for thin slab casting, precipitation is always fine.

Two possibilities could account for this lack of agreement between the commercial and laboratory experiences. The first is that solidification during continuous casting is slower, allowing sufficient segregation of titanium to occur to give rise to coarse precipitation, so that there is less titanium available to precipitate out in a fine detrimental form during straining. The other possibility is that the cooling conditions used in laboratory tests after casting are not sufficiently precise to simulate the commercial continuous casting cooling conditions. Laboratory tests have mostly used an average cooling rate of 60~200°C/min, representing the average cooling conditions below the surface. Commercially, the cooling conditions are more complex, as can be seen from Fig.2.6. The strand is cooled rapidly at first to a minimum temperature, after which the temperature rises by 100°C. This is followed by temperature oscillations, the temperature falling as the sprays impinge on the surfaces, and then rising again as the strand goes between the rolls. It has been shown that these temperature oscillations, particularly when under-cooling, can encourage more abundant and finer precipitation.

## **Copper**

A potential steel processing problem associated with Cu and other residual elements is cracking during continuous casting, which may on occasions be related to the more classical hot shortness phenomenon. Metallic elements that remain in the steel in small quantities after refining is complete and which are not deliberately added to steel are defined as residuals, as they are always present to some degree. Some elements, like copper and tin remain because they cannot be preferentially oxidized when normal steelmaking methods are used. The main processing problem caused by the presence of residual elements in steels is hot shortness. Hot shortness results directly from the fact that residual elements more noble than iron, such as copper, tin, nickel, arsenic and antimony, are not oxidized when steel is reheated. Consequently, as iron is removed preferentially from the

surface layers, these residual elements build up progressively in the subscale layer. In the case of Cu this results in a low melting point phase which melts at the grain boundaries during rolling.

To avoid hot shortness, Melford [151] has suggested that  $Cu+6(Sn+Sb) < k$ , where  $k$  depends on the degree of enrichment which in turn depends on the furnace atmosphere, time in furnace and the temperature.

Cu is the major cause of hot shortness since it can enrich to a level exceeding its solubility limit in austenite (9%) and such enrichment is possible under conditions of severe oxidation. At reheating temperatures in the range 1100~1200°C, the Cu rich phase that precipitates is molten (melting point of Cu is 1080°C) and tends to penetrate the austenite grain boundary leading to surface cracks during subsequent rolling operations [151]. In contrast, Ni has been shown to have a beneficial effect, since it stabilizes austenite and increases the solubility of Cu, preventing the precipitation of Cu. Fisher [152] has studied the effect of Ni additions on the prevention of the molten Cu rich phase and shown that the Ni: Cu ratio must be in the range 1.5 to 2.0 to increase the solubility of Cu in austenite so that hot shortness is avoided. He has also pointed out that while a Ni: Cu ratio of 1.5 to 2.0 is required for Ni to increase the solubility of Cu in  $\gamma$  sufficiently to prevent liquid phase formation, ratios of 1:1 or less can be effective by promoting oxidation and subscale occlusion at temperatures as low as 1150°C.

Wolf [153, 154] has reported that residual Cu causes surface cracks and points out that these intergranular cracks are affected by the mode of secondary cooling. Severe cooling reduces scaling but raises thermal stresses. Because of this, softer cooling is generally preferred despite greater residual enrichment by scaling. Air mist spraying, which would reduce thermal stresses have been found to result in significantly enhanced scaling and this should be accompanied by residual enrichment. However, Lewis [155] disputes this inference, finding no difference in enrichment between casts given a variety of different secondary cooling conditions, including air mist spraying.

Wigman and Millet [156] of Nucor steel have also noted that in thin slab casting, the Cu level must not exceed 0.15%Cu if checking in of the slabs during rolling is to be avoided. When melt-in copper exceeds 0.15% a similar addition of Ni is required to prevent cracking from occurring.

Hannerz [90] has examined Cu the most extensively up to levels of 1% in a 0.07%C, 1.5%Mn plain C-Mn steel but could find no significant influence of Cu on hot ductility at

temperatures  $>700^{\circ}\text{C}$ . These steels were heated to  $1350^{\circ}\text{C}$  and cooled at  $60^{\circ}\text{Cmin}^{-1}$  to the test temperature and tested in an argon atmosphere. Ductility below  $700^{\circ}\text{C}$  was impaired by the 1% Cu addition but this could be due to copper precipitation from the 1% Cu in solution. He contrasts his laboratory results with the commercial observations of Cu causing poor surface quality and cracks and indicates the need to carry out tensile tests in an oxidising atmosphere.

Mintz et al. [157] has looked into the effect of oxidation in more detail. Both C-Mn-Al and C-Mn-Nb-Al steels containing Cu and or Ni up to 0.5% were examined. No effect of Cu or Ni was found on the hot ductility when the steels were solution treated at  $1330^{\circ}\text{C}$  and cooled to the test temperature, independent as to whether a protective or oxidising atmosphere was used. Tensile samples cast directly after melting and tested under an argon atmosphere were again found not to be influenced by compositional changes.

Only when the tensile specimens were cast and allowed to cool in air was the deleterious effect of copper on hot ductility obtained and this could be prevented by a similar addition of nickel, (0.25%, of each), Fig.2.66.

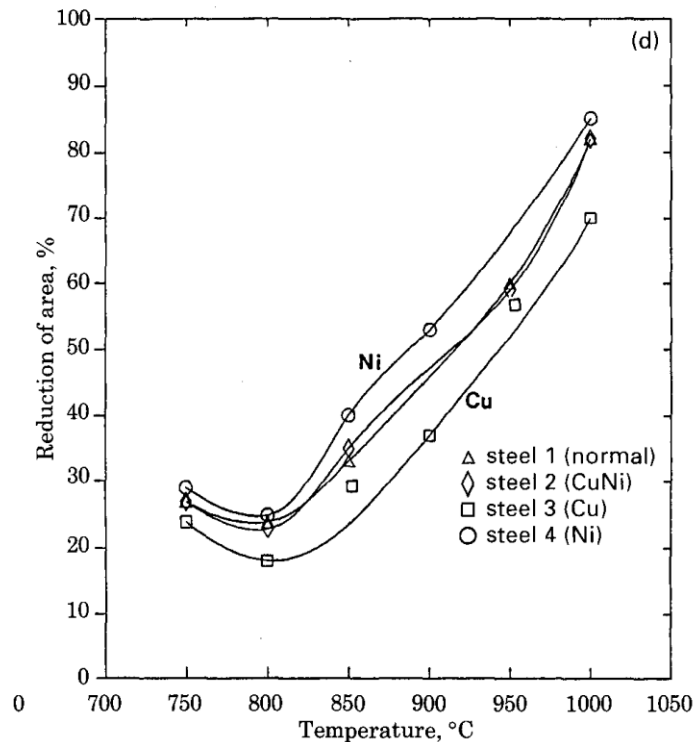


Fig.2.66 Hot ductility curves for boron as-cast C-Mn-Al-Nb steels tested in "air" (argon flow discontinued) steel1, low residual, steel 2, 0.25%Cu, 0.25%Ni, steel 3, 0.5%Cu, steel 4, 0.5%Ni [157].

No evidence for Cu rich films penetrating along the  $\gamma$  boundaries was found, ruling out conventional hot shortness as the explanation. The deterioration could be explained by the observation of fine copper sulphides (or oxysulphides) particles at the boundaries, Fig.2.67, which had formed on cooling as a result of oxidation and the presence of Cu, according to the reaction:  $2\text{MnS} + \text{O}_2 + 4\text{Cu} = 2\text{Cu}_2\text{S} + 2\text{MnO}$  [158].

The need to have cast conditions in order to produce these sulphides probably arises because an increased segregation of Cu is required for the above reaction to proceed to any degree. Ni, by increasing the solubility of Cu in iron, might be responsible for a reduced driving force for Cu precipitation.

It was pointed out in this laboratory work [157], that the oxidation conditions were very much less severe than during continuous casting. In continuous casting, the water cooling and reheating as the strand passes through the rolls provides enhanced conditions for oxidation, and therefore this work may underestimate the influence of Cu on hot ductility. It was suggested that although the laboratory work had indicated that a Ni:Cu ratio of 1:1 would maintain good ductility, it was felt that the more severe oxidizing conditions present during continuous casting would lead to a greater residual enrichment requiring a higher Ni addition and a Ni:Cu ratio closer to 2:1. It was also recommended that, since copper sulphides were the cause of the poor ductility, sulphur levels should be kept low.

Except for this investigation all the other hot ductility examinations have been carried out using an inert atmosphere. Generally, when an inert atmosphere is used the influence of Cu on hot ductility is confusing with no clear conclusions.

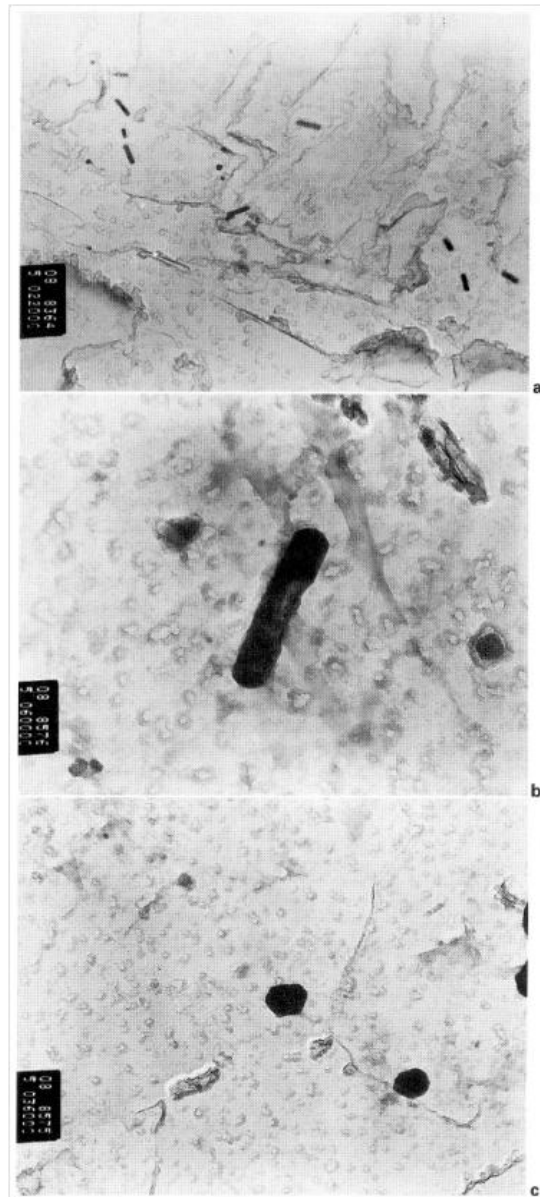


Fig.2.67 Micrographs obtained using transmission electron microscopy (TEM) showing copper sulphide particles at  $\gamma$  grain boundaries (X18500) and b, c enlarged views of copper (oxy) sulphide showing their various shapes (X51600, X30300) [157].

Comineli et al. [159] have shown that when Cu is added to a plain C-Mn steel (0.1%C, 0.5%Mn), increasing the Cu addition from 0.1 to 0.5%Cu has little influence on the hot ductility after melting and cooling at 25°C/min or 200°C/min to the test temperature. With an HSLA Ti/Nb (0.015%Ti and 0.03%Nb), 0.1%C, 1.5%Mn steel, again very similar hot

ductility curves were obtained at the cooling rate of 200°C/min for a Cu free steel compared to a similar steel containing 0.3%Cu. However, at a slower cooling rate, of 25°C/min, ductility was much improved for both steels but even more so for the Cu containing steel in the temperature range 800~1000°C. Coarser precipitation was present at the slower cooling rate and the Cu containing steel gave significantly coarser precipitation in accord with its better ductility. Comineli et al's explanation is to suggest that either Cu increases the activity of C and N or that because Cu retards dynamic recovery and dynamic recrystallisation through solute drag, the number of vacancies produced during deformation increase. This leads to an increase in the kinetics of the carbonitride precipitation [159]. However, both Cu and Ni lower the transformation temperatures (nickel has a much bigger effect) and this could also account for any beneficial effect of these elements on hot ductility at the higher temperature end of the trough as moving the hot ductility trough to lower temperature will allow earlier dynamic recrystallisation and better ductility. Mintz et al. [160] in another study using an inert atmosphere found that after melting and cooling at 25°C/min, a 0.5%Cu addition to a 0.11%C, 1.2%Mn steel gave RA values 10% lower than for the Cu free steel throughout the temperature range 750~950°C. Adding Ni (0.3 or 0.5%) restored the ductility.

Nagasaki and Kahara [134] have examined the influence of Cu (0.5%) and Sn (0.01%) on ultra low and plain 0.2%C steels with a very low Mn content of <0.01. Three strain rates were examined  $10^{-2}\text{s}^{-1}$ ,  $1\text{s}^{-1}$  and  $200\text{s}^{-1}$  to cover the strain rate range encountered during the straightening operation as well as when hot rolling. The tensile specimens were heated to 1350 °C and then cooled at 600°C/min. Ductility was generally very good for the ultra low C (0.001%C), low S steels,  $\geq 70\%$  RA, even when Sn was present as shown in Fig.2.68. However, when S was present, ductility deteriorated at 950 °C to 40 and 50% RA for the Cu (0.5%) and Sn (0.01%) containing steels, respectively but only when tested at the highest strain rate, Fig.2.69. The cause of this deterioration in ductility is believed to be the segregation of S to the grain boundaries forming fine precipitates of FeS [134].

For the 0.2%C steel the normal deep ductility trough was found, this being most marked at the slowest strain rate as shown in Fig.2.70. For the conditions relevant to continuous casting  $10^{-2}\text{s}^{-1}$ , the trough occurred at a lower temperature, 800°C, corresponding to the transition temperature from austenite to ferrite and its depth increased with S and Sn content. However, inter-granular failure occurred not within the ferrite film but at the interface between the ferrite band and the austenite grain surface. Examination of the fractured surfaces at the minimum ductility, with Auger spectroscopy, showed that Sn and S segregate to the boundaries but there was no evidence for Cu segregation. It was suggested that when S and Sn segregate they can retard grain boundary migration allowing voids to

form and coalesce at the grain boundaries. S segregation occurred probably because of the steels low Mn level ( $\leq 0.035\% \text{Mn}$ ).

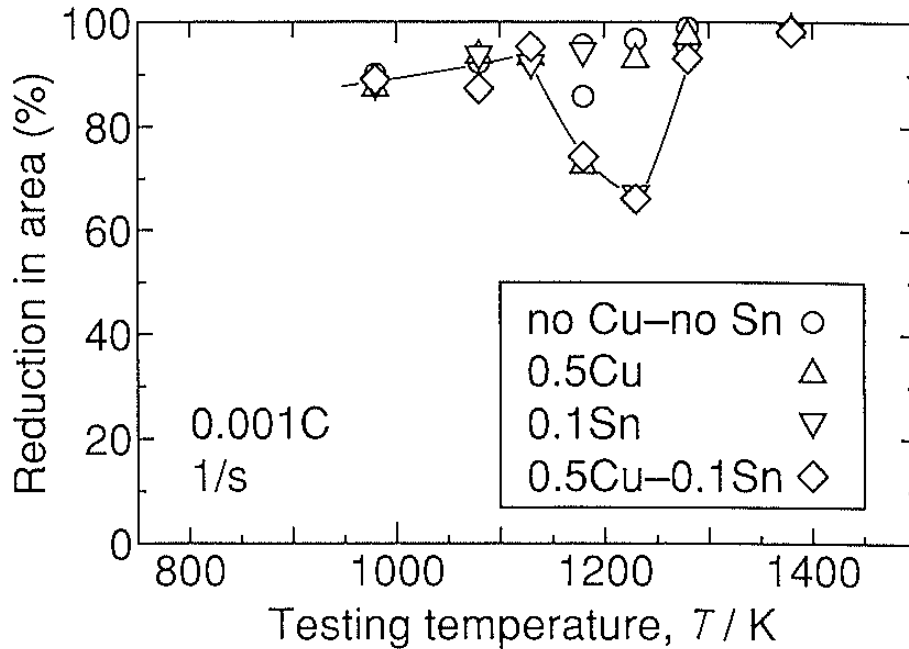


Fig.2.68 Hot ductility for the high purity ultra-low carbon steels containing copper and/or tin deformed at  $1\text{s}^{-1}$  [134].

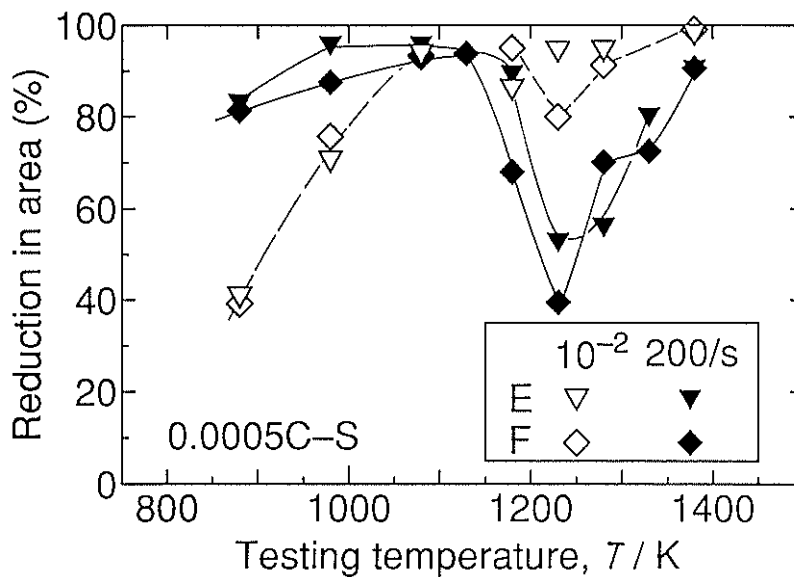


Fig.2.69 Effect of copper on the hot ductility of ultra-low carbon steels containing 0.004% sulphur deformed at  $10^{-2}\text{s}^{-1}$  and  $200\text{s}^{-1}$  [134].

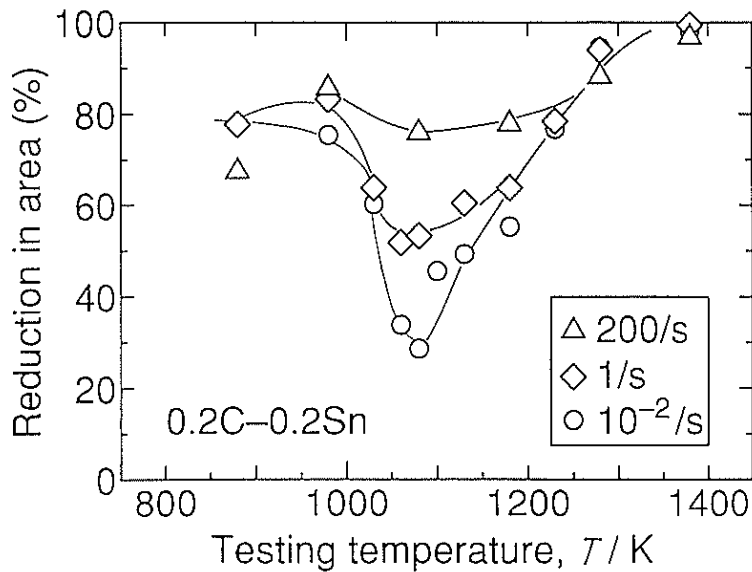


Fig.2.70 Hot ductility for the 0.2% carbon steel containing 0.2% tin deformed at  $10^{-2}\text{s}^{-1}$  and  $200\text{s}^{-1}$  [134].

Matsuoka et al. [135] have carried out a similar exercise on steels with C contents in the range 0.002 to 0.15% C, and 0.27% Mn at one strain rate  $10^{-3}\text{s}^{-1}$  and have found supporting results with regards to the influence of Cu (0.04%) and Sn (0.05%) but not S. In their work the tensile specimens were heated to  $1250^{\circ}\text{C}$  and cooled at  $300^{\circ}\text{C}/\text{min}$ . Hot ductility in the temperature range  $800\sim 900^{\circ}\text{C}$  decreased with increase in C and there was a further deterioration with the addition of Cu and Sn as shown in Fig.2.71, although Sn had much the bigger effect. For these higher S, Mn steels (Mn/S ratio of  $\sim 20:1$ ), S was found not to have a significant influence on the ductility. Auger was again used but only Sn segregation was detected. They put the deterioration in ductility down to the following: (1) the presence of the pro-eutectoid ferrite along the austenite grain boundaries (2) segregation of Sn to the boundaries (3) the increase in deformation resistance shown by the load/elongation curves between the pro-eutectoid ferrite and the austenite just below the  $A_{e3}$  that occurs on adding Sn.

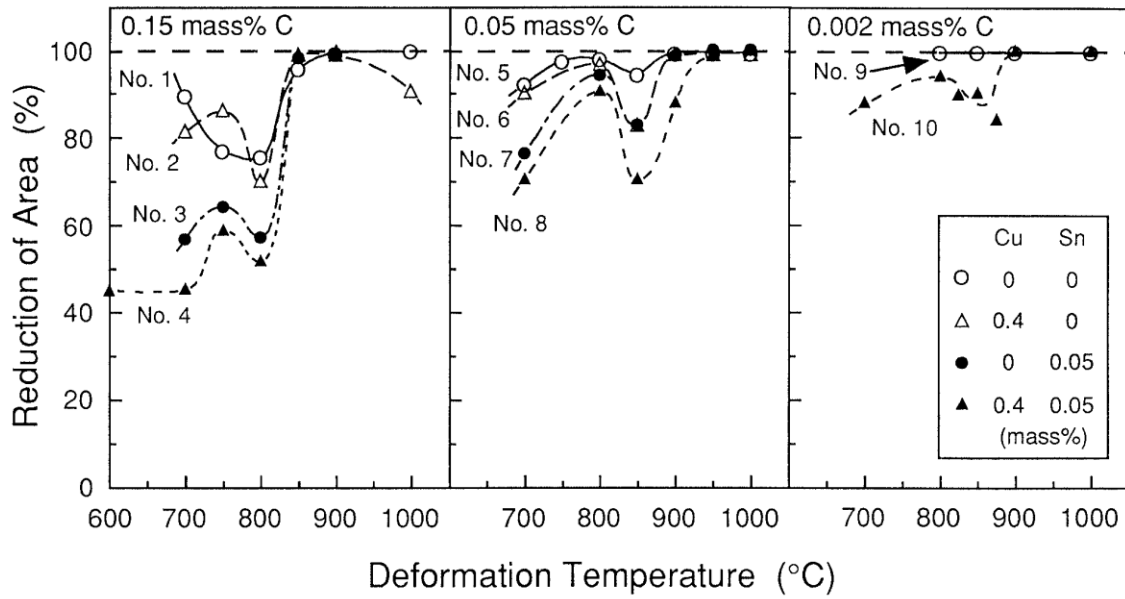
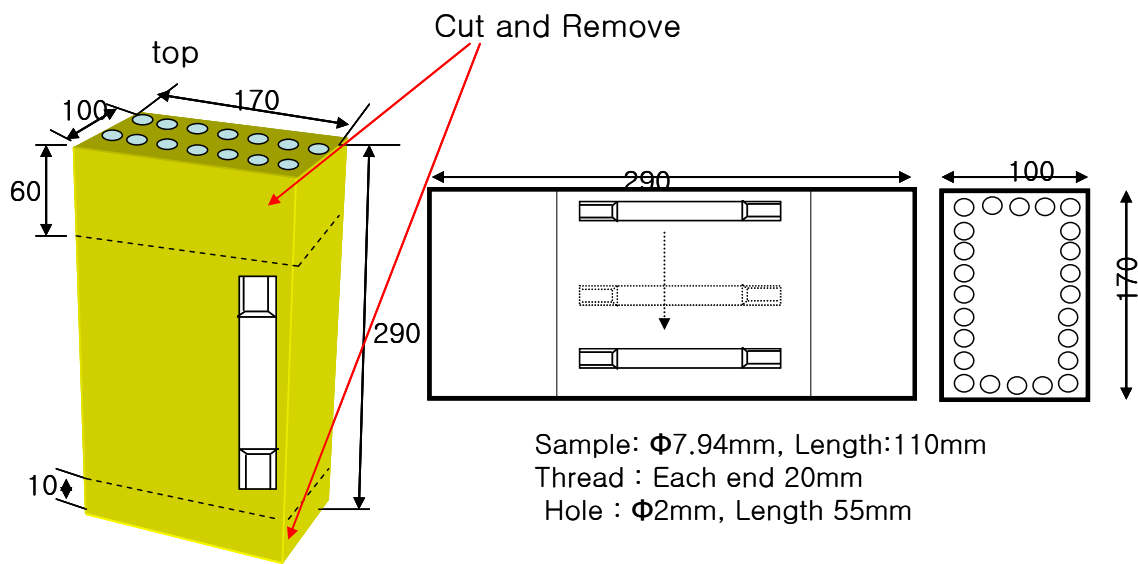


Fig.2.71 Effects of deformation temperature and Cu and/or Sn addition on the hot ductility of steels with various C content [135].

## CHAPTER 3: EXPERIMENTAL METHODS

### 3.1 Preparation of specimens

The steels were produced as experimental 50kg vacuum melt ingots which after removing the shrinkage cavity at the top of ingot had dimensions 170x220x100mm. The tensile samples were machined from the as cast ingots, as shown in Fig.3.1



- **Remark:** Remove 2mm from surface

Fig.3.1 Position and dimensions of tensile specimens taken from as cast ingot.

Tensile specimens were either tested at the City University using an induction heater for melting or at POSCO using a Gleeble when the tensile samples were only re-heated to 1300~1350°C. All machining was carried out by POSCO.

The tensile samples for induction type tensile testing machine were 110mm in length and normally 7.94mm in diameter. Each end of the samples was threaded with 5/16 BSF (British Standard Fine) thread which enabled them to be screwed into the grips of the tensile test machine. They also had a 2mm diameter hole drilled in the centre that ran up to the mid-point of the length of the sample in order to allow access for a thermocouple into the melt zone. A schematic diagram of the samples is shown in Fig.3.2.

Normally the samples would be of 7.94mm in diameter, yet previous testing of TWIP steels had found that it suffered from thermal expansion on solidification, breaking the silica tube. Unlike other steels such as transformation induced plasticity (TRIP) steels that did not thermally expand, TWIP caused difficulties in accommodating the silica tube of 8mm in diameter that surrounds the melt zone. This governed the decision to re-machine the samples to a 7.7mm diameter and the as-received samples were found using a micrometer to have a diameter of  $7.72 \pm 0.005\text{mm}$ . In practice 7.72mm samples resulted in reduction of area (RA) results of only a 1~2 percent higher than that of 7.94 mm samples.

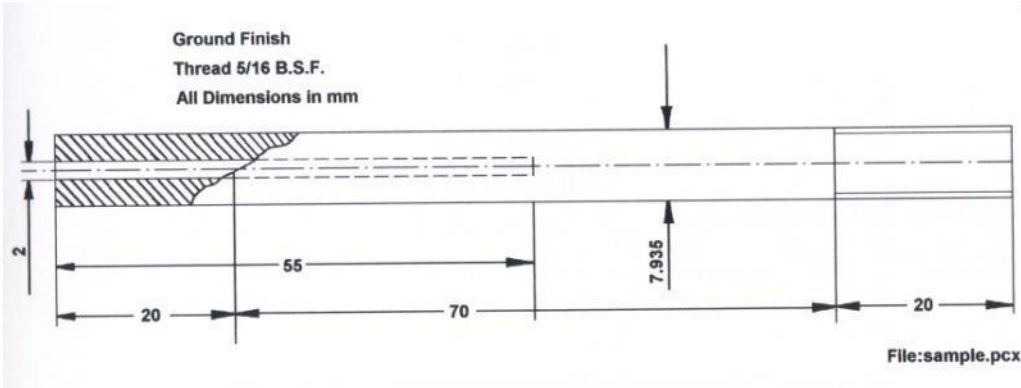


Fig.3.2 Details of the tensile test sample used when testing was carried out in the induction heated unit at the City University London.

Cylindrical specimens were machined from as cast ingots for the Gleeble machine, with a 10mm diameter and 120mm in length and the details of such specimens are shown in Fig.3.3

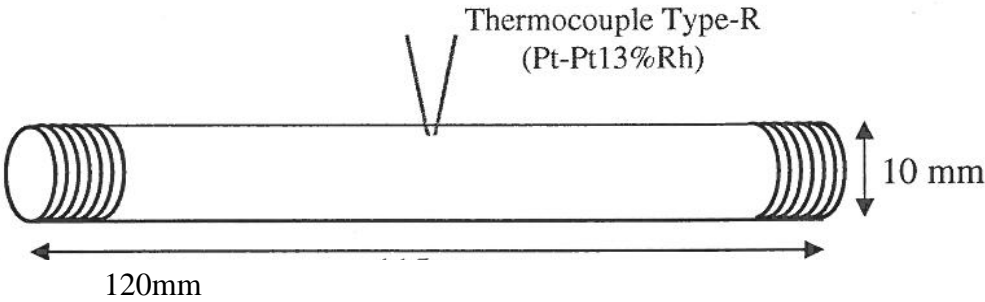


Fig.3.3 Geometry of Gleeble specimen.

## **3.2 Equipment for tensile testing**

### **3.2.1 Hot tensile testing machine**

Of all the laboratory tests, the one that has proved the most popular for the study of transverse cracking is the simple hot tensile test [20-23]. Generally, tests are carried out using a servo hydraulic load frame equipped with either a furnace or an induction heater, in a protective atmosphere.

To enable specimens to be cast “in situ” the tensile testing equipment used consisted of an induction furnace and tensometer. The City University London’s hot tensile test rig used a converted tensometer to which an induction heating device had been fitted. The induction heater was controlled by a device that in turn was programmed and monitored by a Personal computer.

The equipment used at City University London is shown in Fig.3.4. The heating section was a large induction generator connected to copper coils, which were wrapped around a silica glass tube. The tube was supported by the grips of the tensometer in which the specimens were placed. This enabled temperature accuracy of  $\pm 5^{\circ}\text{C}$  to be obtained in the central 22mm molten zone. Temperature measurements were taken using R type thermocouple (platinum/platinum-13% rhodium). Figure 3.5 shows the photograph of test equipment outlined above.

The melt zone was approximately 22mm long (11mm either side of the midpoint of the sample). The molten steel was contained in a silica tube that had 0.2mm diametrical clearance of the sample. Protection from oxidation was achieved by surrounding the sample with a large silica glass tube through which argon was passed. This is shown schematically in Fig.3.6.



Fig.3.4 Layout of test equipment.

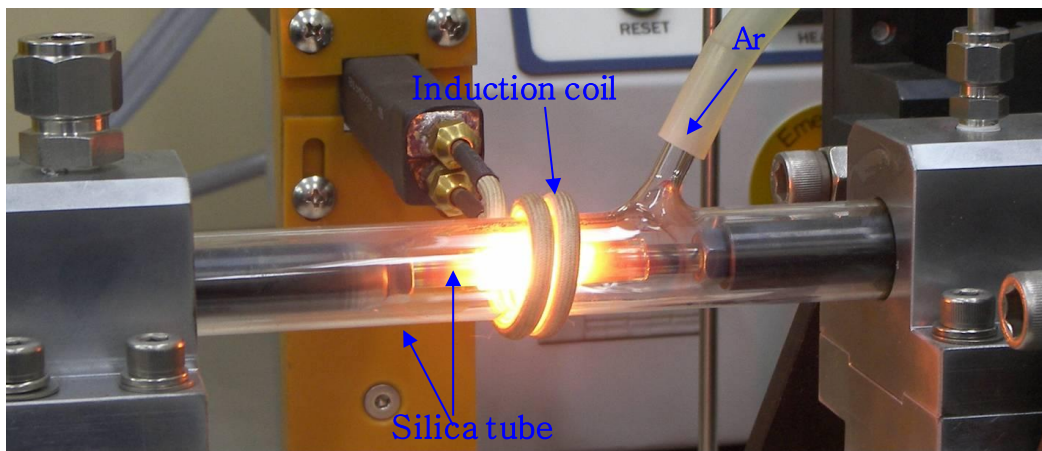


Fig.3.5 Testing arrangement for the hot ductility tests in the as cast condition.

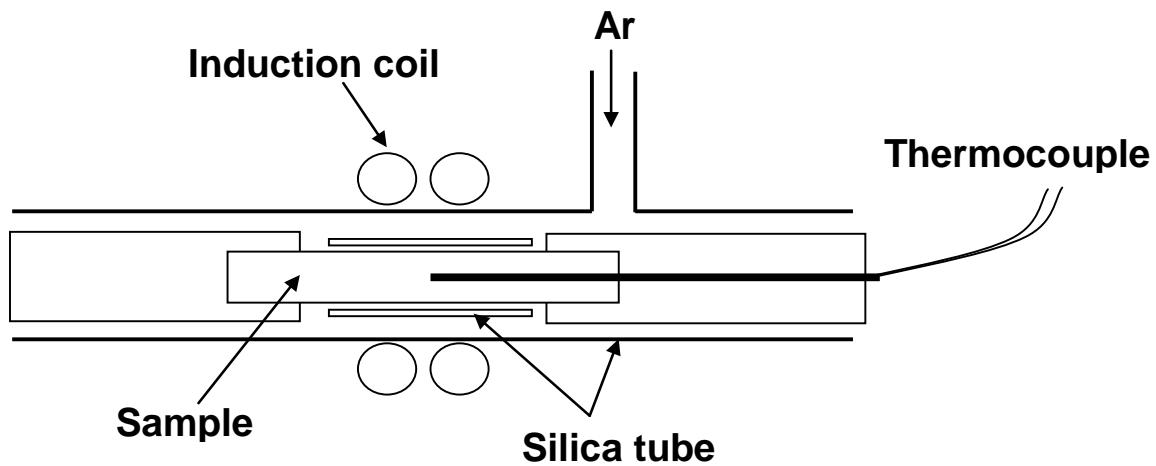


Fig.3.6 Schematic diagram of testing rig at the City University London.

### 3.2.2 Gleeble 3500

The Gleeble machine has also proved to be popular for the investigation of hot ductility because of its ability to melt samples and versatility in simulating thermal cycles. In this case, heating is by electrical resistance, which has the advantage that there is no practical limit to the possible rate of heating, and temperature gradients are again kept to a minimum. Sample cooling can be achieved by several methods such as simple cooling by anvil/grips or by any combination of air/inert gas/water quenching. Testing can be done in either ambient or inert atmosphere or alternatively under vacuum. The testing is done fully automatic, or with a limited manual control. It is possible to deform under uniaxle tensile and compressive or plain strain compressive conditions at the desired temperature. Lay out of test equipment is shown in Fig.3.7. A schematic diagram of the Gleeble testing arrangement is shown in Fig.3.8. In order to control the temperature of specimen an R type thermocouple (platinum/platinum-13% rhodium) is spot welded onto the specimen at the middle of the span.

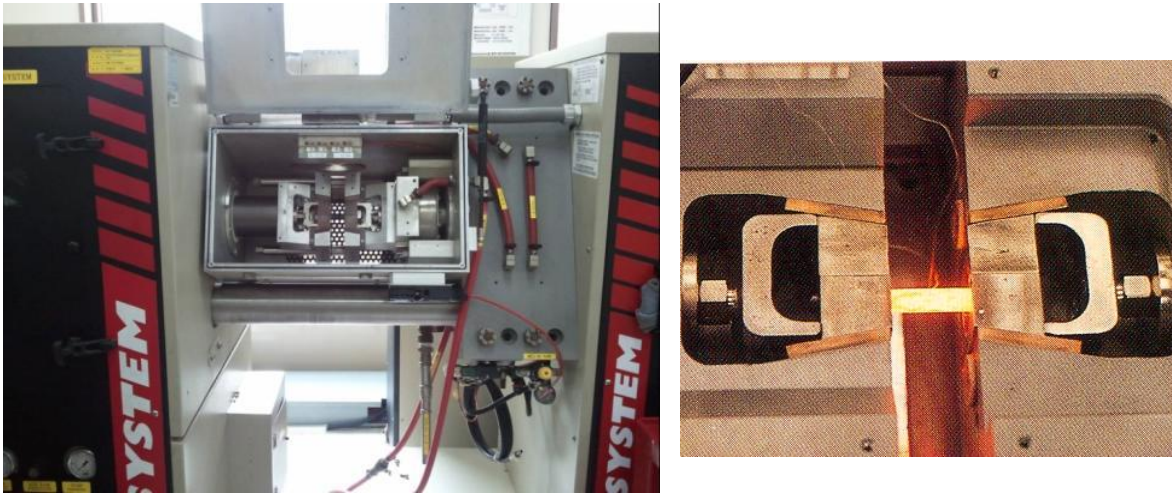


Fig.3.7 Layout of Gleeble 3500.

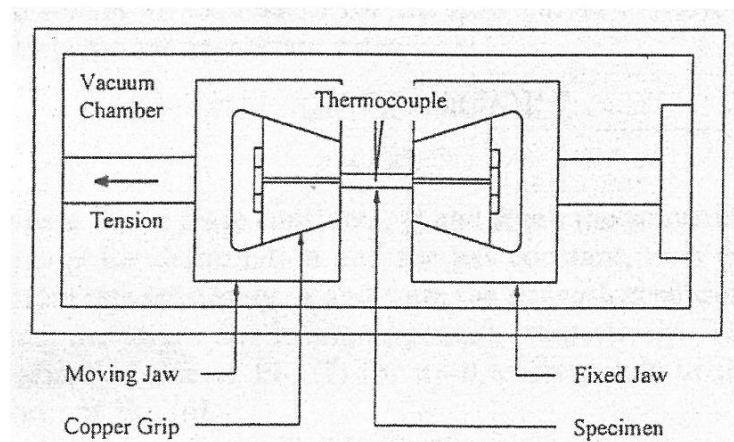


Fig.3.8 Testing arrangement for carried out the hot ductility tests when re-heating to 1250~1350°C using the Gleeble.

### 3.3 Evaluation of hot ductility

Once the samples had failed they were immediately gas quenched with argon in order to preserve the grain structure and fracture surface present at the time of failure. The sample area was measured using vernier calipers.

As the sample were often not of uniform cross section 8 measurements were taken of the final diameter of each samples(four for each half sample) at 90° intervals of rotation. The

average was then used to calculate reduction of area values employing the formula below

$$RA(\%) = (D_i^2 - D_f^2) / (D_i^2 - 2^2) \times 100$$

Where  $D_i$  = initial diameter

$D_f$  = final diameter

The number 2 in the equation for RA arises due to the drilled 2mm hole for inserting the thermocouple.

The reduction of area for the Gleeble samples was measured using a stereo microscope. Fig.3.9 shows the geometry of sample after fracture. Reduction of area at fracture was calculated as follow

$$RA(\%) = (A_0 - A_f) / A_0 \times 100$$

Where  $A_0$  = cross-sectional area before test

$A_f$  = cross-sectional area after test



Fig.3.9 Geometry of sample after fracture.

### 3.4 Metallography

#### 3.4.1 Optical Microscopy (OM)

After measurement of the final diameter, the sample was mounted in a hot cured resin, in a mounting machine, polished to 1 micron and etched in 2% Nital solution or Picric acid solution for examination under the optical microscope.

Firstly, one half of the fractured sample is cut along the radial axis exposing the fracture surface. This sample-section is then transferred to a mounting press where it was filled with

transpotic powder and compression heated. Upon cooling, a plastic block is produced that has to be further machined to bring the fracture surface of the cut section to the surface. The next stage of preparation is polishing. Three grinding pads, 240, 400 and 600 grit silicon carbide papers were used consecutively. The specimens were polished with 6 $\mu$ m followed by a 1 $\mu$ m-diamond grained polisher, the fracture surface then having a refined mirrored appearance.

Etching involves using various abrasive chemicals to expose the surface microstructures. Different chemicals are required for different steel compositions and it was trial and error to achieve successful results. The best results for the investigated TWIP steel was achieved by washing the surface with ethanol, and applying a 2% Nital solution. This still did not fully etch the grain boundaries and a Picric Acid etch was therefore added.

Microscopy had to follow swiftly from etching as the exposed fracture surface is prone to oxidation. The microscope used had lenses which gave magnifications of 50, 100, 400 and 1000 times and was connected to a computer for image capture.

### **3.4.2 Scanning Electron Microscopy (SEM)**

SEM examinations being carried out on the fractured tensile specimens on sections taken close to the point of fracture, the other half of the sample was used for fracture examination of the fractured surface. The type of fracture and the compositions of the particles were identified. Fracture examinations were carried out using a JSM-6700F Jeol Field Emission Scanning Electron Microscope (FE-SEM), operating at 30KV accelerating voltage. Field Emission Gun analyzer (FEG) was used to identify the precipitates that were present on the fracture surface.

### **3.4.3 Transmission Electron Microscopy (TEM)**

The morphology and chemical composition of precipitates were determined by using a JEM-2100F Jeol Field Emission Transmission Electron Microscope (FE-TEM) on carbon replicas taken from tensile specimens.

Tensile specimens were taken and a longitudinal region including the fracture was mounted in a clear plastic. They were subsequently ground down close to the center of the sample and polished with increasingly fine diamond pads until a final polish with 1 $\mu$ m diamond paste.

The samples were then etched with a 2% Nital (Nitric acid and ethanol) solution. Following this, the samples were washed and then coated with a layer of carbon approximately 1µm thick by arc evaporation of a carbon rod in a vacuum chamber.

The deposited carbon layer was then removed by immersing the samples in a 10% Nital solution. The resulting carbon film was placed on to small nickel grids and examined with the TEM. All microscopic and electron microscopic examinations were carried out at POSCO.

#### **3.4.4 Secondary Ion Mass Spectrometry (SIMS)**

Boron is a light element with an atomic number of 5, and presents special problems when it comes to determining grain boundary concentration profiles needing high spatial resolution [161]. For example Electron probe micro analyser (EPMA) and STEM-EDS suffer from low sensitivity for boron. SIMS and particle tracking autoradiography (PTA) have spatial resolution of the order of 1µm and Auger electron spectroscopy (AES) requires that the grain boundary surface can be exposed.

However because SIMS has a high spatial resolution of ~1 µm combined with an excellent B-detection sensitivity of <10ppm [161]. It is ideal for obtaining a relatively quick picture of the B distribution within the grains and grain boundaries.

In preparation for SIMS analysis the surfaces were mechanically polished and carefully cleaned. SIMS analyses were performed with a Cameca IMS 6F instrument using 12.5KeV  $O_2^+$  as primary ions. The sample voltage was +4.5KeV, the ion beam current 500nA, field of view 250µm and the detection ion was  $^{11}B$ . The negatively charged secondary ion emitted from the surface was used to obtain mass-resolved ion images.

When analysing the B distribution the  $^{11}B^{16}O_2^-$  signal on mass 43, was the strongest B channel recorded. However, the Al as  $^{27}Al^{16}O^-$  interfered with the B signal in the mass 43 images. The  $^{11}B$  signal was therefore used to form the images in all SIMS analyses.

## CHAPTER 4: THE INFLUENCE OF Al AND N ON THE HOT DUCTILITY OF TWIP STEELS

### 4.1 Introduction

The mechanism which gives the TWIP steels their exceptional ductility and high strength is one which depends on having a fully austenitic structure which has low stacking fault energy. Extensive twinning then occurs on deformation giving a high work hardening rate so preventing “necking” from occurring during the forming operation. This is best achieved by having a high Mn level [3, 5]. In order to achieve these properties the stacking fault energy must be controlled. If it is too high then twinning does not occur and if too low martensite will form.

Aluminium additions at the 1~2% level as well as reducing the stacking fault energy also improve the low temperature toughness but more importantly have been shown to prevent delayed fracture after the steel has been deep drawn[1]. However, Al is known when added in small amounts  $\geq 0.04\%$  to give transverse cracking problems for steels with the peritectic C level due to AlN precipitation at the austenite grain boundaries [20]. The influence of these very much higher Al levels on hot ductility in these TWIP steels has not been explored. Therefore the influence of high Al and N contents on TWIP steels was a first consideration. Without the addition of microalloying elements the strength of this high Al TWIP steels in the final product is ~800MPa.

### 4.2 Experimental

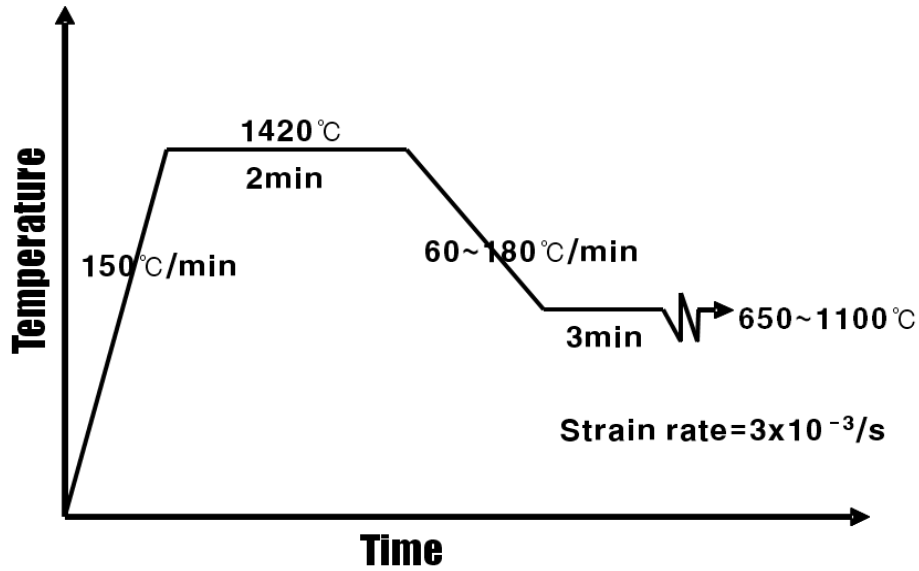
In the simple hot ductility test, conditions are kept as close as possible to those pertaining to the commercial continuous casting operation. The tensile specimen is heated to a high temperature to dissolve all the microalloying elements or as in the present case melted. It is then cooled at the average cooling rate that the strand undergoes to test temperatures in the range 1000 to 700°C; this being the temperature range in which poor ductility occurs in a tensile test and is the same temperature range in which cracking occurs when the strand is unbent at the straightener.

Although the simple hot ductility test is a good simulator of the continuous casting operation there are nevertheless important differences; one of the most important being that in the continuous casting, cooling conditions are quite complex and very different from those used in the simple test. The temperature on cooling from the melting point is

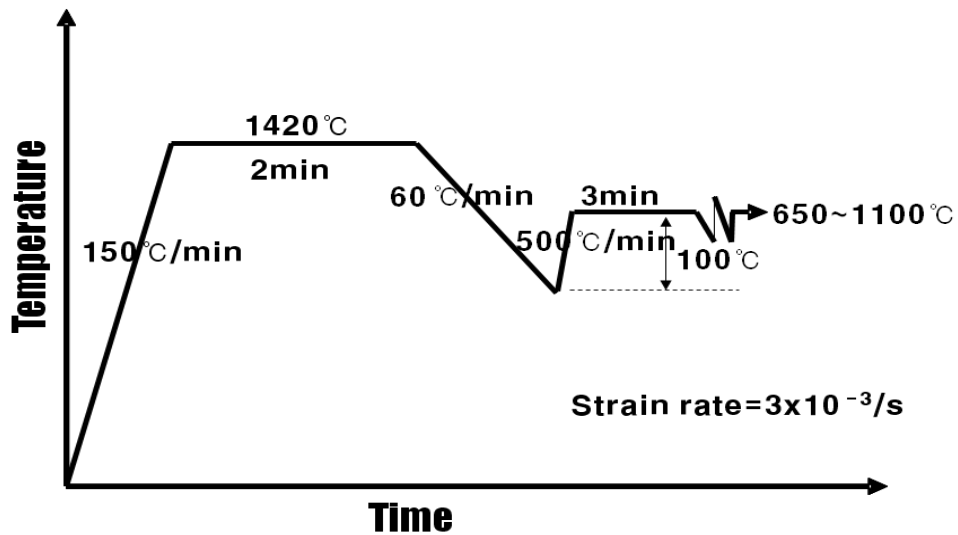
observed to fall rapidly, reach a minimum (primary stage of cooling) and then increase again and this is followed by the temperature cycling the temperature falling much more slowly to the straightener (secondary stage of cooling). During this stage, the temperature first rises as the strand goes into the guide rolls and then falls as it exits and the water sprays impinge on the surface. Experimentally, it is difficult to carry out this complex cycling treatment but it has been found that by putting in an under cooling step the agreement between the experimental work and commercial experience is much enhanced [149].

It is proposed in the present examination to, as well as testing using the simple cooling programme to also simulate the continuous casting operation more accurately by introducing an under-cooling step. The influence of cooling rate was also explored. Generally, 60°C/min was used which corresponds to the average cooling rate close to the surface where the cracks form for 220mm thick slab.

The tensile samples were initially heated at 150°C/min to 1420°C, the melting point where they were held for 2 minutes. They were then cooled at 60°C/min to either the required test temperature or if under cooled to 100°C below the test temperature. If under cooling was carried out, the samples were then immediately reheated at 500°C/min to the test temperature. Once the sample had reached the test temperature, it was held for 3 minutes before straining to failure. The test temperatures were in the range of 650°C to 1100°C. The tensile specimens were strained to failure at a strain rate of  $3 \times 10^{-3} \text{ s}^{-1}$  based on a gauge length of 22mm. The two temperature profiles used are shown, respectively in Figures 4.1(a) and 4.1(b) for without and with under-cooling. In addition samples from selected steels were given a faster cooling rate of 180°C/min, without under cooling, this cooling rate being chosen to correspond to the average cooling rate for thin slab casting, 50mm thick slab.



(a)



(b)

Fig.4.1 Temperature profile used (a) without and (b) with under cooling step.

The composition (wt.%), of the high Al, TWIP steels are given in Table 4.1.

The steels were all high C (0.6%) with 18%Mn except for steel 2 which was made having 22%Mn. Two levels of Al were examined very low and  $<0.05\%$ , steels 1~2 respectively and high 1.50% Al, steels 3~6. The N level was generally high 0.01 to 0.02% except for steel 6 (0.004%N). Steels 1~5 were laboratory melts but steel 6 was a commercial melt and this

had both a low N and lower S level (0.002%S compared to 0.006%S for the laboratory made steels) as well as having present Cr and a small amount Ni.

Table 4.1 Compositions of TWIP steels, wt%

Steel	C	Si	Mn	P	S	Al	N	Cr	Ni
1	0.61	0.05	18.07	0.009	0.006	0.047	0.0130	0	0
2	0.61	0.09	21.97	0.010	0.0066	<0.02	0.0160	0	0
3	0.61	0.07	18.09	0.009	0.0062	1.53	0.0095	0	0
4	0.61	0.06	18.10	0.010	0.0061	1.52	0.0170	0	0
5	0.61	0.05	18.16	0.010	0.006	1.52	0.0230	0	0
6	0.61	0.07	17.45	0.021	0.002	1.42	0.0043	0.55	0.22

### 4.3 Results

The hot ductility curves for the low Al containing steels (steels 1 and 2), and the high Al containing steels (steels 3~5) are given in Figs4.2 and 4.3 respectively and that for the commercially cast steel (steel 6) are shown in Fig.4.4 (top curve). It can be seen from Figs 4.2 and 4.3 that adding 1.5%Al causes the hot ductility to deteriorate in the temperature range 800~900°C from ~38% RA (Fig.4.2) to ~20% RA. Also as the N level increases from 0.01% (steel 3) to 0.023% (steel 5) there is a further decrease in ductility, Fig.4.3. The commercially cast high Al containing steel with the low N and S level (steel 6 in Fig.4.4) had improved ductility (~39% RA in the temperature range 800~900°C) similar to that given by the low Al containing steels.

In the laboratory cast high N, 1.5%Al containing steels (Fig.4.3), there was a tendency for the ductility to be worst in the temperature range 800~850°C and to recover slowly with further increase in temperature.

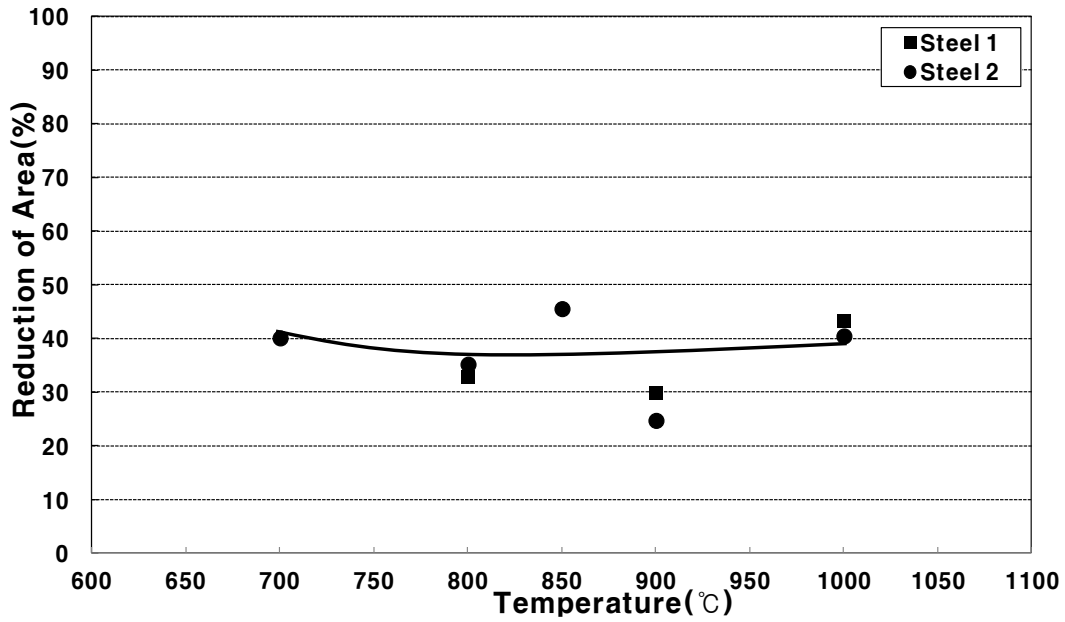


Fig.4.2 Hot ductility curve for low Al steels, steels 1 and 2. (Cooling rate: 60°C/min)

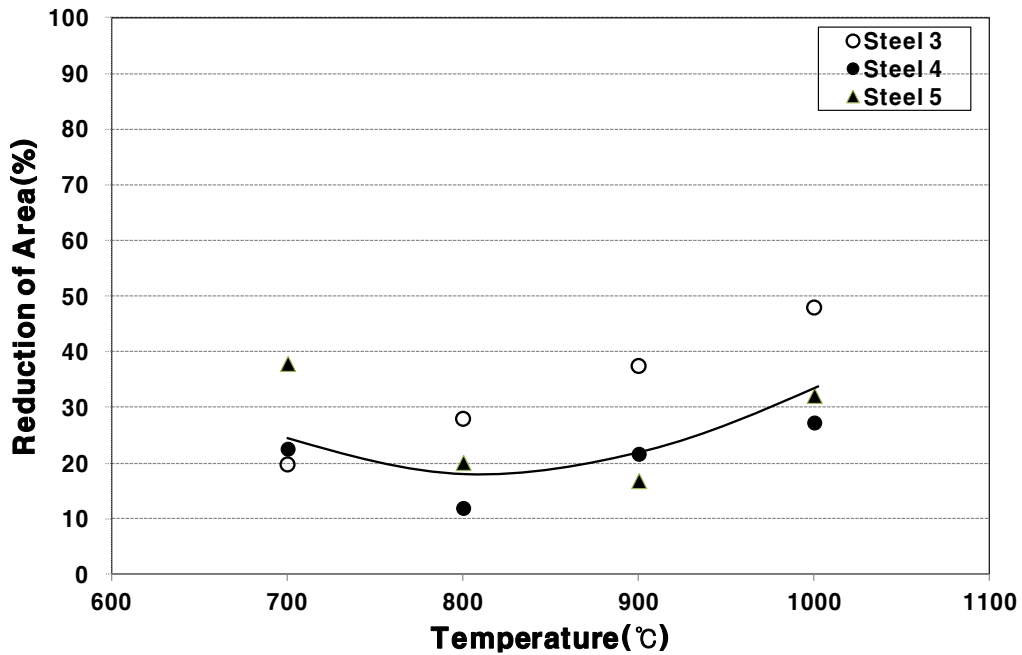


Fig.4.3 Hot ductility curves for high Al steels, steels 3(0.0095%N), 4(0.017%N) and 5(0.023%N). (Cooling rate: 60°C/min)

Introducing an under cooling step as in Fig.4.1 (b) results in a deterioration in ductility, with the RA decreasing by ~20% (Fig.4.4). A similar deterioration in ductility occurred for this steel when the cooling rate was increased from 60 to 180 °C/min without the under cooling step (Fig.4.4)

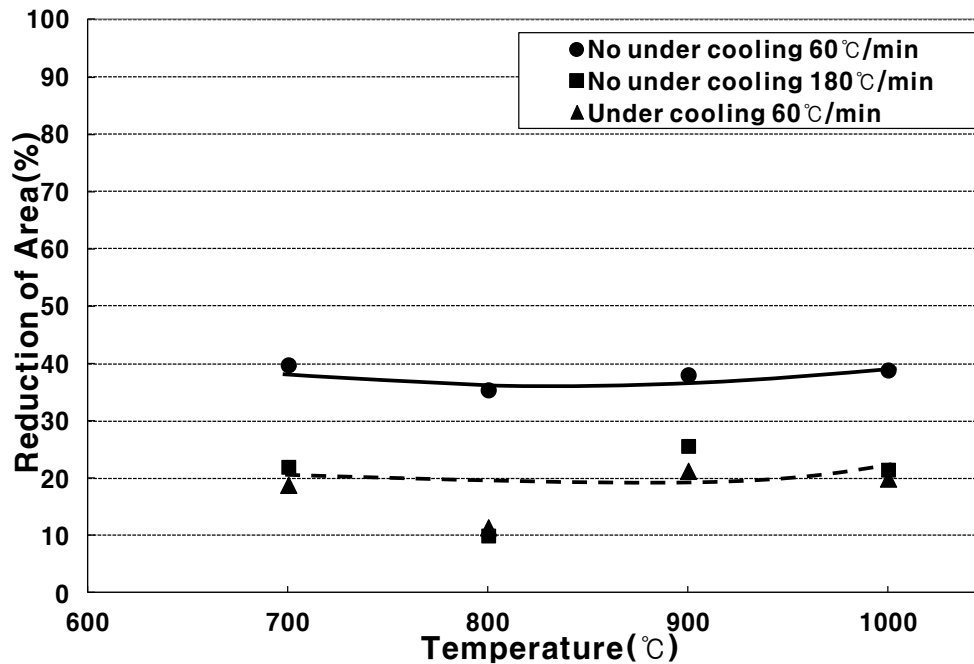


Fig.4.4 Hot ductility curves for 1.42%Al, 0.0043%N TWIP steel (steel 6), after cooling at 60°C/min and 180°C/min and after introducing the under- cooling step.

A smaller decrease in ductility was observed on increasing the cooling rate from 60°C/min to 180°C/min for the higher N steel(steel 5), the RA being on average 7% lower at the faster cooling rate(Fig. 4.5)

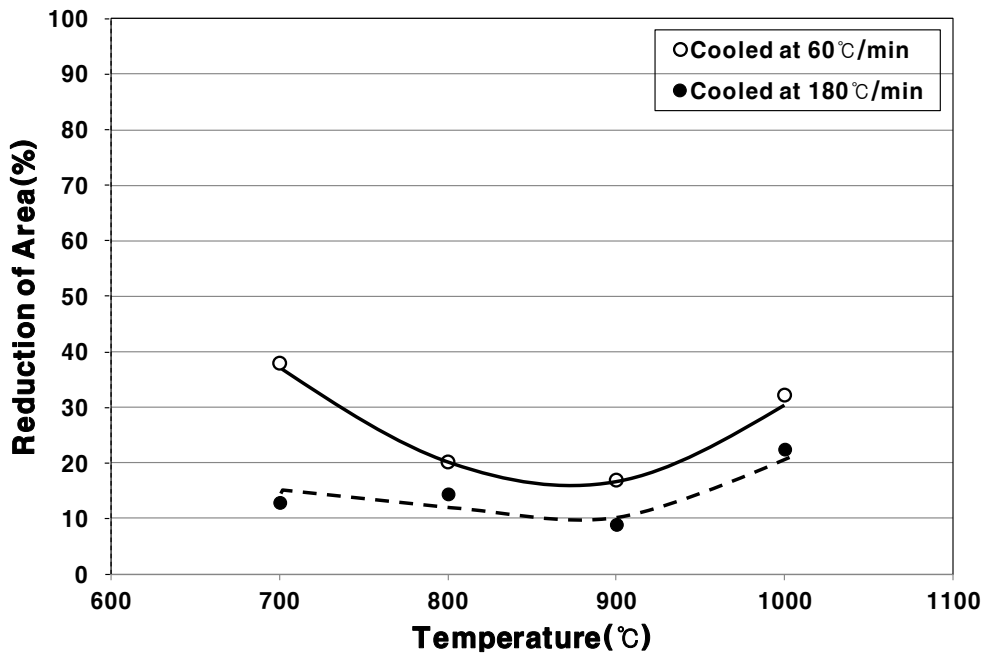


Fig.4.5 Hot ductility curves for high Al and high N steel (steel 5), at two cooling rates, 60°C (solid line) and 180°C/min (dashed line).

The microstructures for two test temperatures were examined 800°C and 900°C for steels 5 and 6, steels with ~1.5%Al, the former having a high N content (0.023%N) and the latter low (0.004%N). The microstructures for these steels at the two test temperatures are given in Figs.4.6 and 4.7 for the low N steel and Figs.4.8 and 4.9 for the higher N steel.

The structures are fully austenitic and the grain boundaries can be seen to contain many precipitates. In the low N, 1.5%Al containing steel, the precipitates were of shorter length than in the higher N steel.

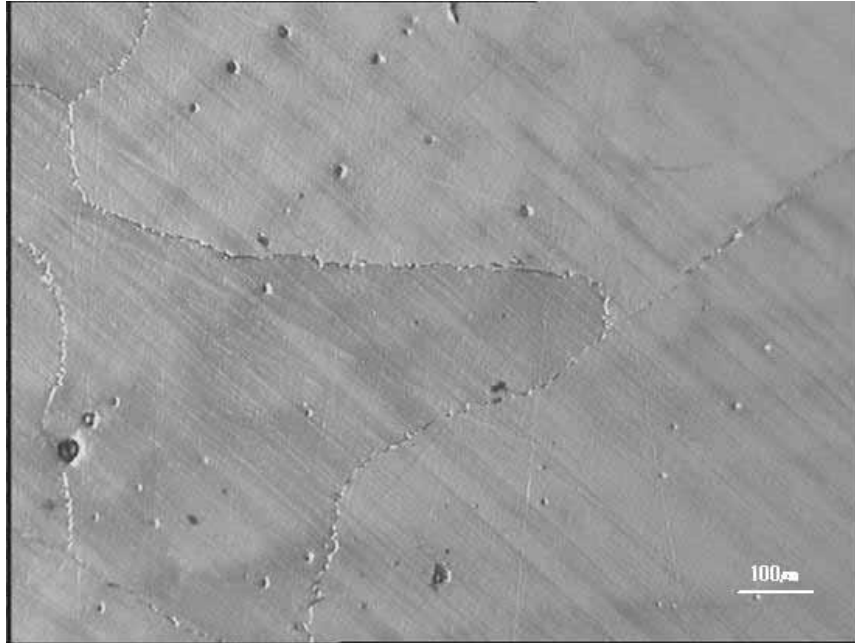


Fig.4.6 Micrograph of TWIP steel, steel 6 (1.42%Al, 0.0043%N) melted and tested at 800°C showing precipitation at austenite grain boundaries.

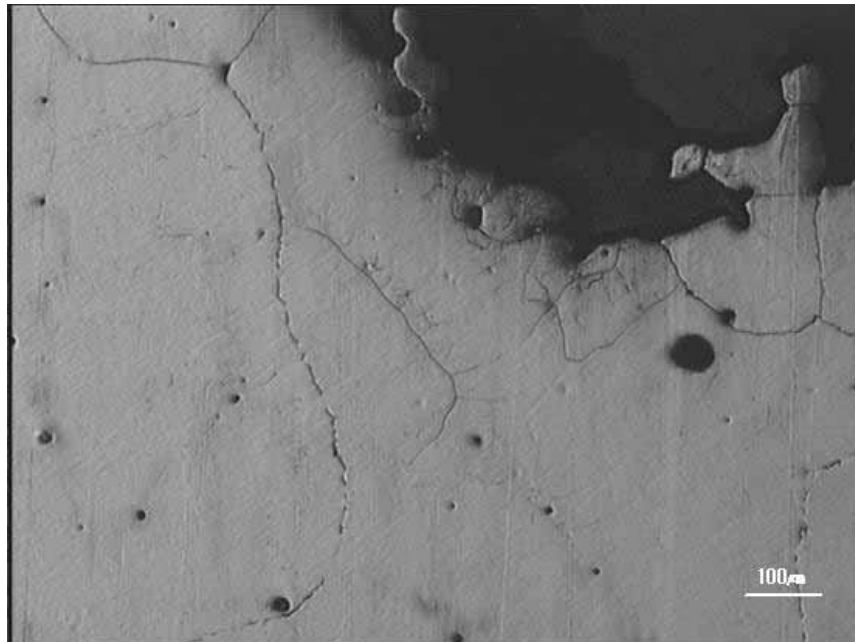


Fig.4.7 Micrograph of steel 6 (1.42%Al, 0.0043%N) melted and tested at 900°C showing precipitation at austenite grain boundaries.

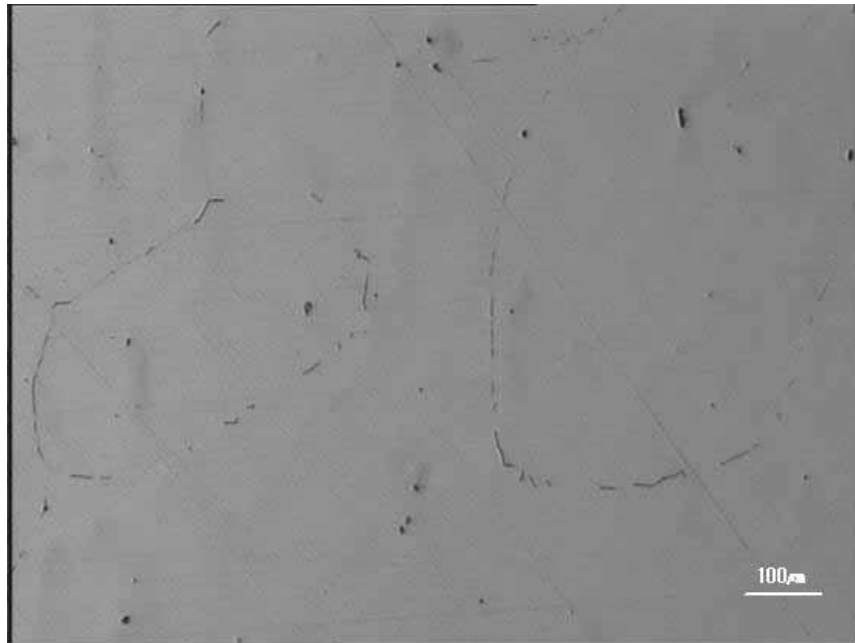


Fig.4.8 Micrograph of TWIP steel 5 (1.53%Al, 0.023%N) melted and tested at 800°C showing longer precipitates at the boundaries compared to the lower N steel 6 (Fig.4.7).

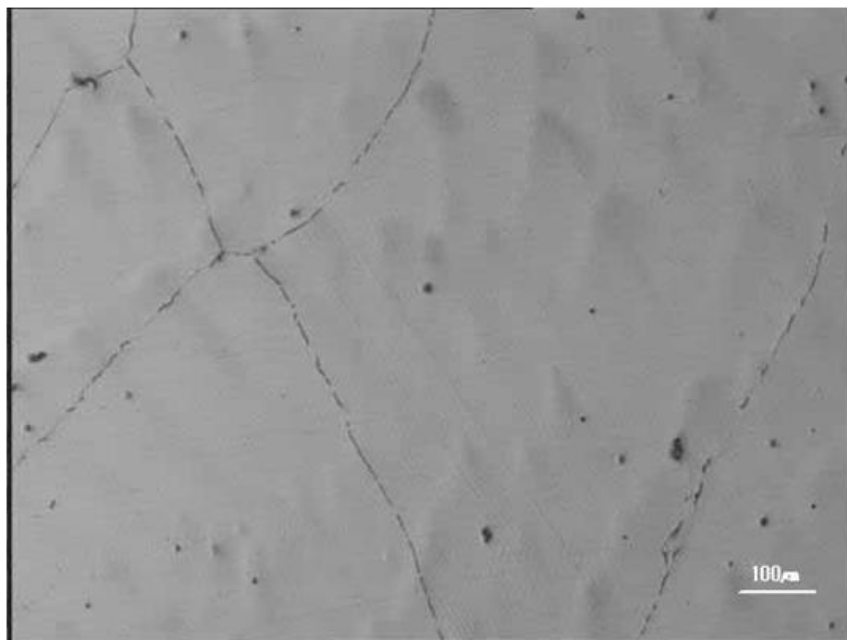
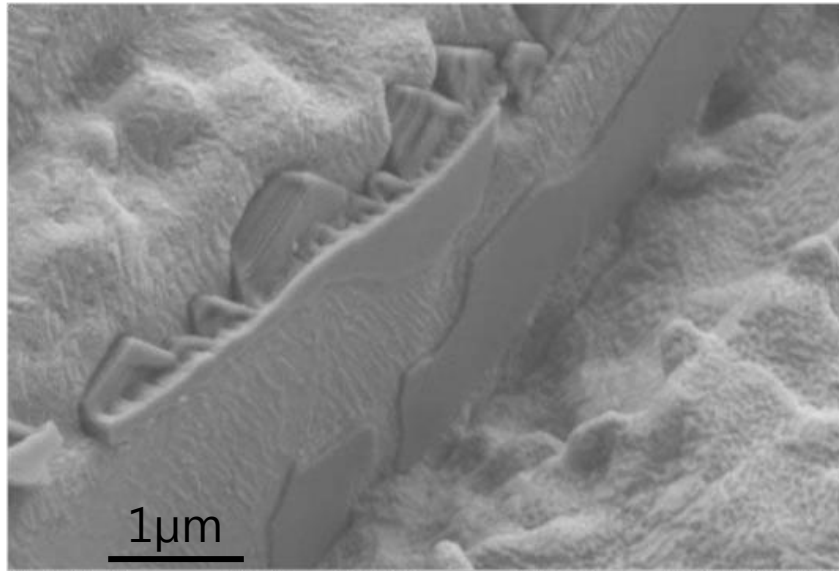
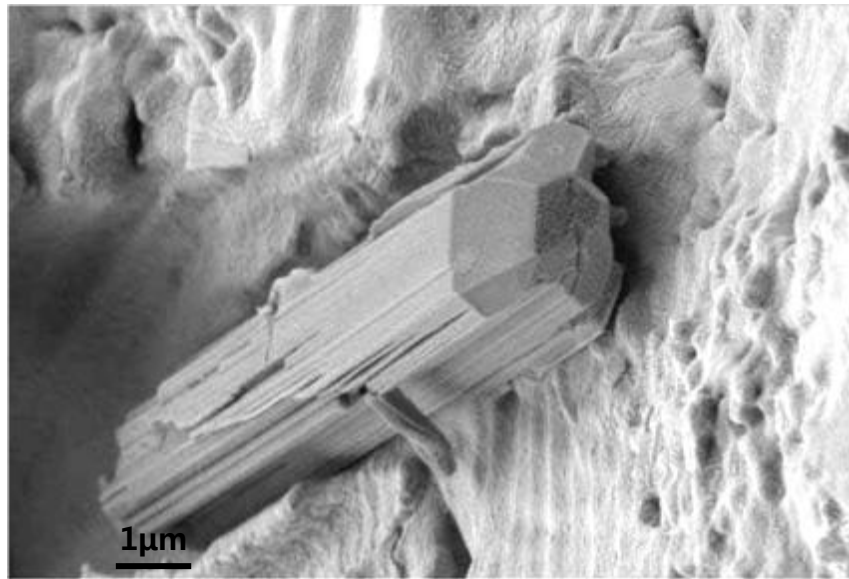


Fig.4.9 Micrograph of TWIP steel 5 (1.53%Al, 0.023%N) melted and tested at 900°C showing extensive precipitation at austenite grain boundaries.

Scanning electron microscope work identified the precipitates at the grain boundary as AlN precipitates (Fig.4.10 (a) and 4.10 (b)). In the higher N containing steel the precipitates were coarser, Fig.4.10 (b)



(a)



(b)

Fig.4.10 Copious precipitation of AlN at the austenite grain boundaries in (a) low N TWIP steel 6 (1.43%Al, 0.0043%N) showing very thin films of AlN at the grain boundaries on the fracture surface and (b) coarse AlN particle at the boundary in a high N, TWIP steel 3 (1.53%Al, 0.01%N). Both steels were tested at 800°C after melting and the fracture surfaces examined.

#### 4.4 Discussion

In HSLA (High Strength Low Alloy) low C steels ductility at both the high temperature and low temperature ends of the trough can recover to almost 100% RA. However, because these steels are fully austenitic one would not expect the ductility to improve at the low temperature end as it does in plain C-Mn and HSLA steels, when ferrite, which has excellent ductility, forms in substantial amounts below the  $A_{r3}$  [162]. Ductility would also be expected to improve markedly at the high temperature end in HSLA steels when dynamic recrystallisation occurs but for these very highly alloyed TWIP steels dynamic recrystallisation does not take place until very high temperatures. Previous work [51] has found that as the C level increases dynamic recrystallisation becomes more difficult and that it is clear from Fig. 4.2 which shows no improvement in ductility even as at high a temperature as  $1000^{\circ}\text{C}$ , that even without the presence of large volume fractions of AlN precipitation that the high C and probably high Mn levels make it increasingly difficult for dynamic recrystallisation to occur.

Previous work [21] on low Al steels tested in the temperature range in which the steels are fully austenitic but unrecrystallised has also found that the ductility remains approximately constant with temperature but ductility is only 40~50% RA so that the ductility of a fully ferritic unrecrystallised steel ( $\approx 100\%$  RA) is far superior to that of unrecrystallised fully austenitic steel. Presumably the increase in grain boundary sliding which occurs with increasing temperature, which would result in deterioration in the hot ductility, is approximately balanced by the increased rate of recovery. This also seems to be the case for the presently examined low Al, TWIP steels, with the RA remaining approximately constant within the temperature range  $700\sim 1000^{\circ}\text{C}$  (Fig.4.2); no dynamic recrystallisation having been observed to take place from metallographic examination. For the laboratory produced high Al containing TWIP steels, although dynamic recrystallisation was not observed, there is a slow improvement in ductility as the temperature increases, suggesting that some grain boundary migration may be taking place (Fig.4.3) or recovery is outweighing grain boundary sliding.

The temperature for the maximum rate of precipitation of AlN is  $815^{\circ}\text{C}$  [163], and the curves for the higher Al containing steels indicate that this test temperature gives the worst ductility (Figs 4.3 and 4.4). Table 4.2 lists the depth of the hot ductility curves at  $800^{\circ}\text{C}$  from Figs 4.2 and 4.3 for the steels examined. It can be seen assuming equilibrium conditions and that the entire N is taken out of solution by Al as AlN that increasing the Al and N contents or increasing the amount of AlN precipitated out results in the ductility decreasing. Ductility will be dependent on both the Al and N levels. Higher N levels favour

more AlN precipitation and higher Al levels favour a greater driving force for AlN precipitation. Thus, both high Al and N levels should be detrimental to ductility.

It therefore appears that from Table 4.2 that the ductility of the high Al, high N, 1.5% Al laboratory cast steels is worse than the low Al containing steels because of the greater volume of AlN particles present at the austenite grain boundaries. The marked AlN precipitation at the austenite boundaries is clearly shown in Figs. 4.6~4.10.

Table 4.2 AlN precipitation and its influence on the minimum depth of the trough

Steel	Mn, wt.%	Al, wt.%	N, wt.%	[Al][N] x 10 <sup>-4</sup>	AlN, wt.%	RA(800°C), %
2	22	0	0.0160	0	0	36
6	17.45	1.42	0.0043	61.1	0.012	39
1	18	0.047	0.0130	6.1	0.038	33
4	18	1.52	0.0170	255	0.050	13
5	18	1.52	0.0230	345	0.067	17

Under-cooling led to worse ductility. In previous work [71, 149], on low Al containing steels, under cooling also gave rise to a deterioration in ductility and this was ascribed to the under cooling causing more AlN to precipitate out. Similar reasoning may apply to the presently examined steels, although with these very high Al and high N steels there would be a much greater chance of achieving equilibrium.

Increasing the cooling rate again led to worse ductility. Previous work [77] on low Al containing HSLA steels has also found this behaviour and it was shown to be due to both a finer AlN particle and MnS inclusion size. Thus for a given volume fraction of particles more extensive coverage of the grain boundaries occurs when the particles are finer but more numerous and it is easier for intergranular cracks to interlink and give failure. This may also be the case for the higher Al containing steels. It is interesting to note that steels giving the best ductility steel 6 had both low S and low N. Previous work [21] has shown that a RA values in the range 35~40% needs to be attained when tensile samples are cooled at an average rate of 60°C/min directly to the test temperature to avoid transverse cracking. Ductility in these TWIP steels is therefore poor and transverse cracking will be a problem. However it can be seen from Fig. 4.11 which also gives the hot ductility curve for an X65 steel [99] that ductility in the critical temperature range 800~900°C is similar for both the HSLA steel and TWIP steels. HSLA steels of the composition given in Fig. 4.11 are nevertheless continuous cast and control rolled without cracking but great care has to be

taken.

As the ductility of these TWIP steels depends solely on the ductility of unrecrystallised austenite, low S and N levels are needed to keep the ductility sufficiently high to avoid transverse cracking and this is probably the reason for steel 6 giving the highest ductility of all the steels examined for the temperature range 700~1000°C.

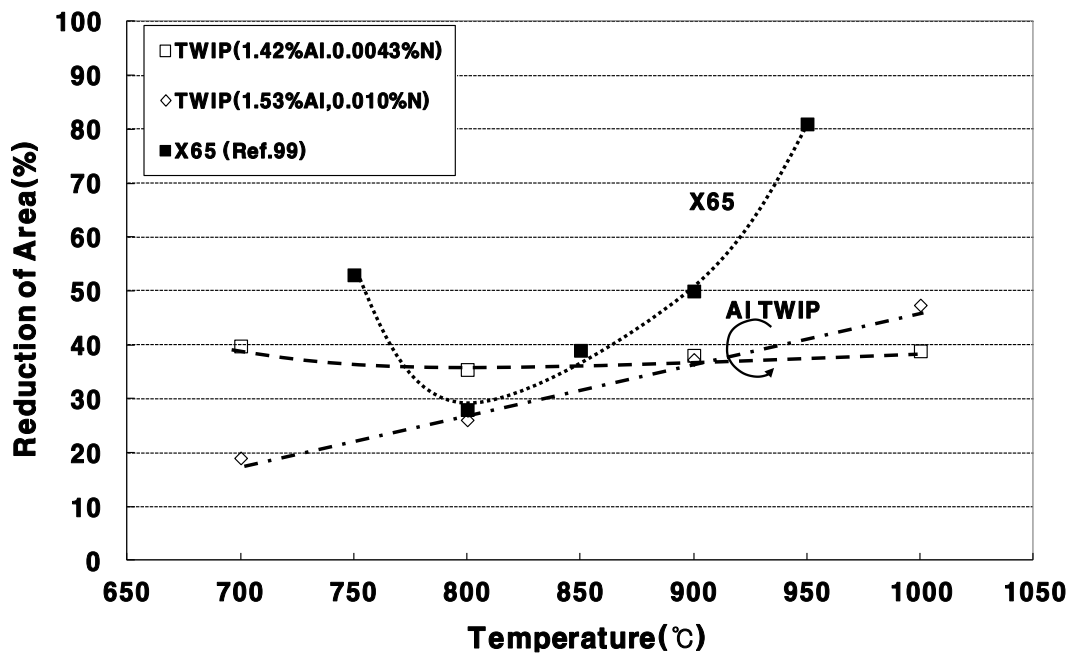


Fig.4.11 Summary of hot ductility curves for the Al containing in the melted “cast in situ” condition and typical hot ductility curve for a 0.1C-0.42Si-1.39Mn-0.007P-0.01S-0.036Al-0.0075N, HSLA steel. Cooling rate in all cases was 60°C/min.

#### 4.5 Conclusions

1. TWIP steels having 0.6%C and 1.5%Al have relatively flat hot ductility curves, the ductility increasing only very gradually with temperature. Because the thin film of ferrite is not present and dynamic recrystallisation does not take place, recovery in ductility at the high and low temperature ends of the trough does not occur.
2. Ductility is generally <40% RA indicating that with these TWIP steels it will be difficult to avoid transverse cracking. The 1.5%Al containing steels had worse ductility than the low Al containing steels because of the presence of large amounts of AlN precipitated at

the austenite grain boundaries.

3. Ductility is dependent on unrecrystallised austenite and therefore to avoid transverse cracking in these TWIP steels, low N and low S levels are recommended so that the volume fraction of second phase particles (AlN and MnS) is low.
4. Introducing an under cooling step to the cooling programme to better simulate the commercial process led to worse ductility.
5. Increasing the cooling rate from 60 to 180°C/min similarly caused deterioration in ductility.

## **CHAPTER 5: HOT DUCTILITY OF Nb/V CONTAINING HIGH Al, TWIP STEELS**

### **5.1 Introduction**

The first exercise had shown that for these high Al, TWIP steels there were going to be difficulties in casting and that when the high N levels were present it was going to make casting even more difficult.

These TWIP steels were also required at a higher strength level, ~1000MPa and a Nb addition was the most likely way of this being achieved. However, Nb containing steels are notoriously difficult to cast. In HSLA steels with 0.1~0.2%C, 1.4%Mn, Nb additions can cause RA value to be as low as 10% in the straightening temperature range [69, 127]. V in contrast has been found to have a less detrimental influence on hot ductility of HSLA steels and when Nb and V together even better ductility can be obtained [112]. V additions have been found to have a much smaller influence than Nb on the hot ductility provided the nitrogen level is low giving rise to a coarser precipitation. There is also some evidence that adding V to an Nb containing steel can improve its ductility by slowing down the rate of precipitation [128].

The hot ductility of Nb/V containing TWIP steels was therefore examined although from previous work on HSLA steels; ductility was likely to be worse than the simpler microalloying free TWIP steels. A lower N level was also chosen (0.007%N) to see whether this might make the difference.

### **5.2 Experimental**

The composition of the Nb/V high Al containing TWIP steels used in the present exercise are given in Table 5.1. The steels contained 0.6%C and 18%Mn. The composition was similar for most of the steels, the N level being 0.007% lower compared to an average N content of ~0.017%N for the Nb/V free high Al containing TWIP steels used in the previous chapter. Two of the steels in Table 5.1, F and AA had low N levels of 0.003%. The Nb level chosen was 0.03% and the V level was set at 0.1%.

The major difference between the steels was in their initial state prior to tensile testing. In the first group, Table 5.1, A-2, B-2 and F, the tensile specimens were all cast in-situ. In the second group, A-1, AB and AA were all heated to 1350°C before tensile testing.

Table 5.1 Composition of Nb/V containing TWIP steels, wt%

Steel	C	Si	Mn	P	S	Al	Nb	V	N	Condition
A-2	0.61	0.21	18.32	0.010	0.005	1.55	0.029	0.12	0.0065	Cast in situ
B-2	0.61	0.21	18.21	0.010	0.005	1.54	0.028	0.12	0.0084	Cast in situ
F	0.61	0.20	18.11	0.011	0.006	1.42	0.032	0.10	0.0029	Cast in situ
A-1	0.61	0.22	18.20	0.010	0.005	1.56	0.028	0.11	0.0068	Machined As-Cast
AB	0.61	0.20	18.03	0.012	0.010	1.41	0.031	0.10	0.0070	Machined Hot-Rolled
AA	0.61	0.19	17.74	0.012	0.009	1.41	0.032	0.10	0.0030	Machined Hot-Rolled

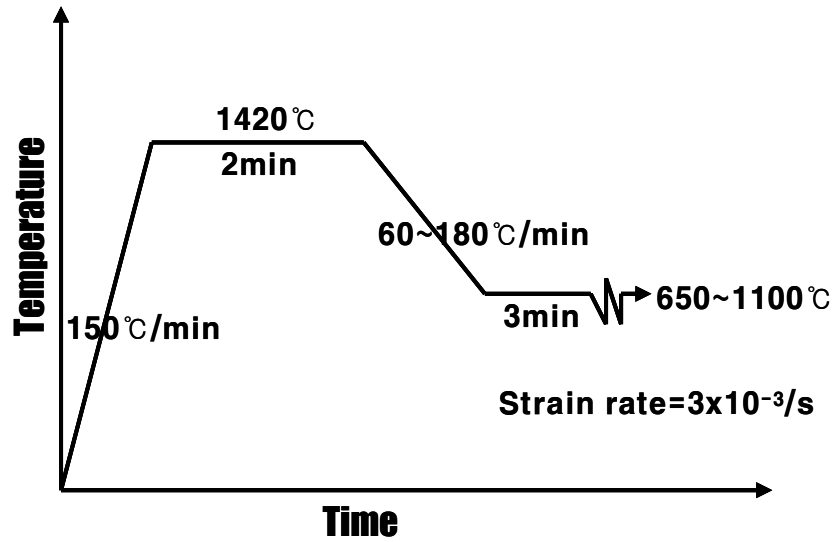
In this case, tensile samples were machined from the as cast ingots or from plates after hot rolling, the samples being taken along the rolling direction. Theoretical calculations by Factsage 6.1 program gave the solidus and liquidus temperatures for the steels, as 1283°C and 142°C, respectively.

Tensile specimens were cast in situ using the induction testing rig at City University London. When cast in situ the tensile samples were 110mm in length and 7.7mm in diameter.

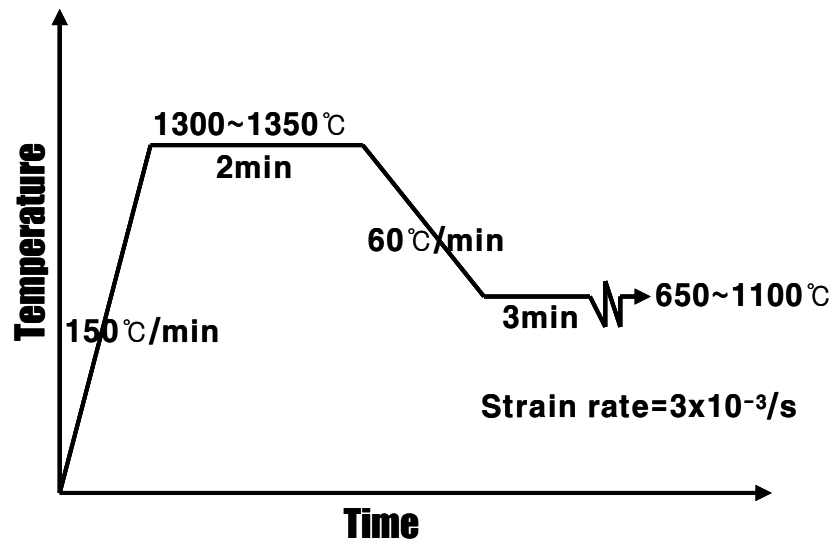
The TWIP steels, A-2, B-2 and F in Table 5.1, were heated to 1420°C so that the samples were fully melted, held for 2 minutes and then cooled to the required test temperature at 60°C/min or 180°C/min for selected steels. The former cooling rate (60°C/min) corresponds to the average cooling rate close to the surface of conventional continuous slab (220mm thick) and the latter (180°C/min) to that for thin slab casting (50mm thick slab). The tensile specimens were strained to failure at the same strain rate of  $3 \times 10^{-3} \text{ s}^{-1}$  based on a gauge length of 22 mm.

Steels A-1, AA and AB were tested using a Gleeble machine. The dimensions of the tensile specimen were 120 mm in length having a diameter of 10mm. For steel A-1, the tensile samples were machined from the as cast ingot, heated to 1300°C held 2 min, cooled at 60°C/min to the test temperature where they were held for 3 min and then strained to failure using a strain rate of  $3 \times 10^{-3} \text{ s}^{-1}$  (denoted “machined as-cast” in the text). For steels AA and AB, the tensile samples were machined from the hot rolled plate after ingot casting. In this case the tensile specimens were heated to a higher temperature of 1350°C, held 2 min and then given the same thermal history and testing as for A-1 (these samples will be referred to as “machined hot rolled”, Table 5.1).

The temperature profiles for the “as cast in situ” and the “machined as cast and hot rolled” specimens are shown in Figs. 5.1 (a) and 5.1 (b), respectively.



(a)



(b)

Fig.5.1 Schematic diagram for the testing conditions for (a) “cast in situ” and (b) “machined as-cast or hot rolled” tensile specimens.

After measurement of the RA, a sample taken close to the point of failure was prepared for metallographic examination. Optical microscopy was performed in order to detect precipitation at the austenite grain boundaries as well as measure the austenite grain size

using the mean linear intercept method.

SEM with analysing facilities was used to examine the fracture surfaces and identify the precipitates that were present on the fracture surface. Carbon extraction replicas were also taken from sections close to the point of fracture and examined using a TEM.

### 5.3 Results

The hot ductility curves for the three “cast in situ” steels are given in Fig.5.2. It can be seen that the ductility for these steels is very poor, the RA values in the temperature range 700~900°C being <20% and there is no significant difference in hot ductility behaviour for these steels even though the total N level varied from 0.0085 to 0.003%N. The curves for “machined as-cast” and “cast in situ” steels with very similar composition are given in Fig.5.3 and again taking into account the scatter, there is no significant influence in hot ductility between the two conditions. In Fig.5.4, the “machined hot rolled” condition is compared with the “machined as cast” and it can be seen that the hot rolled condition gives better ductility and increasing the N level makes the ductility worse.

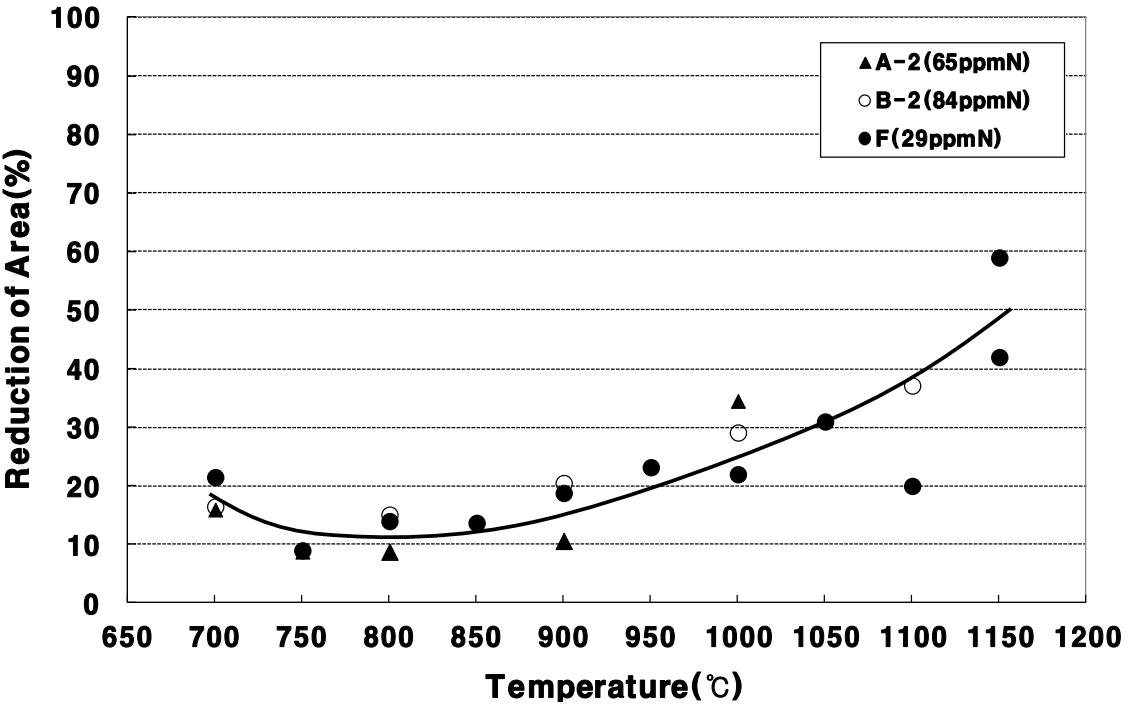


Fig.5.2 Hot Ductility curves for Nb/V TWIP steels, in the “cast in situ” condition. (Cooling rate: 60°C/min)

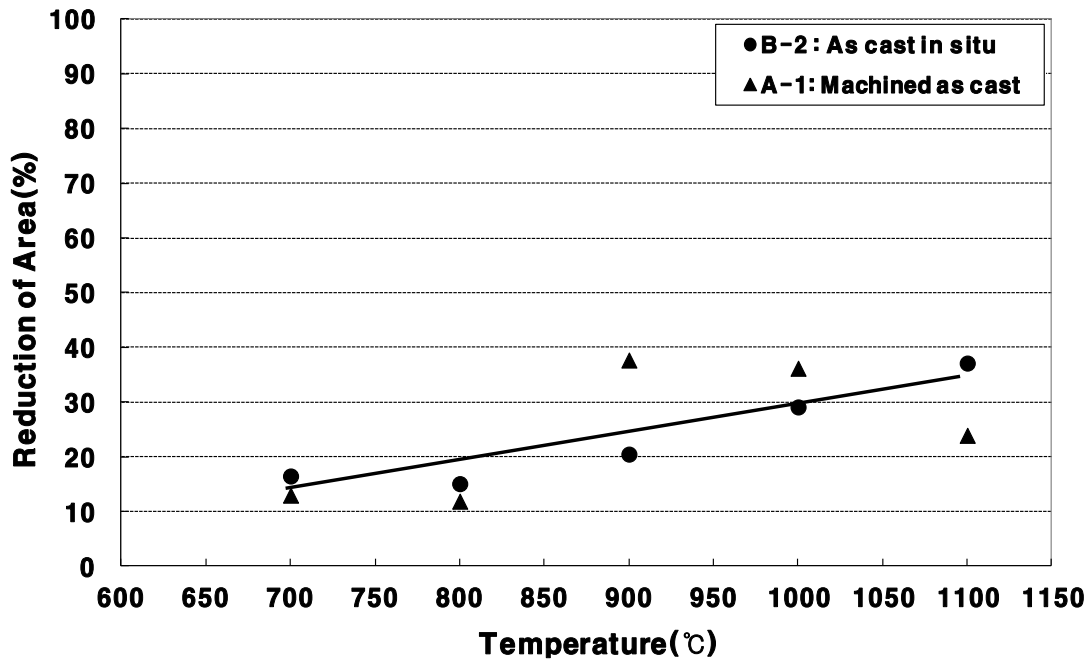


Fig. 5.3 Hot ductility curves for “machined as-cast” and “cast in situ” steels of similar composition

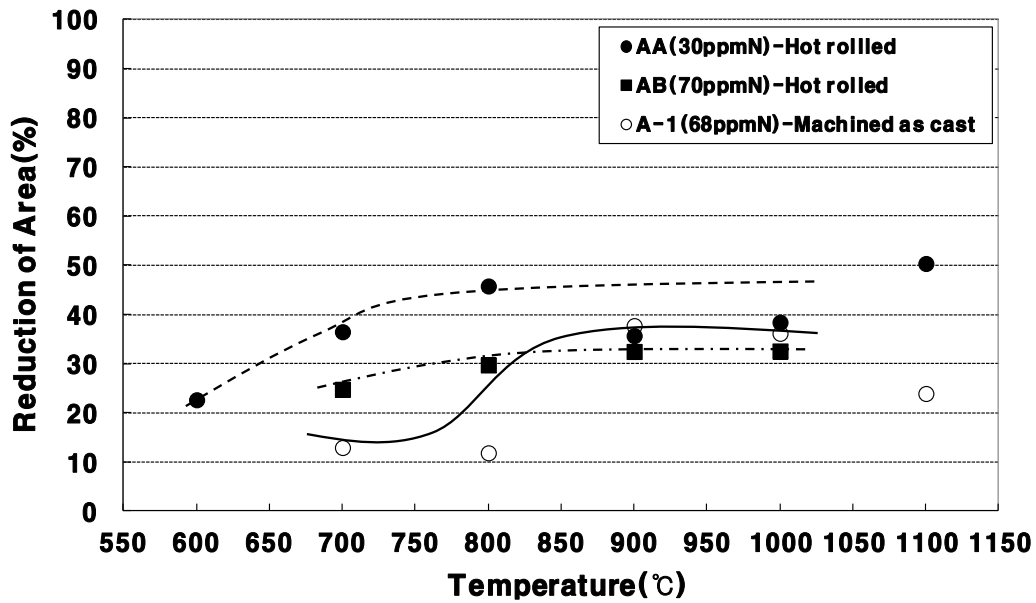


Fig.5.4 Hot ductility curves for "machined hot rolled" (dashed curves) and "machined as-cast" steel (solid curve).

The effect of increasing the cooling rate from 60°C/min to 180°C/min is given for the two steels, B-2, (0.0084%N) and F, (0.003%N) in Fig.5.5. While increasing the cooling rate for the higher N steel led to only a very small decrease in the ductility, for the lower N steel a substantial decrease in ductility was observed, ductility being as low as 5% RA throughout the temperature range 750~950°C.

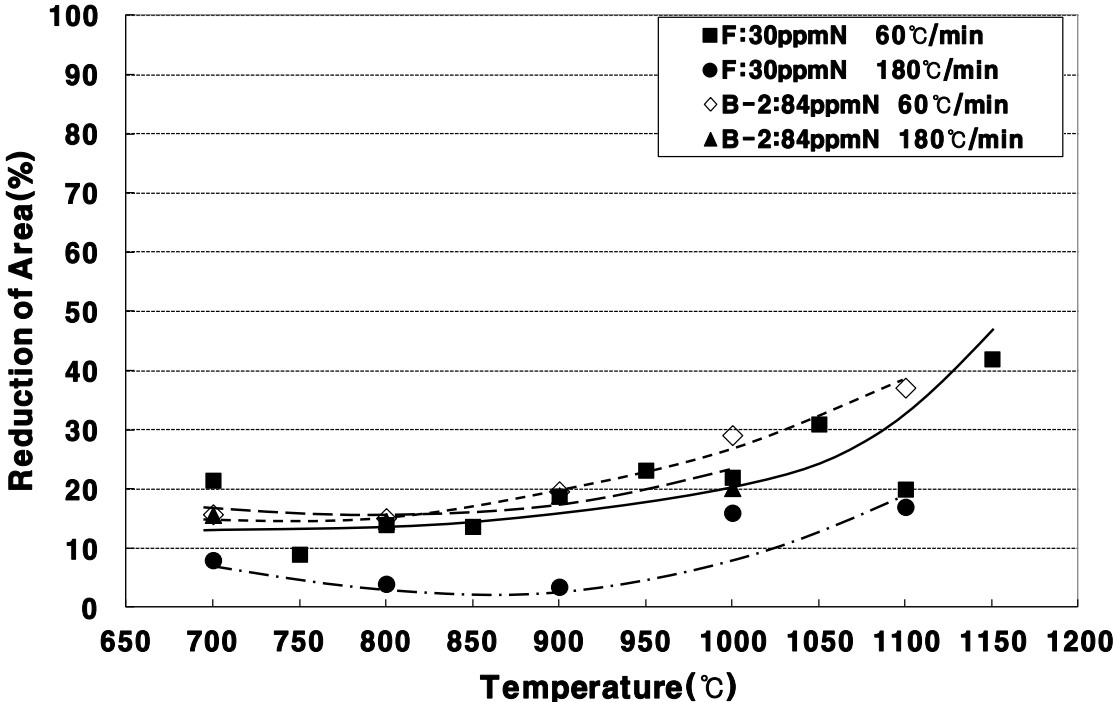


Fig.5.5 Influence of cooling rate on the hot ductility of low and higher N, Nb/V containing TWIP steels.

The steels were all fully austenitic from solidification temperature to room temperature and as no phase transformation occurs on re-heating to 1300~1350°C no grain refinement can take place. As a consequence the grain size for the “cast in situ” and “machined as-cast” tensile specimens was similar at ~ 325µm. Hot rolling caused the grain size to refine and for the “machined hot rolled” condition the austenite grain size was 150µm.

The change in microstructure on testing in the temperature range 700 to 1100°C was similar for all three conditions and only the micrographs for the “machined as cast” condition are shown in Fig.5.6. Marked precipitation at the boundaries occurred at 700°C, Fig.5.6 (a) and

as the temperature of testing increased the precipitation became less, there being little present above 1000°C, Fig.5.6 (e).

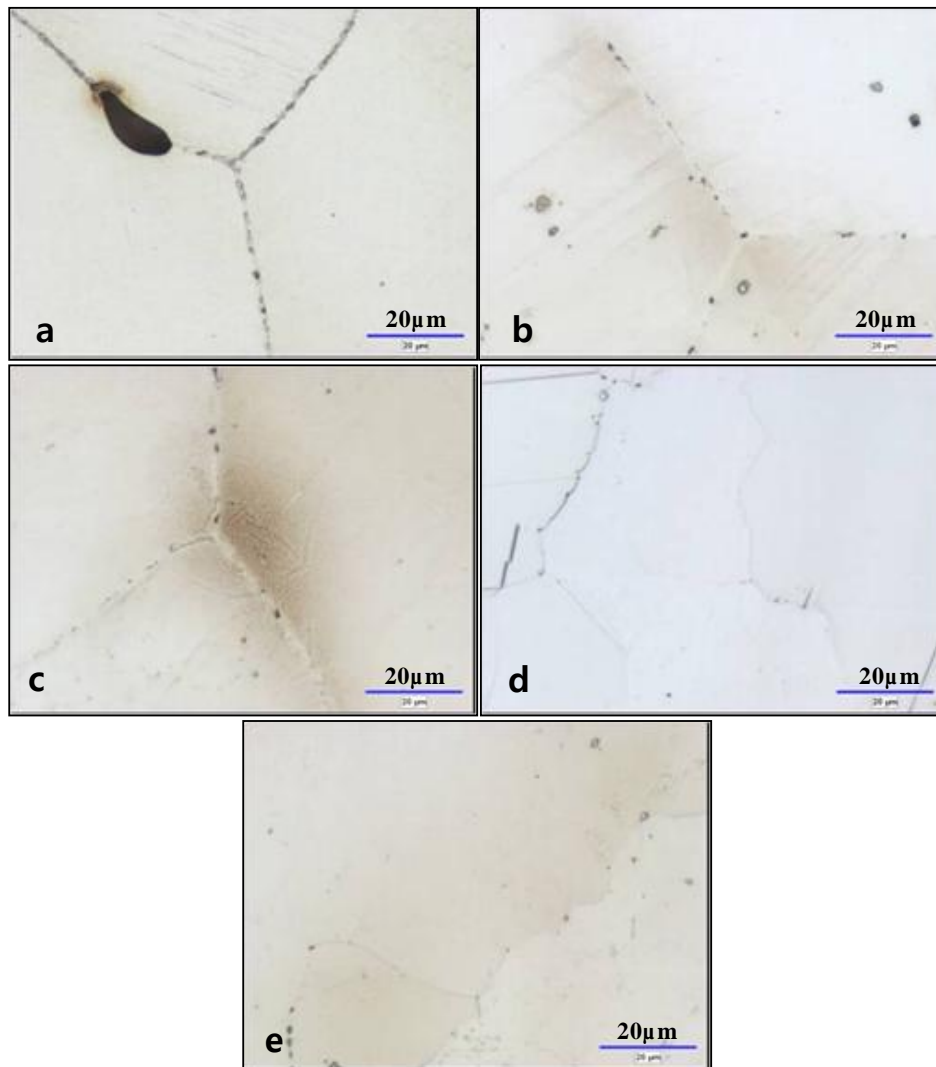


Fig.5.6 Micrographs of as cast steel, A-1, (0.0068%N) tested at (a) 700°C, RA 13%, (b) 800°C, RA 12%, (c) 900°C, RA 38%, (d) 1000°C, RA 36%, (e) 1100°C, RA 24%

Evidence for dynamic recrystallisation occurring was only found at very high temperatures, 1100~1150°C when ductility was seen to improve as shown in Fig.5.7 for the “cast in situ” steel F.

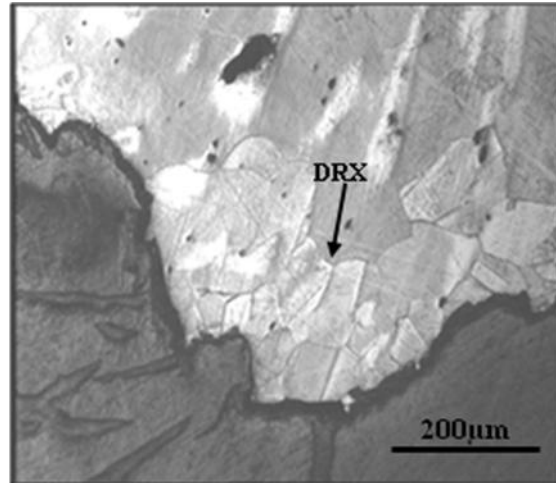
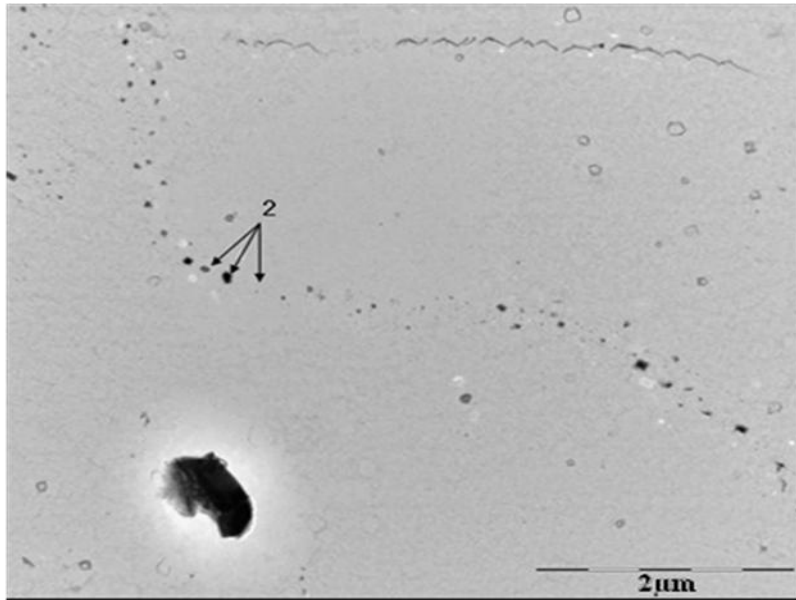


Fig.5.7 Dynamic recrystallisation (DRX) at the fracture surface for steel F (“cast in situ”) tested at 1150°C. (RA was 50%)

TEM work on the hot rolled high Al, Nb/V TWIP steel, using carbon replicas taken from sectioned tensile specimens close to the point of fracture have clearly identified precipitates of Nb(C, N) and VN at the boundaries as well as Nb(C, N) in the matrix. The typical precipitation found at the austenite boundary is shown in Fig.5.8 (a) and the associated analysis of the particles that are present is given in Fig.5.8 (b).

It should be noted however, that the V peaks are very small compared to the Nb suggesting there is little VN considering the large amount of V (0.1%) present in the steel. It may be that because of the high Al and presence of Nb both competing for N in solution that there is in fact little N available for forming VN.



(a)

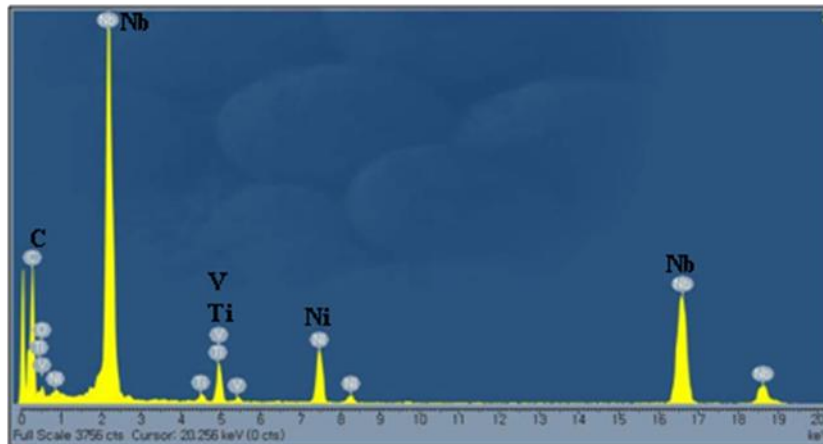


Fig.5.8 (a) typical precipitation found in the Nb/V steels with associated analysis for particles (Steel A-1 was “machined as-cast” and tested at 700°C) and (b) position 2 in (a) showing strong Nb peaks with much smaller V peaks.

Coarse precipitates of AlN (6μm) were also located within the grains but were not associated with the austenite grain boundaries (Fig.5.9).

Fine Nb(C, N) precipitation was found at the grain boundaries and within the matrix, Fig.5.10.

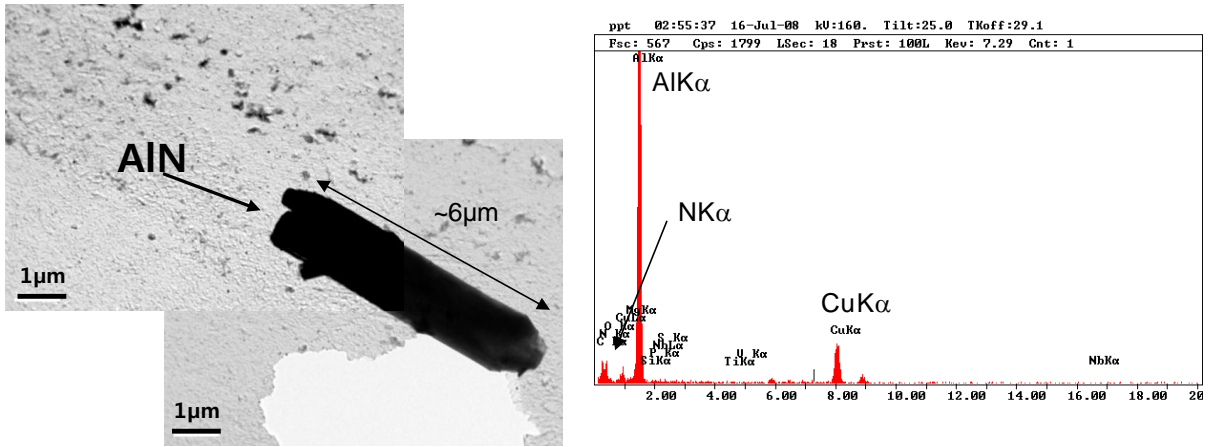


Fig.5.9 Very coarse AlN precipitation not associated with the grain boundaries in steel AB, "machined hot rolled".

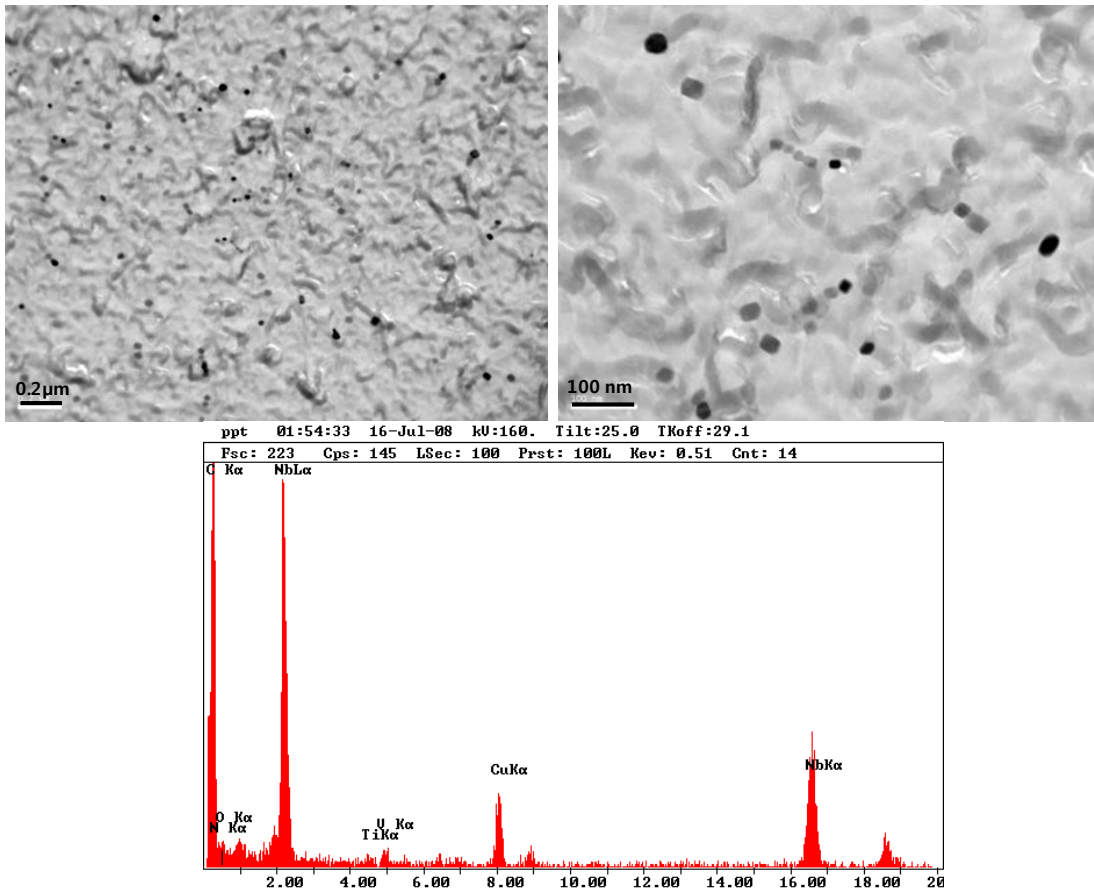
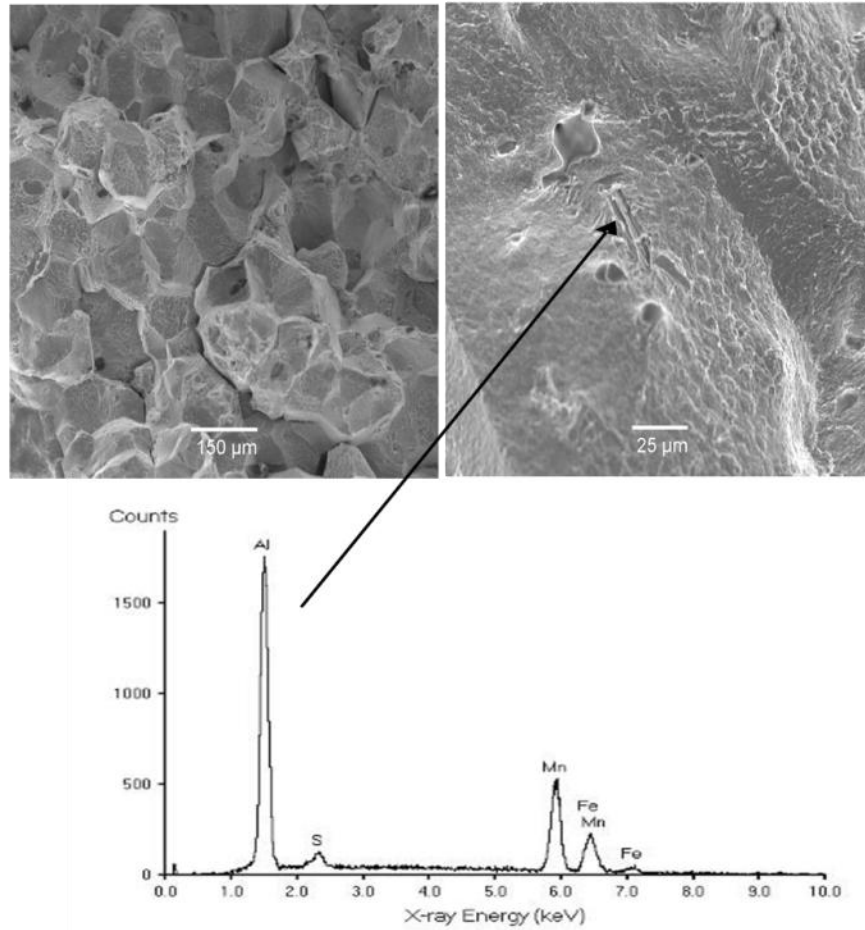
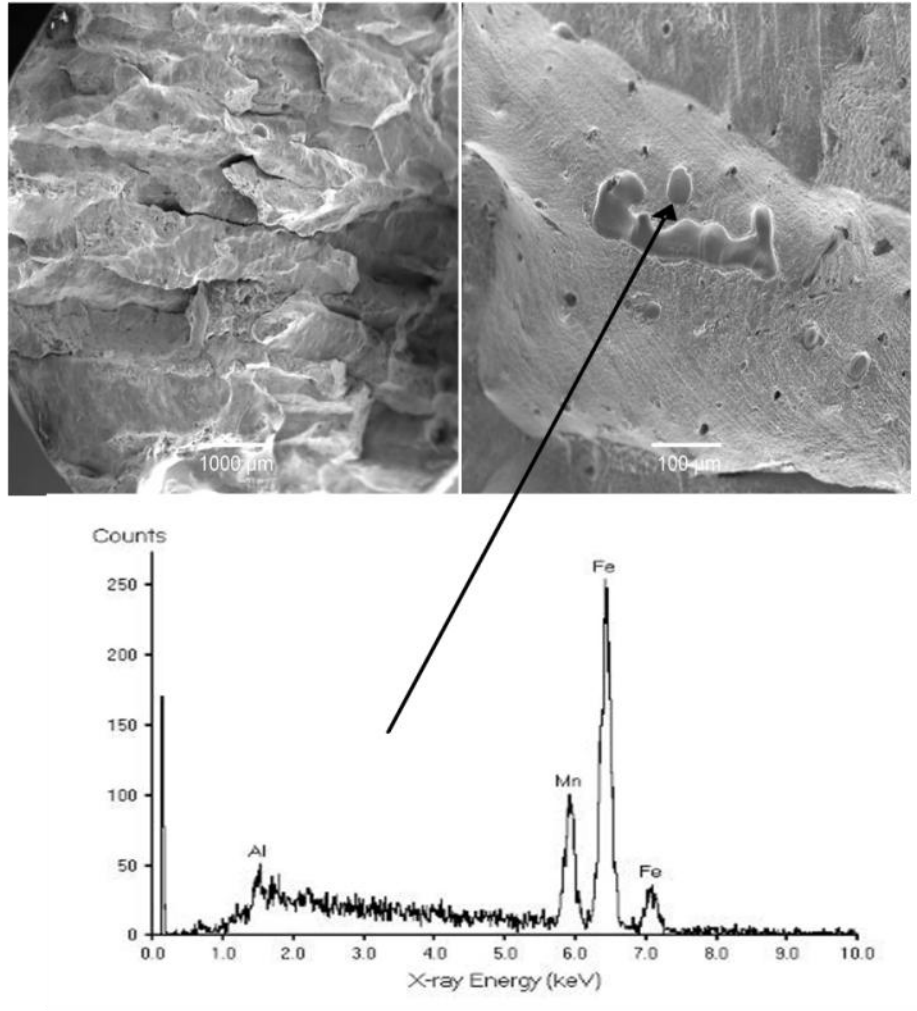


Fig.5.10 Fine Nb(C, N) precipitation (12~40nm) within the austenite grains in steel AB, "machined hot rolled".

Examination of the fractured surfaces using the SEM showed evidence for this dendritic AlN precipitation in the TWIP steels as shown in Fig.5.11 which also shows the intergranular failure appearance for a tensile specimen tested at 700°C. It should be noted that intergranular failures were observed for all the tensile specimens up to temperatures as high as 1000°C.



(a)



(b)

Fig.5.11 Films of AlN found on the fracture surface of (a) “machined as rolled” and (b) “machined as-cast” steels tested at 700°C.

## 5.4 Discussion

The ferrite transformation which normally plays a large part in accounting for the hot ductility behaviour of HSLA steels [20] is absent in these steels, the TWIP steels being fully austenitic. The factors that influence hot ductility are the austenite grain size and the precipitation processes that occur at the austenite grain boundaries and within the matrix. Dynamic recrystallisation by further refining the grain size and allowing the cracks forming along grain boundaries to become isolated can also lead to a considerable improvement in the hot ductility. However, dynamic recrystallisation was not observed in these steels until

very high temperatures  $\geq 1100^{\circ}\text{C}$  and does not occur during the straightening operation in continuous casting as the strain involved is too low and the grain size too coarse.

It should be noted that because of the high Mn level and low melting point of the steel, the austenite grain size is significantly finer than found in the Nb containing 1.4%Mn HSLA (High Strength Low Alloy) line pipe steels. In the latter case, the as cast grain size is 1~2mm whereas in the present instance is  $\sim 325\mu\text{m}$ , almost an order in magnitude finer.

Grain size is important in controlling ductility behaviour for the following reasons [20]:

(i) When the failure mode is intergranular, the crack aspect ratio which controls the stress concentration at the tip of a crack is greater the coarser the grain size.

(ii) It is harder to propagate cracks by grain boundary sliding at triple points in finer grained steels.

(iii) The increased specific grain boundary area in finer grained steel (for a given volume of precipitate) reduces the precipitate density on the grain boundaries.

Finer grain sizes require a smaller critical strain for dynamic recrystallisation so that recrystallisation leading to an even finer grain size is encouraged and intergranular cracks become isolated.

The influence of grain size on ductility is shown in Fig.2.16 (chapter 2), for steels with 1.4%Mn and it can be seen that whereas refining the grain size from 1~2mm to  $325\mu\text{m}$  leads to little improvement in ductility refining the grain size further to  $150\mu\text{m}$  leads to a significant improvement,  $\sim 15\%$  increase in the RA value in accord with the present results [20]. The grain size of these TWIP steels are therefore at the threshold of when significant changes to ductility might take place.

Hence, when comparing the ductility of “machined as cast” tensile specimens with “machined hot rolled” tensile specimens, it should be noted that the hot rolling breaks down the as cast structure and refines it so that its grain size is refined from  $325\mu\text{m}$  to  $\sim 150\mu\text{m}$  and in consequence the ductility improves. Unfortunately, there is little one can do to refine the austenite grain size during continuous casting so that grain size will always be  $\sim 325\mu\text{m}$ .

The second factor in these steels affecting hot ductility is the precipitation processes and it is these that give rise to the ductility trough and poor ductility. The steel is a complex steel, having high Al, Nb and V present, all of which can give rise to precipitation in the austenite. Both Nb(C, N) and VN can precipitate rapidly during tensile testing [20]. For typical microalloying composition for Nb and V, the nose temperature for Nb(C, N) precipitation is  $950^{\circ}\text{C}$  whereas it is about  $885^{\circ}\text{C}$  for VN [164]. The very high Al level would also favour AlN precipitation up to very high temperatures and AlN can be particularly detrimental to

hot ductility as AlN precipitates mainly at the austenite grain boundaries and as seen from this work precipitates is a dendritic film. The cause of the continued poor ductility <40% RA, even to as high a temperature as 1100°C is probably due to the presence of AlN at the austenite grain boundaries in these high Al containing steels restricting dynamic recrystallisation from occurring and reducing the ductility by encouraging crack growth by grain boundary sliding. These fine films of AlN at the austenite grain boundaries, however, are notoriously difficult to extract from sections but examination of the fractured surfaces clearly shows their presence (Fig. 5.11).

In all these cases, the precipitates that are formed in the austenite will be mainly nitrides rather than carbides (Nb(C, N) is mainly a carbide precipitate but does contain a substantial amount of N when precipitated in the austenite) and hence the nitrogen level becomes again of the utmost importance in controlling the ductility.

Ductility is therefore likely to be very poor in the temperature range 800~950°C because of Nb(C, N) and VN precipitation but even at higher temperatures when the precipitates are not present AlN will be preventing ductility from recovering to its full potential for unrecrystallised austenite. As previously mentioned, even when no precipitates are present the ductility of unrecrystallised austenite only reaches at most 50% RA, but a value of 40% is sufficient to avoid transverse cracking [21].

Previous work [75] has always shown that increasing the cooling rate in ferrite/pearlite steels leads to a loss of ductility because faster cooling rates result in finer precipitation as well as finer sulphides at the austenite grain boundaries and finer precipitation within the matrix. Although inclusion and particle size were not examined in the present research work, it seems reasonable to expect similar behaviour to that shown by the HSLA steels. The finer precipitation increases the flow stress on the boundary as well as shortening the distance between the particles at the boundaries making it easier for inter-granular cracks to open up and propagate along the boundary. Although the steels in the present work are austenitic it is likely that the cause of the deterioration on faster cooling is the same and the S and N levels should be as low as possible to restrict the number of particles.

A summary of all the present and previous work from Chapter 4 is given in Fig.5.12 and shows that adding Nb/V to a high Al TWIP steel results in a significant loss in ductility for the temperature range 800~1100°C. The X65 steel [99] given a similar testing programme as shown in Fig.5.1 (a) is also included in the diagram. This Nb containing steel with its relatively low Al level can just about be cast without transverse and edge cracking occurring. Recent work [21] has shown that provided the straightening temperature would

give a RA value in excess of 35% cracking should not be a problem. The hot ductility curves for the high Al, Nb/V free TWIP steels have a similar depth to this X65 steel but the trough is much wider. However, when Nb/V are present the depth of the trough markedly increases to such levels that there is little influence of the N content on the hot ductility and to avoid cracking in this steel, straightening would have to be carried out at temperatures in excess of 1100°C a temperature too high for conventional straightening during continuous casting. Thus even at this lower N level of 0.007% cracking is still likely to be a problem.

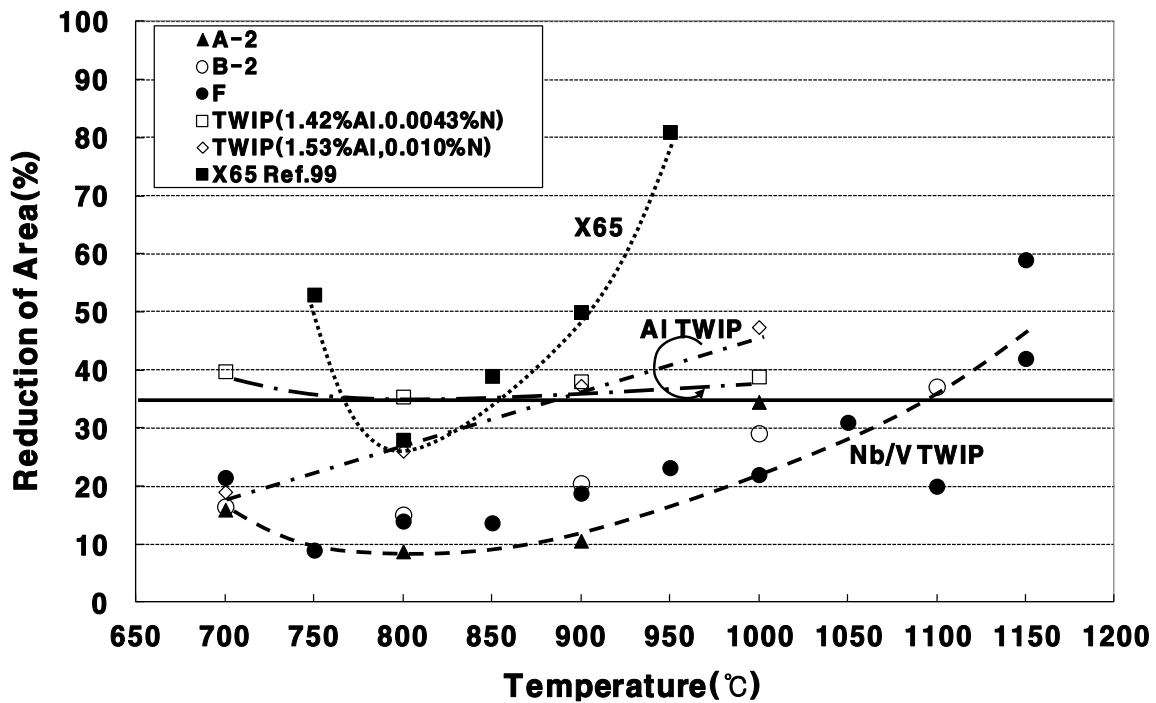


Fig.5.12 Summary of hot ductility curves for the Al containing Nb/V free high N TWIP steels and the Nb/V containing high Al TWIP steels in the melted “cast in situ” condition also included is a typical hot ductility curve for 0.1C-0.42Si-1.39Mn-0.007P-0.01S-0.036Al-0.0075N steel. Cooling rate in all cases was 60°C/min.

## 5.5 Conclusions

1. Adding Nb and V to the high Al containing TWIP steel resulted in worse ductility.
2. Increasing the cooling rate from 60 to 180°C/min after melting causes the ductility to further deteriorate but the deterioration is dependent on the N level, high N levels

producing only a very small reduction in the ductility, probably because ductility is so poor.

3. The hot ductility of “machined hot rolled” TWIP steels is better than “machined as-cast” TWIP steels. This is because hot rolling refines the austenite grain size.

## CHAPTER 6: INFLUENCE OF S ON HOT DUCTILITY OF HIGH Al, TWIP STEELS

### 6.1 Introduction

It is clear from the previous chapters that for these austenitic steels, it is the MnS inclusions and precipitates which control the hot ductility. Hence the AlN level and MnS volume fraction should be kept as low as possible, i.e. low N and S levels. Impurity segregation weakening the boundaries could also be important in particular the S level and the P level. In the present exercise the influence of S level on the hot ductility of TWIP steels has been examined.

### 6.2 Experimental

The compositions of the 3 steels are given in Table 6.1. The compositions were similar, Al, N and P levels being the same, (1.5%Al, 0.0085%N, 0.023%P) the only difference being the S level which ranged from 0.003 to 0.023%. A small amount of Ca was added to steel 1 so as to reduce S to a low level.

The Mn level was very high, 18%, so heating to 1250°C would not be expected to cause any of the MnS inclusions to go back into solution. (From the Factsage programme, the solidus is 1270°C and liquidus is 1420°C).

A Gleeble machine was used to carry out the tests. Samples were re-heated to 1250°C and cooled at 60°C/min to the test temperature as shown in Fig.6.1. As in the previous chapters, optical metallography, SEM and TEM examinations were carried out on the broken tensile specimens.

Table 6.1 Compositions of TWIP steels, wt-%

Steel	C	Si	Mn	P	S	Al	N	Ca
1	0.615	0.20	18.30	0.022	0.0032	1.51	0.0080	<0.003
2	0.612	0.19	18.30	0.024	0.0100	1.53	0.0093	0
3	0.603	0.20	18.30	0.023	0.0230	1.52	0.0093	0

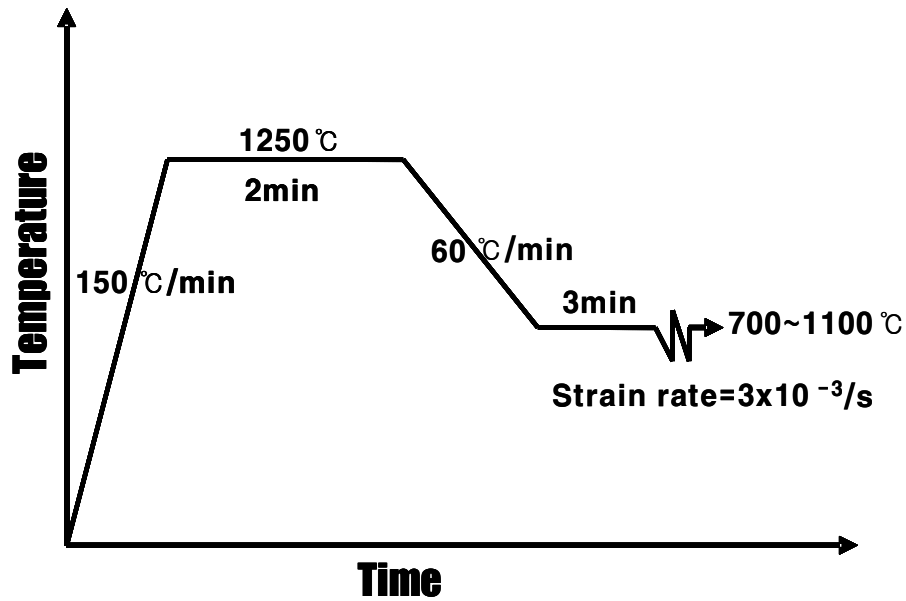


Fig.6.1 Schematic diagram of the processing route for the tensile specimens

### 6.3. Results

The hot ductility curves are given in Fig.6.2. The 0.010 and 0.023%S steels have very similar hot ductility curves, ductility being  $\leq 40\%$  RA throughout the temperature range under examination, 700~1100°C. The low S steel although having similar ductility to the higher S steels, within the temperature range 700~900°C, gave reduction of area values of 50~60% at temperatures above 900°C. The higher S steels gave as much as 30~35% lower RA values in this temperature range, Fig.6.2.

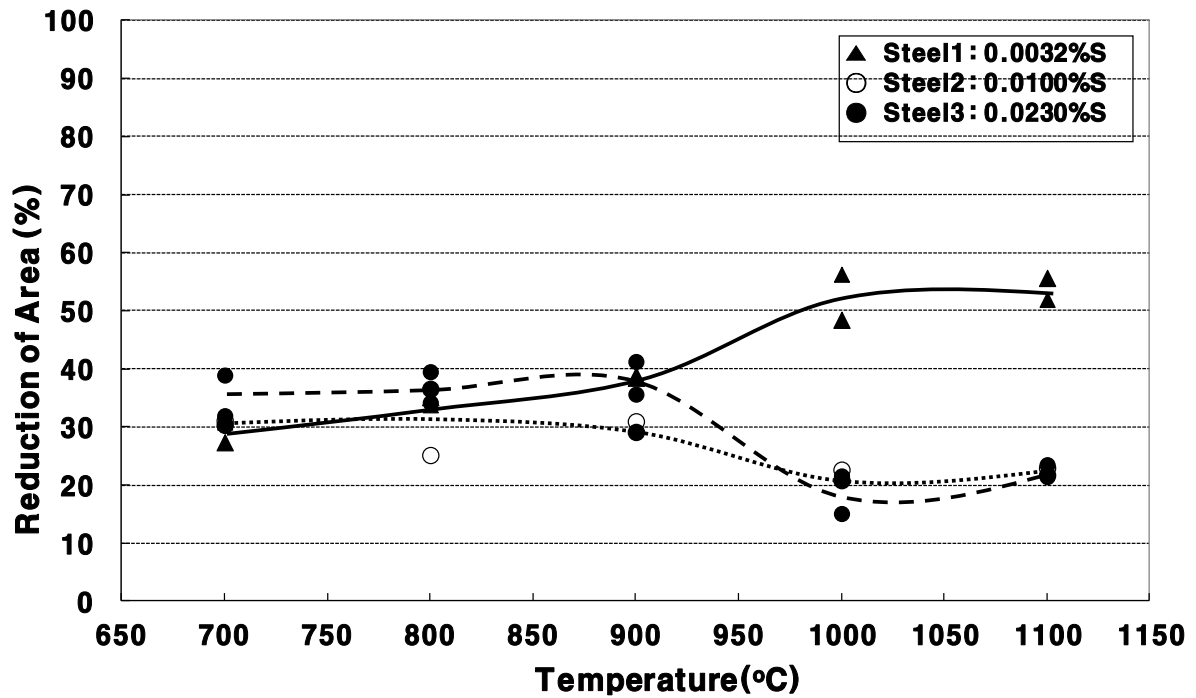


Fig.6.2 Hot ductility curves for the three TWIP steels with varying sulphur contents.

The microstructures of the three steels are given in Figs. 6.3 (a), (b) and (c) for the 0.003, 0.010 and 0.023% S, steels, respectively. The volume fraction of coarse particles present can be seen to increase markedly as the S level increases from 0.003 to 0.01 but there is a much smaller increase on raising the S level from 0.010 to 0.023%. (It can be seen that although there are particles at the austenite grain boundaries, many of these precipitates are at the dendritic boundaries of which only a few become the final austenite grain boundaries). Cracks were frequently observed along these boundaries (Fig. 6.3).

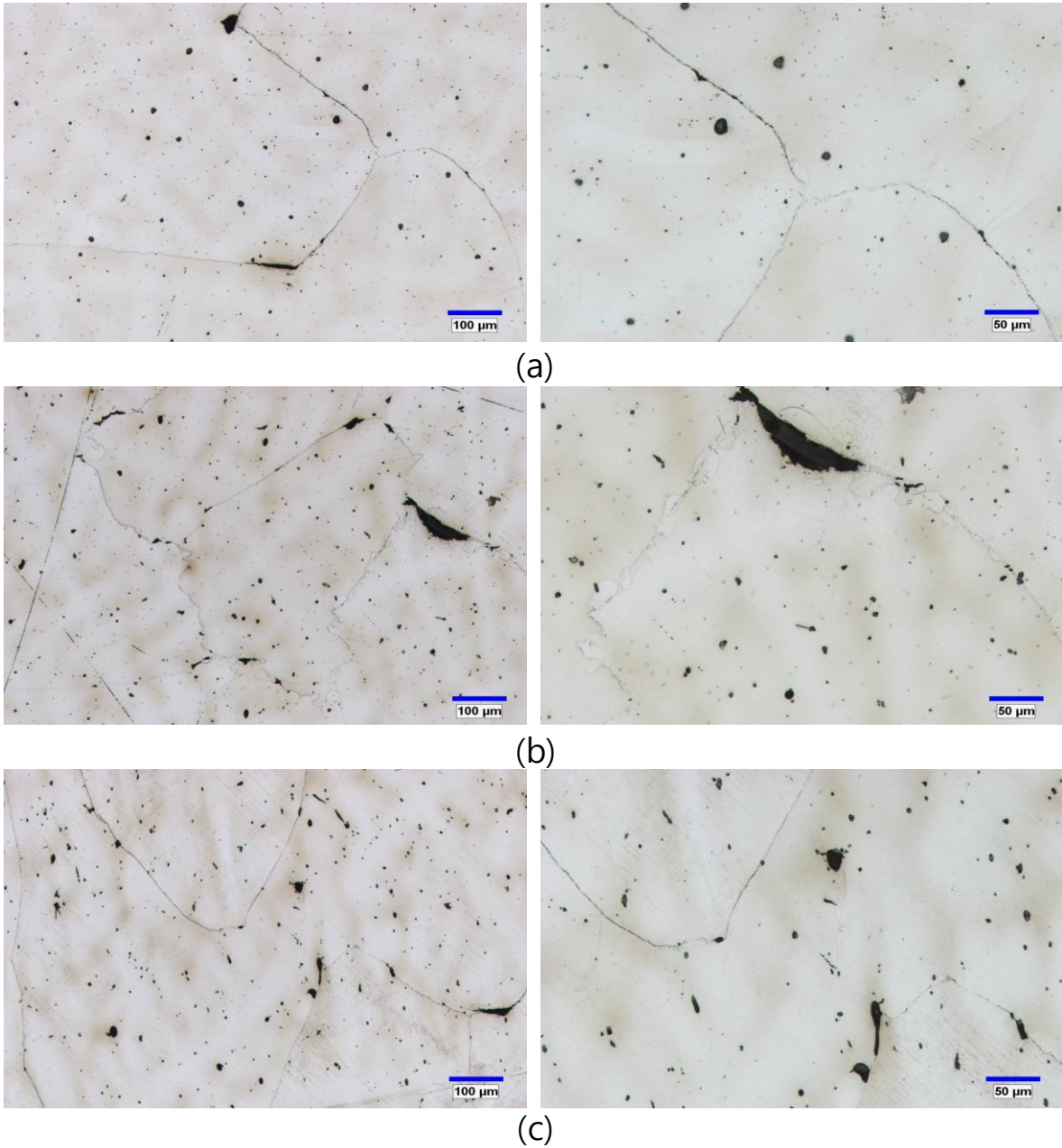


Fig.6.3 Microstructures for the 3 steels examined (a) 0.003%S, (b) 0.010%S, (c) 0.023%S at two magnifications (Optical Microscopy).

The analysis spectra of the particles could be divided into essentially three types: MnS inclusions with Ca, pure MnS inclusions and AlN (Fig. 6.4).

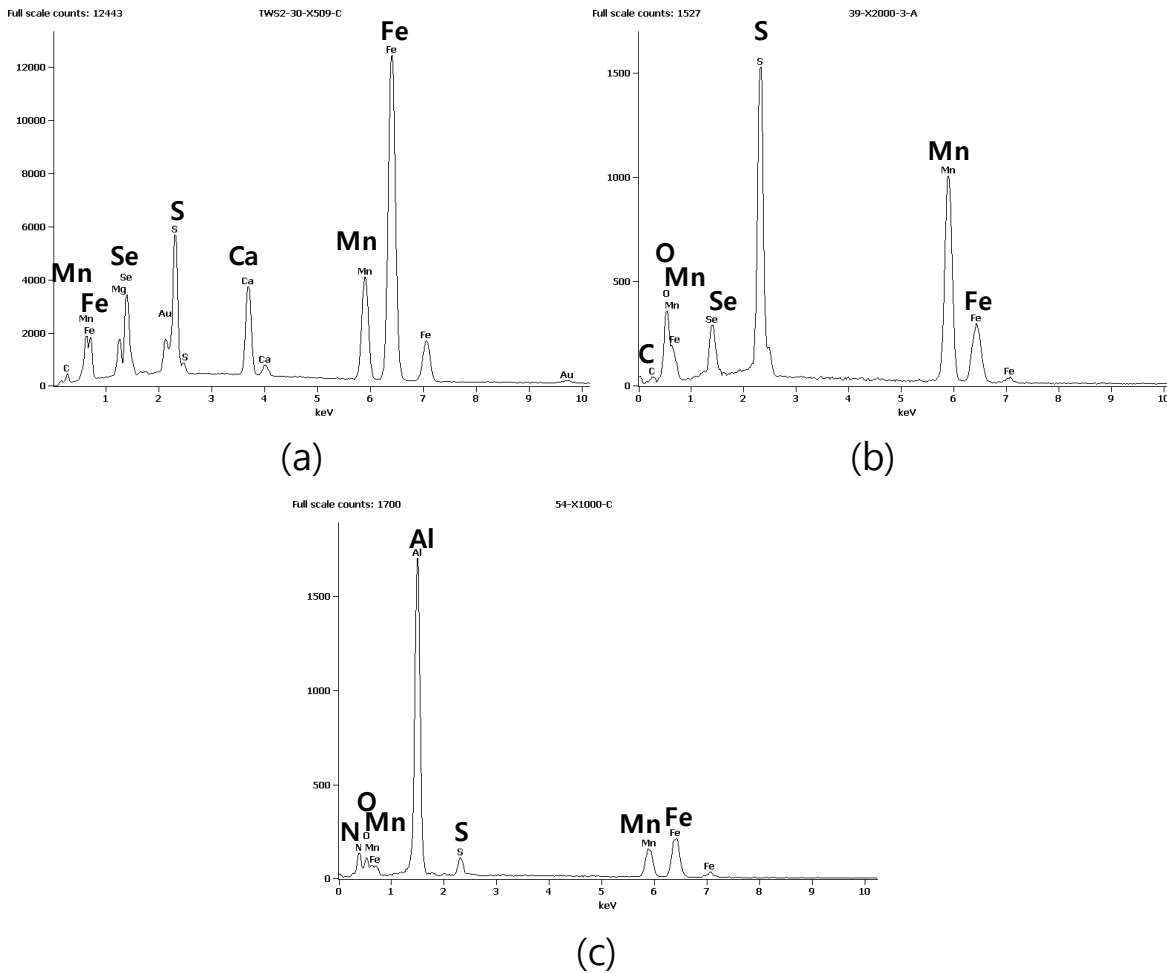


Fig.6.4 Types of analysis spectrum (a) MnS inclusions containing Ca, (steel 1) (b) Pure MnS inclusions, (steels 1, 2 and 3) (c) AlN (steels 1, 2 and 3).

SEM examination indicated that the sulphides in all the steels have curved irregular shapes although spherical in nature, Fig.6.5. The low S steel contains AlN precipitates and manganese sulphide inclusions which occasionally contained Ca, Figs. 6.5 (a). The AlN particles in the low S steel are hexagonal plates and very coarse 4~20 $\mu$ m, Fig. 6.6 and the MnS with Ca inclusions are fine generally less than a micron but spherical in shape. There was the occasional coarse sulphide 2~3 $\mu$ m. Most of the precipitation appears within the matrix of the austenite.

Table 6.2 summarises the findings for the very low S steel 1 and also the higher S, steel 2, 0.01%S.

Table 6.2 Inclusion and precipitate sizes and shapes in low S and higher S steels

Inclusion type	Steel	
	0.003%S (Steel1)	0.010%S (Steel2)
Sulphide	Size	< 1 $\mu\text{m}$ Occasional coarse 2~3 $\mu\text{m}$
	Shape	Irregular curved
AlN-Hexagonal	4~30 $\mu\text{m}$	Finer 1~3 $\mu\text{m}$
AlN-Dendrite rods	Occasional	1 $\mu\text{m}$ thick, 5~20 $\mu\text{m}$ long

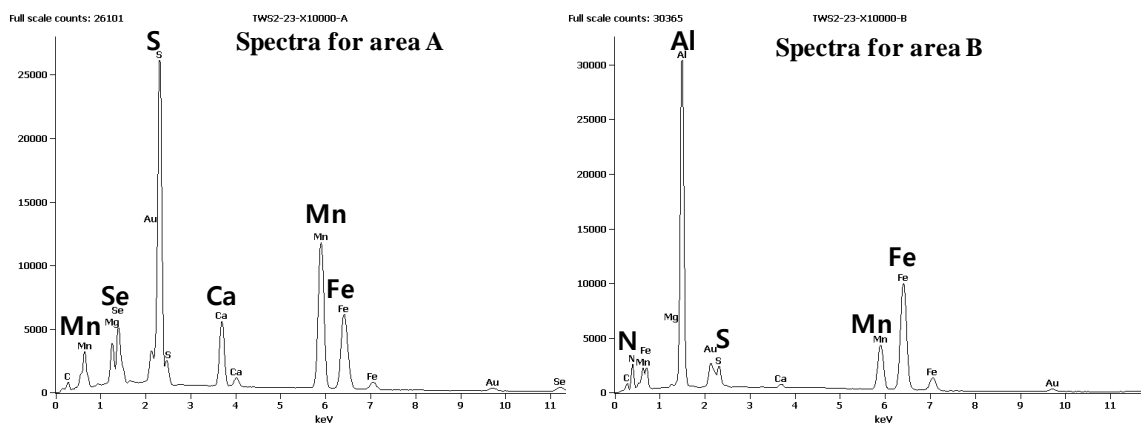
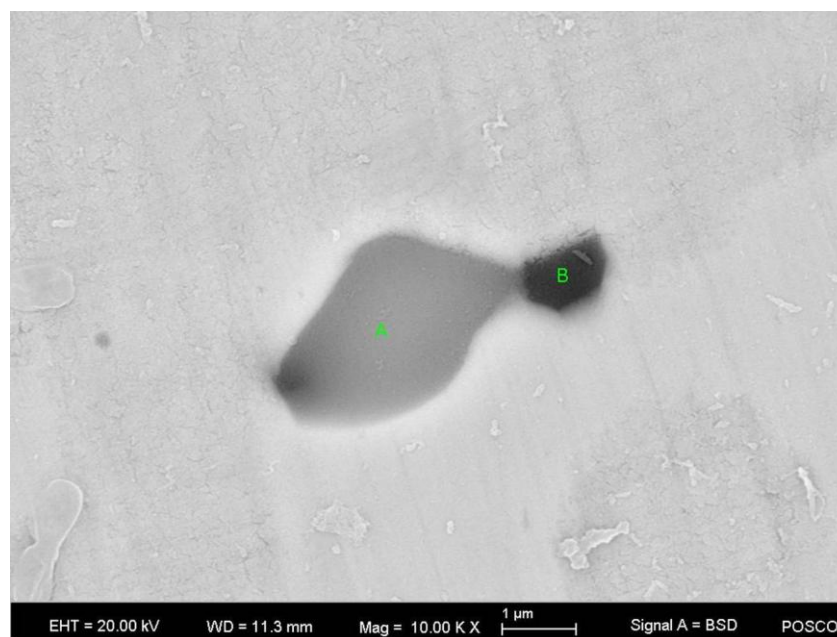


Fig.6.5 (a) Low S, 0.003%steel, grey colour is CaMnS and black is AlN, with analysis spectrums (SEM).

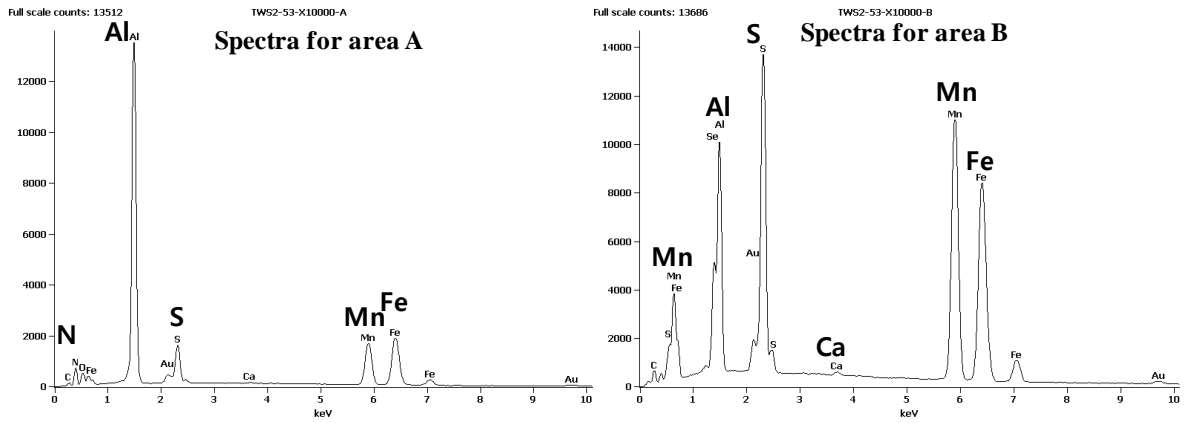
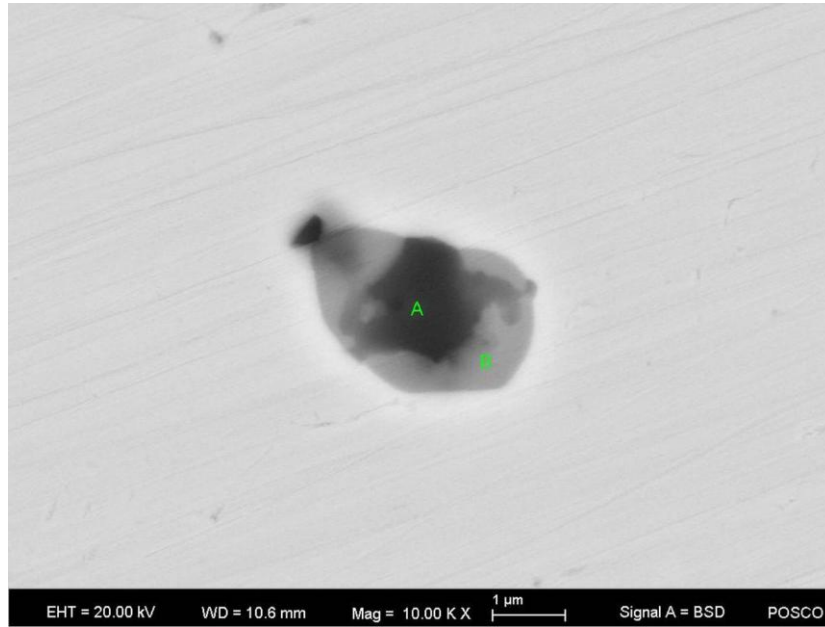


Fig.6.5 (b) Higher S steel, 0.01%, grey is MnS (B), black AlN(A) and dark grey is a mixture of MnS and AlN with their analysis spectrums (SEM).

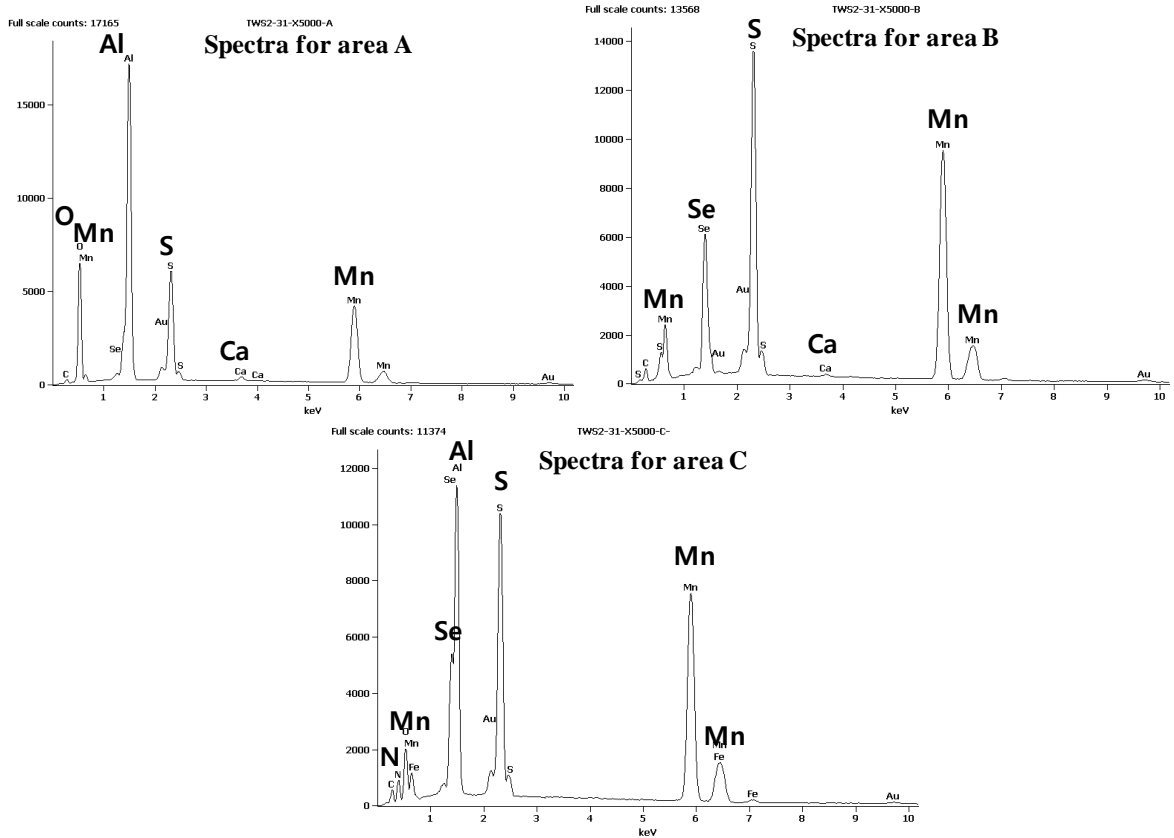
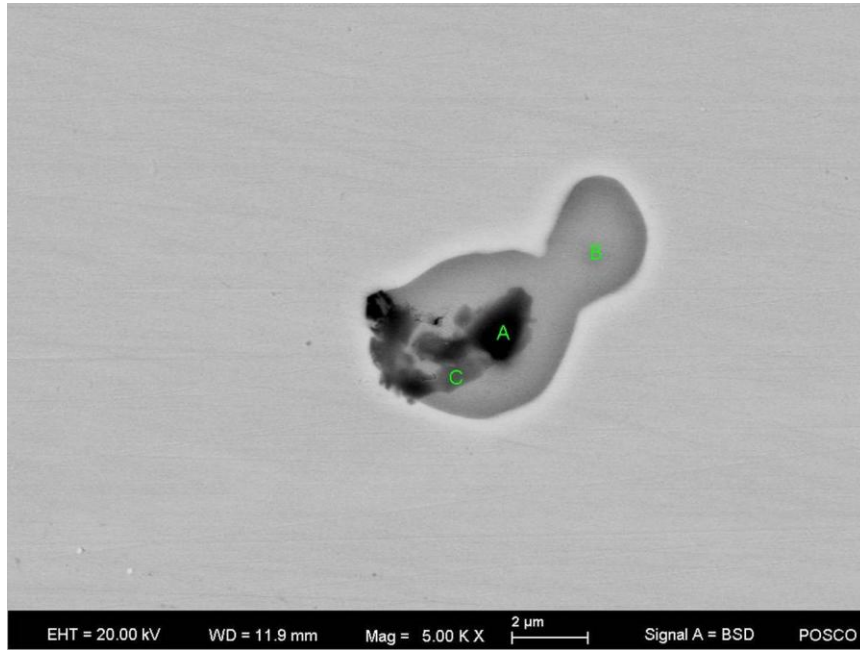


Fig.6.5(c) Higher S steel, 0.01%, grey is MnS (B), black AlN (A) and dark grey is a mixture of MnS and AlN (C), with analysis spectrums (SEM).

Fig.6.5 Sulphides and AlN particles present in (a) low S, 0.003% steel, grey colour is CaMnS and black is AlN, (b) and (c) higher S steel, 0.01%, grey is MnS, black AlN and dark grey is a mixture of MnS and AlN.

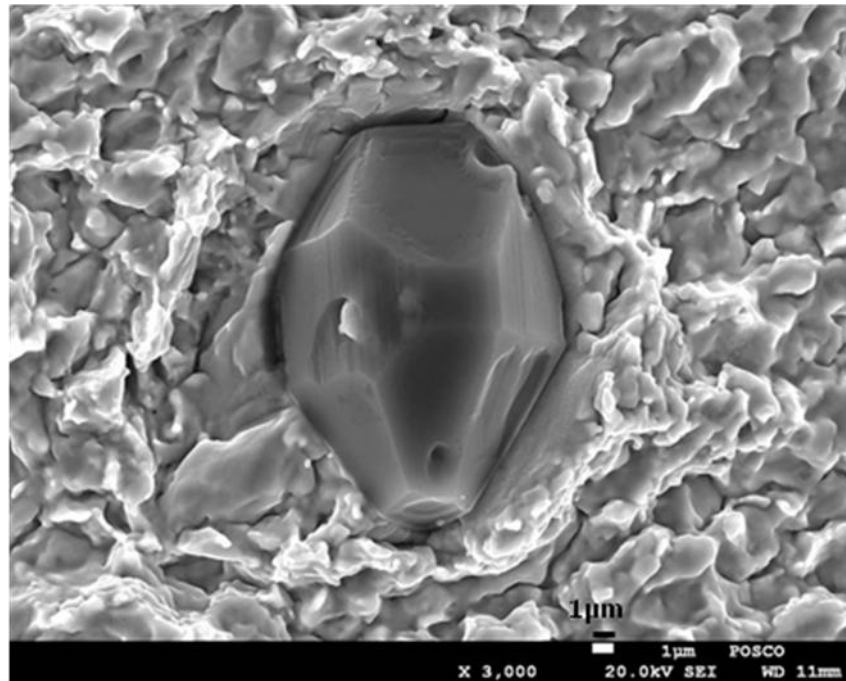


Fig.6.6 Large hexagonal AlN particle in low S steel (SEM).

For the 0.01% S steel, the mode of precipitation is very different. There is a mixture of coarse, hexagonal AlN plates, finer than in the low S steel, 1~3 μm but more importantly there are dendritic rods of AlN, 1 μm thick and 5 to 20 μm long in size and much coarser MnS inclusions of average length 3 μm and of irregular shape. The dendritic rods are situated at the dendritic boundaries which at times become the austenite grain boundaries. In all cases on the fracture surfaces of the higher S steels, a MnS inclusion was always associated with the dendritic AlN rod, Fig.6.7 (a).

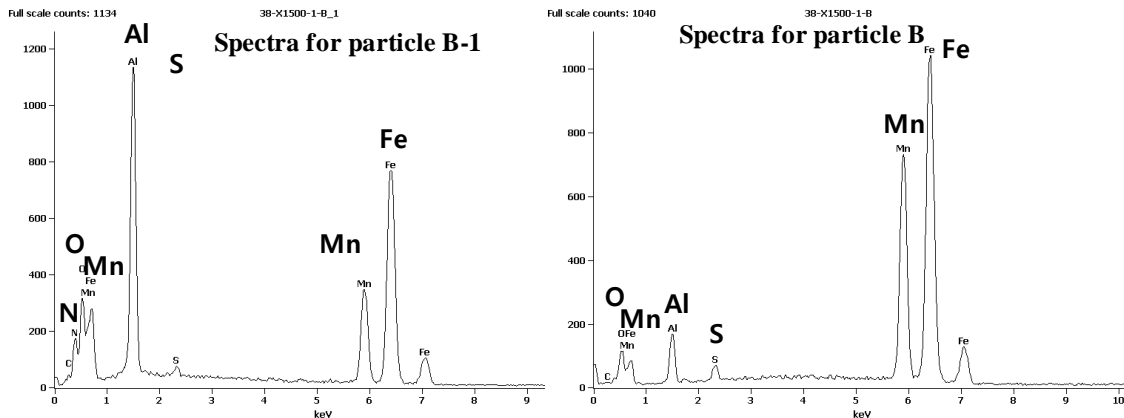
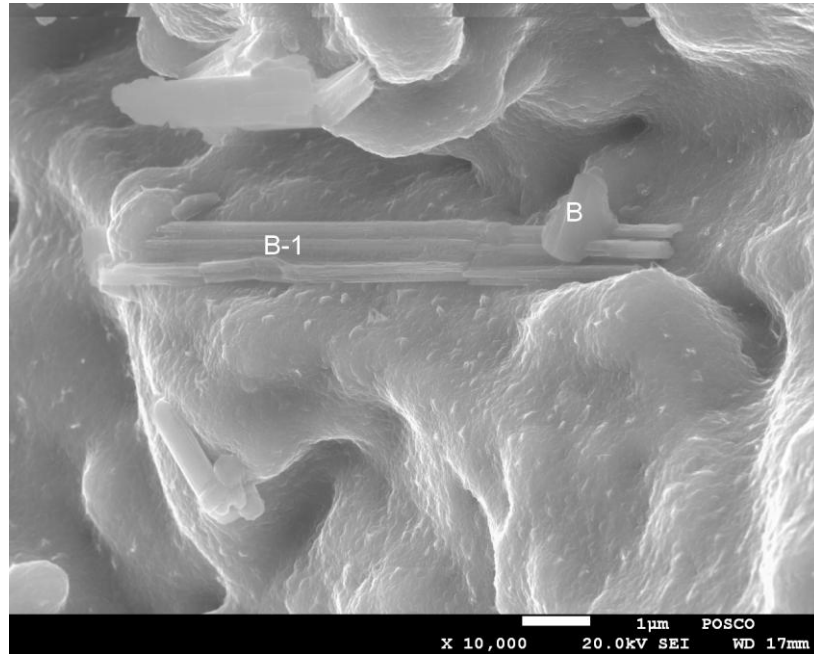


Fig.6.7 (a) AlN dendritic rod shaped precipitate, B-1 present in higher S steels on fracture surface. Note associated MnS inclusion B in Fig. 6.7(a) (SEM).

Whereas Ca was often associated with the sulphide inclusions in the low S steel (Fig 6.5 (a)) in the higher S steels, the sulphides were pure MnS, Figs 6.5(b) and (c). These inclusions always seemed to be associated with an AlN particle, being sometimes adjacent as in Fig. 6.5(a) and at times within the sulphide inclusions, Fig. 6.5(b) and (c). In the higher S steels dendritic rod shaped AlN particles were present, Fig. 6.7(a), B-1 in the figure, but again were always associated with a MnS inclusion, B in figure.

More examples of these coarse dendritic AlN found in the higher S steels are shown in Fig. 6.7(b) and (c). Again these dendritic rods A-1 in Fig. 6.7(b) and A and C in Fig. 6.7(c) were always associated with finer “oval” shaped MnS inclusions, An in Fig. 6.7(b) and B in Fig.6.7(c).

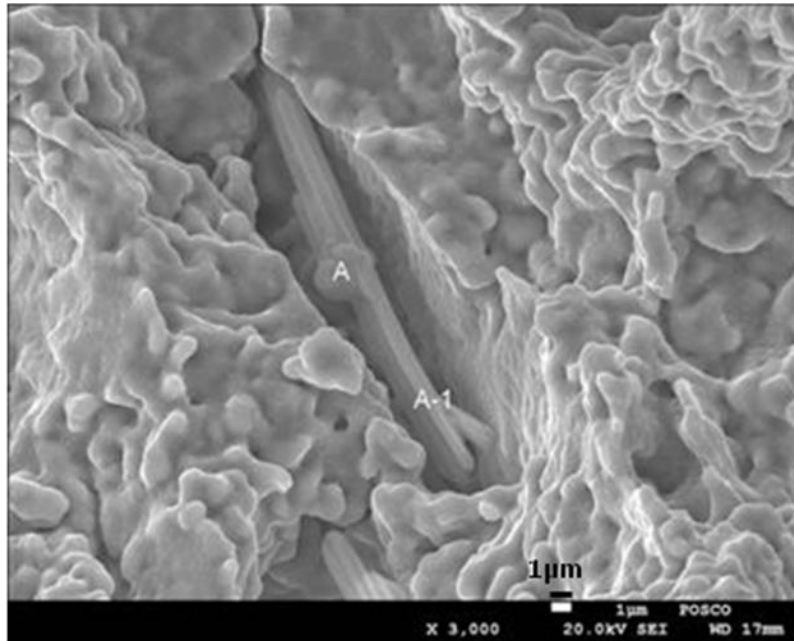


Fig.6.7 (b) Dendritic AlN rod on fracture surface, A-1 with associated MnS inclusion (A) in higher S steels (SEM).

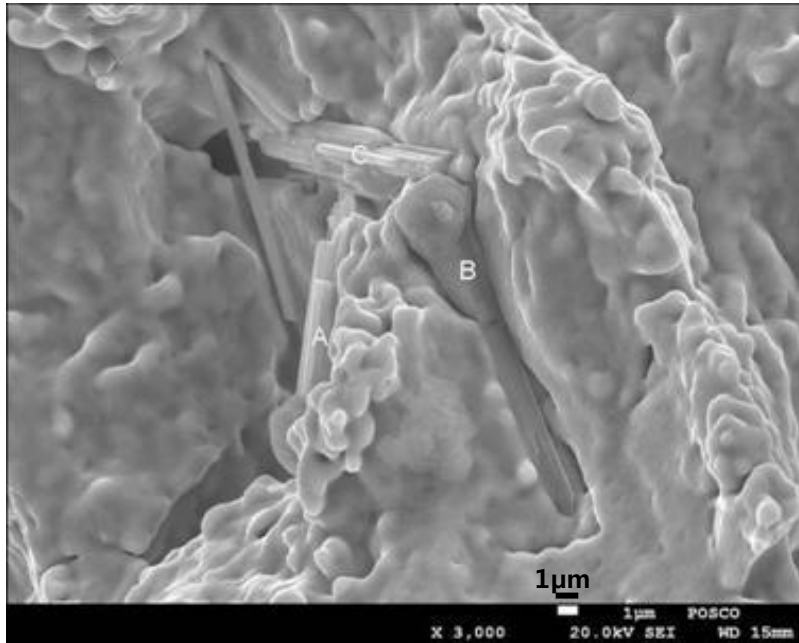


Fig.6.7(c) Dendritic AlN rods on fracture surface, A and C with associated MnS inclusion in higher S steels, B (SEM).

Fig.6.7 Further examples of these dendritic AlN rods associated with MnS inclusions.

The fracture surfaces of these higher S steels, Fig.6.8 were very flat and often decorated with these AlN rods (arrowed in Fig.6.8 (b)). Cracks were frequently observed at the boundaries.

An extreme example of the coarseness of these AlN dendritic rods is shown in Fig.6.9, for the 0.010%S steel.

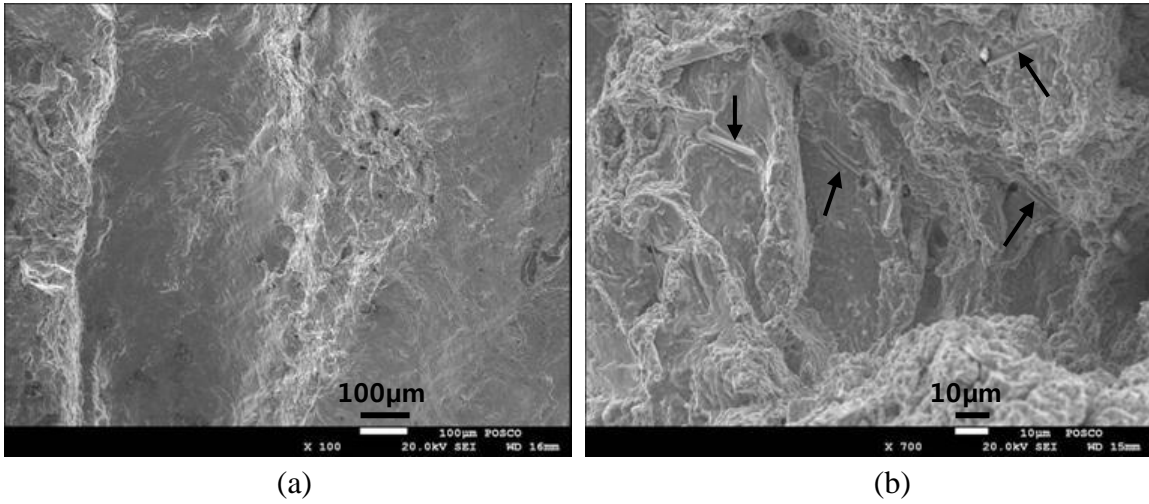


Fig.6.8 Flat intergranular fractures formed by grain boundary sliding are encouraged by the long interdendritic AlN rods in high S steels (SEM).

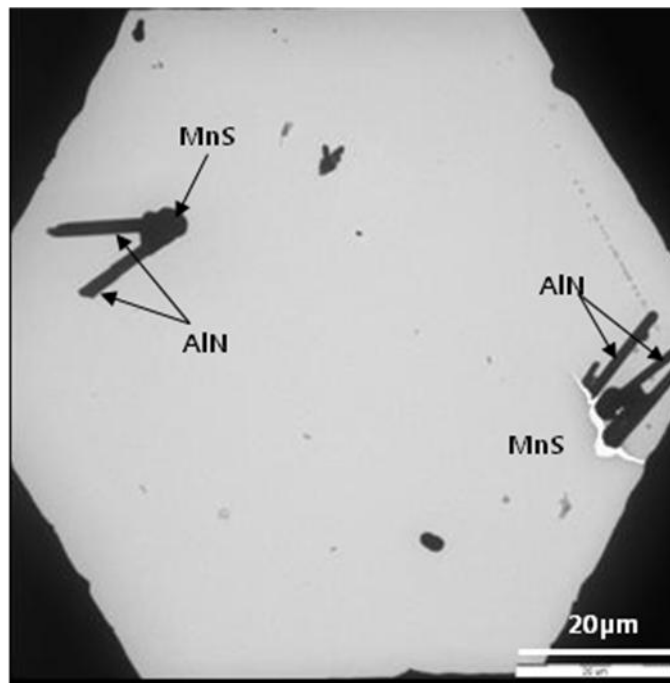


Fig. 6.9 Very coarse AlN dendritic rods found in higher S steels (TEM) with sulphides at their ends.

In contrast to the higher S steels, the low S steel rarely showed a dendritic AlN rod. Large hexagonal plates of AlN were observed instead, Fig. 6.10.

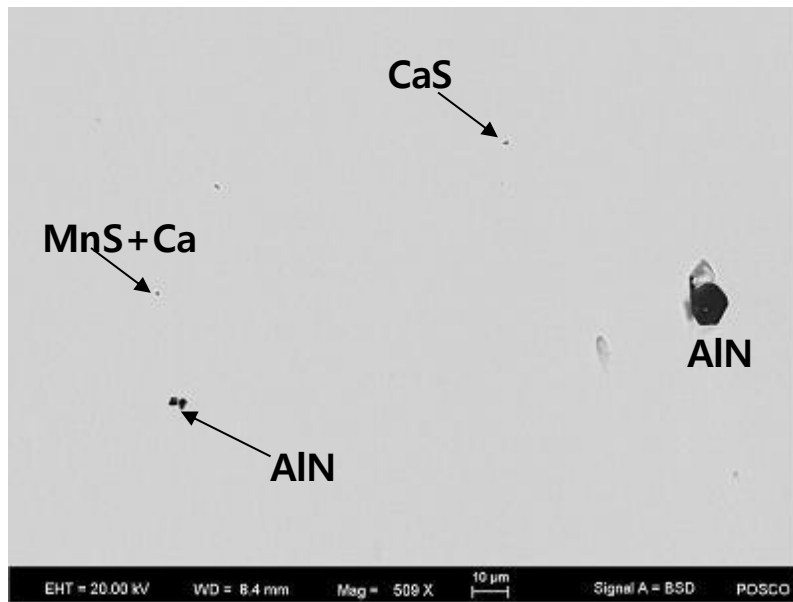
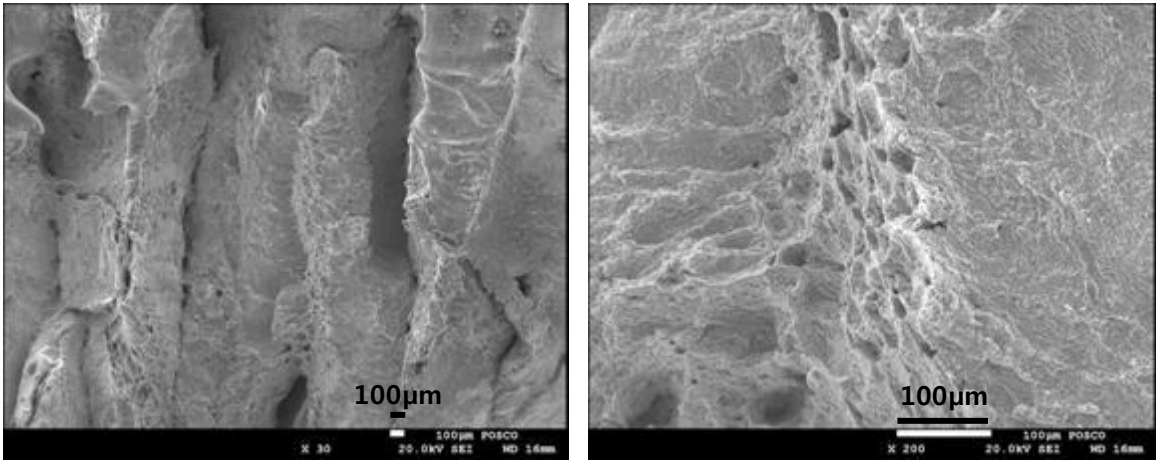


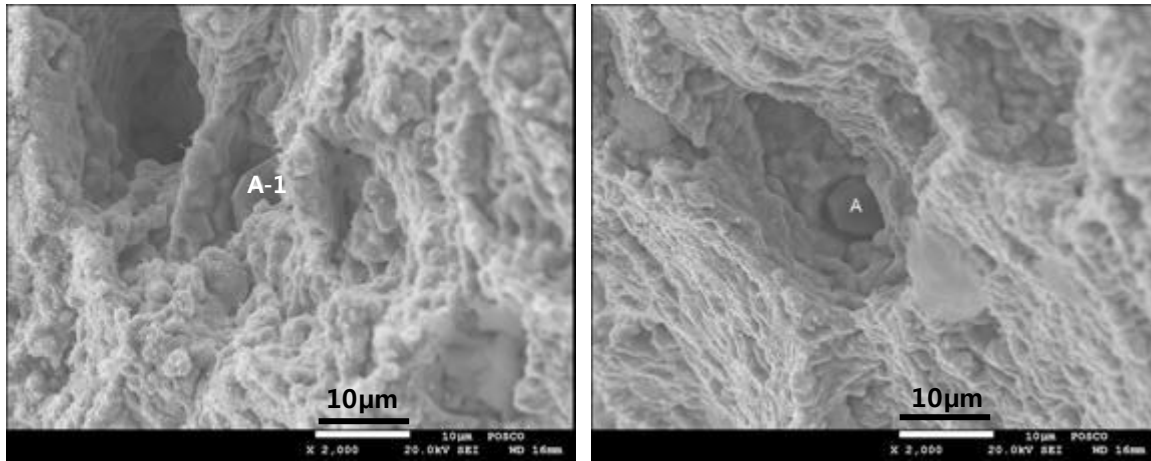
Fig.6.10 A typical area for the low S steel is shown in which coarse hexagonal AlN particles are present and very fine MnS sulphide inclusions containing Ca.

The fracture appearance at 1000°C for the low S steel is shown in Fig. 6.11. Fracture was much more ductile with hexagonal AlN particles being present in the matrix, An in Figs. 6.11(c) and (d).



(a)

(b)



(c)

(d)

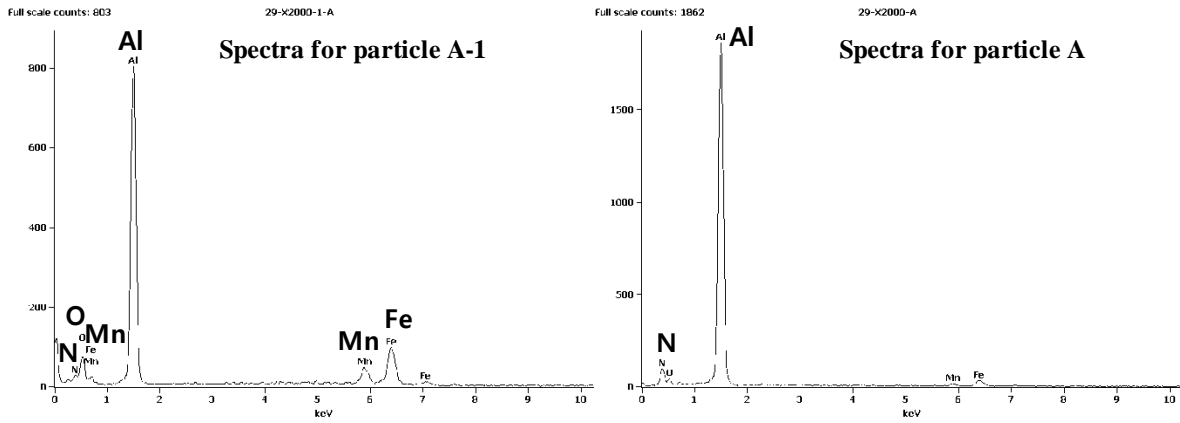


Fig.6.11 Typical fracture surface of low S steel showing the presence of plate AlN particles (SEM).

In the higher S steels, the AlN rods were often present in the matrix but although they are not always situated at the austenite grain boundaries, they were sufficiently long to readily extend cracks to the boundaries and cause intergranular failure. The cracks in the boundaries are readily seen in Fig.6.12. There is no indication that the highest S steel (0.023%S) has more or longer AlN rods than in the 0.010%S steel.

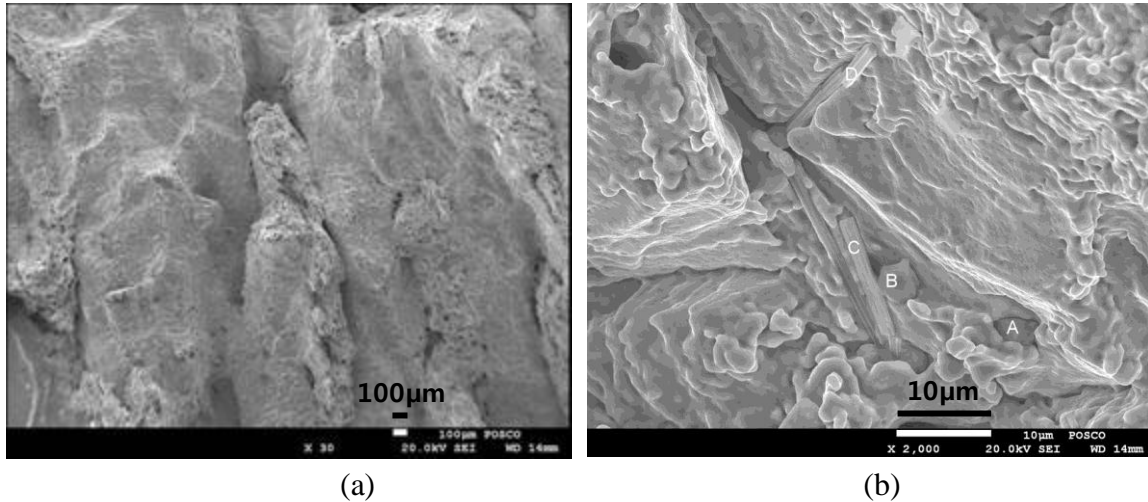


Fig. 6.12 Fracture surface in 0.023% S steel at 900°C (SEM).

The big difference between the AlN precipitation patterns in the steels are clearly seen in the network of random areas on the electron microscope grid for replicas, taken from sections of the tensile specimens close to fracture, Fig. 6.13(a), (b) and (c) for the 0.003, 0.010 and 0.023% S steel, respectively. Whereas none of these coarse rods are observed in the low S steel, only hexagonal precipitates, in the higher S steels there are many of them.

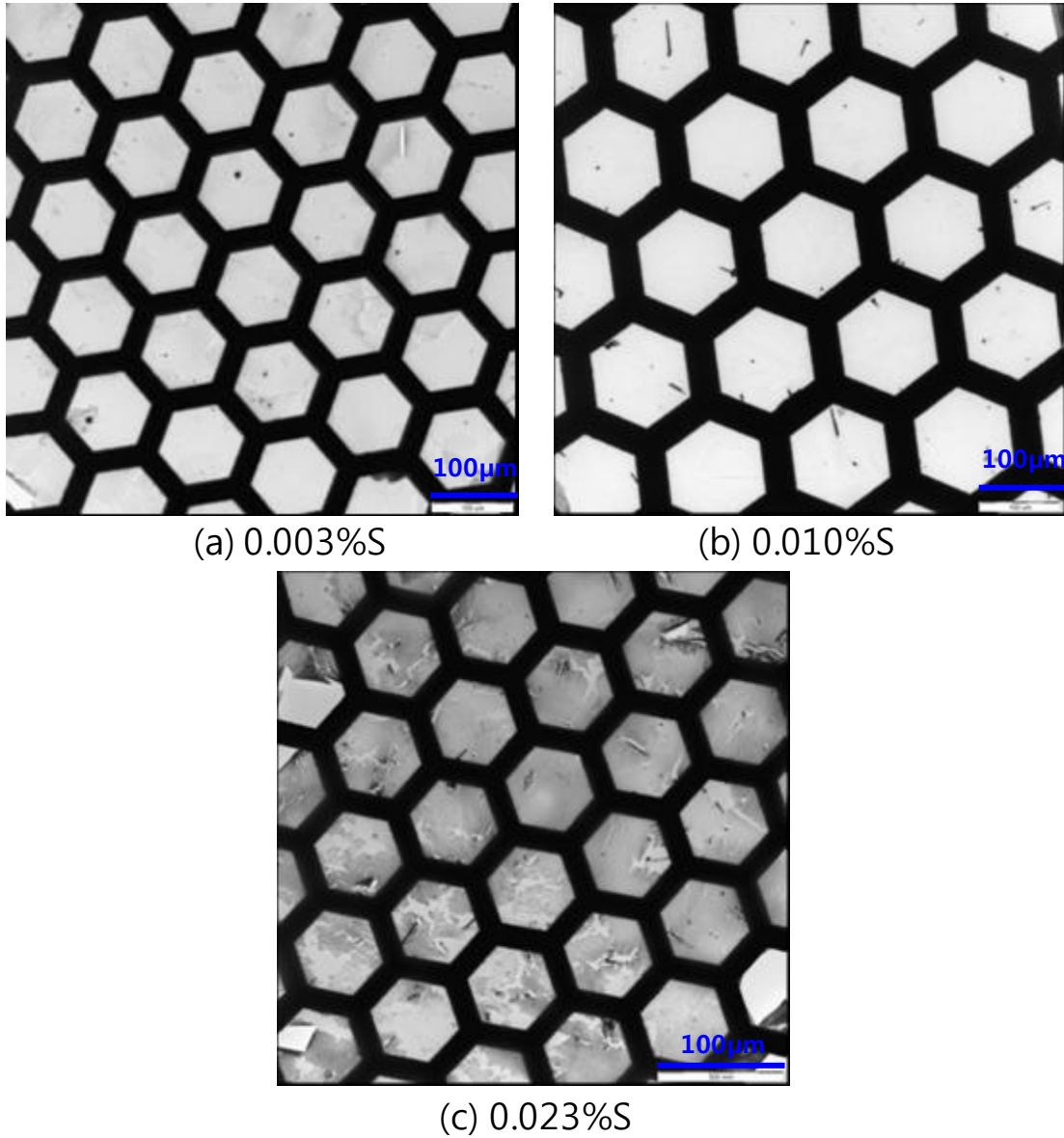


Fig.6.13 Electron microscope grids showing the absence of these long AlN rods in the low S steel (a) but their presence in the higher S steel (b) and (c) (TEM).

#### 6.4. Discussion

There was no evidence for dynamic recrystallization for the test temperature range 700~1100°C from metallographic examinations near fracture, the grain structure remaining coarse with no evidence of new finer grains. Ductility in the austenite without dynamic recrystallization is a balance between recovery which improves the ductility and grain

boundary sliding which encourages crack formation and growth. It has been found that for the temperature range under examination when there is no precipitation they nearly balance each other out, so there is often little change in the RA values with temperature [165]. Examination of the grain size for these steels indicates that this is similar for all of them being in the range 200~300 $\mu$ m. It has also been found from the literature that when dynamic recrystallization doesn't take place the ductility of austenite is relatively low, RA values being in the range 40~50% compared to 90~100% when dynamic recrystallisation takes place [75].

For these steels solidification takes place directly from the liquid to the austenite. Solidification starts at 1420°C and is complete when the temperature reaches 1270°C. This accounts for the finer austenite grain size (200~300 $\mu$ m) compared to that found in HSLA steels (1mm) when solidification takes place at much higher temperatures (1440°C) [167]. Because there is no further phase change on cooling many of the inclusions will be situated at the austenite grain boundaries where they will have the greatest effect in controlling the hot ductility.

The tensile specimens were taken from the as cast ingots and the sulphides and coarse rod shaped AlN precipitates that are observed probably formed prior to solidification. The high Mn level in these steels would prevent any of the sulphides going back into solution at the reheating temperature of 1250°C. Thus as no dynamic recrystallization was observed throughout the testing temperature range examined, it is likely that the sulphides are situated where they would be after casting. Similarly, the coarse AlN particles will have no tendency to go back into solution at 1250°C. It is therefore reasonable to assume that the precipitate size, morphology and location in the microstructure are the same in the tensile specimens as in the as cast ingot.

It can be seen from Fig.6.3 that increasing the S level from 0.003 to the range 0.01~0.023% results in a greater volume fraction of particles and increasing the S from 0.003 to 0.010% in the austenitic TWIP steels results in a 35% decrease in the RA for the temperature range 1000~1100°C, Fig.6.2. In these steels there will be both copious precipitations of AlN and MnS at the boundaries and within the matrix. Increasing the S level will increase the volume fraction of inclusions. However, as shown in Fig.6.2, only when the S level is reduced to very low levels does the ductility improve.

Increasing the S content as well as increasing the volume fraction of sulphides might be expected to increase their size in accord with the observations (Table 6.2). However, in the case of AlN, the volume fraction of AlN hardly alters, Table 6.3 assuming equilibrium

conditions occur, but the precipitation pattern changes from plate like hexagonal particles situated in the matrix for the low S steel to for the higher S steels, finer hexagonal plate AlN particles and coarse long dendritic rods of AlN at or close to the austenitic grain boundaries, Table 6.2. It suggests that the change in the precipitation may be related to the nucleation association of MnS and AlN and that the AlN particles need MnS inclusions before they can precipitate out in the melt.

If equilibrium conditions apply then the volume fraction of MnS and AlN would be as shown in Table 6.3. The volume fractions of AlN and MnS were calculated using ThermoCalc programme.

Table 6.3 Volume fraction of MnS and AlN assuming equilibrium conditions.

Steel	Composition wt.%				Volume Fraction x10 <sup>-4</sup>		
	Mn	S	Al	N	AlN	MnS	Total
Steel1	18.3	0.003	1.51	0.0080	5.15	0.938	6.088
Steel2	18.3	0.010	1.53	0.0093	5.96	3.124	9.084
Steel3	18.3	0.023	1.52	0.0093	5.95	7.330	13.28

It can be seen from Table 6.3 that the volume fraction of AlN is similar for the three steels, but the volume fraction of MnS increases markedly with S contents. It is likely that the massive dendritic rod like AlN precipitates which are present in the higher S steels, rather than the sulphides lead to brittle failure at higher temperatures, Figs. 6.7 and 6.9. These rods form at or close to the austenite boundaries and are particularly detrimental to the ductility as they encourage intergranular fracture.

There does seem to be a strong relationship between the nucleation of sulphides and the AlN particles and that MnS inclusions are required for precipitation of AlN to take place in the melt. If there are insufficient sulphides present then precipitation of AlN occurs mainly as coarse hexagonal platelets. It would appear that these plates nucleate more readily at the very low S level. Thus, when there are few sulphides that are fine, as in the low S steel, precipitation of these rod like particles in the melt does not take place, but when the S level increases so that there is an ample supply of MnS inclusions to precipitate out with, AlN precipitates firstly as hexagonal plates and then in a dendritic rod like form causing the steel to remain brittle at the higher temperatures

In accord with this argument, it is interesting to observe that although ductility decreases on

increasing the S from 0.003 to 0.010, there is no significant further decrease on increasing the S from 0.010 to 0.023%. If equilibrium conditions are applied, one would expect ductility to continually decrease as the S level increased.

The presence of the long rods of AlN at the boundaries ensures that no recovery in ductility can occur at high temperatures, and ductility will indeed get even worse as grain boundary sliding increases. In contrast for the very low S steel recovery takes place, outweighing the detrimental effect of grain boundary sliding, as the AlN particles are now in the matrix and there is less AlN precipitated.

Work by Abushosha et al. [100] on plain C-Mn steels (~0.1%C, 1.4%Mn) has also shown, the influence of sulphur on the ductility of as cast ferrite/pearlite C-Mn steels is only small. On increasing the S level from 0.002% to 0.016% the ductility depreciates by about 5% when the thin film of ferrite is present and 10% when the steel is fully austenitic.

Lankford has also suggested that increasing the Mn content increases the driving force for precipitation of MnS, and this increases precipitation within the matrix rather than more detrimentally, at the austenite boundaries [17]. This may be why the very high Mn level in these steels causes so much precipitation within the matrix.

In the higher S steels, there is some indication that ductility improves at temperatures below 950°C and this may be related to the reduced grain boundary sliding that occurs. Behaviour for all three steels is indeed similar for temperatures  $\leq 900^\circ\text{C}$  (Fig.6.2), which again is probably related to grain boundary sliding being much reduced. Grain boundary sliding is very much encouraged by particles at the boundaries provided the temperature is high enough to cause significant sliding and this would seem to be the case for the presently examined steels.

The present results have some similarity with the work of Osinkolu et al. [114] in that they found that AlN reduced hot ductility in ultrahigh purity steels only by pinning the boundaries so that S was able to segregate and pin them. Thus, when the S levels were very low (<0.001%), the hot ductility was excellent even when a high volume fraction of AlN was present both at the austenite grain boundaries and within the matrix [114]. The present work differs importantly in that instead of segregation of sulphur to the boundaries being invoked as the cause, it appears that AlN precipitation only takes place when sulphides are present and when the sulphur level is reduced to a very low level only a few AlN particles are able to precipitate out.

## 6.5 Conclusions

1. Reducing the S level to 0.003% leads to improved ductility in the temperature 950~1100°C, with RA values being 50~55%.
2. Higher S levels of 0.010 and 0.023% give similar hot ductility curves to each other giving poor ductility achieving only RA values of 20% in the temperature range 950~1100°C.
3. The poor ductility in the higher S steels is more of a consequence of the change in the precipitation pattern from coarse hexagonal plate AlN, which are mainly within the matrix and so have little influence on the hot ductility, to very long dendritic rod precipitates, which are situated at the dendritic or close to the austenite grain boundaries. This dendritic precipitation was rarely observed in the low S steel.
4. The MnS inclusions appear to act as nucleation sites for the precipitation of AlN. Below a certain volume fraction of sulphides, the AlN precipitation is very much reduced so that only hexagonal AlN plates are formed which are not situated at the austenite grain boundaries.
5. It is strongly recommended that to reduce the incidence of transverse cracking in these steels a very low S is a necessary requirement.

## CHAPTER 7: INFLUENCE OF B AND Ti ON HOT DUCTILITY OF HIGH Al TWIP STEELS

### 7.1 Introduction

From the previous chapter, for the temperature range 700~1000°C, the RA values for Nb/V TWIP steels were <20%, well below that needed to avoid transverse cracking. Even without Nb/V, the simpler high Al TWIP steels only marginally meet the 35~40% RA criterion required to avoid transverse cracking and then only with low S and N levels. There is therefore a need to find ways of improving the hot ductility of high Al TWIP steels to make them more amenable to casting and this is where adding Ti with B might be a solution.

Boron has been found generally to improve the hot ductility of steels, particularly those containing Nb, but very close control of processing conditions has to be made, including the cooling rate to the tensile testing temperature range [90, 132, 133, 136, 138, 140, 170, 175, 177, 179, 180]. If BN is allowed to precipitate in a fine form, this leads to very poor ductility (i.e. fast cooling) [37]. Nevertheless, the benefits to ductility from adding B are such that it will often give much better ductility than shown by simple plain C-Mn steels in which there are no precipitates present, which suggests that it is in some ways strengthening the boundaries [37].

Many investigations [37, 90, 132, 133, 136, 138, 140, 170, 175, 177, 179, 180] have been carried out to establish the conditions required to obtain the beneficial effect of adding B on hot ductility. These can be summarised as follows:

- 1) The cooling rate should be 6~100°C/min, the lower cooling rate being preferred [147, 175, 177, 179].
- 2) S levels must be kept low to reduce the volume fraction of MnS. These inclusions are believed to be preferred sites for the B to segregate to rather than the austenite grain boundaries [178]. A total Mn/ total S ratio of at least 30/1 is also recommended to prevent the formation of the low melting point FeMnS inclusions [177].
- 3) Low N levels or Ti additions are needed to remove the N and prevent the formation of BN [37, 147].

However, even when these conditions are met there is no guarantee that a B addition will lead to improved ductility. The difficulty in improving the hot ductility of these high Al TWIP steels needs exploring.

## 7.2 Experimental

The compositions of the steels are given in Table 7.1. The steels had 0.6%C and 18%Mn. As in the previous chapter all the TWIP steels were highly alloyed having  $\geq 1\%$ Al with sufficient Mn to ensure that the steel would remain austenitic at room temperature. Steel 1 contained no addition of Ti and B and a relatively high N content, 0.008%N. Steel 2 was similar steel but with Ti and B. The Ti present was enough to ensure all the N should be combined as TiN so that the B when not combined as a carbo-boride might be expected to be in solution, thus available to migrate to the boundaries. TiN also can be less detrimental to the ductility than AlN provide it is sufficiently coarse [37].

Table 7.1 Composition of steels examined, wt.%

Steel	C	Si	Mn	P	S	Al	Nb	Ti	B	N	Condition
1	0.61	0.20	18.3	0.022	0.003	1.51	0	0	0	0.008	re-heated
2	0.55	0.09	16.6	0.024	<0.003	1.12	0	0.038	0.0021	0.007	re-heated

For these two steels 1 and 2, the samples were re-heated to 1250°C and tested on a Gleeble machine. In the text, this condition is referred to as “re-heated”. The tensile samples were machined from the as-cast ingots in the direction of casting and were of 120mm length and 10 mm diameter. The samples were initially heated at 150°C/min to 1250°C after which they were held for 2mins. They were then cooled to test temperatures in the range 700~1200°C at a cooling rate of 60°C/min held for 30secs at temperature and strained to failure using a strain rate of  $3 \times 10^{-3} \text{ s}^{-1}$ . The temperature profile is shown in Fig.7.1.

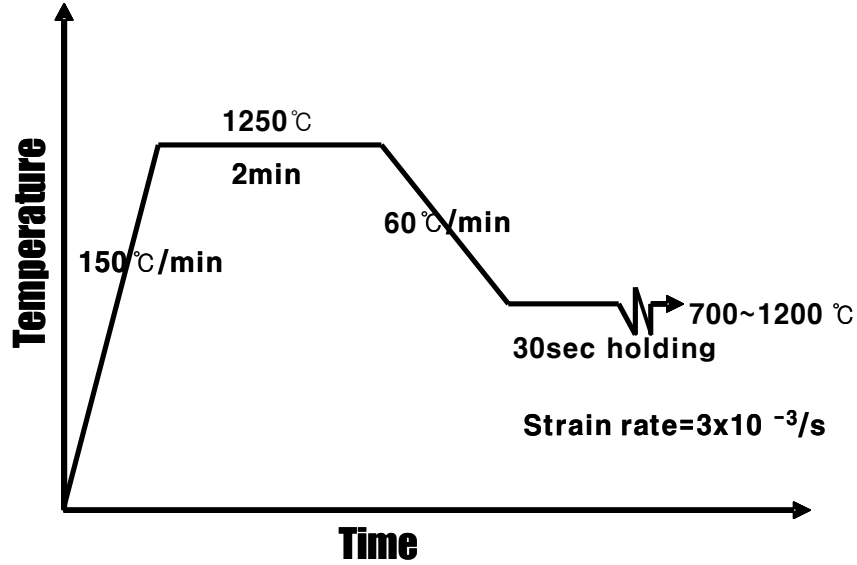


Fig.7.1 Schematic diagram of the processing routes for the tensile specimens for samples machined from the ingots and heated to 1250°C.

Once a tensile sample had failed it was immediately gas quenched with argon in order to try and preserve the grain structure and the fracture surface present at the time of failure. The hot ductility curves of RA against the test temperature were determined as well as the grain size. Metallography was carried out using the SEM (scanning electron microscope) and the TEM (transmission electron microscope). The SEM examination was carried out on sections taken close to the point of fracture and the fracture surfaces were also analysed for the type of fracture and identification of the particles. TEM examination was performed on carbon extraction replicas taken from sections close to fracture. A nickel grid was used.

### 7.3 Results

The grain size for the “re-heated” to 1250°C, steels was ~350µm. The hot ductility curves for the “reheated” Nb free steels 1 and 2 are given in Fig.7.2. It can be seen that the B treated steel, steel 2 gives better ductility for the test temperature range below 950°C but above this temperature, ductility drops below 40% RA and is worse than the B free steel, steel 1.

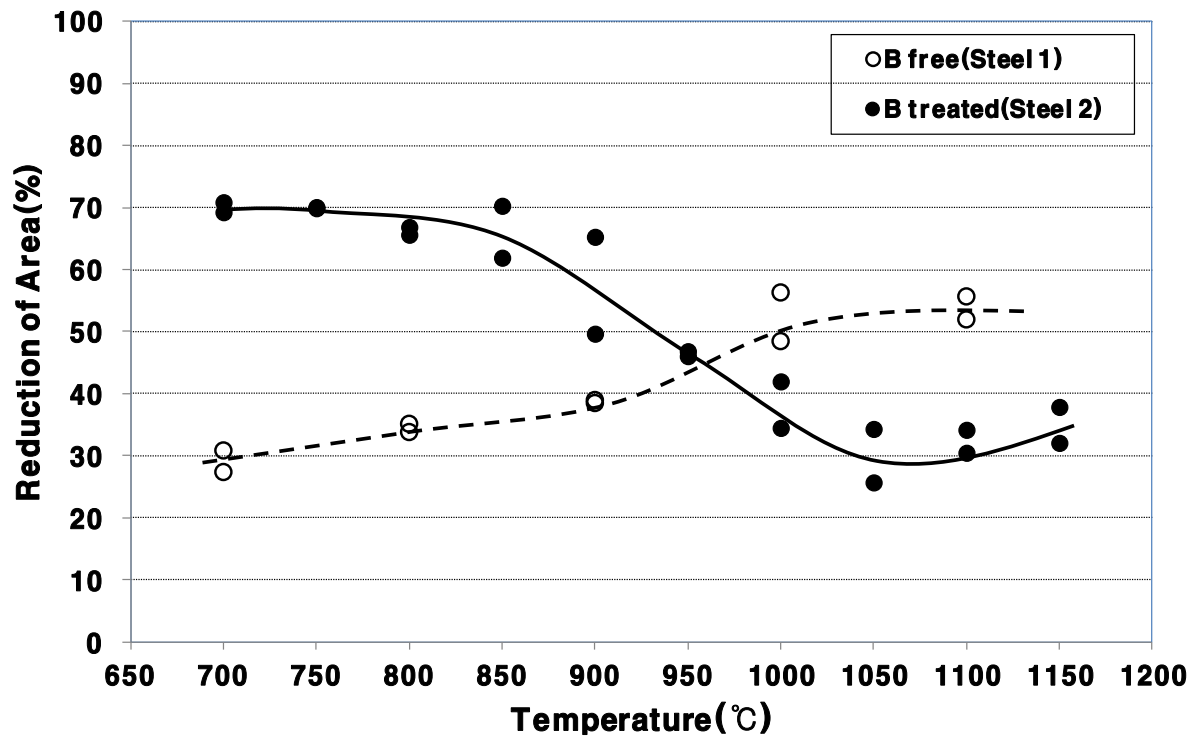
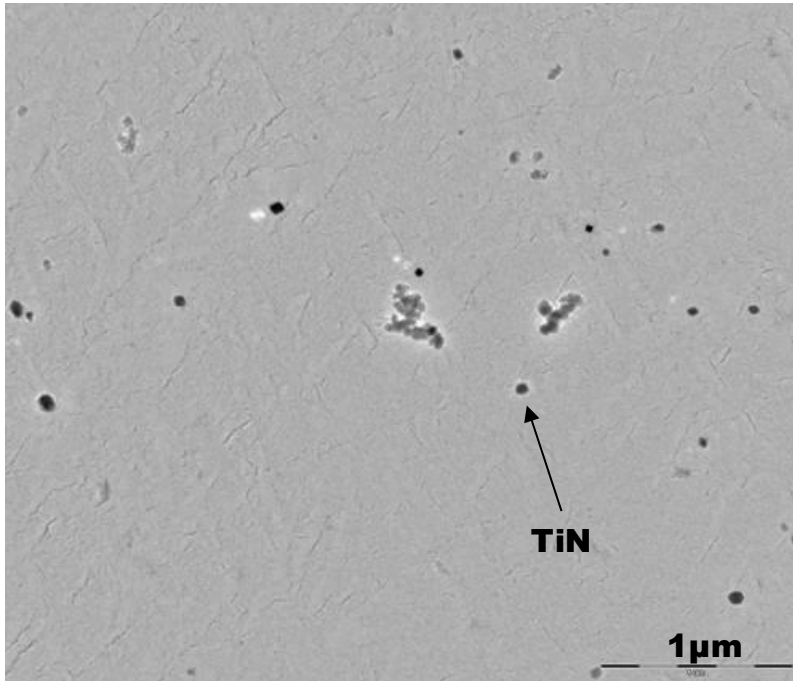
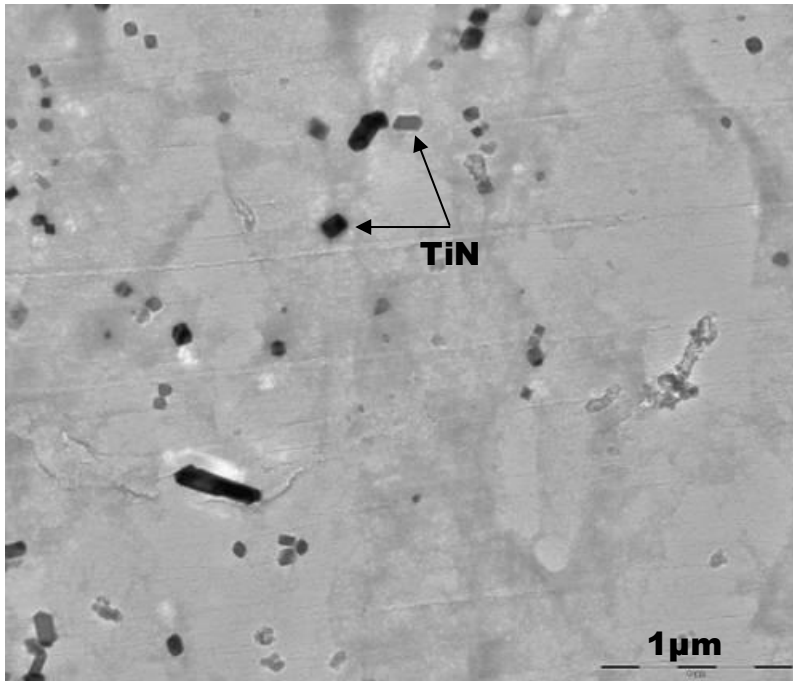


Fig.7.2 Hot ductility curves for Ti-B free steel 1 and Ti-B containing steel 2 after “re-heating” to 1250°C and cooling at 60°C/min to the tensile test temperature.

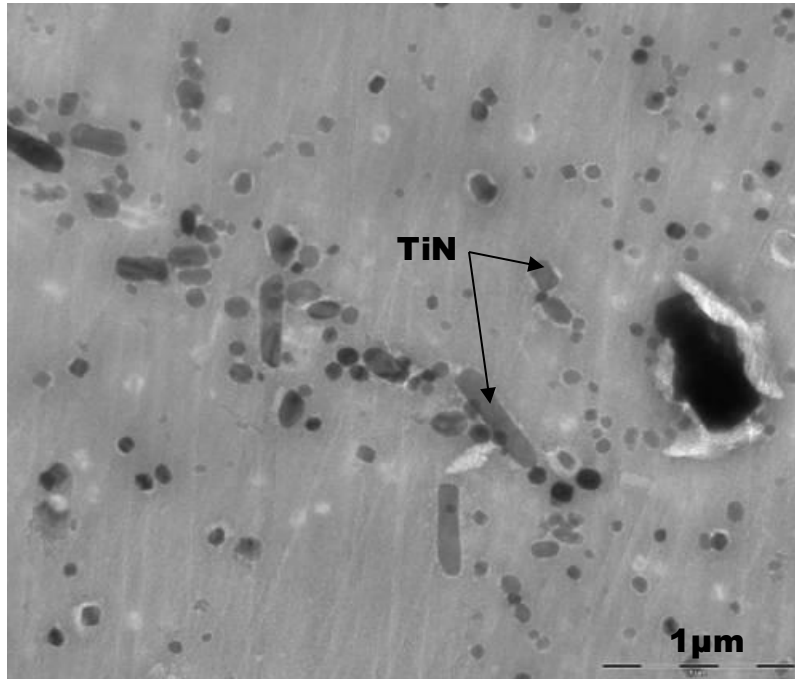
TEM photographs from samples taken from the tensile specimens of the boron treated reheated steel 2 tested in the temperature range 800~1100°C are given in Figs 7.3 (a) ~ (d). At 800°C, Fig.7.3 (a), mainly very coarse TiN particles were present. At 950°C, Fig.7.3 (b), rods of TiN and finer cubic particles of TiN were found. At 1050°C, Fig.7.3 (c) the rod particles were very coarse but copious precipitation of finer TiN particles was also present. At 1100°C, Fig.7.3 (d), mainly very coarse TiN particles were observed.



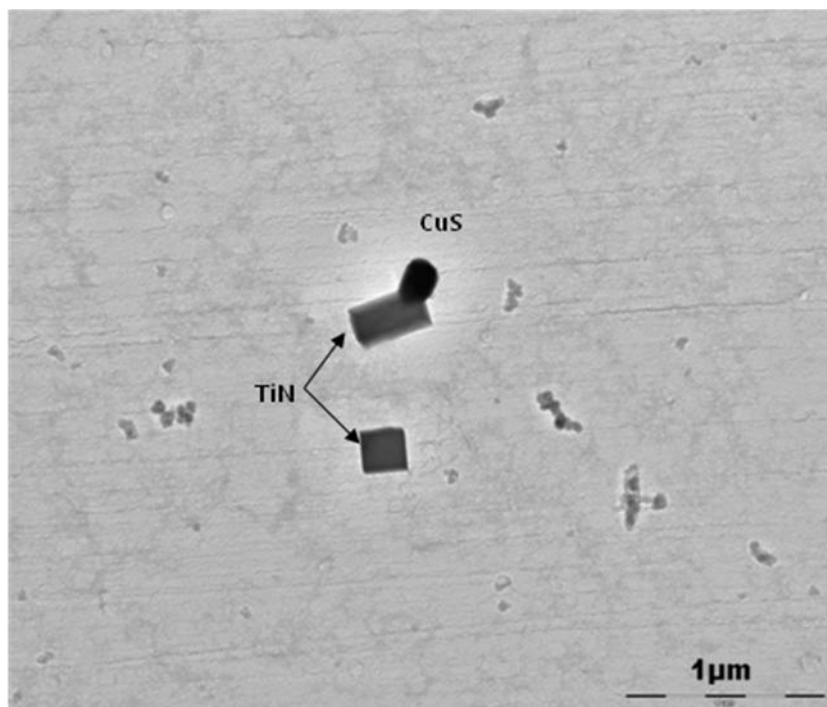
(a) Tested at 800°C, RA 66%



(b) Tested at 950°C, RA 46%,



(c) Tested at 1050°C, RA 34%



(d) Tested at 1100°C, RA 34%

Fig.7.3 Change of TiN particle distribution and size with increasing test temperature from 800 to 1100°C for “re-heated” steel 2 (0.038%Ti, 0.0021%B).

For the B-Ti containing steel 2, AlN was not detected at the austenite grain boundaries or within the grain interior. This compares with steel 1 which showed marked AlN precipitation at the boundaries in Fig.7.4.

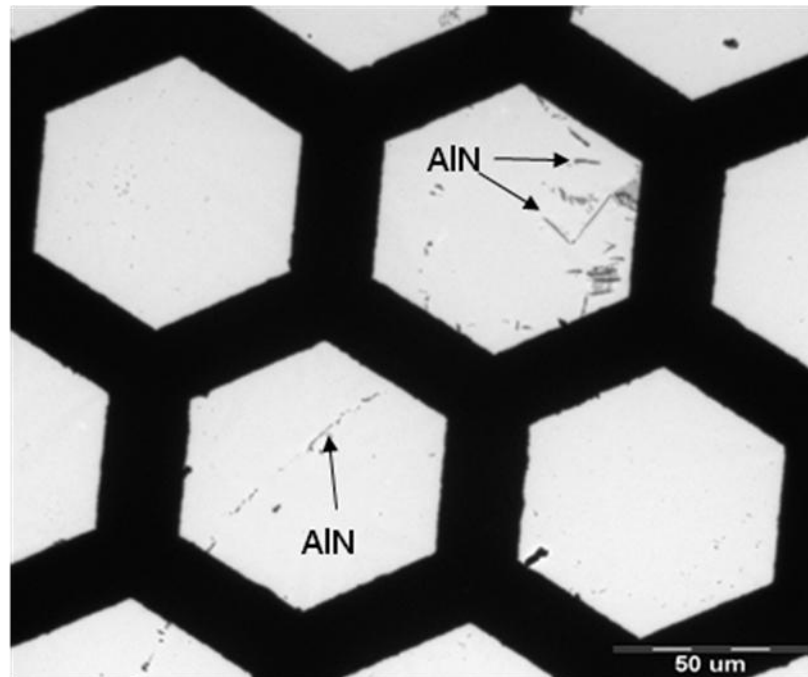


Fig.7.4 Copious precipitation of very coarse AlN particles at the austenite grain boundaries in the Ti-B free TWIP steel, steel 1 “reheated” to 1250°C and cooled at 60°C/min.

## 7.4 Discussion

### Previous work

TWIP steels being fully austenitic means that the ductility at the straightening operation in continuous casting is a balance between 1) the degree of grain boundary sliding which controls the length of cracks, 2) the precipitation in the matrix and grain boundary, which aids sliding and the joining up of developing cracks, and 3) the rate of recovery which reduces the stress acting on the boundary [37]. Because they are so highly alloyed, dynamic recrystallisation in TWIP steels, when tensile tested, requires a very high temperature and probably occurs too late to prevent crack growth from causing failure [166]. This is very different to the lower Mn, HSLA steels which recrystallise more easily leading to grain refinement, isolation of cracks and high ductility values at temperatures >950°C. Increasing the temperature above 900°C in the TWIP steels does lead to some small improvement in

ductility, as shown in Fig.5.12 in chapter 5 and this may possibly derive from some coarsening of the particles or increased recovery.

Grain boundary sliding and crack propagation become easier, the greater the precipitate volume fraction and the finer the particles, particularly at the boundaries [37]. Hence an increase in the S level which controls the amount of sulphides that can form, but more importantly for Ti-B free TWIP steels, such as steel 1, an increase in the [Al][N] product and N level, which controls the amount of AlN precipitated, will be detrimental to ductility [2]. This is particularly so for AlN, since AlN precipitates preferentially at the austenite grain boundaries. The problem with casting these high Al, TWIP steels is clearly shown in Fig.7.4 where there is copious precipitation of very coarse AlN particles at the austenite grain boundaries and the films of AlN at the austenite grain surfaces lead to “rock candy type failures”. AlN precipitation at the grain boundaries has also been shown to depend on MnS inclusions to seed its precipitation [168] and in the simpler high Al, TWIP steels having no microalloying elements, once the S level is less than 0.01% preferably 0.003%, there are insufficient nucleation sites for AlN to form at the boundaries and in consequence ductility improves [168]. However even with a low S as in steel 1, the steel only marginally achieves the 35~40% RA requirement for the straightening temperature range 800~950°C, Fig.7.2.

Ti additions by preventing AlN precipitation at the grain boundaries would be expected to improve ductility, but only from previous work, if the TiN precipitates are coarse [37]. Fine precipitation can be very detrimental to the ductility. This means that cooling rates have to be slow to ensure the TiN precipitates out in a coarse form.

### **Hot ductility of “re-heated” to 1250°C steels**

Although useful information on the hot ductility of Ti containing TWIP steels can be found from the hot ductility curves for the “re-heated” condition, there being no dynamic recrystallisation or refinement of grain size via transformation, re-heating does have the disadvantage in not reproducing the precipitation processes that occur on melting and cooling to the test temperature.

To understand the hot ductility curve in the “reheated” condition it has to be appreciated that reheating to 1250°C after melting will take a small amount of the Ti and N back into solution which will then be available for precipitating out again on cooling and holding at the test temperature.

According to the equilibrium solubility equation of Wada and Pehlke [176]

$$\log(\text{wt.}\% \text{Ti})(\text{wt.}\% \text{N}) = -14400/T + 4.94 \text{ where } T \text{ is in K.}$$

0.0008% N goes back into solution in the 0.038%Ti, steel 2, at 1250°C which is sufficient to account for the finer precipitation observed on cooling to temperatures in the range 800~1100°C, Figs.7.3(b) and (c).

The majority of TiN particles present on reheating at 1250°C will be those formed on melting and shortly after casting and will be very coarse but some can go back into solution and can then re-precipitate in a fine form.

At 800°C there appears to be insufficient time for much re-precipitation of TiN in a fine form to take place, Fig.7.3 (a). As the temperature increases, presumably the nose of the PTT (Precipitate-Temperature-Time) diagram is reached, and precipitation is marked, Fig. 7.3(c). Ductility can be seen to fall dramatically as the temperature of 1050°C is approached and this deterioration in ductility in steel 2, Fig.7.2 in the test temperature range from 800°C to 1050°C corresponds to the appearance of this fine TiN precipitation.

Above this temperature again the time is probably too long for extensive precipitation and precipitates that now form can grow rapidly and are coarse. These coarse precipitates formed at 1100°C would have little influence on the hot ductility, Fig.7.3(d) and ductility remains poor, Fig.7.2, probably because this temperature is close to the temperature range when incipient melting at the grain boundaries can occur which is sensitive to the segregation of elements such as P and S [181].

### **Role of B on the hot ductility of “re-heated” steels**

The improvement in ductility which occurs in the lower temperature range 700~950°C in steel 2, Fig.7.2 could be due to either the removal of N by the Ti preventing AlN precipitation at the austenite grain boundaries or B segregation to the boundaries.

Work by Perrot-Simonetta and Kobylanski [170] clearly shows that if free B can segregate to the austenite grain boundaries, then ductility is improved but if it is allowed to precipitate as BN at the boundaries, ductility can be very poor. They suggest B segregates to the boundaries and repels S, enhancing metallic bonding so reducing cavity nucleation and cavity growth during grain boundary sliding. Work by Karlson et al. [172] using SIMS (Secondary ion mass spectrometry) technique has shown that B segregates to the boundaries in stainless steel and this segregation is dependent on cooling rate.

Zhang et al. [141] have also found that the B segregation is very dependent on cooling rate. Using Auger electron microscopy they showed that B segregates to austenite grain boundaries in low C, Nb containing steels (0.046%Nb, 0.0007%B) and the segregation is non-equilibrium. When their steel was quenched from 1200°C and held at 900°C for various times it was found that a B peak occurred first followed by P and then S after a long time. Under non equilibrium conditions the excess vacancies produced on quenching, combine with the impurities and the complex diffuses to the grain boundary where dissociation occurs and the boundary region enriches in impurities [141]. However, at the same time there is also the reverse diffusion of impurities away from the boundary through normal diffusion which reduces the concentration at the boundaries. The cooling rate is therefore important. If the cooling rate is too high then insufficient time is available for all the B/vacancy complexes to reach the grain boundaries and segregation is reduced. If the cooling rate is too slow then reverse diffusion dominates, again leading to a reduced segregation at the boundary. There is thus an optimum cooling rate range in which segregation can take place. For boron, they found, in accord with the work of Yamamoto et al. [175] and Chown [177], that the maximum segregation occurred when the cooling rate was ~10°C/min with reduced segregation taking place at 100°C/min. In the present instance the cooling rate of 60°C/min would be expected to give some improvement in ductility but not the maximum. It is likely that much of the improvement in ductility in the temperature range 700~950°C in these “reheated” steels is due to Ti preventing the precipitation of AlN and forming coarse precipitates of TiN instead.

## 7.5 Conclusions

1. The addition of ~0.002%B and 0.04%Ti to a high Al TWIP steel improved the hot ductility for the temperature range 700~950°C after re-heating to 1250°C, and cooling at 60°C/min to the test temperature. The RA values in excess of 40% were obtained indicating that transverse cracking would be avoided using this regime. However, the N level in these steels was relatively low for nominally high N steels.
2. Reheating to 1250°C causes some of the N and Ti to be taken back into solution and this can re-precipitate on cooling to the test temperature in a fine form giving poor ductility. As a result ductility was quite poor,  $\leq 40\%$  RA for test temperatures  $> 950^\circ\text{C}$ .

## CHAPTER 8: INFLUENCE OF B AND Ti ON HOT DUCTILITY OF ‘AS-CAST’ HIGH Al, Nb CONTAINING TWIP STEELS

### 8.1 Introduction

From the previous chapter 5, the temperature range 700~1000°C, the RA values for Nb/V TWIP steels were  $\leq 20\%$ , well below that needed to avoid transverse cracking. Although the addition of B and Ti seems to have to some degree “solved” the problem of cracking in the simpler high Al TWIP steels there is no guarantee this would be the case for the higher strength Nb containing steels. An investigation was therefore carried out into establishing the hot ductility of a Nb containing high Al TWIP steel with a Nb-B-Ti high Al, TWIP steel. To make the conditions more relevant to the continuous casting process the Nb-B-Ti TWIP steel was cast and cooled at two different cooling rates from the melting point, 60 and 12°C/min. It has been shown that both B segregation to the boundaries and coarsening of the TiN particles, both of which improve ductility, are favoured by slower cooling rates.

### 8.2 Experimental

The compositions of the two Nb steels examined are given in Table 8.1. Steel 1 was a Nb containing steel, free of Ti and B. Steel 2, as well as having Ti and B present also had an addition of Nb.

Table 8.1 Composition of steels examined, wt.%

Steel	C	Si	Mn	P	S	Al	Nb	Ti	B	N	Condition
1	0.60	0.02	17.9	0.024	0.0036	1.19	0.050	0	0	0.011	re-heated
2	0.55	0.07	18.3	0.022	0.0020	1.19	0.016	0.049	0.0021	0.006	As-cast

For steel 1, the samples were re-heated to 1250°C and tested on a Gleeble machine. In the text, this condition is referred to as “re-heated”. The tensile samples were machined from the as-cast ingots and were of 120mm length and 10 mm diameter. The samples were initially heated at 150°C/min to 1250°C after which they were held for 2mins. They were then cooled to test temperatures in the range 700~1200°C at a cooling rate of 60°C/min held for 30secs at temperature and strained to failure using a strain rate of  $3 \times 10^{-3} \text{s}^{-1}$ .

The specimens for steel 2 were melted with an induction furnace. In the text, this condition

is referred to as “as-cast”. The tensile samples were initially machined from the as cast ingots as cylinders having a length of 110mm and diameter 7.7mm. Each tensile sample was inserted in a close fitting silica tube which was surrounded by another tube through which argon flowed and placed in a tensile machine. Only the central length of the sample, a length of 12 mm was melted. A hole 2mm in diameter had been drilled from one end of the sample to its centre so that a thermocouple could be inserted to control the temperature. The samples were initially heated at 150°C/min to the melting point 1410°C, where they were held for 2minutes. They were then cooled at either 60 or 12°C/min to test temperatures in the range 700~1200°C, the procedure being then the same as for the Gleeble samples. The temperature profile is shown in Fig.8.1.

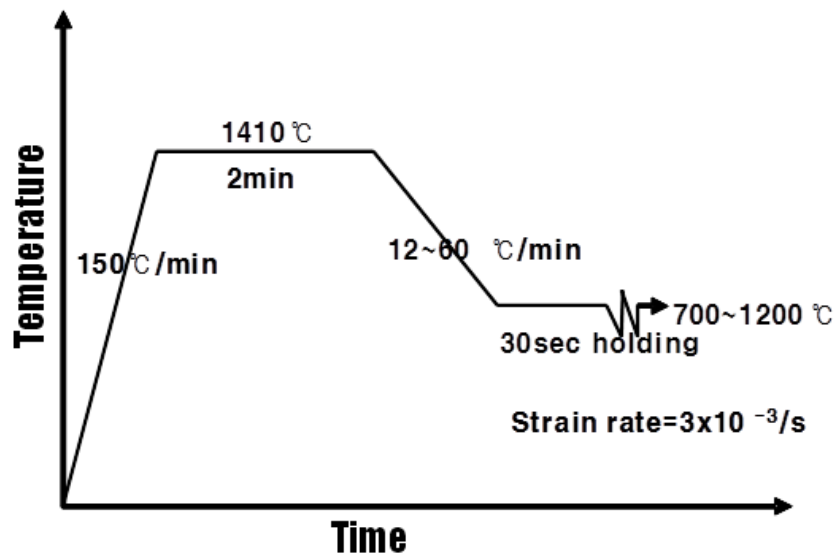


Fig.8.1 Hot ductility curves for samples machined from the ingots and re-melted at 1410°C; “as-cast”.

### 8.3 Results

The hot ductility curves for the Ti-B-Nb high Al, TWIP steel 2 are shown in Fig.8.2 for cooling rates of 12 and 60°C/min after melting, the as-cast” condition. Also included is the hot ductility for steel 1, re-heated to 1250°C and cooled at 60°C/min.

For the “as-cast” Nb, Ti-B containing steel, steel 2, Fig.8.2 (solid curve), ductility was very poor, ~10% RA throughout the temperature range 700~1200°C, when the cooling rate was 60°C/min. Reducing the cooling rate to 12°C/min (solid curve) produced a significant

improvement in ductility, the RA values being in the range 37~60% in the temperature range 800~1050°C. TEM work was not carried out on this steel to look for fine Nb(C, N) and TiN precipitation but from previous work on HSLA steels, using cooling rates in the range 25~100°C/min after melting these fine detrimental precipitates, which are responsible for fracture, are likely to be present [78, 79, 131]. Included also in Fig.8.2 is the hot ductility curve(dashed curve) for, steel 1, “re-heated” to 1250°C and cooled at 60°C/min which illustrates how poor the ductility is in these TWIP steels at this cooling rate when Nb is present singly or with Ti and B.

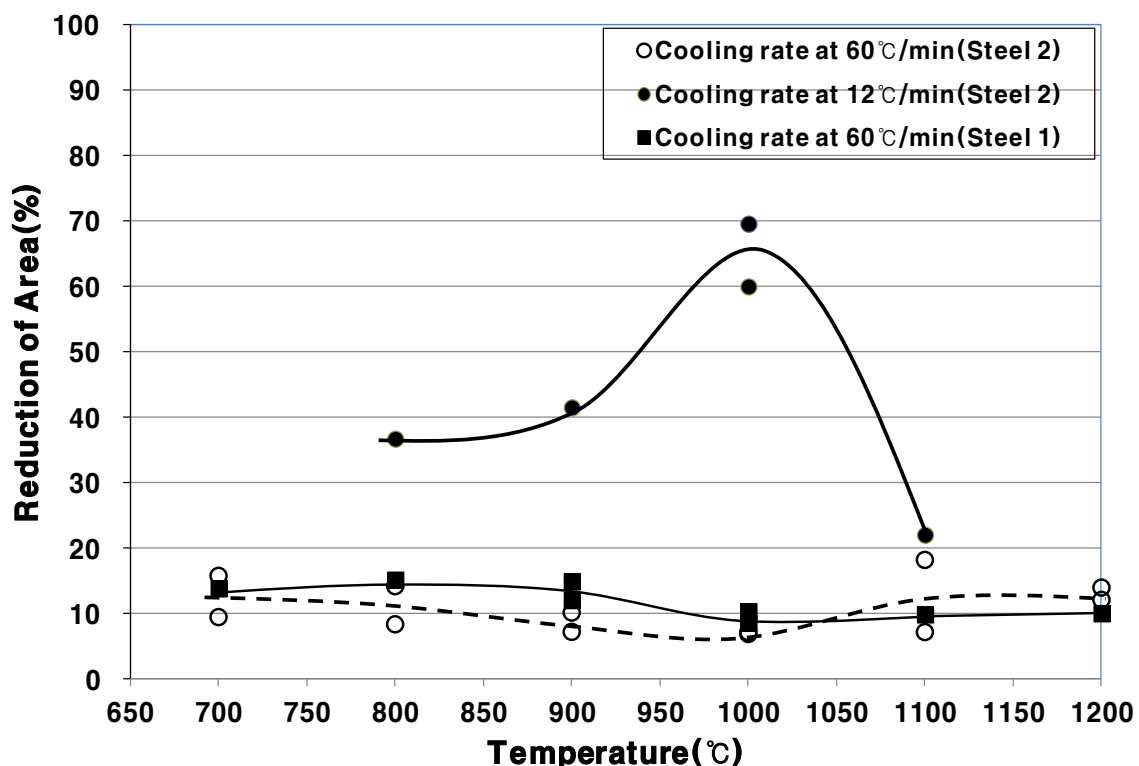
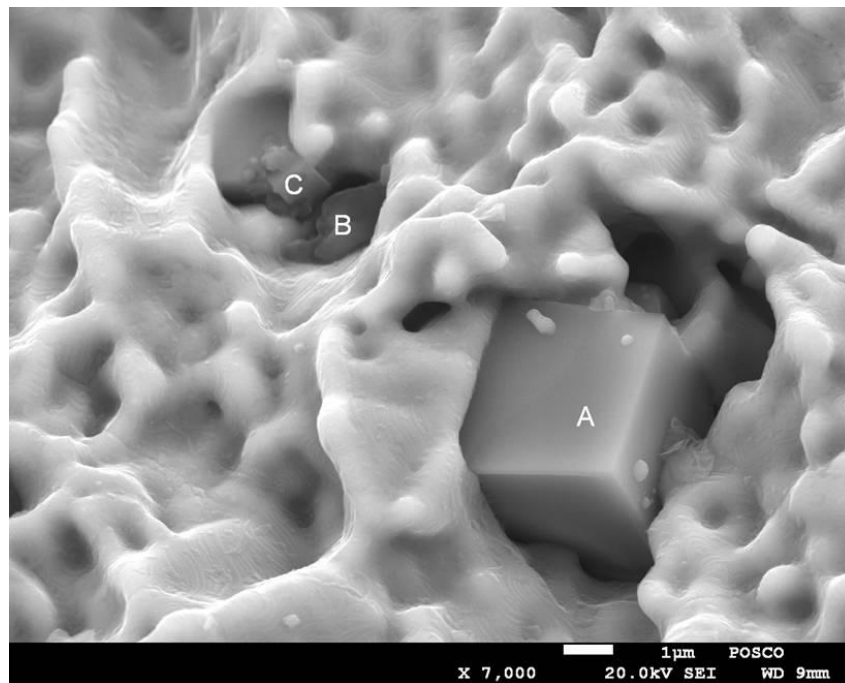


Fig.8.2 Hot ductility curves for cooling rates of 12 and 60°C/min for the Nb, Ti-B steel 2 after melting, the “as-cast” condition. Also included is the hot ductility curve for steel 1, “re-heated” to 1250°C and cooled at 60°C/min.

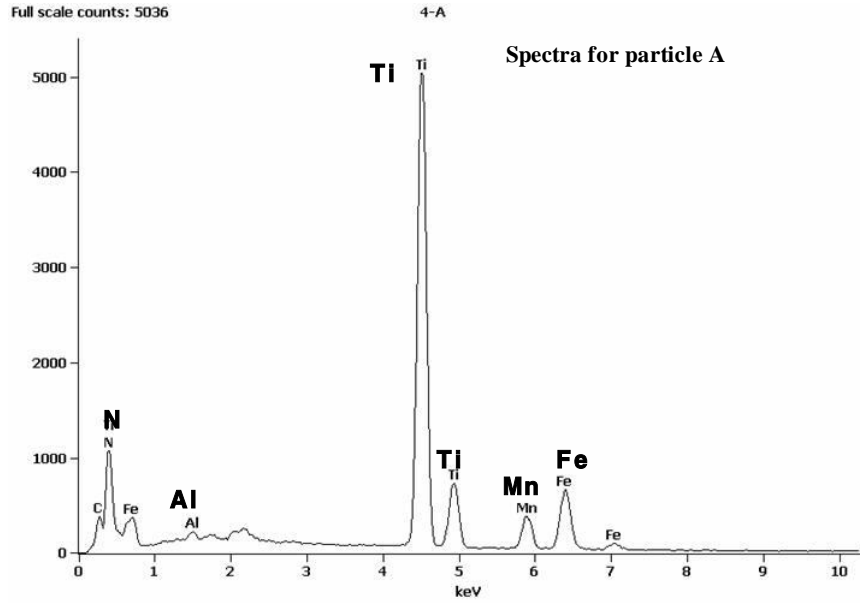
For steel 2, the fracture appearance of the “as-cast” tensile specimens cooled at 60°C/min was inter-granular and coarse TiN particles were present on the fracture surface, Fig.8.3 (a). The hot ductility for the “re-heated” Ti-B free, Nb containing high Al TWIP steel, steel 1 (dashed curve in Fig.8.2) can be seen to give very poor ductility throughout the temperature

range 700~1200°C. For this Ti free steel 1, gross precipitation of AlN precipitation occurred at the austenite grain boundaries but this time in addition there was a fine precipitation of Nb(C, N) in steel 1, Figs.8.4 (a) and (b), respectively. Most of the precipitates shown in the low magnification photograph, Fig.8.4 (a) are AlN. Coarse dendritic precipitation of AlN was also observed, Fig.8.4(c). In contrast, for the Ti containing steel 2, AlN was not detected at the austenite grain boundaries or within the grain interior.

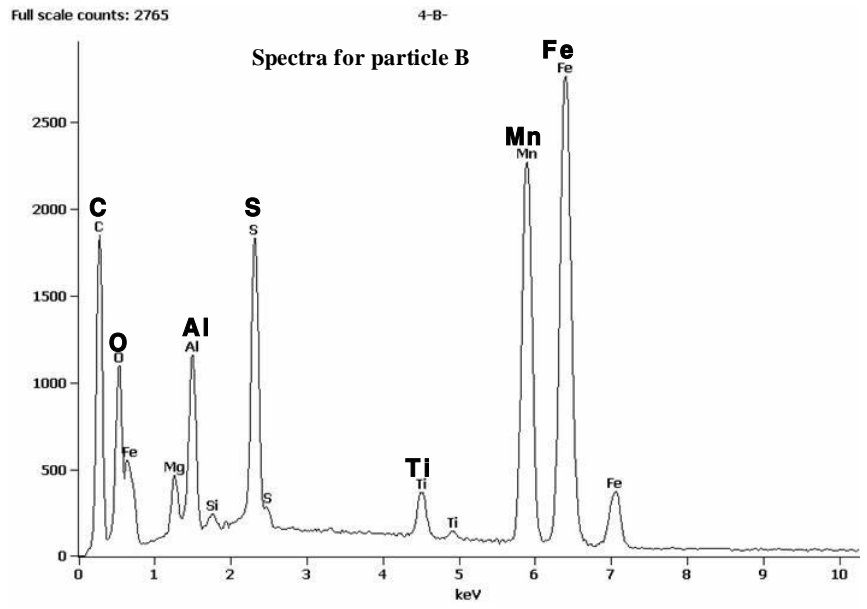
Although the “reheated” Nb steel (dashed curve) chosen for comparison did contain a higher N level and Nb content it does indicate how poor the ductility is when Nb is present as the “re-heated” condition invariably gives better ductility than the “as-cast”.



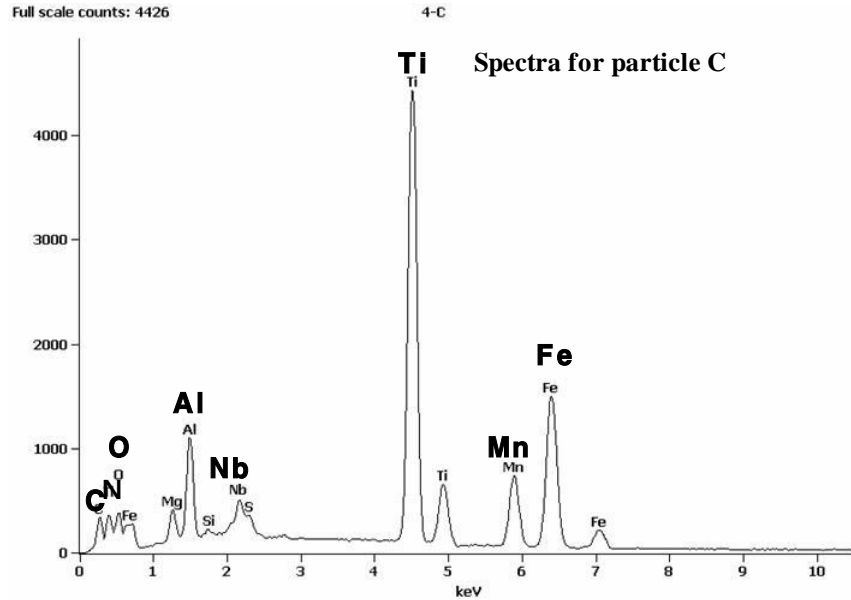
(a) Fracture surface (SEM)



(b)

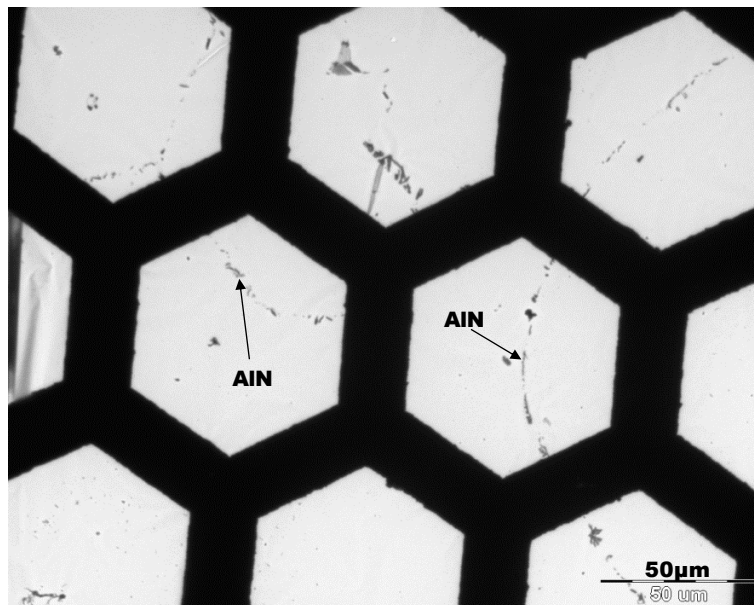


(c)

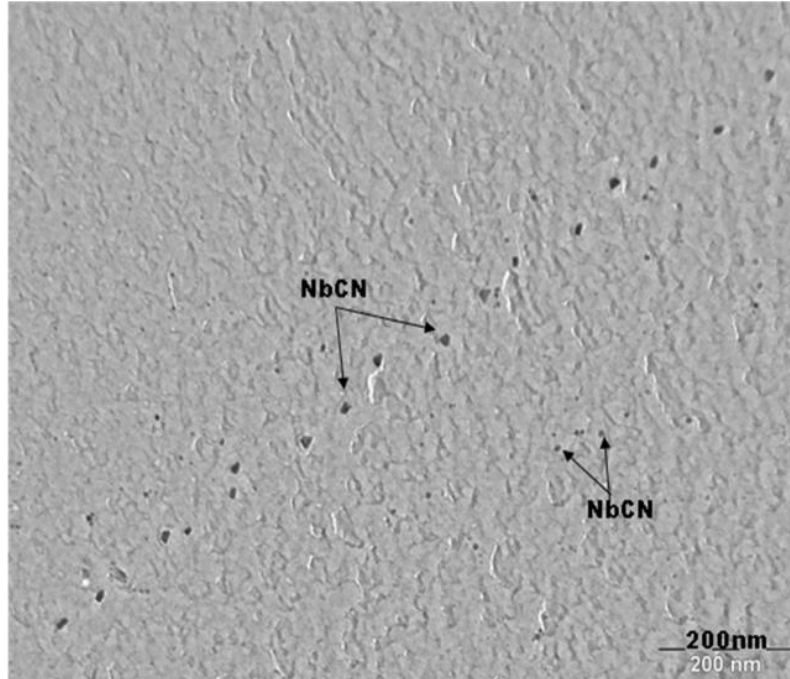


(d)

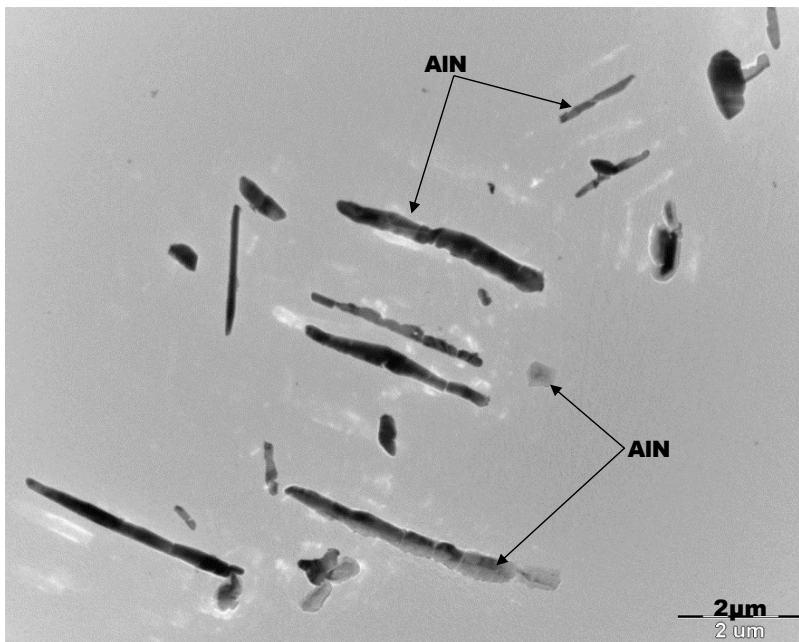
Fig.8.3 Coarse TiN particles in the “as-cast” steel 2, cooled at 60°C/min, (a) fracture surface showing the presence of precipitation particles A, B and C with typical analysis (b) mainly TiN particles with occasionally a trace of Al (c) mainly MnS particles with Alumina (d) TiN particles with more substantial amounts of Nb. Sample was fractured at 800°C.



(a)



(b)



(c)

Fig.8.4 AlN and Nb(C, N) precipitation in the Ti-B free TWIP steel, steel 1 “reheated” to 1250°C and cooled at 60°C/min. (a) Copious precipitation of very coarse AlN particles at the austenite grain boundaries (b) Fine (Nb(C, N)) precipitation at the boundaries (c) dendritic precipitation of AlN.

## 8.4 Discussion

Nb containing high Al, TWIP steels is particularly difficult to cast being prone to transverse, edge and corner cracking and therefore two cooling rates, 60°C/min, and a slower cooling rate of 12°C/min were examined. The “as-cast” state was chosen to be more representative of the continuous casting operation, particularly for Ti containing steels where re-heating does not take all the TiN particles back into solution, as is the case when the steel is melted.

The Nb-Ti TWIP steel in the as-cast state, Fig.8.2, when cooled at 60°C/min, gives terrible ductility (10% RA) throughout the temperature range 700~1200°C. This is due most likely from previous work on HSLA steels to fine precipitation of NbC at the boundaries and within the matrix. This fine precipitation occurs when the steel is deformed during the straightening operation [79, 131].

Turkdogan [68] has suggested that the addition of Ti to the melt reduces transverse cracking by coarsening the precipitates of Nb and V, thereby eliminating their effect on ductility. During the later stages of solidification, most of the N would be expected to precipitate in a relatively coarse form as TiN in the inter-dendritic boundaries. These coarse particles then serve as nucleation sites for equilibrium precipitation of NbC at higher temperatures. Turkdogan calculated, by the time the temperature had reached 1200°C during solidification, most of the Nb would be precipitated as NbC on the coarse TiN particles so that the detrimental fine strain induced NbC precipitation would not occur at lower temperatures. Abushosha et al. [78, 79] and Comineli et al. [131] suggest from their work that 60°C/min is too fast to achieve this and slower cooling rates  $\leq 25^\circ\text{C}/\text{min}$  are required. This is substantiated by the finding in the present work, Fig.8.2 that decreasing the cooling rate to 12°C/min results in a substantial improvement in the hot ductility, RA values being  $\geq 35\%$  for the temperature range 800~1000°C, the temperature range typically used in the straightening operation. In the present work it cannot be established whether this improvement is due to B segregation to the boundaries or coarsening of the TiN particles, both of which are enhanced by slower cooling rates. However, Zarandi and Yue [138] have clearly shown in their work that it is B that is responsible for the improvement in ductility, as in their investigation Ti was present in both B containing and B free steels. Zarandi and Yue using a more commercial cycling treatment including primary and secondary cooling have shown with a low C (0.015~0.05%), Nb (0.035~0.05%) Ti-stabilised containing steel, that when 0.004~0.005%B is added, boron not only improves the ductility in the  $\gamma + \alpha$  phase field but does so also in the  $\gamma$  temperature range, RA values above 40% being achieved throughout the temperature range, 700~1050°C, Fig.8.5. This compared with ~20%RA for the B free steel for the same temperature range.

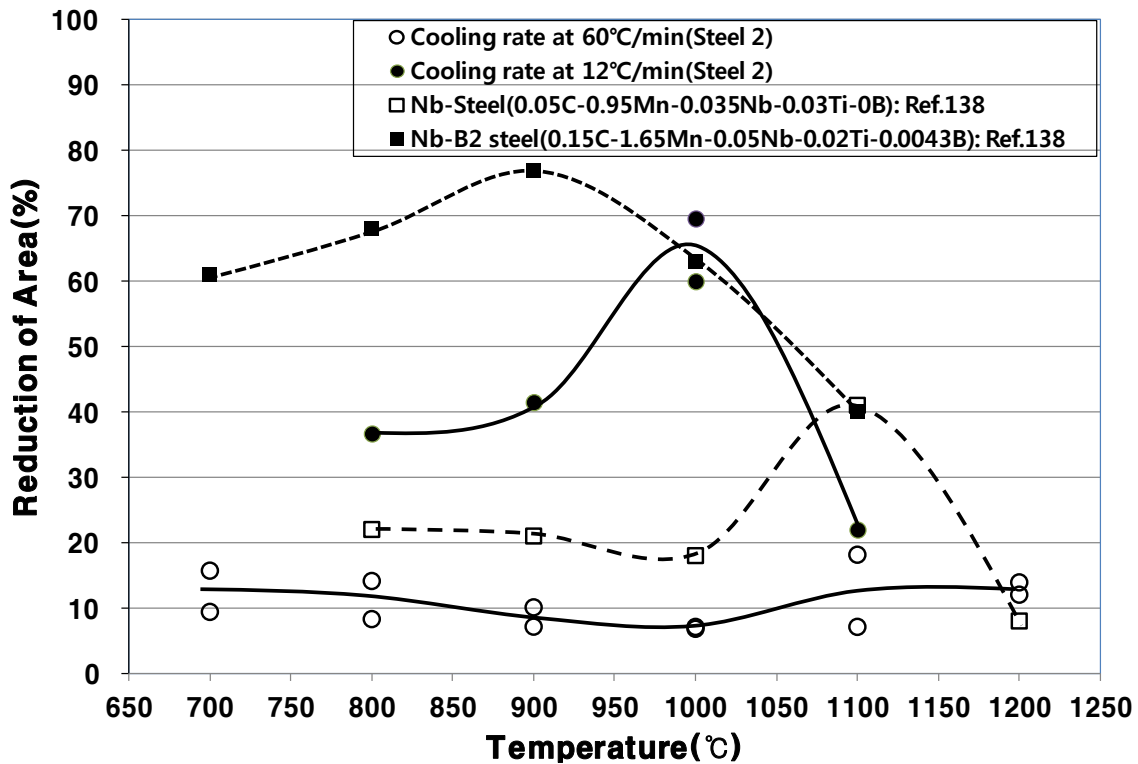


Fig.8.5 Hot ductility curves for “as-cast” steel 2 at the two cooling rates, 60 and 12°C/min compared to Zarandi and Yues’ curves for HSLA, Nb containing steels with and without B using a secondary cooling rate of 15°C/min.

Their steels contained as in the present investigation sufficient Ti to combine with all the N. They suggest that the improvement in ductility of the austenite could be due to either non-equilibrium segregation of the boron and niobium to the  $\gamma$  boundaries, strengthening them or earlier nucleation and growth of Nb containing precipitates so coarsening them and leading to a softer  $\gamma$  lattice.

The curves (dashed lines) obtained by Zarandi and Yue [138], Fig.8.5 is shown with the presently derived curves (solid lines) for comparison. Their average secondary cooling rate was 15°C/min compared to the single cooling rate of 12°C/min used in the present work. For this slow cooling rate, considering that the compositions are very different, they both show similar trends in that on cooling, the ductility increases reaches a peak and then decreases. The most important part of the present work is that when a slow cooling rate of

12°C/min is used in the temperature range 800~1000°C, ductility is adequate to prevent transverse cracking occurring in the Ti-B containing high Al, TWIP steels. The importance of a slow cooling rate in avoiding cracking as well as the need for low N contents in continuous cast B bearing low C and Mn steels containing Mo has also been shown by Cho et al. [147].

Following recommendations based on the present work; a low S level, sufficient Ti to combine with the entire N, a B addition and a slow secondary cooling rate, transverse cracking was avoided in both the lower and higher strength high Al containing TWIP steels.

### **Importance of secondary cooling rate**

The best laboratory simulation is always to have a high primary cooling rate followed by a slower secondary cooling rate as occurs in the commercial operation. However, simpler test conditions are always sought after. It is probably the slower, secondary cooling process that is most important in controlling ductility as this allows time for segregation and growth of precipitates to occur. Certainly, not including a primary fast cooling rate and only using a slower secondary cooling stage in the tensile test produces ductility results which can be used to predict the likelihood of transverse cracking occurring.

Although the average of the cooling rates for the faster primary and slower secondary cooling rate, corresponding to 60°C/min has in the past been taken for the cooling rate experienced just below the broad face of the strand for 220mm thick strand, a cooling rate closer to 10~15°C/min should be used as this corresponds more closely to the secondary cooling rate used in the continuous casting operation. However, because most of the past work in the literature has used this cooling rate of 60°C/min or higher, the most appropriate slower cooling of 10~15°C/min makes comparison with past work, difficult. Nevertheless, a strong recommendation will be made at the end of this thesis for all future work to be carried out at this slower cooling rate.

## **8.5 Conclusions**

1. The ductility of Nb containing high Al, TWIP steels is very poor in the as-cast condition. Adding B and Ti still gave rise to extremely poor ductility when a cooling rate of 60°C/min was used. Reducing the cooling rate to 12°C/min caused the ductility to improve so that RA values were now close to the 35~40% RA value required to avoid transverse cracking. It is recommended that to avoid transverse cracking, the secondary cooling rate should not be higher than  $\approx 60^\circ\text{C}/\text{min}$  in these Nb containing high Al, TWIP

steels. It should however, be noted that the N level was relatively low in this steel, 0.006% and more work is required to establish the influence on the ductility of higher N steels.

2. Microstructures were always fully austenitic so that the improvement in ductility is either due to the non-equilibrium segregation of boron to the austenite grain boundaries or Ti combining with N avoiding AlN precipitation at the boundaries or a combination of both. Clearly more work is required to identify the ultimate cause.
3. Following all these recommendations, i.e. a low S level, slow secondary cooling rate, a Ti level above the stoichiometric for TiN and a boron addition of 0.002%, transverse cracking was avoided in these very difficult to cast high strength TWIP steels.

## CHAPTER 9: INFLUENCE OF B ON HOT DUCTILITY OF HIGH Al TWIP STEELS

### 9.1 Introduction

In the previous chapter it has been shown that Ti and B are required to give good ductility and avoid transverse cracking. Without these additions these high Al, TWIP steels can only just achieve the 35~40% RA (reduction of area) benchmark required to avoid transverse cracking from occurring even with low N and S levels. However, an addition of Ti sufficient to combine with the entire N, as well as a B addition and a low S level has enabled casting to be carried out successfully at POSCO even in high N (0.01%N) steels and when Nb is present. Fracture, when the hot ductility is poor is always intergranular and therefore strengthening the boundary regions is of importance [37]. B is one of the few segregates which are believed to be beneficial to ductility. Perrot-Simonetta and Kobylanski have suggested that B prevents S segregating to the boundaries [170]. Cooling rate is also important and average cooling rates in the range 10 to 100°C/min are needed; the lower the cooling rate in this range, the more effective B is in improving ductility [141, 175, 177].

The complexity of all these various factors makes it difficult to be sure not only what are the essential ingredients required to give good ductility in high Al, TWIP steels but the mechanisms which give rise to any improvement.

This is particularly so when Ti and B are present together. It is not clear from the previous chapter whether the improved ductility that has been found in high Al, TWIP steels on adding Ti and B is due to B diffusing to the boundaries, strengthening them or Ti removing all the N as TiN, so preventing the detrimental to ductility film of AlN precipitating out at the austenite grain surfaces or a combination of both.

This investigation has been designed to explore more fully the role of B in determining the hot ductility of high Al containing, TWIP steel and to see whether it is possible to establish experimentally B segregation to the boundaries using SIMS (secondary ion mass spectrometry).

### 9.2 Experimental

The compositions of the high Al containing TWIP steels are given in Table 9.1.

Steels 1, 2 and 3 were similar high Al TWIP steels with  $\approx 0.04\%$ Ti and  $\approx 0.002\sim 0.0025\%$ B. Steel 2 had a small addition of Ni, 0.43%, and Steel 3 had a lower Al, N and S level than the others. Steel 4 was of otherwise similar composition to this group but contained no B and was used as a base to compare the hot ductility of Ti containing steels with boron, steels 1~3, to a Ti containing steel without boron. Of these steels the B-Ti steel 1 was the closest in composition to steel 4; the B free Ti containing TWIP steel. Steel 5 had a higher Ti level of  $\sim 0.10\%$  but again was otherwise of similar composition to steels 1~3.

Table 9.1 Compositions of the high Al containing TWIP steels, wt.%

Grade	C	Si	Mn	P	S	Al	Ti	B	N	Ni
Steel 1	0.59	0.03	17.9	0.024	0.0046	1.51	0.042	0.0026	0.0093	0
Steel 2	0.60	0.02	18.0	0.025	0.0032	1.48	0.041	0.0026	0.0094	0.43
Steel 3	0.55	0.09	16.6	0.024	<0.003	1.12	0.038	0.0021	0.0070	0
Steel 4	0.62	0.04	17.9	0.025	0.0043	1.53	0.041	0	0.0092	0
Steel 5	0.55	0.07	17.6	0.019	0.0014	1.44	0.098	0.0017	0.0090	0

The tensile samples were machined from the as-cast ingots and were of 120mm length and 10mm diameter and were tested on a Gleeble machine. As for most of this thesis, the samples were initially heated at  $150^\circ\text{C}/\text{min}$  to  $1250^\circ\text{C}$  after which they were held for 3mins. They were then cooled to test temperatures in the range  $700\sim 1200^\circ\text{C}$ , the cooling rate always being  $60^\circ\text{C}/\text{min}$ , after which the samples were held 30secs and strained to failure using a strain rate of  $3\times 10^{-3}\text{s}^{-1}$ . The temperature profile is shown in Fig.9.1.

Once a tensile sample had failed it was immediately gas quenched with argon in order to try and preserve the grain structure and the fracture surface present at the time of failure.

The hot ductility curves of RA against the test temperature were determined as well as the grain size. SEM (scanning electron microscope) examination was carried out on sections taken close to the point of fracture and the fracture surfaces were also analysed for the type of fracture and identification of the particles. TEM (transmission electron microscope) examination was performed on carbon extraction replicas taken from sections close to fracture. A nickel grid supported the carbon replica in the microscope. The SIMS analysis was performed with a Cameca IMS 6F instrument to establish the presence of B at the boundaries. The conditions used during the SIMS analysis detection were as follows:

$\text{O}_2^+$  was the bombarding ion on the etched surface, the field of view being  $250\mu\text{m}$  and the detection ion  $11\text{B}$ . The negatively charged secondary ions emitted from the surface were used to obtain the mass-resolved ion images. All the areas examined were checked first to

ensure there was a boundary in the field of view.

SEM examination was first carried out on a simpler high Al, TWIP steel free of both Ti and B (Steel 1 in chapter 7), to examine the influence of high Al on the fracture appearance. The steel had been given the same schedule as shown in Fig.9.1.

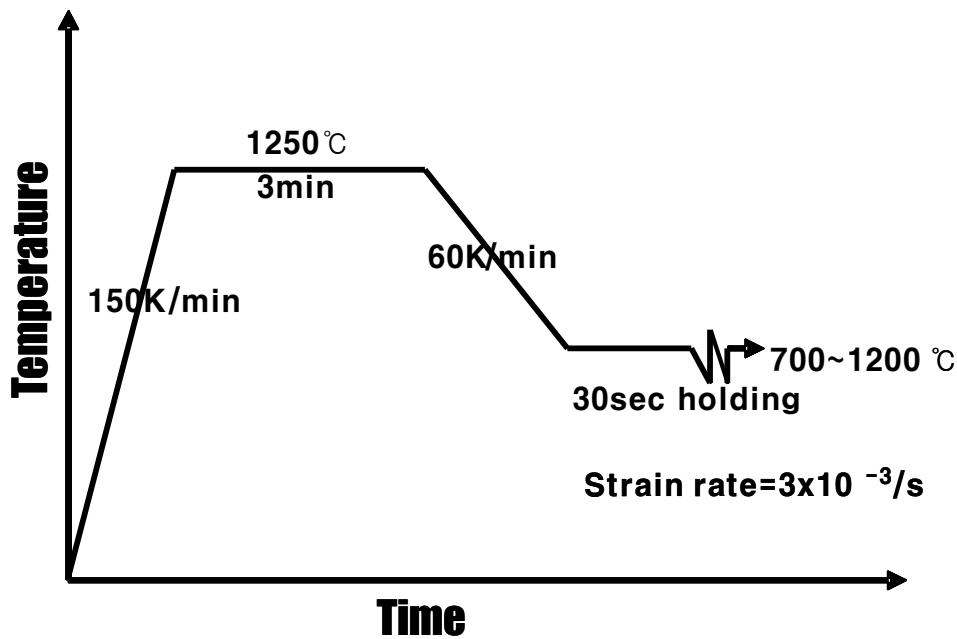


Fig.9.1 Schematic diagram of the heating and cooling programme used in the investigation.

### 9.3 Results

In the hot ductility curves in Fig.7.2 in chapter 7, it can be seen that there is a substantial improvement in the hot ductility in the temperature range 700~900°C when Ti and B are present but it is not clear whether this improvement is due to the presence of Ti or B or both and hence the need for further examination.

To establish the role of these elements in improving ductility more clearly the hot ductility curves of the presently examined TWIP steels which contained both Ti and B, steels 1~3 were compared to a similar Ti containing steel which was free of B, (steel 4). These curves are given in Fig.9.2 and show (compositions in Table 1) that the ductility of the Ti containing TWIP steels with a B addition, steels 1~3 (solid curves), are better than the Ti

containing and B free steel of otherwise similar composition, steel 4 (dashed curve). B in itself is therefore giving a benefit to the ductility. Compositions of steels 1 to 4 although similar do have differences which might influence the hot ductility. Steels 2 and 3 gave the best ductility of the three Ti-B steels. Steel 3 had the lowest N and S contents which probably accounts for its better ductility. Steel 1 gave the worst ductility of the three B treated steels having both a high N level and the highest S content. It is not clear why steel 2 gives such good ductility but the presence of the small Ni addition may possibly be the reason. The best comparison of the hot ductility curves is with those of steels 1 and 4 which have very similar compositions and clearly show that the boron containing steel 1 has better ductility than the B free Ti containing steel, steel 4.

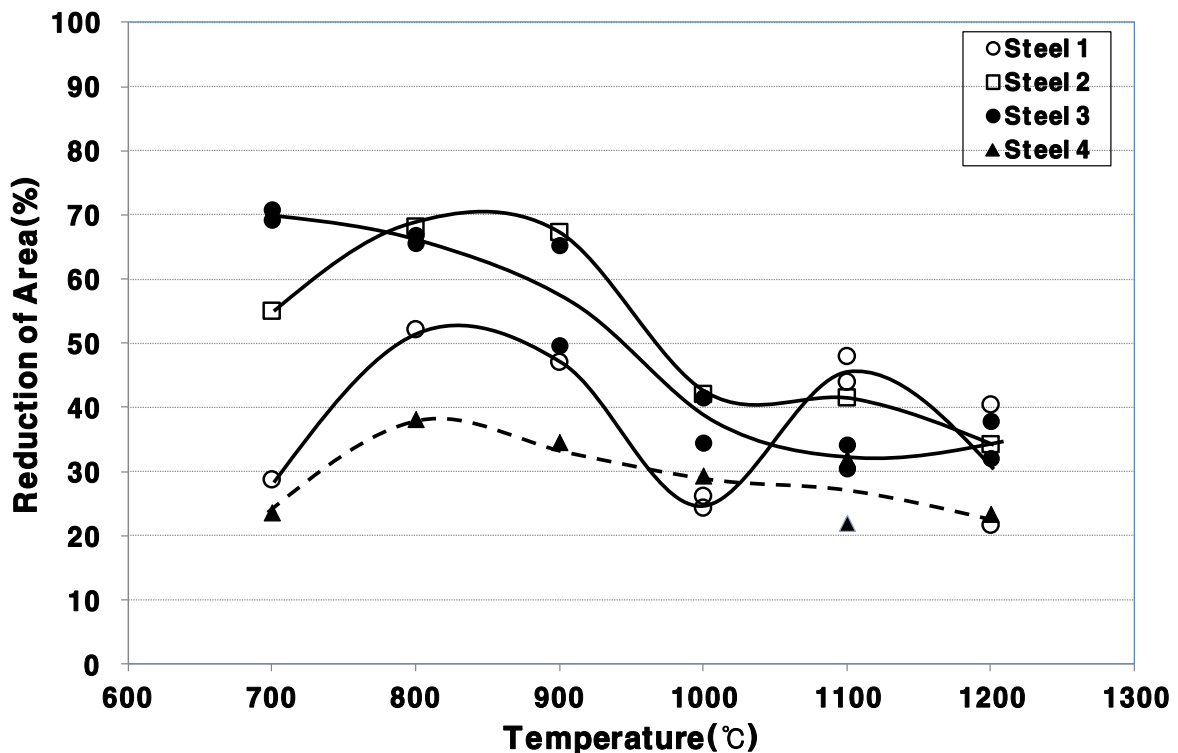


Fig.9.2 Hot ductility curves for B-Ti high Al, TWIP steels, Steels 1~3 compared to the hot ductility curve for a B free, Ti containing high Al, TWIP steel, Steel 4.

The SIMS results for all the B containing steels are given in Figs 9.3, 9.4, 9.5 and 9.6 for the steels containing B, steels 1, 2, 3 and 5 respectively. It can be seen that in all cases B has segregated to the boundaries throughout the temperature range 700~1200°C. The B

concentration is always more intense in the temperature range 700~800°C when it is possible that BN or Fe<sub>23</sub>BC<sub>6</sub> precipitation occurred but B is also present at the boundaries at temperatures > 800°C when precipitation is unlikely.

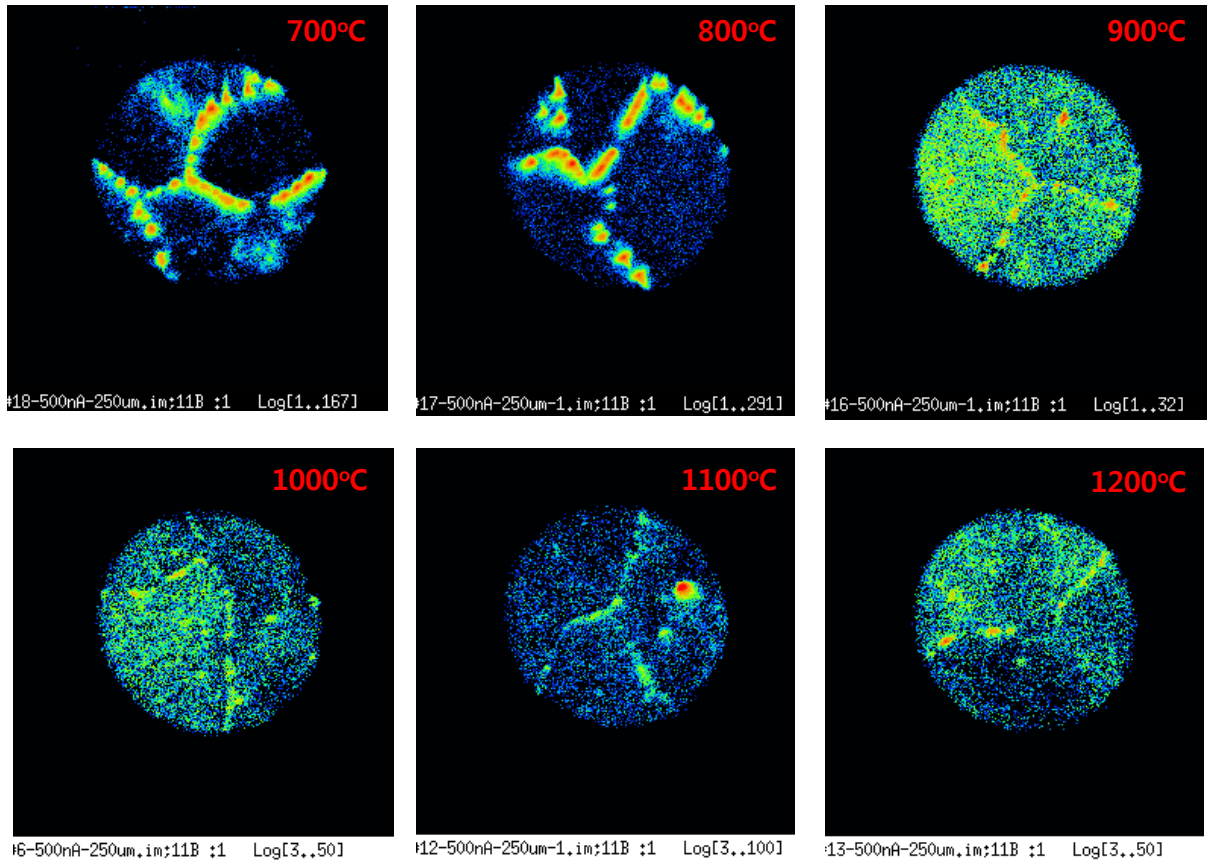


Fig.9.3 SIMS photographs for steel 1 (1.51%Al, 0.042%Ti, 0.0026%B, 0.0093%N) for the test temperature range 700~1200°C.

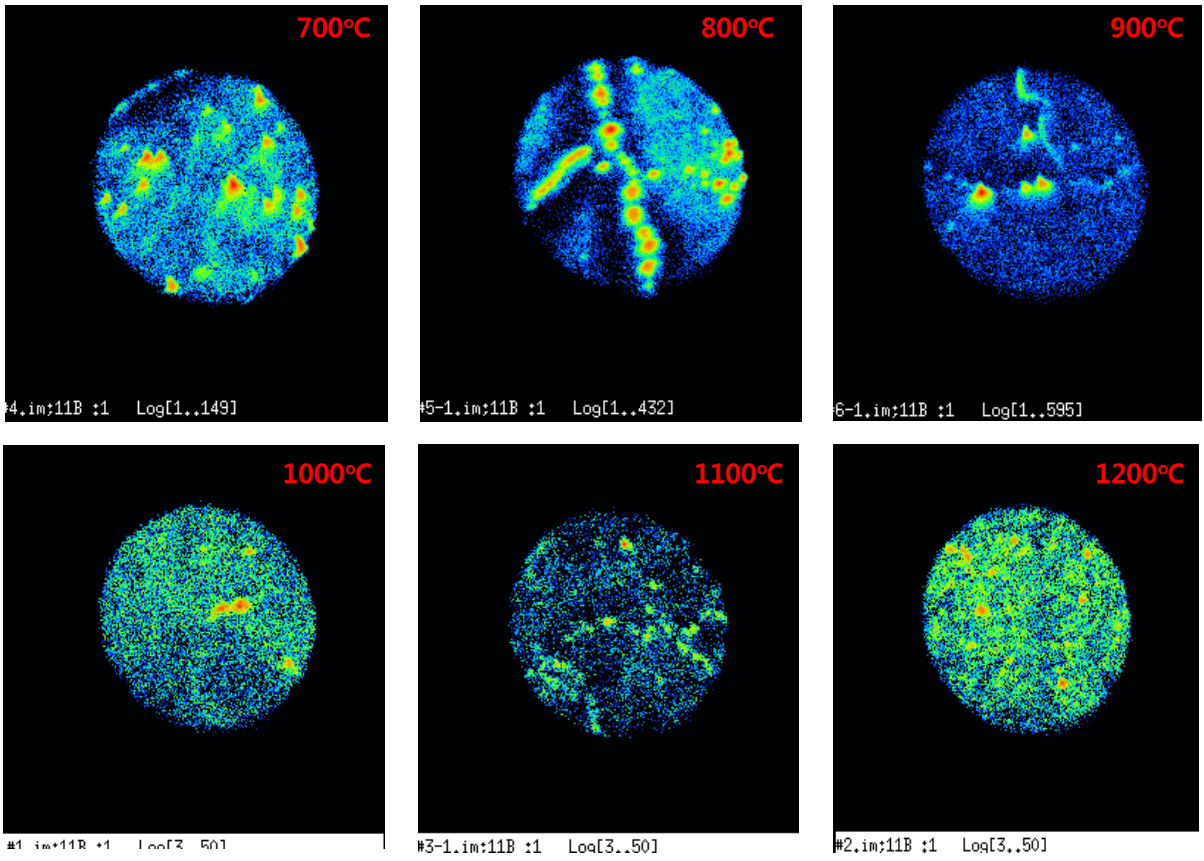


Fig.9.4 SIMS photographs for steel 2 (1.48%Al, 0.041%Ti, 0.0026%B, 0.0094%N) for the test temperature range 700~1200°C.

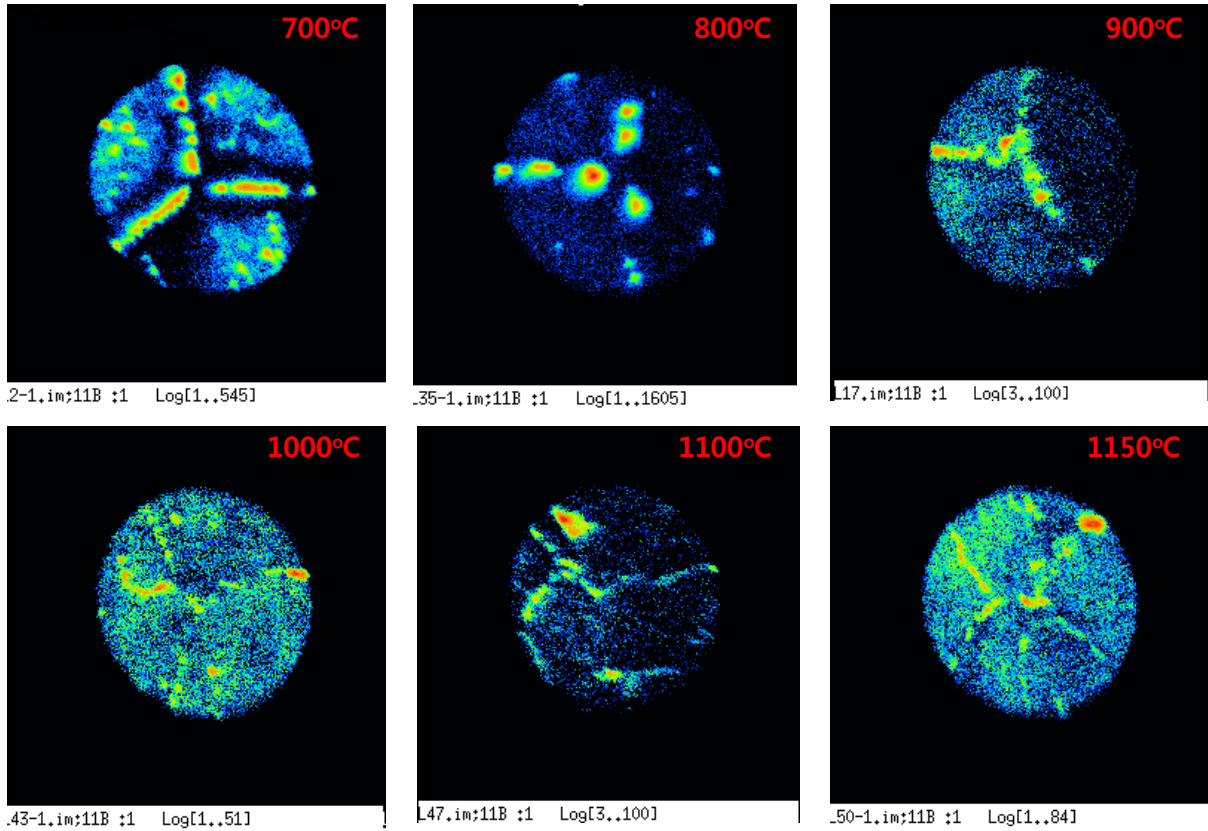


Fig.9.5 SIMS photographs for steel 3 (1.12%Al, 0.038%Ti, 0.0021%B, 0.007%N) for the test temperature range 800~1150°C.

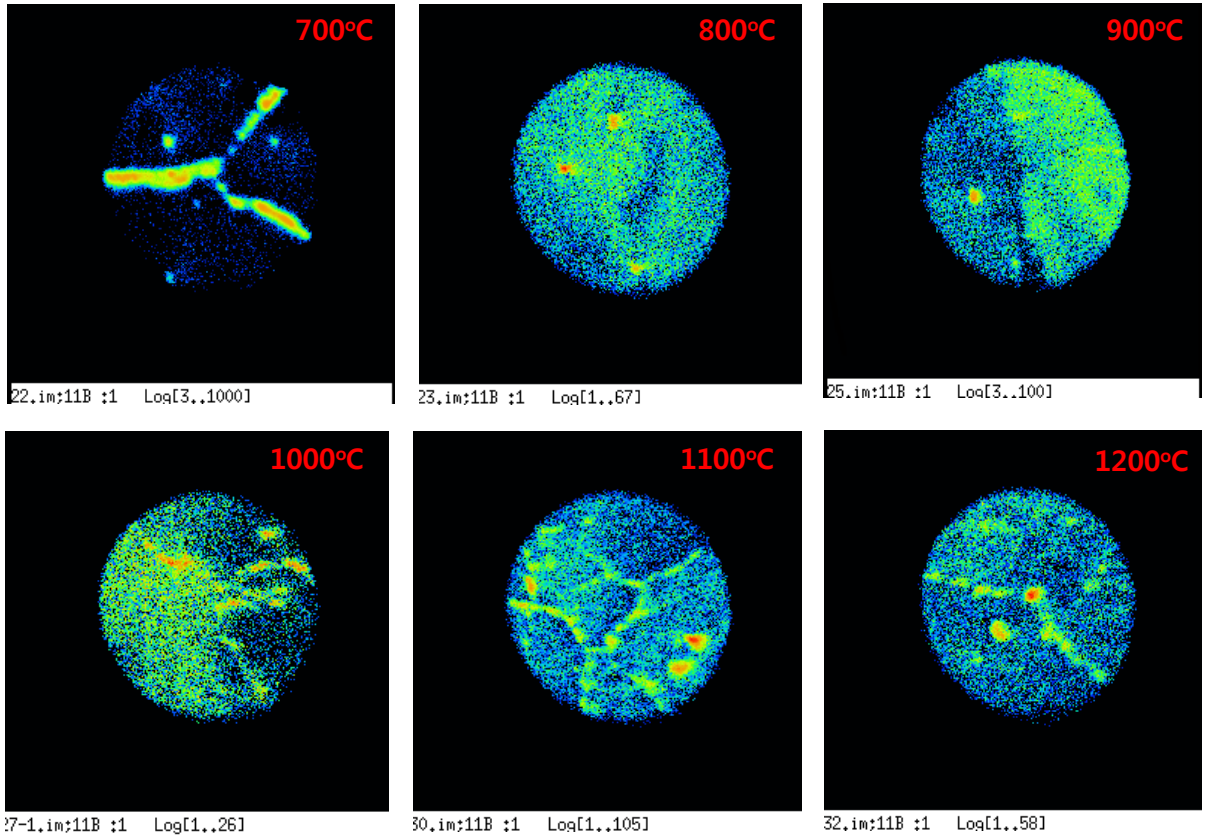


Fig.9.6 SIMS photographs for steel 5 (1.44%Al, 0.098%Ti, 0.0017%B, 0.009%N) for the test temperature range 700~1200°C.

Finally, the hot ductility curve for steel 5, the Ti-B steel with a very high Ti level (0.1%Ti) is shown in Fig.9.7. The corresponding SIMS photographs are given in Fig.9.6. It can be seen from Fig.9.7 that on heating to 1250°C and cooling to the test temperature, ductility does not fall rapidly at temperatures > 900°C, as observed in the ~0.04% Ti-B steels, Fig.7.2 and Fig.9.2 but remains high >40% RA throughout the temperature range 800~1200°C.

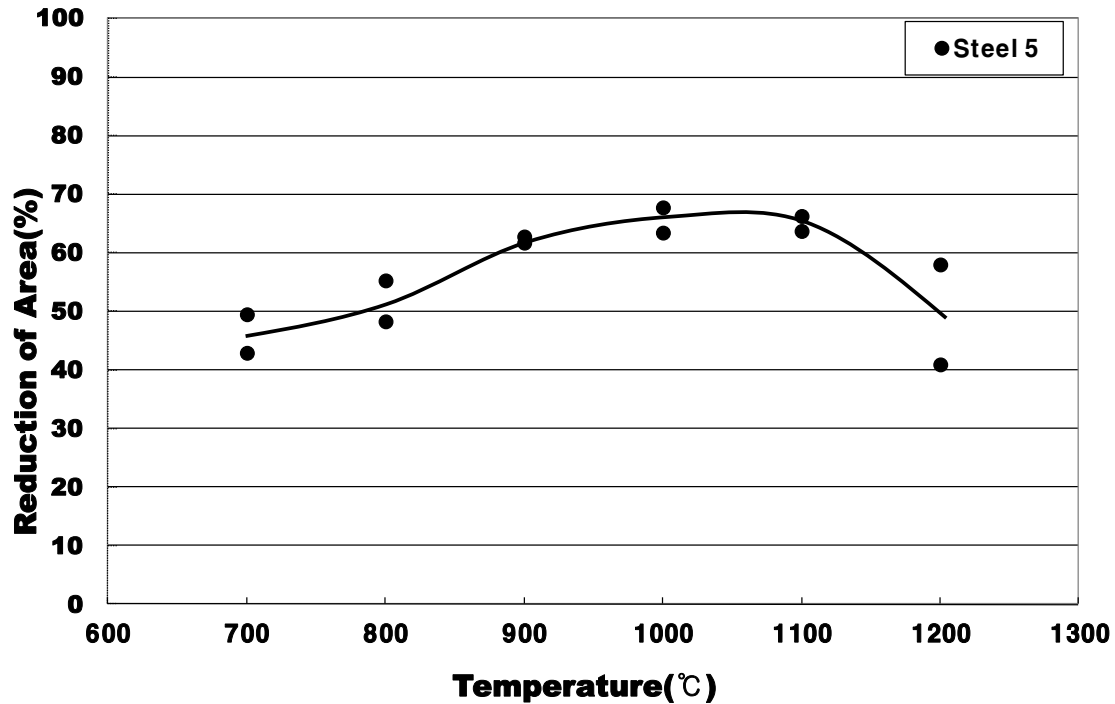
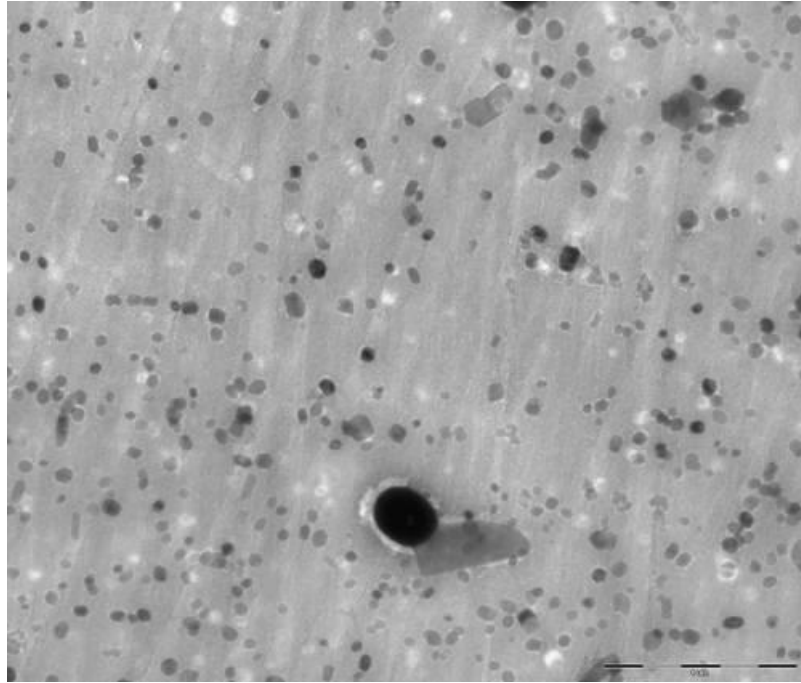
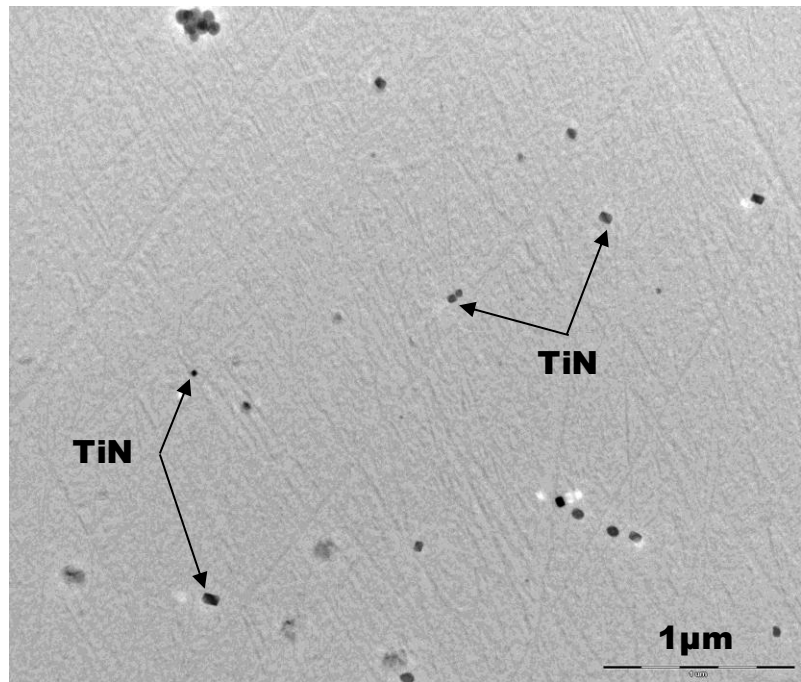


Fig. 9.7 Hot ductility curve for high Ti-B containing steel, steel 5, after heating to 1250°C.

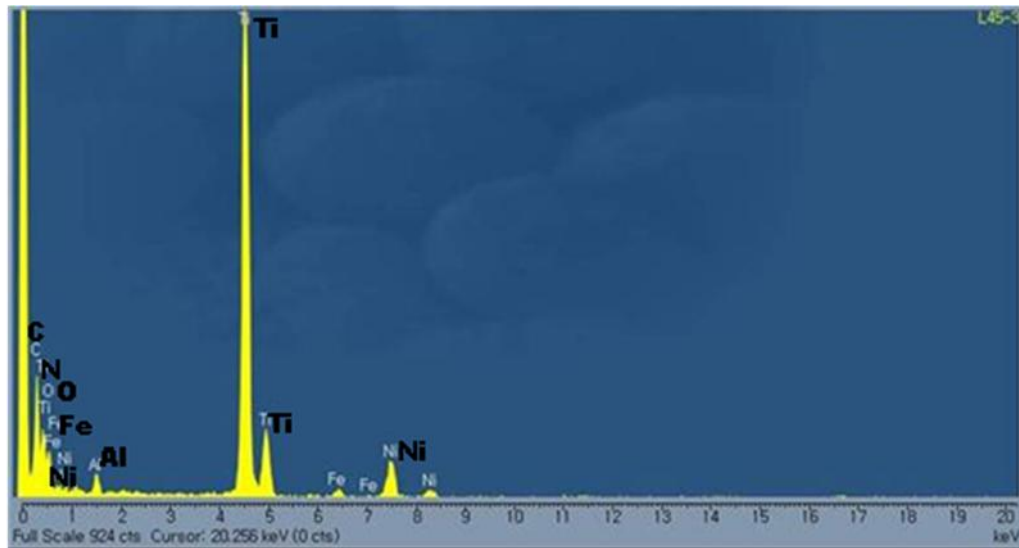
Two generations of TiN precipitation were observed in the  $\sim 0.04\%$  Ti containing TWIP steels (steels 1~3), when heated to 1250°C and cooled to the test temperature. One was cubic in shape  $\sim 200\text{nm}$  in size which precipitated on solidification of the melt and the other a much finer precipitate  $\sim 10\text{nm}$  that came out during cooling from 1250°C and reprecipitated at test temperatures in the range 950~1100°C. In contrast, in the case of the high Ti containing steel (0.1%Ti) very few fine particles were found. The reduction in the number of finer particles is clearly seen in the higher Ti containing steel by comparing the precipitation in a steel with  $\approx 0.04\%$  Ti Fig. 9.8(a), steel 3 with steel 5, Fig.9.8(b), the steel with  $\approx 0.1\%$  Ti.



(a)



(b)



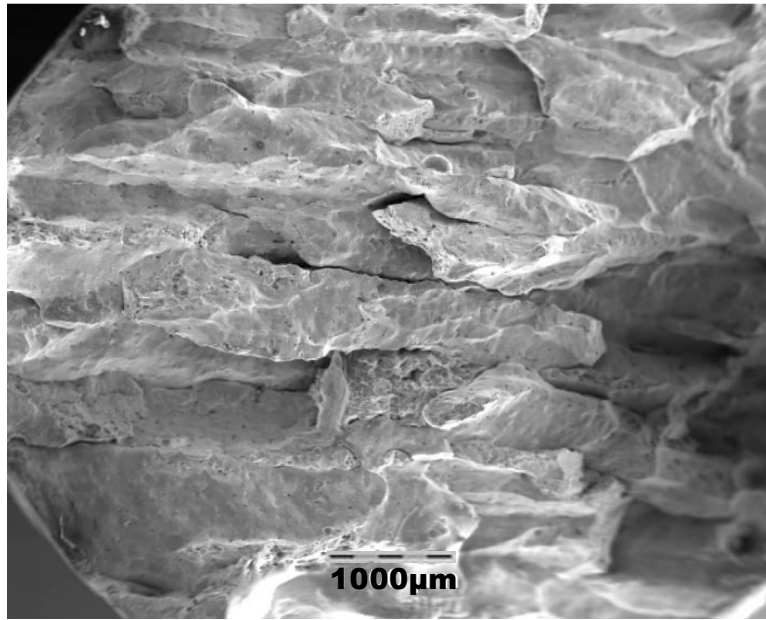
(c)

Fig.9.8 Particle distribution for (a) 0.04%Ti steel 3, heated to 1250°C and cooled to the test temperature of 1050°C and (b) 0.1% Ti, steel 5, tested at 1000°C and (c) typical analysis for the fine particles.

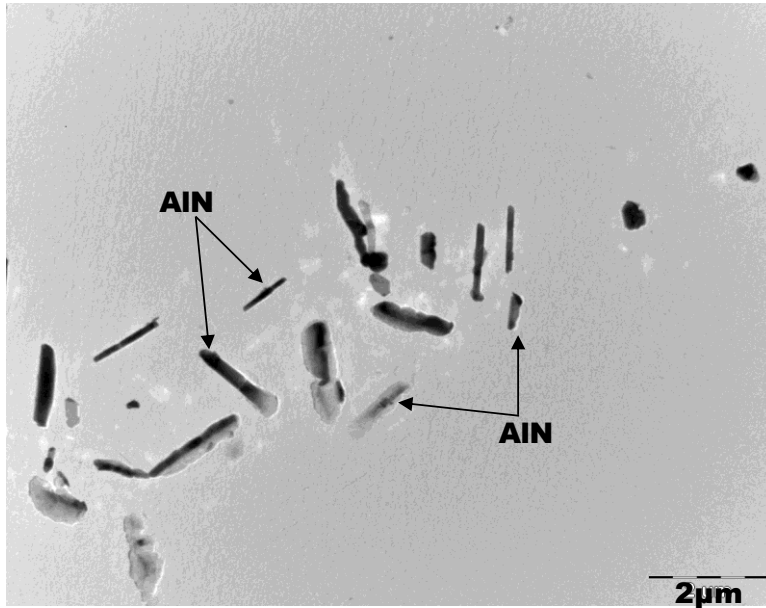
#### 9.4 Discussion

TWIP steels are fully austenitic and as such differences in the hot ductility curves between boron free and boron containing Ti, TWIP steels of otherwise similar composition depend on the precipitates and inclusions that are present as well as segregation of B to the boundaries. Increasing the volume fraction of precipitates/inclusions and reducing their size will result in ductility deteriorating [37]. Their distribution in the grain structure is also important, since precipitation at the grain boundaries is always the most detrimental to ductility [37].

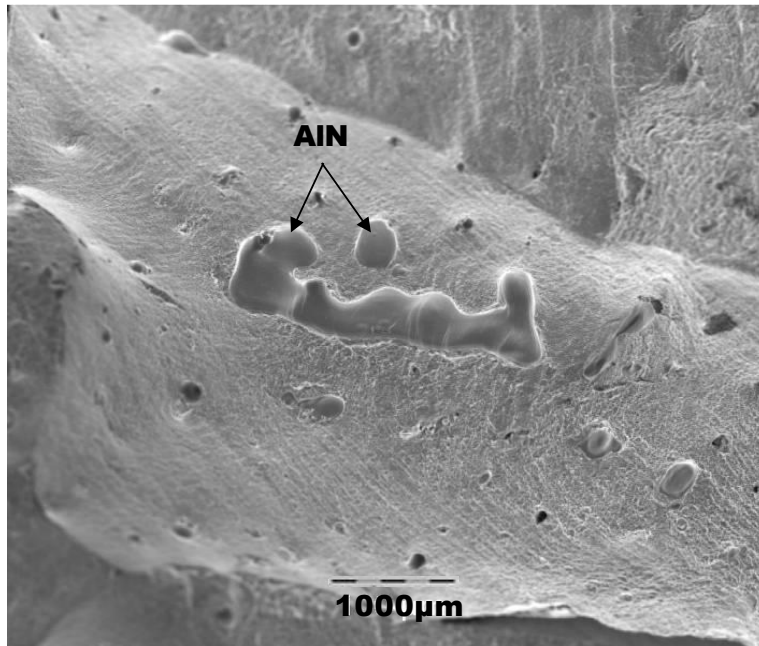
Having both Ti and B and Al additions, means, that there is great competition for the N. Wilson and Gladman [130] point out that when B and Al are present together, although AlN is more stable than BN, because B is such a small atom it can diffuse more rapidly and BN forms rather than AlN. However, when Ti is present, Ti will always combine preferentially with the N and the size and volume fraction of the TiN particles will dictate the ductility. The high Al, TWIP steels that are free of Ti and B, curve steel 1, in Fig.7.2 have been shown to give poor ductility. Rock candy failure are common, Fig.9.9(a) as AlN precipitates at the austenite boundaries as shown in Fig.9.9(b) and as a thin film over the grain surface, Fig.9.9(c) [167].



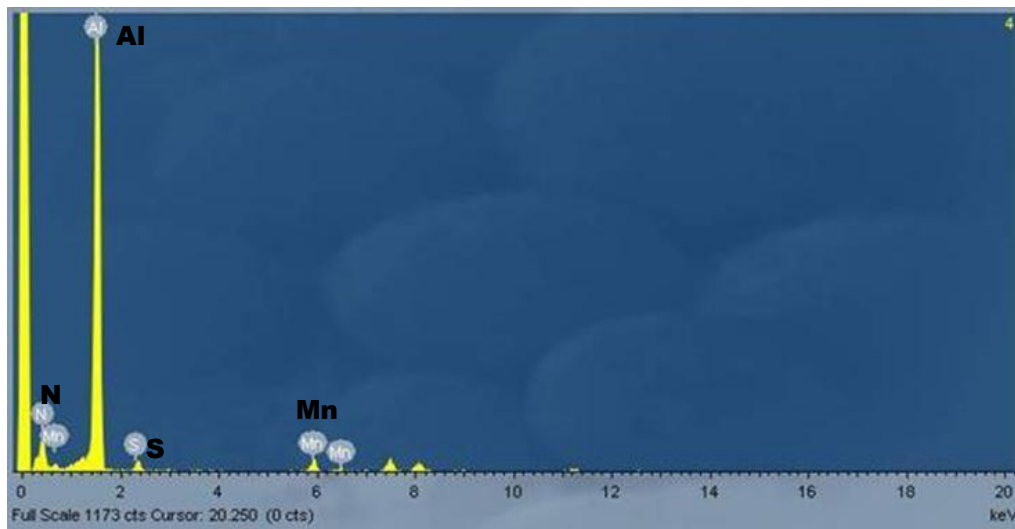
(a)



(b)



(c)



(d)

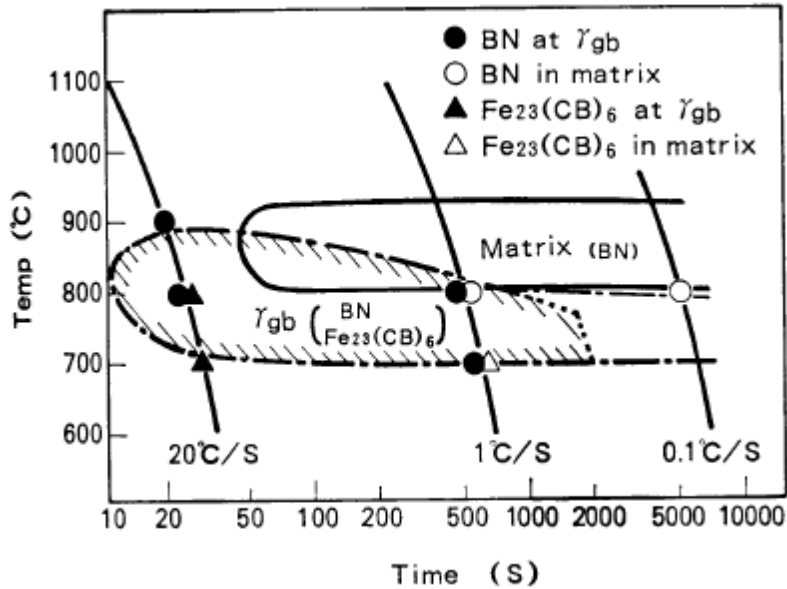
Fig.9.9 AlN films on the grain surface of as-cast high Al TWIP steels having no Ti or B present [167]. (a) Intergranular failure (b) AlN precipitation at the austenite grain boundaries (c) AlN film on fracture surface (d) analysis of particles

It might be expected that Ti would be beneficial to ductility even in a fine form as TiN precipitates more randomly, whereas AlN precipitates preferentially at the austenite grain surfaces. However, fine precipitation of TiN in the matrix when it occurs is very detrimental to ductility [78, 79, 131, 169].

B, being such a small atom can segregate easily to the boundaries and this has been observed in many studies [161, 172~174]. Karlsson et al. [172] have used SIMS analysis recently to detect B segregation to the boundaries in stainless steel. Samples were quenched from a range of temperatures from 900 to 1250°C and cooled at various cooling rates to room temperature. Segregation of B to the boundaries became more intense the higher the quenching temperature indicating that it was non equilibrium. Slower cooling rates also gave more intense segregation.

There are many techniques for studying grain boundary segregation and the SIMS technique is a very good technique for studying B segregation because it has both a high lateral resolution of 1µm and can detect B at very low levels <10ppm in an iron matrix [172]. More importantly it has a wide field of view making it of all the techniques available for examining segregation FIM (field ion microscope), AES (auger electron spectroscopy), PTA (particle tracking autoradiography) etc, one of the easiest to use. The technique has the disadvantage that it is not able to show with certainty whether the B is in a precipitate or an element in solution at the boundaries and the concentration of B in solution is therefore not defined except qualitatively by the intensity.

Examination of all the SIMS photographs, Figs.9.3~9.6 shows evidence of B segregation throughout the temperature range 700~1200°C. There seems to be a tendency for this segregation to be very intense in the temperature range 700~800°C when B will have probably precipitated out as BN or Fe<sub>23</sub>(CB)<sub>6</sub>, at the boundaries as shown by the PTT (precipitation-time-temperature) diagram established by Yamamoto et al, Fig.9.10 [175].



**Time-Temperature-Precipitation curves of BN and  $\text{Fe}_{23}\text{CB}_6$**   
 Fig.9.10 PTT diagrams for BN and  $\text{Fe}_{23}(\text{CB})_6$  [175].

It can be seen from Fig.9.10 that the nose of the PTT diagram for BN and  $\text{Fe}_{23}(\text{CB})_6$  occurs at  $800^\circ\text{C}$  and for the cooling rate of  $60^\circ\text{C}/\text{min}$  used in the present investigation ( $1^\circ\text{C}/\text{S}$  in Fig.9.10, thick solid line) precipitation of BN takes place between  $700\sim 800^\circ\text{C}$  [175]. Thus the intense regions at the boundaries shown in the SIMS photos at  $700\sim 800^\circ\text{C}$ , Figs. 9.3~9.6 corresponds most likely to the precipitation of BN or  $\text{Fe}_{23}(\text{CB})_6$ . The hot ductility curves for the 0.04% Ti-B containing steels, Fig.9.2 all show similar characteristics, ductility being good in the temperature range  $700\sim 900^\circ\text{C}$ , which corresponds to when the B concentration at the boundaries would be a maximum and deteriorating rapidly as the temperature approaches  $1000^\circ\text{C}$  above which there is little further change, Fig.7.2 and Fig.9.2. Although at higher temperatures  $>800^\circ\text{C}$ , the intensity of B segregation is less, Figs.9.3~9.6, B segregation has nevertheless taken place, even at as high a temperature as  $1200^\circ\text{C}$ . The previous chapter has shown that the decrease in ductility that occurs at temperatures  $>900^\circ\text{C}$  is due to some of the TiN going back into solution on re-heating to  $1250^\circ\text{C}$  and re-precipitating out in a fine form, Fig.9.8(a). According to the equilibrium solubility equation of Wada and Pehlke [176] in the case of the 0.04%Ti steels, steels 1~3  $\approx 0.001\%N$  goes back into solution at  $1250^\circ\text{C}$ . In contrast for the 0.1%Ti, steel 5, very little N goes back into solution at  $1250^\circ\text{C}$  ( $0.0003\%N$ ) and in consequence there is good ductility throughout the temperature range 700 to  $1200^\circ\text{C}$ , Fig.9.7 as the Ti rich, fine precipitation,

detrimental to ductility is very much reduced, compare Fig.9.8(a) with Fig.9.8(b). B can now segregate to the boundaries giving an improvement in ductility over the whole temperature range examined.

Previous work on as-cast Ti containing HSLA steels (high strength low alloy steels) [78, 79, 131] has shown, that slowing the cooling rate from 100~25°C/min on cooling from the melt leads to a considerable improvement in ductility due to coarsening of the particles. This has also been shown to occur for a Ti-Nb high Al, TWIP steel in the previous chapter. It seems likely that if the cooling rate after casting in the presently examined steels had been reduced to  $\leq 25^\circ\text{C}/\text{min}$ , ductility would have been better than that found at the present cooling rate of 60°C/min. The slower cooling rate would have resulted in a coarsening of the TiN particles leaving B to exercise its full potential in improving ductility over the whole of the temperature range 700~1100°C.

However, as well as TiN precipitation, being very sensitive to cooling rate, so is B segregation. Zhang et al. [141] have shown that for the ultra-low C steel they examined, cooling from 1050°C resulted in the maximum segregation occurring when the cooling rate was  $\sim 10^\circ\text{C}/\text{min}$  in accord with the work of Yamoto et al. [175] and Chown and Cornish [177]. Hence, slower cooling rates of 10~15°C/min would be recommended to give better ductility [171] as this allows more B to segregate to the boundaries as well as coarsening the TiN precipitates. In testing it is always better to use a more accurate simulation of the continuous casting conditions which includes both the primary and secondary cooling stages of casting, shown in Fig 2.8, as has been shown in some of the more recent work [169], rather than the average cooling rate for the two cooling regimes as in this work. However, it is probable that generally, it is the secondary cooling rate which controls the ductility during casting rather than the primary. This is very convenient as the average secondary cooling rate used commercially is commonly 10~15°C/min, which gives the optimum benefit to ductility from both Ti and B and probably accounts for these steels being free of cracks after the straightening operation.

## Summary

The present work has shown using a cooling rate of 60°C/min that the presence of B in addition to Ti gives better ductility for the temperature range 700~900°C. From previous work on boron containing TWIP steels [141, 175, 177] even better ductility would be expected if the cooling rate was slower, closer to 10°C/min and such a secondary cooling rate may be needed to avoid transverse cracking.

The SIMS examination indicates that B segregates to the boundaries and this is therefore the most likely cause of better ductility; B strengthening the bonding at the boundaries.

However, the role of Ti is also important, because it combines preferentially with the N preventing AlN from precipitating at the boundaries and allowing B to un-impedingly segregate there. Hence, sufficient Ti must be present to combine with all the N. TiN precipitation can in itself be very detrimental to ductility and the cooling rate is again important to ensure that the TiN precipitates are sufficiently coarse to have little influence on cooling after melting. An average cooling rate of 12°C/min has been found to achieve this [78, 79, 131]. It is probable from the commercial experience of not encountering cracking in these steels on continuous casting that a normal secondary cooling rate, which is close to the average cooling rate of 12°C/min, will achieve the same benefits to ductility and avoids transverse cracking. This cooling rate will give the Ti and B additions the necessary conditions to give good ductility and avoid cracking

## 9.5 Conclusions

1. Both 0.04%Ti and 0.002%B are required to ensure good hot ductility in high Al, high N TWIP steels. Sufficient Ti is needed to remove the entire N as TiN so preventing AlN precipitating as films over the austenite grain surfaces. B is also needed as it can segregate to the boundaries and strengthen them.
2. A SIMS technique has successfully shown that B segregates to the boundaries in these Ti containing TWIP steels throughout the temperature range 700~1200°C.
3. Although the present work has used a cooling rate of 60°C/min, it is believed from the commercial experience of casting these steels and the past literature, that a slower cooling rate 10~15°C/min commensurate with the average cooling rate during secondary cooling in continuous casting will give even better ductility. This slower cooling rate will result in the optimum segregation of B as well as coarsening the TiN precipitates so they are no longer effective in reducing the ductility.

## CHAPTER 10: SUMMARY AND CONCLUSIONS

In order to gain a better understanding of the likelihood of cracking in TWIP steel slabs, hot tensile tests were performed. The tensile samples were generally heated to 1250~1300°C and cooled down to test temperatures in the range 1100 to 700°C or on occasions melted in situ with the same processing route so as to simulate the continuous casting process.

1. The influence of high Al levels (1~1.5%Al) on hot ductility in TWIP steels was explored. Ductility is generally <40% RA indicating that with these TWIP steels it will be difficult to avoid transverse cracking. The 1.5%Al containing steels had worse ductility than the low Al (0.02%Al) containing steels because of the presence of large amounts of AlN precipitated at the austenite grain boundaries. Ductility in these TWIP steels is dependent on unrecrystallised austenite and therefore to avoid transverse cracking low N and low S levels are recommended so that the volume fraction of second phase particles (AlN and MnS) is low.
2. The TWIP steels were also required at a higher strength level, ~1000MPa and an Nb addition was the most likely way of this being achieved. Because Nb steels are noted for giving poor ductility in HSLA steels V, which from previous work had been found beneficial to the ductility by slowing down the rate of Nb precipitation was added. The hot ductility of the Nb/V containing TWIP steels was therefore examined and expected ductility was worse than the simpler microalloying free TWIP steels but better than in V free, Nb containing steel. A lower N level (0.007%N) was also chosen to see whether this might make the difference by reducing the amount of precipitation. Increasing the cooling rate from 60 to 180°C/min after melting caused the ductility to further deteriorate but the deterioration was dependent on the N level, although the higher N levels produced only a very small reduction in the ductility, probably because ductility is so poor.
3. Because of the likely importance of second phase particles the influence of S level on the hot ductility of these TWIP steels was examined. The hot ductility of three steels having S contents of 0.003, 0.01 and 0.023% were investigated. Reducing the S level to 0.003% improved ductility with RA values being 50~55% in the temperature range 950~1100°C but higher S levels of 0.010 and 0.023% give similar hot ductility curves to each other giving poor ductility achieving only RA values of 20%. The poor ductility in the higher S steels is more a consequence of the change from coarse hexagonal plates of AlN, which are mainly within the matrix and so

have little influence on the hot ductility, to very long dendritic rod precipitates, which are situated at the dendritic or close to the austenite grain boundaries. This dendritic precipitation was rarely observed in the low S steel.

The MnS inclusions appear to act as nucleation sites for the precipitation of AlN. Below a certain volume fraction of sulphides, the AlN precipitation is very much reduced so that only hexagonal AlN plates are formed which are not situated at the austenite grain boundaries.

4. Clearly when high free N levels are present in these non-microalloyed steels, ductility is poor and transverse cracking will be a problem. Adding Ti to remove the N was therefore explored. Furthermore because of the success of adding B in improving the hot ductility in HSLA steels when the entire N was removed, additions of the two elements in combination were also examined.

An investigation was carried out into establishing the hot ductility of a Nb containing high Al, TWIP steel with compared to a Nb-B-Ti high Al, TWIP steel. To make the conditions more relevant to the continuous casting process the Nb-B-Ti TWIP steel was cast and cooled at two different cooling rates from the melting point, 60 and 12°C/min.

The ductility of Nb containing high Al, TWIP steels was found to be very poor in the as-cast condition. Adding B and Ti still gave rise to extremely poor ductility when a cooling rate of 60°C/min was used. However reducing the cooling rate to 12°C/min caused the ductility to improve to 40% RA in the temperature range 800~1050°C, the RA value required to avoid transverse cracking. It is recommended that to avoid transverse cracking, the secondary cooling rate during continuous casting should not be higher than  $\approx 12^\circ\text{C}/\text{min}$  in these Nb containing high Al, TWIP steels.

5. Refining the grain size from 325 $\mu\text{m}$  to 150 $\mu\text{m}$  produced good ductility (as-cast to wrought grain size by rolling before straightening) but this is not possible commercially.
6. In the commercial operation there are two cooling regimes. The first has a very high cooling rate (primary cooling) and the second is much slower (secondary cooling). This secondary cooling rate is often in the range 8~15°C/min. The close agreement between the commercial results and the laboratory hot ductile tests at 12°C/min in predicting the onset of cracking suggests that it is probably the slower secondary cooling process that is the most important in controlling ductility as this allows time for segregation and the growth of precipitates to occur. In the past, the cooling rate used has been taken as the average of the cooling rates for the faster primary and slower secondary cooling rate. The latter has been taken as 60°C/min the cooling rate experienced just below the broad face

of the strand for 220mm thick strand. However, the present work suggests that a cooling rate closer to 10~15°C/min should be used as this corresponds more closely to the secondary cooling rate used during the continuous casting operation. This of course makes comparison with past work in the literature difficult since most of this work has used a cooling rate of 60°C/min or higher.

7. An investigation was carried out using SIMS to establish whether B could be detected at the grain boundaries and the presence of B segregation was established for all the B containing steels throughout the temperature range 600~1200°C.
8. Hence in practice, both 0.04%Ti and 0.002%B are required to ensure good hot ductility in high Al, TWIP steels having 0.009%N. Sufficient Ti is needed to remove all the N as TiN so preventing AlN precipitating as films over the austenite grain surfaces and B is also needed as it can segregate to the boundaries and strengthen them.
9. Following all these recommendations, i.e. a low S level, slow secondary cooling rate, a Ti level above the stoichiometric for TiN and a boron addition of 0.002%, transverse cracking was avoided in these very difficult to cast high strength TWIP steels.

## **FUTURE WORK**

The following suggestions are made for future work.

1. More hot ductility testing on these TWIP steels are required at the slower cooling rate of 12°C/min, in the “as-cast” state, this being more in keeping with the commercial continuous casting operation. Ideally, both having a primary and secondary cooling regime should be used.
2. P has also been shown to cause cracking problems in high C steels when P segregates to the grain boundaries forming a low melting point iron phosphide eutectic. The influence of P on the hot ductility of these TWIP steels needs investigating,
3. Of most importance in the present work is the need to find out whether high N contents resulting from casting using an electric arc furnace can be used with these Ti, B steels as long as there is sufficient Ti to combine with the entire N. To date only relatively low N levels (0.007%) has been examined whereas commercially N contents are typically 0.01% for steel produced via the electric arc route.

## REFERENCES

1. Y. G. Kim, T. W. Kim and S. B. Hong: "High Strength Formable Automotive Structure Steel", Proceedings of ISATA, Aachen, Germany, Sep., 1993, p269.
2. T. W. Kim, S. H. Park and Y. G. Kim: *Materia Japan*, 36, 1997, p502~504.
3. G. Frommeyer, U. Brux and P. Neumann: "Supra-Ductile and High-Strength Manganese-TRIP/TWIP Steels for High Energy Absorption Purposes", *ISIJ International*, 43, 2003, p438~446
4. C. Scott, N. Guelton, S. Allain, M. Faral: "The Development of a New Fe-Mn-C Austenitic Steel for Automotive Applications", *Development in Sheet Products for Automotive Application*, Organized by James R. Fekete and Roger Pradham, *La Revue de metallurgie-CIT*, Vol.103, Issue 6, June 2006, p293
5. G. G. Chin, S. J. Kim, I. R. Shon: "Development of High Strength TWIP Steels", *Trends in Metals & Materials Engineering*, 2006, No.4, p12.
6. K. Brimacombe and K. Sorimachi: "Crack Formation in the Continuous Casting of Steel", *Metallurgical Transactions*, 1977, 8B, p489~505.
7. ISIJ: "History of Continuous Casting Technology in Japan", ISIJ, Tokyo, Japan, 1996
8. N. A. McPherson and A. McLean: "Transverse Cracking in Continuously Cast Products", *Continuous Casting*, Volume 8, The Iron and Steel Society, 1997.
9. M. M. Wolf: "Initial Solidification and Strand Surface Quality of Peritectic Steels", *Continuous Casting*, Volume 9, The Iron and Steel Society, 1997.
10. Schmidt, L., Josefsson, A.: *Scandinavian Journal of Metallurgy*, Vol. 3, 1974, p193.
11. M. Hater, R. Klages, B. Redenz and K. Taffner: "Results From a Curved Mould Continuous Casting Machine Making Pipe and Plate Steel", *Open Hearth Proceedings*, AIME, 1973, p 202~217.

12. S. Harada, S. Tanaka, H. Misumi, S. Mizoguchi and H. Horiguchi: "A Formation Mechanism of Transverse Cracks on CC Slab Surface," ISIJ International, 30, 1990, p 310~316.
13. N. A. McPherson and R.E. Mercer: "Continuous Casting of Slabs at BSC Ravenscraig Works", Ironmaking and Steelmaking, 1980, 167~179.
14. B. Mintz and J. M. Arrowsmith: "Hot-ductility behaviour of C-Mn-Nb-Al Steels and its relationship to crack Propagation During the straightening of Continuously Cast Strand", Materials Technology, 1979, 6, p24~32.
15. T. H. Coleman and J. R. Wilcox: "Transverse Cracking in Continuously Cast HSLA Slabs Influence of Composition", Materials Science and Technology, Vol.1, 1985, p80~83.
16. B. Patrick and V. Ludlow: "Development of Casting Practices to Minimise Transverse Cracking in Microalloyed Steels" Rev. Metall. 1994, 91 p1081~1089.
17. W. T. Lankford: "Some considerations of Strength and Ductility in the Continuous Casting Process", Metallurgical Transactions, 1972, p1331~1357.
18. H. Zhang et al.: "Effect of Niobium on Continuous Casting Solidification Structures of HSLA Steels" in "HSLA Steels Metallurgy and Applications", Beijing 1985, p445~453.
19. Y. Maehara, K. Yasumoto, H. Tomono, T. Nagamichi and Y. Omomri: "Surface Cracking Mechanism of Continuously Cast Low Carbon Low Alloy Steel Slabs" Materials Science and Technology, 1990, 6, p793~806.
20. B. Mintz, S. Yue and J.J. Jonas: "Hot Ductility of Steels and its Relationship to the Problem of Transverse Cracking During continuous Casting", International Materials Reviews, 1991, Vol.36, No.5, p187~217.
21. B. Mintz: "The Influence of Composition on the Hot Ductility of Steels and to the Problem of Transverse Cracking", ISIJ International, 1999, 39, p833~855.
22. H. G. Suzuki et al.: "Embrittlement of Steels Occurring in the Temperature Range from 1000 to 600°C", Transactions ISIJ, 1984, 24, p169~177.

23. C. Ouchi and K. Matsumoto: "Hot Ductility in Nb-bearing High Strength Low-alloy Steels", Transactions ISIJ, 1982, Vol.22, p181~189.
24. B. G. Thomas, J. K. Brimacombe and I. V. Samarasekera: "The Formation of Panel Cracks in Steel Ingots: A State-of-the-Art Review," *ISS Trans.*, 7, 1986, p7~20.
25. M. Suzuki, H. Hayashi, H. Sshibata, T. Emi, I.J.Lee: "Simulation of Transverse Crack Formation on Continuously Cast Peritectic Medium Carbon Steel Slabs", Steel Research, 1999, 70, p412~419.
26. M. Teshima, T.Kitagawa, S. Miyahara, H. Funanokaea, K.Ozawa and K. Okimoto: "The Secondary Cooling Technology of Continuous Casting for Production of High Temperature and High Quality Slab", *Tetsu to Hagane*, Vol. 74, 1988, p1282~1289.
27. Y. Maehara, H. Tomono and Y. Ohmori: "Stress Relaxation During Hot Deformation of Austenite", Transactions ISIJ, 1987, 27, p499~505.
28. I. G. Davies, K. Thomas, J. Goringe and K. A. Broome: "Continuous Casting at British Steel Stocksbridge Works", Ironmaking and Steelmaking, Vol.13, 1986, p40~45.
29. K. C. Mills, T. H. Billany, A. S. Normanton, B. Walker and P. Grieveson: "Causes of Sticker breakout during Continuous Casting", Ironmaking and Steelmaking, Vol.18, 1991, p253~265.
30. M. Hashino, M. Tokuda and T. Watanabe: "Melting Behavior of Mould Powders for Continuous Casting", *Tetsu to Hagane*, Vol. 68, 1982, p152.
31. W. R. Irving and A. Perkins and R.Gray: "Effect of Steel Chemistry and Operation Parameters on Surface Defects in Continuously Cast Slabs", Ironmaking and Steelmaking, Vol.11, 1984, p146~151.
32. E. Takeuchi and J. K. Brimacombe: "Effect of Oscillation Mark Formation on the Surface Quality of Continuously Cast Steel Slabs", Metallurgical Transactions B, Vol.16B, 1985, p605~625.
33. Offerman, C, Dacker, C. A., Enstrom, C.: Scandinavian Journal of Metallurgy, Vol. 10, 1981,35, p115.

34. Birat, J. P., Larrecq, M., Le Bon, A., Jeanneau, M., Poupon, M., Senaneuch, D.: Steel Making Procs., Vol 64, 1981, p53.
35. Schmidt, L., Josefsson, A.: Scandinavian Journal of Metallurgy, Vol. 3, 1974, p193.
36. Mintz. B., Stewart. J. M., Crowther. D. N.: "Influence of Micro-alloying Additions on the Hot Ductility of Steels Heated Directly to the Test Temperature", Transactions ISIJ, Vol. 27, 1987, p366.
37. B. Mintz and D. N. Crowther:"Hot Ductility of Steels and Its Relationship to the Problem of Transverse Cracking in Continuous Casting", International Materials Reviews, 2010, Vol.55, No.3, p168~196.
38. B. Mintz: " Importance of  $A_{r3}$  Temperature in Controlling Ductility and Width of Hot Ductility Trough in Steels, and its Relationship to Transverse Cracking", Materials Science and Technology, February, 1996, Vol.12, p132~138.
39. Shi Shu XIE, Joo Dong LEE, U-Sok YOON and Chang Hee YIM:" Compression Test to Reveal Surface Crack Sensitivity between 700 and 1100°C of Nb-bearing and High Ni Continuous Casting Slabs", ISIJ International, Vol.42, 2002, No.7, p708~716.
40. L. E. Cepeda, J. M. Rodrigu ez-Ibabe, J. J. Uccola, M.vFuentes: "Influence of dynamic recrystallisation on hot ductility of aluminium killed mild steel", Materials Science and Technology, 1989, Vol.5, p1191~1199..
41. K. M. Bank, A.Tuling, and B. Mintz: "The Influence of Thermal History on Hot Ductility of Steel and its Relationship to the Problem of Cracking in Continuous Casting", Materials Science and Technology, 2012, Vo.28, No.5, P536~542.
42. J. R. Wilcox and R. W. K. Honeycombe:"Hot Ductility of Nb and Al Microalloyed Steels Following High Temperature Solution Treatment", Materials Science and Technology, 1984, 11, p217~225.
43. J. R. Wilcox, R. W. K. Honeycombe: "Effect of precipitation on Hot Ductility of Niobium and Aluminium Microalloyed Steels", Materials Science and Technology, Vol.3, No.10, 1987, p849~854.
44. A. Cowley, R. Abushosha, and B. Mintz: "Influence of  $A_{r3}$  and  $A_{e3}$  Temperature on

- Hot Ductility of Steels”, *Materials Science and Technology*, Vol.14, July, 1998, p1145~1153.
45. B. Mintz, R. Abushosha and A. Cowley: “Preliminary Analysis of Hot Ductility Curve in Simple C-Mn Steels”, *Materials Science and Technology*, Vol.14, March, 1998, p222~226.
46. B. Mintz, J. R. Wilcox and D. N. Crowther: "Hot Ductility of Directly cast Steels" *Materials Science and Technology*, 1986, Vol.2, p589~594.
47. Evans, H. E.: *Creep Fracture*, Pergmon Press., 1984.
48. H. C. Chang and N. J. Grant: “Mechanism of inter crystalline fracture”, *Trans. AIME*, 1956, 206, p44.
49. Gandhi: in ‘Flow and fracture at elevated temperature’, 83, 1983, *Materials Science Seminar*, American Society for Metals.
50. P. J. Wray: *Materials Technology*, 1981, 8, p466.
51. D.N. Crowther and B. Mintz: “Influence of Carbon on Hot Ductility of Steels”, *Materials Science and Technology*, Vol.2, July, 1986, p671~676.
52. H. J. McQueen and J. J. Jonas: in ‘Recovery and recrystallization during high temperature deformation in plastic deformation of metals’, New York, Academic Press., 1975, Vol.6, p393~493.
53. B. Mintz and J. J. Jonas: “Influence of strain rate on production of deformation induced ferrite and hot ductility of steels”, *Materials Science and Technology*, 1994, 10, p721~727.
54. B. Mintz, J. Lewis and J. J. Jonas: ”Importance of Deformation Induced Ferrite and Factors which Control its Formation”, *Materials Science and Technology*, Vol.13, March, 1997, p379~388.
55. J. Lewis, J. J. Jonas and B. Mintz:” The Formation of Deformation induced Ferrite during Mechanical Testing”, *ISIJ International* Vol.38, 1998, No.3, p300~309.

56. D. N. Crowther and B. Mintz: "Influence of Grain Size and Precipitation on Hot Ductility of Microalloyed Steels", *Materials Science and Technology*, 1986, 2, p1099~1105.
57. M. J. Luton and C. M. Sellars: *Acta metallurgica*, 1969, 17, p1033.
58. D. N. Crowther, Z. Mohamed and B. Mintz: "Influence of Micro-alloying Additions on the Hot Ductility of Steels Heated Directly to the Test Temperature", *Transactions ISIJ*, Vol.27, 1987, p366~375.
59. D. N. Crowther, Z. Mohamed and B. Mintz: "The Relative Influence of Dynamic and Static Precipitation on the Hot Ductility of Microalloyed Steels", *Metallurgical Transactions A*, Vol.18A, November, 1987, p1929~1939.
60. Yasumoto, K., Maehara, Y., Ura, S., Ohmori, Y.: "Effects of sulphur on hot ductility of low-carbon steel austenite", *Materials Science and Technology*, 1985, 2, p111.
61. H. Suzuki, S. Nishimura and S. Yamaguchi: "Characteristic of Hot ductility in steels subjected to the melting and solidification", *Transactions ISIJ*, Vol.22, 1982, p48~56.
62. Gittins, A., Tegart, W. J. McG.: *Metals Forum*, 1981, Vol. 4, P 57.
63. D. N. Crowther and B. Mintz: "Influence of Grain Size on Hot Ductility of Plain C-Mn Steels", *Materials Science and Technology*, Vol.2, September, 1986, p951~955.
64. V. Kutuma Rao, D. M. R. Taplin and P. R. Rao: *Metallurgical Transactions A*, Vol. 6A, 1975, p 77~86.
65. C. M. Sellars: *Hot Working and Forming Processes*, (ed. C.M. Sellars and G. J. Davis), 3, 1980, London, The Metal Society.
66. Y. Maehara, K. Yasumoto, Y. Sugitani and K. Gunji, "Effect of Carbon on Hot Ductility of As cast Low Alloy Steels", *Transactions ISIJ*, Vol.25, 1985, p1045~1052.
67. P. J. WRAY: *Metallurgical Transactions A*, Vol. 15A, 1984, p2059.
68. E. T. Turkdogan: "Causes and Effects of Nitride and Carbide precipitation in HSLA Steels in Relation to Continuous Casting", *Steelmaking Conference Proceedings*, Vol.70,

1987, p399~416.

69. Y. Maehara and Y. Ohmori: "The Precipitation of AlN and NbC and the Hot Ductility of Low Carbon Steels", *Materials Science and Engineering*, 62, 1984, p109~119.
70. X. P. Li, J. K. Park, J. Choi and C. H. Yim: "The Effects of Ferritic Transformation on Hot Ductility of Medium Carbon Steel", *Metals and Materials*, Vol.5, No.5, 1999, p25~32.
71. G. I. S. L. Cardoso, B. Mintz and S. Yue: "Hot Ductility of Aluminium and Titanium Containing Steels with and without Cycle Temperature Oscillation", *Ironmaking and Steelmaking*, 1995, Vol.22, No.5, p365~377.
72. E. T. Turkdogan, S. Ignatowicz and J. Pearson: *J. Iron Steel Inst.*, 1955, 180, p349~354.
73. B. Mintz: "Understanding the Low Temperature End of the Hot Ductility Trough in Steels", *Materials Science and Technology*, January, 2008 Vol.24, p112~120.
74. A. Cowley, and B. Mintz: "Relative Importance of Transformation Temperature and Sulphur Content on Hot Ductility of Steels", *Materials Science and Technology*, Vol.20, November, 2004, p1431~1439.
75. R. Abushosha, S. Ayyad and B. Mintz: "Influence of cooling rate and MnS inclusion on hot ductility of steels", *Materials Science and Technology*, Vol.14, March, 1998, p227~235.
76. B. Mintz, R. Abushosha, S. Y. Ayyad and G. I. S. L. Cardoso: HSLA '95. *Proceeding of the Conference on HSLA steels*, China Science and Technology Press, Beijing, China, October, 1995, p342-345.
77. R. Abushosha, S. Ayyad and B. Mintz: "Influence of Cooling Rate on Hot Ductility of C-Mn-Al and C-Mn-Nb-Al Steels", *Materials Science and Technology*, Vol.14, March, 1998, p346~351.
78. R. Abushosha, O. Comineli and B. Mintz: "Influence of Ti on Hot Ductility of C-Mn-Al Steels", *Materials Science and Technology*, Vol.15, March, 1999, p278~286.
79. R. Abushosha, R. Vipond and B. Mintz: Influence of titanium on hot ductility of as cast

- steels”, *Materials Science and Technology*, vol.7, 1991, p613~621.
80. B.Mintz, J.M. Stewart and D.N.Crowther: “ The Influence of Cyclic Temperature Oscillation on Precipitation and Hot Ductility of a C-Mn-Nb-Al Steel, *Transactions ISIJ*, Vol.27, 1987, p 959-964.
81. K.Suzuki, S.Miyagawa, Y.Saito and K.Shiotani: “Effect of Nitride Forming Elements on Precipitation of Carbonitride and High Temperature Ductility of Continuously Cast Low Carbon Nb Containing Steel Slab“, *ISIJ International* Vol.35, 1995, No.1, p34~41.
82. A.M. El-Wazri, F. Hassani, S. Yue, E. Es-Sadiql, L. E. Collins and K. Iqbal: ” The Effect of Thermal History on the Hot Ductility of Microalloyed Steels”, *ISIJ International* Vol.39, 1999, No.3, p253~262.
83. T. Saeki, S. Oguchi, S. Mizoguchi, T. Yananoto, H. Matsui and A. Tsuneoka: *Tetsu-to-Hagane*, 1982, 68, p1773.
84. T. Matsumiya, T. Saeki, J. Tanaka and T. Ariyoshi: *Tetsu-to-Hagane*, 1982, 68, p1782.
85. A. Grill, K. Sorimachi and J. K. Brimacombe: *Metallurgical Transactions.*, 1976, 7B, p177.
86. Y. Sugitani and M. Nakamura: *Tetsu-to-Hagane*, 1979, 65, p1702.
87. M. Wolf and W. Kurtz: *Metallurgical Transactions.*, 1981, 12B, p85.
88. S. N. Singh and K. E. Blazek: *Journal of Metals*, October, 1974, 26, p17.
89. K. Yasumoto, T. Nagamichi, Y. Maehara and K.Gunji, “Effect of Alloying Elements and Cooling Rate on Austenite Grain Growth in Solidification and the Subsequent Cooling Processes of Low Alloy Steels”, *Tetsu to Hagane*, Vol.73, 1987, No.14, p1738~1744.
90. N. E. Hannerz: “Critical Hot Plasticity and Transverse Cracking in Continuous Slab Casting with Particular Reference to Composition”, *Transactions ISIJ*, Vol.25, 1985, p149~158.
91. W. Jaeger, C. Klinkenbug and H. Pircher: *Proceeding of Thermec 2000*, International

conference on 'processing and manufacture of advanced materials' Las Vegas, USA, December 2000, Section A1, Vol.117/3.

92. B. Mintz, A. Tuling and A. Delgado, "Influence of Silicon, Aluminium, Phosphorus and Boron on Hot Ductility of Transformation Induced Plasticity Assisted Steels", *Materials Science and Technology*, Vol.19, December, 2003, p1721~1726.
93. K. W. Andrews: *Journal of Iron steel Institute*, 1965, 203, p721~727.
94. B. Sundman, B. Jansson and J. O. Anderson: *Calphad*, 1985, 9, 3.
95. H. Kobayashi: "Hot-ductility Recovery by Manganese Sulphide Precipitation in Low Manganese Mild Steel", *ISIJ International* Vol.31, 1991, No.3, p268~277.
96. Y. Ohmori and Y. Maehara, "High temperature ductility of AISI 310 austenitic stainless steels", *Materials Science and Technology*, Vol.2, June 1986, p595~602.
97. A. Nagasaki, A. Aizawa, J. Kihara: "Influence of Manganese and Sulfur on Hot Ductility of Carbon Steels at High Strain Rate", *Trans. ISIJ*, Vol. 27, 1987, No. 6, p506~512.
98. T. Kizu and T. Urabe: "Hot Ductility of Sulfur-containing Low Manganese Mild Steels at High Strain Rate", *ISIJ International* Vol.49, 2009, No.9, p1424~1431.
99. B. Mintz, Z. Mohamed and R. Abu-shosha: "Influence of Calcium on Hot Ductility of Steels", *Materials Science and Technology*, Vol.5, July, 1989, p682~688.
100. R. Abushosha, R. Vipond and B. Mintz: "Influence of Sulphur and Niobium on Hot Ductility of As Cast Steels", *Materials Science and Technology*, 1991, 7, p1101~1107.
101. B. Mintz and Z. Mohamed "Influence of manganese and sulphur on hot ductility of steels heated directly to temperature", *Materials Science and Technology*, 1989, Vo.5, December, P1212~1219.
102. S. H. Wang, Z. Y. Liu, W. N. Zhang, G. D. Wang, J. L. Liu and G. F. Liang: "Microstructure and Mechanical Property of Strip in Fe-23Mn-3Si-3Al TWIP Steel by Twin Roll Casting", *ISIJ International*, 2009, Vol. 49, No. 9, p1340~1346.

103. Liao Hongjun, Mao Zhengdong, Wang Lintao, Zhu Jun, Li Yuan and Zhan heng: Study on the surface cracking in hot rolled plates of Fe-23Mn-2Al-V austenitic steel”, Baosteel Technical Research, Vol.5, No1, Mar 2011, p60~64.
104. Wolfgang Bleck, Kriangyut Phiu-on, Christoph Heering and Gerhard Hirt:”Hot Workability of as-Cast High Manganese-High Carbon Steels”, steel research int. Vol.78, 2007, No.7, p536~545.
105. Hamada, AS, Karjalainen, LP: “Hot ductility behaviour of high-Mn TWIP steels” Materials Science and Engineering A, Vol. 528, No. 3, Jan 2011, p1819~1827.
106. Hamada, AS, Karjalainen, LP and M.C.Somani: “The influence of aluminum on hot deformation behavior and tensile properties of high-Mn TWIP steels”, Materials Science and Engineering A, Vol. 467, 2007, p114~124.
107. B. Mintz and R. Abushosha, “Effectiveness of hot tensile test in simulating straightening in continuous casting”, Materials Science and Technology, 1992, 2, p171~177
108. H. G. Suzuki, S. Nishimura and Y. Nakamura: "Improvement of Hot Ductility of Continuously Cast Carbon Steels”, Trans ISIJ, 1984, 24, p54~59.
109. T. A. Bloom, D. R. Fosnacht and D. M. Haezebrouk; “ The Influence of Phosphorous on the Properties of Sheet Steel Products and Methods Used to Control Steel Phosphours Level in Steel Product Manufacturing –Part 1” I & SM, 1990, September, p35~41.
110. M. M. Wolf: “Effects of tramp elements in continuous casting” , Ironmaking and Steelmaking, 1985, Vol.12, No.6, p299~301.
111. J.S.Rege, M.Hua, C.I.Garcia and A.J.Deardo: “The Segregation Behavior of Phosphorus in Ti and Ti+Nb Stabilized Interstitial-Free Steels”, ISIJ International Vol.40, 2000, No.2, p191~199.
112. B. Mintz and R. Abushosha: "Influence of Vanadium on Hot Ductility of Steel" Ironmaking and Steelmaking, 1993, 20, p445~452.
113. B. Mintz, A. Cowley, C. Talian, D. N. Crowther and R.Abushosha: “Influence of P on Hot Ductility of High C, Al, and Nb Containing Steels”, Materials Science and

- Technology, Vol.19, February, 2003, p184~188.
114. G. A. Osinkolu, M. Tacikowski and A. Kobylanski, "Combined Effect of AlN and Sulphur on Hot Ductility of High Purity Iron-base Alloys", *Materials Science and Technology*, Vol.1, July, 1985, p520~525.
115. R. Kiessling: "Non-metallic inclusions in steel", part II, 1966, London, The Iron and Steel Institute.
116. F. Vopodivec, M. Torkar, M. Jakupovic: "Intergranular precipitation of sulphide during cooling of steel from solidification", *Materials Science and Technology*, 1987, Vol.3, p372~377.
117. Y. Maehara and T. Nagamichi: "Effect of Sulphur on hot ductility of niobium containing low carbon steels during low strain rate deformation" *Materials Science and Technology*, Vol.7, 1991, p915~920.
118. T.Inoue, T.Inazumi, Y.Hosoya: "Effects of carbon and sulfur contents on hot-ductility of medium carbon steels", *Tetsu-to-Hagane*, 2001, Vol.87, No.8, p552~556.
119. B. Mintz, R. Abushosha, O. G. Cominelli and S. Ayyad: *Procs. of the 7<sup>th</sup> Int. Symposium on Physical Simulations*, Jan., 1977, Iron Steel Inst. Japan, Eds. H.G.Suzuki, T.Sakai and F.Matsuso, p 449~459.
120. S. Hasebe: *Tetsu-to Hagane*, 1963, Vol.49, No3.p 200.
121. B. Mintz: "Hot Dip Galvanising of Transformation Induced Plasticity and Other Intercritically Annealed Steels", *International Materials Reviews*, 2001, Vol.46, No.4, p169~197.
122. A. Tuling, J. R. Banerjee, and B. Mintz: "Influence of peritectic phase transformation on hot ductility of high aluminium TRIP steels containing Nb", *Materials Science and Technology*, Vol.27, No.11, 2011, p1724~1731.
123. B. Chamont, P. Chemelle and H. Blasusser: *Proc. Conf. on 'Physical simulation techniques for welding, hot forming and continuous casting'*, Ottawa, Canada, 1988, CANMET, MTL, 92-43TR, 11~ 48.

124. H. Su, W. D. Gunawadarna, A. Tuling and B. Mintz: "The Influence of Al and P Additions on the Hot Ductility of Steels" *Materials Science and Technology* 2007, Vo.23,p1357~1366.
125. P. Sricharoenhal, C.Nagasaki and J.Kihara: "Hot Ductility of High Purity Steels Containing Niobium", *ISIJ International*, 1992, Vol. 32, No.10, p1102~1109.
126. J. Y. Fu, C. I. Garcia, S. Pytel and A. J. De Ardo: "Hot Ductility of Continuously Cast Microalloyed Steels" in "Processing Microstructure and Properties of High Strength, Low Alloy Steels", Pittsburgh, 1987, p 27~38.
127. B. Mintz and J. M. Arrowsmith: "Influence of Microalloying Additions on Hot Ductility of Steels", *Sheffield Int. Conf. on Hot Working and Forming Processes*, Ed. by C. M. Sellars and G. J. Davies. Metal Soc., London, 1979, p 99~103.
128. K. Banks, A. Koursaris, F .F. Verdoorn and A. Tuling: "Precipitation and hot ductility of low C-V and low C-V-Nb microalloyed steels during thin slab casting". *Materials Science and Technology*, Vol.17, December 2001, p1596~1604.
129. K. M. Banks, A.Tuling and B.Mintz: "The Influence of V and Ti on the Hot Ductility of Nb Containing of Peritectic C Contents", *Materials Science and Technology*, 2011, Vo.27, No.8. p1309~1314.
130. F. G. Wilson and T. Gladman:"Aluminium Nitride in Steel", *International Materials Reviews*, 1988, Vol.33, No.5, p221~286.
131. O. Comineli, R. Abushosha and B. Mintz: "Influence of Titanium and Nitrogen on Hot Ductility of C-Mn-Nb-Al Steels", *Materials Science and Technology*, Vol.15, September, 1999, p1058~1068.
132. S. K. Kim, J. S. Kim and N. J. Kim: "Effect of B on the hot ductility of Nb containing steel." *Metallurgical and Materials Transactions A*, Vol.33A, 2002, March, p701~704.
133. E. Lopez-Chipres, I. Mejia, C. Maldona, A. Bedolla-Jacuinde, J.M. Cabrera: "Hot ductility behaviour of boron microalloyed steels.", *Materials Science and Engineering A*, Vol.460-461,2007, p464~470.
134. C. Nagasaki and J. Kihara: "Effect of Copper and Tin on Hot Ductility of Ultra-low

- and 0.2% Carbon Steels”, ISIJ International Vol.37, 1997, No.5, p523~530.
135. H. Matsuoka, K. Osawa, M. Ono and M. Ohmura: “Influence of Cu and Sn on Hot Ductility of Steels with Various C Content”, ISIJ International Vol.37, 1997, No.3, p255~262 .
136. S. H. Song, A. M. Guo, D. D. Shen, Z. X. Yuan, J. Liu, T.D. Xu: “Effect of boron on the hot ductility of 2.25Cr1Mo steel “, Materials and Engineering A Vol.360,2003, p 96~100.
137. Nachtrab, W T, Chou, Y T: “The Effect of Tin, Aluminum, and Nitrogen on the Hot Ductility of a Carbon-Manganese Steel Between 700-1200°C”, Metall. Trans. A. Vol. 19A, 1988, No.5, p1305~1309.
138. Faramarz Zarandi and Steve Yue: “The Effect of Boron on Hot Ductility of Nb-microalloyed Steels”, ISIJ International, Vol.46, 2006, No.4, p591~598.
139. M. Lagerquist and R. Lagneborg: “The influence of boron on the creep properties of austenitic stainless steel”, Scandinavian Journal of Metallurgy, 1, 1972, p81~89.
140. H. W. Luo, P. Zhao, Y. Zhang and D. J. Dang: "Effect of boron on hot ductility of low C low alloyed `steel", Materials Science and Technology, Vol.17, 2001, p843~846.
141. Z. L. Zhang, Q. Y. Lin and Z. S. Yu: “Non-equilibrium intergranular segregation in ultra low C steel”, Materials Science and Technology, Vol.16, 2000, p305~308.
142. S. H. Song, T. D. Xu, Z. X. Yuan, Z. S. Yu: ”Equilibrium Grain Boundary Segregation and the Effect of Boron in B-doped Fe-30wt%Ni Austenitic Alloy”, Acta Metall. Mater. 39, 1991, p 909.
143. X. L. He, Y. Y. Chu, J. J. Jonas: “A Method of Determining the Diffusion Coefficient of Vacancy-Solute Atom Complexs During the Segregation to Grain boundaries”, Acta Metall., 37, 1989, p147.
144. M. P. Seah: “Adsorption-induced Interface Decohesion”, Acta Metallurgica, 28 (1980) p955~962.
145. S. H. Song, R. G. Faulkner and P. E. J. Flewitt:”Effect of Boron on Phosphorus-

- induced Temper Embrittlement”, *Journal of Materials Science*, 34 (1999), p5549.
146. K. C. Cho, D. J. Mun, J. Y. Kim, J. K. Park, J. S. Lee and Y. M. Koo: “Effect of Boron Precipitation Behavior on the Hot Ductility of Boron Containing Steel”, *Metallurgical and Materials Transactions A*, Vol.41A, 2010, June, p1421~1428.
147. K. C. Cho, D. J. Mun, M. H. Kang, J. S. Lee, J. K. Park and Y. M. Koo: “Effect of Thermal Cycle and Nitrogen Content on the Hot Ductility of Boron-bearing Steel”, *ISIJ International* Vol.50, 2010, No.10, p839~836.
148. K. C. Cho, D. J. Mun, Y. M. Koo and J. S. Lee: “Effect of niobium and titanium addition on the hot ductility of boron containing steel”, *Materials Science and Engineering A* 528, 2011, p3556~3561.
149. C. Spradbery and B. Mintz: “Influence of undercooling thermal cycle on hot ductility of C-Mn-Al-Ti and C-Mn-Al-Nb-Ti steels”, *Ironmaking & steelmaking* , Vol.32, No.4. 2005, p319~324.
150. H. Luo, L. P. Karjalainen, D. A. Porter, H. M. Liimatainen, Y. Zhang: “ The Influence of Ti on the Hot Ductility of Nb-bearing Steels in Simulated Continuous Casting Process”, *ISIJ International*. Vol. 42, 2002, No.3, p273~282.
151. D. A. Melford: *Residuals Additives and Materials Properties*, Ed, by A. Kelly, D. WP'ashley. E. D. Hondros and C. Lea. The Royal Society. London, 1980, p89~103.
152. G. L. Fisher: *J. Iron Steel Inst.*, 207 (1969), No 7, p1010.
153. M. M. Wolf: *Effects of tramp elements in continuous casting*”, *Ironmaking & Steelmaking*, 12(1985), No. 6, p299.
154. M. M. Wolf : “ Fine Intergranular Surface Cracks in Bloom Casting”, *Trans ISIJ*, 24 (1984), p351~358.
155. P. J. Lewis: “Residual enrichment effects in continuous casting”, *Ironmaking & Steelmaking*, 20(1993), 6, p126.
156. S. L. Wigman and M. D. Millet: *Scaninject VI, International Conference on Refining Processes*, Lulea. Sweden, (1992), p1~17.

157. B. Mintz, R. Abushosha and D. N. Crowther: "Influence of small additions of copper and nickel on hot ductility of steels", *Materials Science and Technology*, 1995, Vol.11, No5, p474.
158. D. A. Melford: *J. Iron Steel Inst.*, 200(1962), No.4, p290.
159. O. Comineli, H. Luo, H-M. Liimatainen and L. P. Karjalainen: "Influence of Cu alloying on hot ductility of C-Mn-Al and Ti-Nb microalloyed steels", *Proceeding IX Conference of Materials Science and Technology*, Madrid, Spain, November, 2003.
160. B. Mintz, O. Comineli and L. P. Karjalainen: "The influence of Ni on the hot ductility of C-Mn-Al, Cu containing steels as a way of preventing hot shortness", *Proceeding 59<sup>th</sup> Annual Conference of ABM*, Sao Paulo, Brazil, 22-24<sup>th</sup> July 2004, *Associacao Brasileira de Metalurgia e Materiais*.
161. T.B.Cameron, J.E.Morrall: in *Boron in steel*, *Proc. Int. Symp. Boron Steels* (Ed. by S.K.Bnerjii and J.E.Morrall), Soc. AIME, New York, 1980, p61~79.
162. B. Mintz: "Understanding the low temperature end of the hot ductility trough in steels", *Materials Science and Technology*, Vol.24, No.1, 2008, p112~120.
163. W. C. Leslie, R. L. Rickett, C. L. Dotson and C. S. Walton: *Trans. ASM.*, 46, 1954, p1470.
164. Y. N. Datur and W. C. Leslie: *Metallurgical and Materials Transactions A*, Vol.12A, 1981, p749~759.
165. G. A. Toledo, O. Campo and E. Lainez: "Influence of Sulfur and Mn/S Ratio on the Hot Ductility of Steels During Continuous Casting", *Steel Research*, 64, 1993, No.6. p293~299.
166. S. E. Kang, A. Tuling, J. R. Banerjee, W. D. Gunawardana and B. Mintz: "The hot ductility of TWIP steels", *Materials Science and Technology*, 2011, 27, No.1, p95~100.
167. S. E. Kang, A. Tuling, I. Lau, J. R. Banerjee and B. Mintz: "The hot ductility of Nb/V containing high Al, TWIP steels", *Materials Science and Technology*, 2011, 27, No.5, p909~915.

168. S. E. Kang, J. R. Banerjee and B. Mintz: "The influence of S and AlN on hot ductility of high Al, TWIP steels", *Materials Science and Technology*, 2012, 28, No, p589~596.
169. K. M. Banks, A. Tuling, C. Klinkenberg and B. Mintz, "The Influence of Ti on the Hot Ductility of Nb Containing HSLA Steels", *Materials Science and Technology*, 2011, Vol.27, No.2, p537~545.
- 170 M. T. Perrot-Simonetta and A. Kobylanski: "Influence of Trace Elements on Hot Ductility of an Ultra High Purity Invar Alloy", *Journal de Physique IV*, 1995, 5, (7), C7-323~334.
171. S. E. Kang, B. Mintz, J. R. Banerjee and E. M. Maina : 'Influence of B and Ti on the hot ductility of high Al and high Al-Nb containing TWIP steels *Materials Science and Technology*, 2013, 29, No.10, p1225~1232.
172. L. Karlsson, H. Norden, and H. Odelius: "Non-equilibrium grain boundary segregation of Boron in austenitic stainless steel-1.Large scale segregation behaviour", *Acta Metall.*, 1988, Vol.36, p1~12.
173. Ph. Maitrepierre, J. Rofes-Vernis and D. Thivellier : Proc. Int. Symp. Boron steels(edited by S.K.Banerjii and J.E.Moral), Metall.Soc. AIME. New York,1980,p1.
174. Y. Ohmori and K. Yamanaki : Proc. Int. Symp. Boron steels(edited by S.K.Banerjii and J.E.Moral), Metall.Soc. AIME. New York,1980,p44.
175. K.Yamamoto, H. G. Suzuki, Y. Oono, N. Noda and T. Inoue, " Formation Mechanism and Prevention Method of Facial Crack of Continuously Cast Steel Slabs Containing Boron", *Tetsu to Hagane*, Vol. 73, 1987, No.1, p115~122.
176. H. Wada and R. D. Pehlke: "Nitrogen solubility and nitride formation in austenitic Fe-Ti alloys ", *Metallurgical and Materials Transactions B*, 1985, 16, p 815~822.
177. L. H. Chown and L. A. Cornish: "Investigation of hot ductility in Al-killed B steels", *Materials Science and Engineering*, 2008, A494, p263~275.
178. M.Tanino:"Precipitation Behaviours of Complex B Compounds in Steels". *Nippon Steel Technical Report No.21*, June 1983, p331~337.

179. I. S. Chung and S. G. Cho: "Effect of cooling rate and strain rate on hot ductility of B steel", Journal of Korean Institute of Metals and Materials, Vol.31, 1993, No.1, p64~72.
180. I. Mejia, A. Bedolla-Jacuinde, C. Maldonado and J. M. Cabrera: "Hot ductility behaviour of a low carbon advanced high strength steel (AHSS) microalloyed with boron", Materials and Engineering A528(2011) , p4468~4474.
181. S. Yue, J. J. Jonas and B. Mintz: 78<sup>th</sup> Steel making and 13<sup>th</sup> Iron making Conf. April 1995, Nashville, "Relationship between hot ductility and cracking during continuous casting of steel", p45~52.
182. Robbins, J. L., Sherby, O. D., Shepard, O. C: J.Iron Steel Inst. Vol.199, 1961, p175.

## APPENDIX A : COMPARISON BETWEEN GLEEBLE TESTING AND INDUCTION TESTING

The composition of the steels that were chosen for examination is given in Table A1 and the hot ductility curves are given in Fig.A1.

Table A1 Composition of steels, wt.%, used for comparing the tensile results from Gleeble with those obtained from Induction heating machine

Steel	C	S	Mn	P	S	Al	Nb	V	N	Remark
A	0.61	0.22	18.2	0.010	0.0048	1.56	0.028	0.113	0.0068	Gleeble
B	0.61	0.21	18.3	0.010	0.0047	1.55	0.029	0.116	0.0065	Induction

The two casts had very similar compositions and therefore would not be expected to lead to any difference in hot ductility behavior. For these two steels A and B, the samples were reheated to 1300°C and tested on a Gleeble machine and Induction heating machine. The samples were initially heated at 150°C/min to 1300°C after which they were held for 3mins. They were then cooled to test temperatures in the range 700~1100°C at a cooling rate of 60 °C/min held for 30secs at temperature and strained to failure using a strain rate of  $3 \times 10^{-3} \text{ s}^{-1}$ . It can be seen that there is quite a significant scatter in the results indicating that the number of samples being tested needs to be increased. Ductility for samples tested using the Gleeble machine for steel A can be seen from Fig.A1 to give generally poor ductility. Below 800°C it averages ~15% RA, whereas above 900°C it averages ~32%. Again the tests carried out on the City University induction equipment fit in reasonably well with those obtained by POSCO using their Gleeble. It should be noted that for both testing modes there will be differences between the surface and centre of the tensile sample. In the case of induction testing, the surface will be hotter than the centre, (~50°C higher), while for the Gleeble it will be the other way round [73]. However, it is clear that ductility improves as the test temperature increases and the major improvement occur for temperatures in excess of 950°C when it would be expected that the Nb and V precipitates would be mainly in solution. The cause of the continued poor ductility < 40% RA even to as high a temperature as 1100°C may well be related to the presence of AlN at the  $\gamma$  grain boundaries in these high Al containing steels restricting dynamic recrystallisation from occurring and reducing the ductility by encouraging crack growth by grain boundary sliding. Although some AlN (high Al peaks are most likely to be AlN) have been observed in the TEM examinations further examination is required to confirm their presence at the higher testing temperatures. Fine films of AlN at the  $\gamma$  grain boundaries are notoriously difficult to extract.

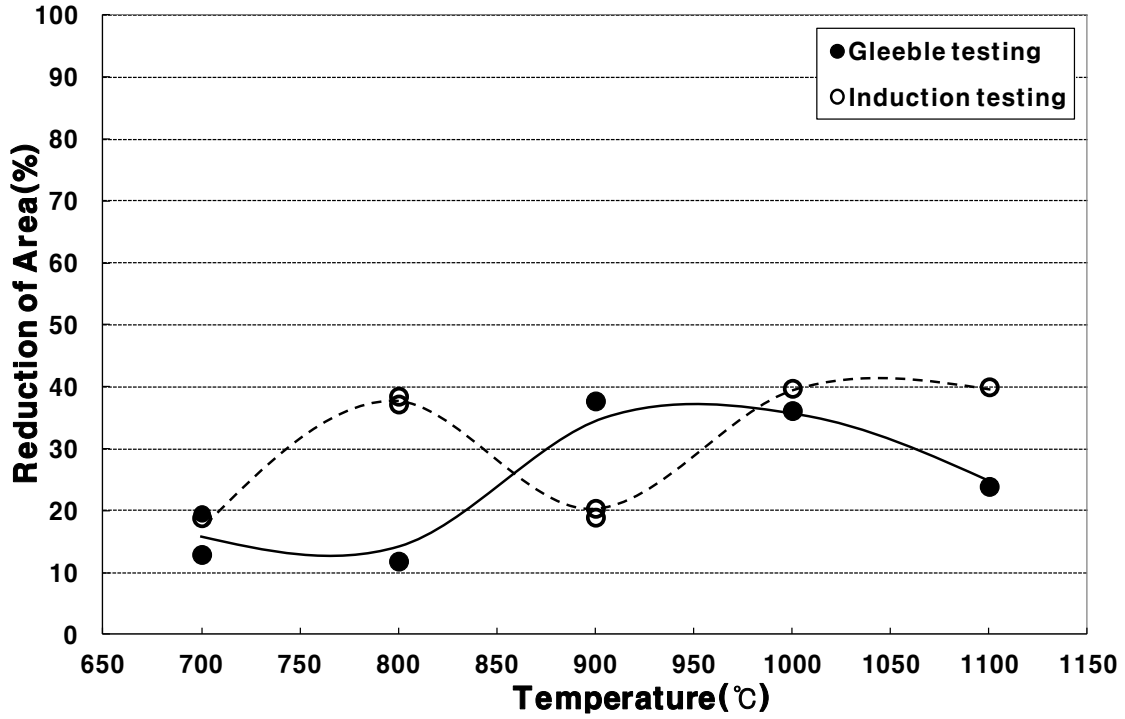


Fig.A1. Comparison of hot ductility behavior between tensile specimens tested using Gleeble with tensile specimens tested using induction heating. Tensile specimens were machined from as cast ingots.

The main conclusion from this exercise is that results from the Gleeble testing and Induction testing are similar and therefore are interchangeable.